Doctoral Dissertation
Doctoral Program in Energy Engineering (30th Cycle)

Innovative solar energy technologies and control algorithms for enhancing demand-side management in buildings

Gianluca Serale
* * * * *

Supervisors
Prof. Marco Perino
Prof. Alfonso Capozzoli

Doctoral Examination Committee:
Prof. Marco Beccali, Referee, Università degli studi di Palermo
Prof. Zhenjun Ma , Referee, University of Wollongong
Prof. Enrico Fabrizio, Examiner, Politecnico di Torino
Prof. Massimo Fiorentini, Examiner, University of Wollongong
Prof. Fabrizio Ascione, Examiner, Università di Napoli Federico II

Politecnico di Torino
2018 May 15th

I hereby declare that, the contents and organisation of this dissertation constitute my own original work and does not compromise in any way the rights of third parties, including those relating to the security of personal data.

…………………………......
Gianluca Serale
Turin, 2018 May 15th

Summary

The present thesis investigates innovative energy technologies and control algorithms for enhancing demand-side management in buildings. The work focuses on an innovative low-temperature solar thermal system for supplying space heating demand of buildings. This technology is used as a case study to explore possible solutions to fulfil the mismatch between energy production and its exploitation in building. This shortcoming represents the primary issue of renewable energy sources. Technologies enhancing the energy storage capacity and active demand-side management or demand-response strategies must be implemented in buildings. For these purposes, it is possible to employ hardware or software solutions. The hardware solutions for thermal demand response of buildings are those technologies that allow the energy loads to be permanently shifted or mitigated. The software solutions for demand response are those that integrate an intelligent supervisory layer in the building automation (or management) systems. The present thesis approaches the problem from both the hardware technologies side and the software solutions side. This approach enables the mutual relationships and interactions between the strategies to be appropriately measured.

The thesis can be roughly divided in two parts. The first part of the thesis focuses on an innovative solar thermal system exploiting a novel heat transfer fluid and storage media based on micro-encapsulated Phase Change Material slurry. This material leads the system to enhance latent heat exchange processes and increasing the overall performance. The features of Phase Change Material slurry are investigated experimentally and theoretically. A full-scale prototype of this innovative solar system enhancing latent heat exchange is conceived, designed and realised. An experimental campaign on the prototype is used to calibrate and validate a numerical model of the solar thermal system. This model is developed in this thesis to define the thermo-energetic behaviour of the technology. It consists of two mathematical sub-models able to describe the power/energy balances of the

flat-plate solar thermal collector and the thermal energy storage unit respectively. In closed-loop configuration, all the Key Performance Indicators used to assess the reliability of the model indicate an excellent comparison between the system monitored outputs and simulation results. Simulation are performed both varying parametrically the boundary condition and investigating the long-term system performance in different climatic locations. Compared to a traditional water-based system used as a reference baseline, the simulation results show that the innovative system could improve the production of useful heat up to 7 % throughout the year and 19 % during the heating season.

Once the hardware technology has been defined, the implementation of an innovative control method is necessary to enhance the operational efficiency of the system. This is the primary focus of the second part of the thesis. A specific solution is considered particularly promising for this purpose: the adoption of Model Predictive Control (MPC) formulations for improving the system thermal and energy management. Firstly, this thesis provides a robust and complete framework of the steps required to define an MPC problem for building processes regulation correctly. This goal is reached employing an extended review of the scientific literature and practical application concerning MPC application for building management. Secondly, an MPC algorithm is formulated to regulate the full-scale solar thermal prototype. A testbed virtual environment is developed to perform closed-loop simulations. The existing rule-based control logic is employed as the reference baseline. Compared to the baseline, the MPC algorithm produces energy savings up to 19.2 % with lower unmet energy demand.

Acknowledgment

My supervisors Alfonso and Marco. Mentors and friends before professors.
My TEBE group colleagues.
My officemates during the PhD (Ylenia, Francesco, and Lorenza).
My co-authors (Alberto, Daniele, Daniele, Francesco, Enrico, and Marco).
My iYfarm teammates (Emanuele, Fabrizio, and Luca).
My SBRC and CHAOS Lab mates.
My students (some of them!).
My Georgios and Lorenza.

Cuore

Identità.
Imprecazione.
Imperativo.

Chapter 1

Introduction

1.1 Background and framework

According to several studies and reports, buildings are responsible for up to 40 % of the global energy needs [1,2,3,4]. Furthermore, in the next future, the total energy consumption of buildings is expected to grow. This fact is mainly due to an increase in the comfort requirements and the population accessing to more comfortable – and as a consequence energy-intensive – buildings. Architects, engineers, and researchers worldwide are trying to cope with this problem, defining sustainable paths of development. This is not a trivial task since buildings are characterised by multi-disciplinary aspects.
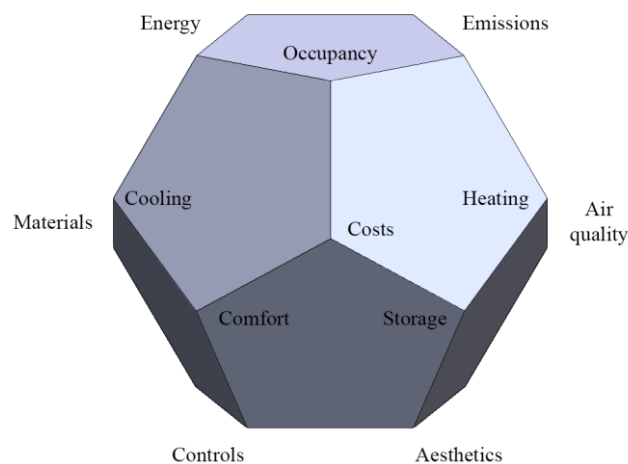
Figure 1. The most unfortunate building dodecahedron. Image courtesy of prof. Forrest Meggers (Princeton University).

To figure out the level of complexity required, the issues concerning sustainable buildings can be compared with those encountered in the batteries development path. Nowadays, batteries are one of the most interesting technologies

of the energy scenario. Nevertheless, some issues should still be addressed to favour a larger-scale and more sustainable market penetration of batteries. These problems mainly concern the energy density, the power density, the initial capital investment cost, and the operating costs. Experts refer to this set of issues as "*the unfortunate tetrahedron*". Buildings are much more complex structures than batteries. Therefore, defining a sustainable path for buildings means dealing with aspects related not only to balances of resources (e.g., costs, materials, emission) and thermo-energetics (e.g., energy, heat, moisture), but also involving the several tangled aspects concerning people (e.g., summer and winter comfort, air quality, aesthetics, ethics, culture, occupancy, etc.). This complex framework led experts to define the building issues as "*the most unfortunate dodecahedron*"!
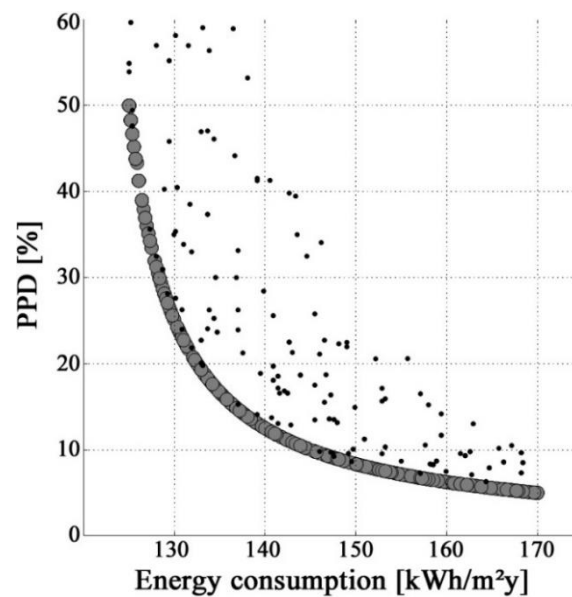
Figure 2. A visualisation of the Pareto front for the reduction of contrasting needs energy consumption vs. improvement of the thermal comfort of occupants (evaluated as Predicted Percentage of Dissatisfied).

Nowadays, researchers investigating this very complex building dodecahedron have a twofold goal. On the one side, the building stakeholders have to *formulate the problem* of building sustainability. In general, this process coincides with the preliminary building design phase. At this stage, all the aspects composing the building dodecahedron should be considered and all their possible combinations investigated. Nowadays, the research activity is focused on figuring out this process using the mathematical formulation of a multi-objective optimization. These objective functions are characterized by contrasting (or conflicting) needs. For instance, the pursuit of obtaining higher levels of comfort can lead to increase the energy demand of buildings dramatically. Likewise, the improvement of building energy performance is accompanied by an increase in the building-related initial investment costs. Many other examples would be possible. In those cases, a single solution that simultaneously optimizes each goal does not exist; whereas it exists a very high number (possibly infinite) of equally optimal solutions. These solutions

are called non-dominated or Pareto optimal solutions. Without additional subjective preference information, all Pareto optimal solutions are considered equally good. The entire set of Pareto optimal solutions – not dominated by any other feasible solutions – is referred to as the Pareto front (or Pareto frontier). *Figure 2* shows an example of Pareto front used to investigate the contrasting needs of thermal comfort and energy consumption.

On the other side, building stakeholders have to *make decisions*. Decision making means to define the trade-off among two or more contrasting objective functions. Defining trade-offs means finding a unique combination between the set of equally good solutions, by appealing to subjective preference information. Practitioners can define these ones using their own experience or the indication of customers. Usually, the number of possible solutions is reduced and regulated by the existence of problem bounds (e.g., economic constraints, or technical feasibility constraints, etc.). Using the previous example, defining a trade-off solution between the contrasting objectives of increasing the occupants' thermal comfort and reducing the building energy demand means to define a valid and unique compromise between two requirements, as highlighted in *Figure 3*. So far, the outcomes of the studies aiming at defining this optimal trade-off led to strongly improve the overall building thermo-energetic performance. As a consequence, the market penetration of efficient buildings' technologies and nearly Zero Energy Buildings strongly increased.
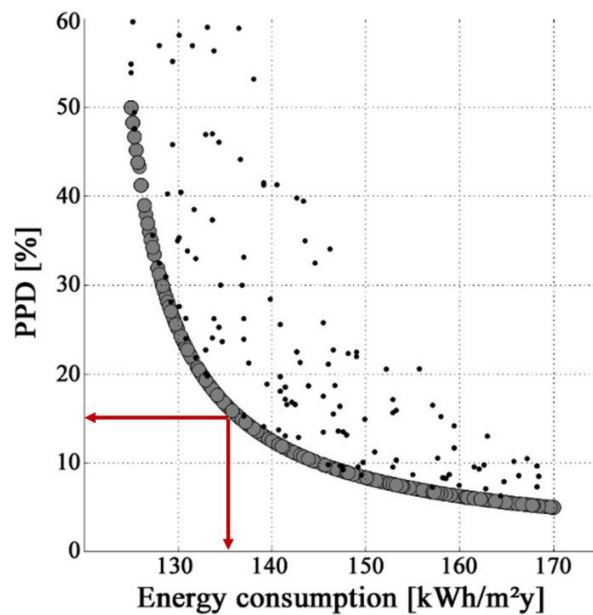
Figure 3. Subjective preferences allow a unique trade-off between the conflicting needs to be determined, individuating the required optimal conditions.

However, moving forward the building design phase and considering the operational lifespan of a building, new challenges must be faced. Indeed, buildings are dynamic systems whose requirements evolve over time. Nowadays, this is more significant and evident than in the past. For instance, the extensive adoption of renewable energy sources - directly integrated into the buildings or connected to

the energy grids - has increased the variation over time of the energy value (evaluated as consumption of resources, as well as energy tariff). Indeed, the energy value strongly fluctuates over time, even with substantial daily differences, according to the stochastic fluctuations of the energy demand and availability. The more the penetration of renewable source, the more stochastic the energy availability. Furthermore, it can be observed a mismatch between these stochastic patterns of energy production and consumption (e.g., in buildings, space heating demand mainly does not occur when solar energy is readily available). This variation of the boundary conditions and requirements also affects the selection of the optimal trade-off on the Pareto front. Indeed, the selection of the correct combination of the parameters must evolve over time, adapting itself to the variation of boundary conditions. For instance, Figure 4 shows how this dynamic behaviour can be applied to the previous example. On the one hand, the case indicated with the black arrow can be representative of conditions where the energy value becomes very low (e.g., when significant renewable energy sources are available), thus the energy consumption becomes no more a primary concern. On the other hand, the case indicated with the red arrow can be symbolic of an increase of energy prices or a decrease of comfort requirements (e.g., during unoccupied periods).
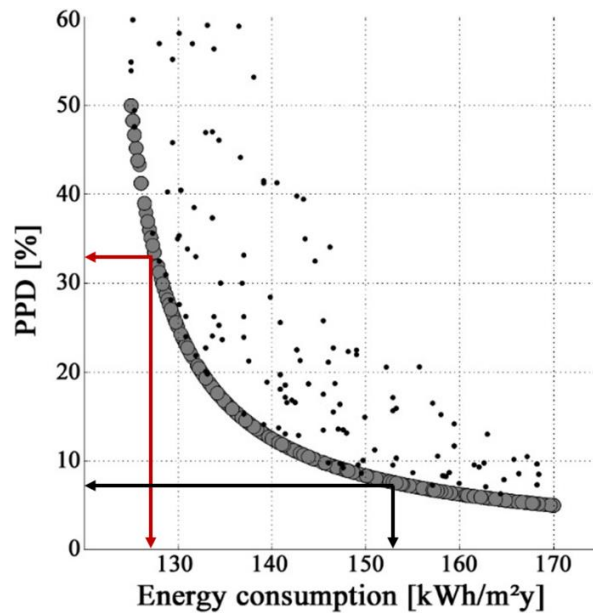
Figure 4. (black arrow) A possible optimal trade-off when energy value is low. (red arrow) A possible optimal trade-off when energy value is high or the building is unoccupied.

The previous scenario has increased the necessity of buildings capable of performing flexible thermal management strategies. Therefore, modern buildings must be able to interact with their occupants and the energy supply grid; to adapt their behaviour to the continuous variation of their needs. Buildings with these properties are often referred to as *responsive buildings*. These responsive buildings assume a fundamental role also in the energy distribution grid, since they can

perform thermal demand response strategies (e.g., active energy storage, peak load shifting, etc.). In this context, new market opportunities are emerging. In detail, software services capable of performing data analytics tools and energy management strategies will play a crucial role in the very next few years. This opportunity represents a shift from the traditional energy and building market that is generally more hardware solutions oriented. Nowadays potential benefits offered by software services are impressive and range from the optimisation of the system design to the active energy demand response management.

The hardware solutions for thermal demand response of buildings are those technologies that allow the energy loads to be permanently shifted or mitigated. In particular, this goal is achieved by exploiting thermal storage, a feature strictly related to the thermal capacity of an element or a structure. *Passive* storage strategies exploit the thermal capacity of the overall building itself (e.g., walls, ceilings, floors, structures). *Active* strategies instead bound the storage functions to a specific element (generally referred to as thermal energy storage unit or tank). Passive and active storage strategies can be combined to enhance the overall storage capabilities of buildings. Furthermore, they can be based on the exploitation of both sensible and latent heat (when a phase change occurs).

The software solutions for demand response are those that integrate an intelligent supervisory layer in the building automation (or management) system. The continuous collection and exchange through the internet of monitored building-related data enhance this feature. Such characteristics are typical of the *smart buildings*. In fact, nowadays electronic components are becoming extremely affordable; thus their deployment in buildings sharply increased in the last decade. This massive implementation has allowed a significant amount of data to be more readily available and accessible. Simultaneously, the increase in computational power and the availability of accurate weather and energy tariff forecast allowed the building designers to explore many possible advanced control strategies for optimising the energy management of buildings. In particular, in the design stage, data-analytics is necessary to define demand/supply profiles and tune the combination of multi-energy systems (e.g., the combination of various renewable energy sources with storage and energy delivery systems). Furthermore, in the design stage, the monitoring system must be accurately selected and installed defining where and which are the most critical variables that must be gathered. In the operating phase, the data can be used for continuous commissioning purposes, the detection of fault occurrence and the re-tuning and optimisation of system controllers. This process consists in the development of an intelligent supervisory layer capable of improving the responsiveness of the building automation system.

1.2 Aim and objectives

Nowadays, it is crucial for the scientific research to deeply investigate both these hardware and software aspects. It is essential to have a vision that considers

both these elements at the same time. In fact, only their correct overlap and integration can lead to effective solutions for the challenges offered by the current energy scenario. The present thesis is based on this vision. The main goal of the work is to investigate hardware technologies and software solutions that enable to reduce the mismatch between energy availability and demand in buildings. For this purpose, a specific case study of a renewable energy system coupled with a storage unit for building space heating was considered as a case study. On the one hand, the thesis investigated all the thermo-energetic aspects influencing the performance of an innovative hardware technology (a slurry PCM-based solar thermal system for building space heating). On the other hand, an innovative close-loop predictive controller was devised to enhance the efficiency of this novel system. This case study allowed several of the challenges required by the modern energy science to be approached and faced. In this perspective, the path of the thesis assumes a broaden vision and the approach adopted can be further generalised to different technologies or systems.

The first part of the thesis is focused on an innovative technological solution of an active latent heat-based thermal energy storage coupled with a solar thermal system. This *hardware solution* allows the gap between renewable energy availability and user energy demand to be permanently shortened. It also mitigates the mismatch between peaks of demand and production. Firstly, this technology was investigated and conceived theoretically. Secondly, experimental tests were performed to define the features required for a storage media capable of exploiting latent heat. Thirdly, physical-mathematical numerical models were developed to perform simulations. These are essential to assess the potential benefits achievable by such a technology. Finally, a full-scale prototype was conceived and realised to investigate the performance of the innovative system experimentally.

Once the technical aspects of this new technology were solved, further questions have arisen: "*Can we obtain the maximum benefits achievable by an innovative technology just adapting the existing control methods developed for other technologies? Or does this innovative technology require to set up control paradigms ad-hoc developed?*". The coupling of innovative technologies with control solutions that effectively exploit the potentialities offered by recent advances in electronics is as significant as the investigation of the technology itself. Therefore, any innovative technological solution requires being controlled optimally to be effective and fully exploit its potential. For this reason, the second part of the thesis is mainly focused on the *software solutions* for demand response. In more detail, this part of the thesis is primarily dedicated to the thermal management of buildings with Model Predictive Control (MPC), a promising control strategy that merges principles of classical feed-back control and optimisation. An MPC algorithm has been devised to regulate the hardware technological solution developed in the first part of the thesis.

The primary scopes of the current thesis can be pinpointed through the following bullet points:

•	investigation of innovative PCM features and properties;

- conceiving, design and prototyping of an innovative technology (*hardware solutions*) capable to enhance the usage of solar radiation and maximise energy storage opportunities. This technology is used as a case-study throughout the entire work;

- development of a calibrated and validated numerical models able to capture thermal dynamics of the prototype elements and to stress its performance according to various boundary conditions;

- assessment of the potentialities offered by the conceived technology in terms of efficiency increase and fulfilling of the mismatch between solar energy availability and building energy demand;

- definition of a clear and exhaustive framework concerning innovative controllers (*software solutions*), with a particular focus on those offering predictive features and recursive optimisation features (MPC based);

- devising of an innovative control algorithm to regulate the prototype under investigation and maximise its performance.

1.3 Research methodologies

Figure 5*, Figure 6, Figure 7, Figure 8* outline the methodological framework and the key-aspects investigated in the present thesis. Even if this research activity has been focused on a specific case study (a solar thermal system exploiting latent heat for space heating of residential buildings), it contains all the various aspects required to correctly approach the full current scientific challenges offered by the energetic scenario.

Chapter 2 is a literature review of the scientific works regarding solar thermal technologies, Phase Change Materials (PCMs) and the combination of these two topics (PCMs in solar technologies). Chapter 3 introduces the concept of a solar thermal system that uses PCM both as heat transfer fluid and as storage media. This Chapter can be further divided into three parts: the theoretical and experimental investigation of the features of the PCM adopted in the system; the conceiving and designing of a full-scale prototype to test the technology; and the development of a physical-mathematical numerical model to describe the dynamical evolution over time of the innovative s

ystem. Chapter 4 presents the results of the research undertaken in Chapter 3. Firstly, the numerical model has been validated with experimental measurements; secondly, the reliable results of the numerical model were used to parametrically assess the system performance under various boundary conditions; finally, experimental results about the full-scale prototype are presented. Chapter 5 switches from the investigation of hardware aspects to the software solutions for intelligent building thermal energy management. In detail, the first part of the Chapter outlines a literature review and a broad framework of the steps necessary to correctly implement an MPC problem in buildings. The second part of the Chapter formulates an MPC algorithm to regulate the technology presented in the

previous chapters. Close-loop simulations were performed to test the controller effectiveness and compare its key performance indicators with those of an existing rule base controller. The Conclusion Chapter outlines and summarises the main findings of the research path. An outlook on the future perspectives is also provided.

References

[1] Pérez-Lombard L, Ortiz J, Pout C. A review on buildings energy consumption information. *Energ build* 2008;40(3):394-98. https://doi.org/10.1016/j.enbuild.2007.03.007.

[2] Allouhi A, El Fouih Y, Kousksou T, Jamil A, Zeraouli Y, Mourad Y. Energy consumption and efficiency in buildings: current status and future trends. *J Cleaner prod* 2015;109:118-30. https://doi.org/10.1016/j.jclepro.2015.05.139.

[3] Cao X, Dai X, Liu J. Building energy-consumption status worldwide and the state-of-the-art technologies for zero-energy buildings during the past decade. *Energ build* 2016;128:198-213.

[4] International Energy Agency. Tracking Clean Energy Progress 2017. Energy Technology Perspectives 2017 Excerpt. 2017 IEA report. Available at: https://www.iea.org/publications/freepublications/publication/TrackingClean EnergyProgress2017.pdf
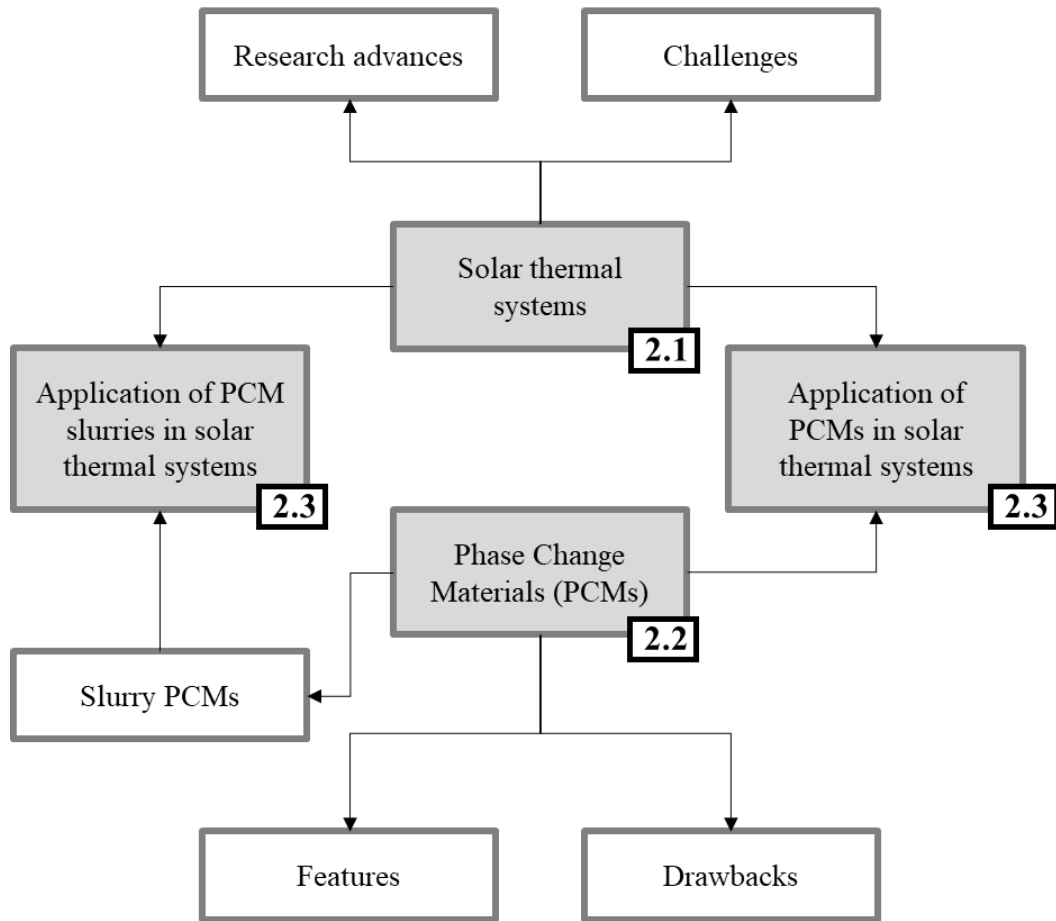
CHAPTER 2

Figure 5. Methodological framework of Chapter 2. Numbers in black-boxes indicate the chapter subsections dealing with the topic.

CHAPTER 3
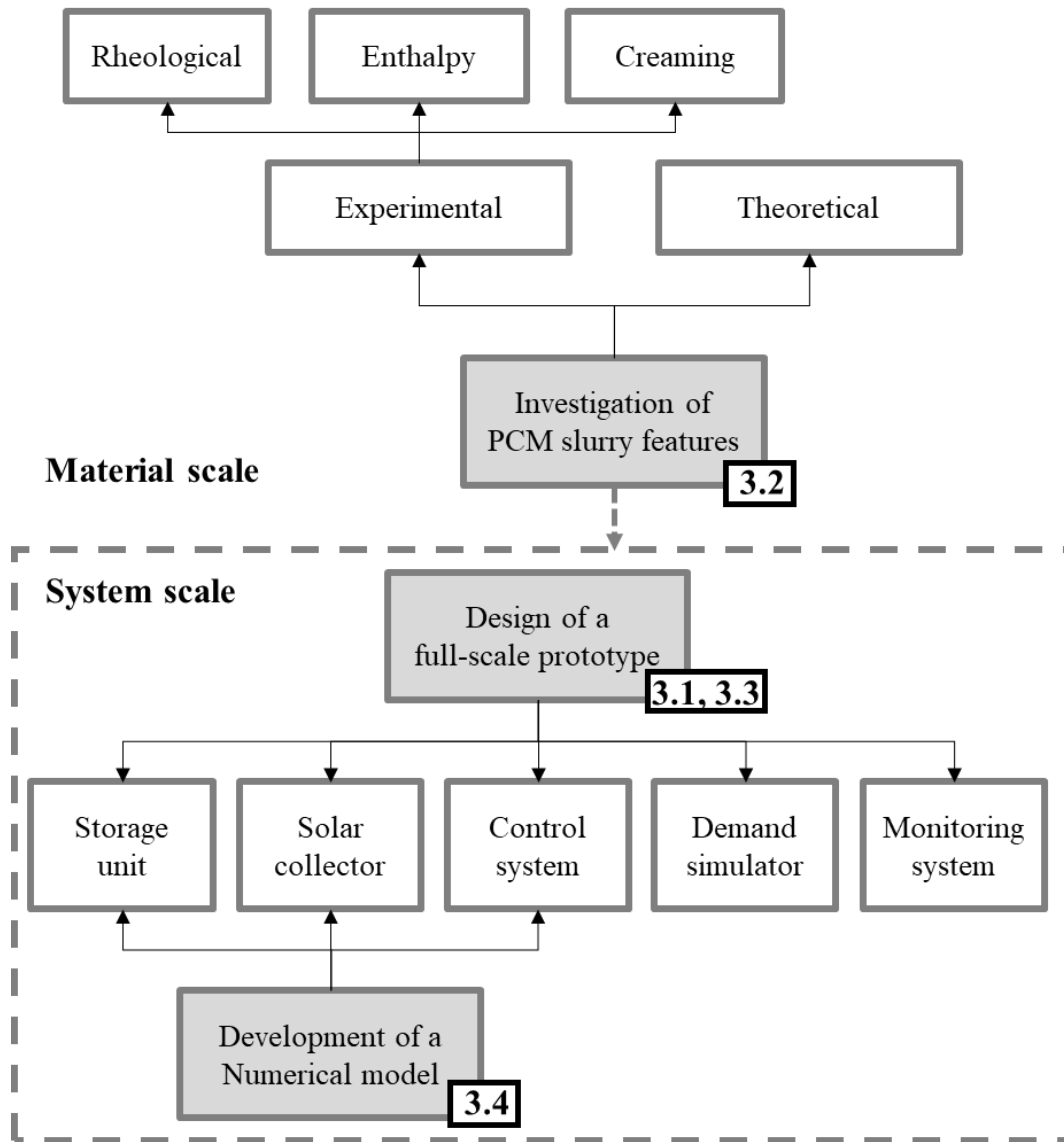
Figure 6. Methodological framework of Chapter 3. Numbers in black-boxes indicate the chapter subsections dealing with the topic.

CHAPTER 4
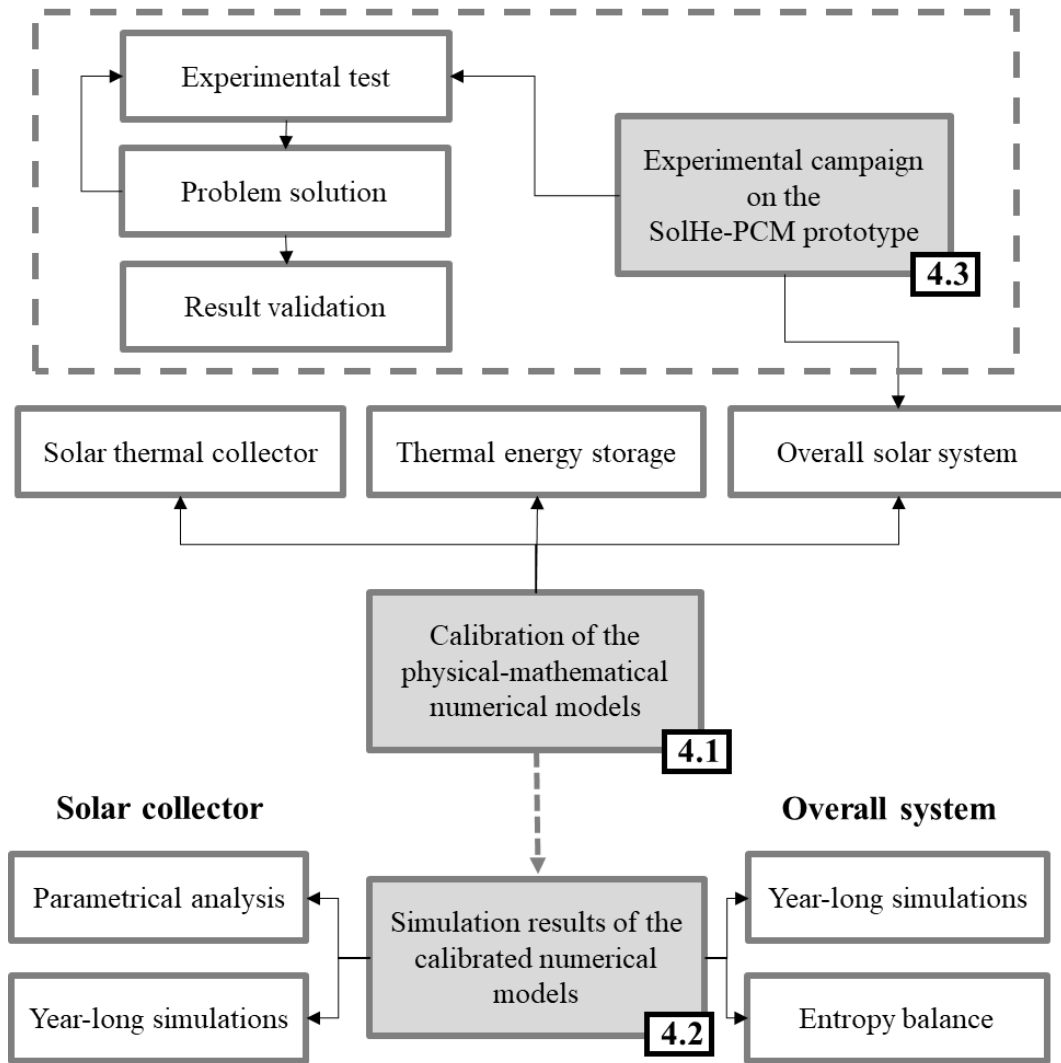
Figure 7. Methodological framework of Chapter 4. Numbers in black-boxes indicate the chapter subsections dealing with the topic.

CHAPTER 5

```
┌──────────────┐   ┌──────────────┐   ┌──────────────┐   ┌──────────────┐
│ Opportunities│   │  Literature  │   │   Problem    │   │ Applications │
│              │   │   review     │   │ formulation  │   │              │
└──────────────┘   └──────────────┘   └──────────────┘   └──────────────┘
```

```
        ┌─────────────────────┐
        │   A framework for   │
        │  Model Predictive   │
        │   Control (MPC)     │
        │                 5.1 │
        └─────────────────────┘
```

MPC literature review

MPC formulation

```
        ┌─────────────────────┐
        │ MPC formulation to  │
        │ control the solar   │
        │  thermal system     │
        │                 5.2 │
        └─────────────────────┘
                 │
        ┌─────────────────────┐      ┌──────────────┐
        │ Problem formulation │─────▶│  Close-loop  │
        │                     │      │ simulations  │
        └─────────────────────┘      └──────────────┘
```

```
┌──────────────┐ ┌──────────┐ ┌──────────────┐ ┌──────────────┐
│  Controlled  │ │ Forecast │ │ Hard and soft│ │  Objective   │
│ system model │ │  model   │ │ constraints  │ │  function    │
└──────────────┘ └──────────┘ └──────────────┘ └──────────────┘
```
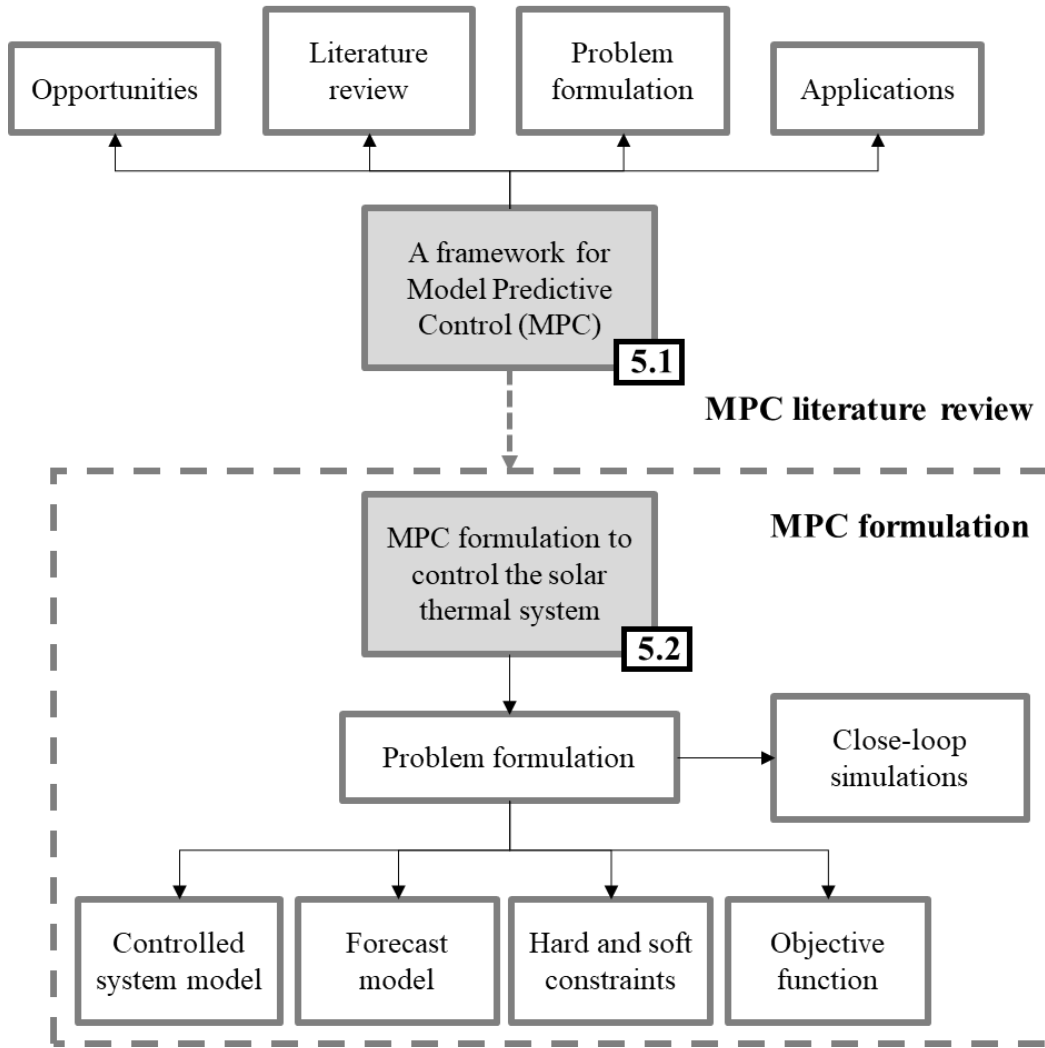
Figure 8. Methodological framework of Chapter 5. Numbers in black-boxes indicate the chapter subsections dealing with the topic.

Chapter 2

Recent advances in building integrated solar thermal systems and Phase Change Materials (PCMs)

The scope of the present Chapter 2 is to investigate the findings achieved so far in the scientific literature about the technologies involved in the work.

In detail, the first part of the chapter (Section 2.1) describes the background of solar thermal technologies. It provides an outlook of the current technologies worldwide adopted and a description of the primary elements composing a solar thermal system.

The following Section 2.2 introduces the Phase Change Materials (PCMs). The PCMs are often used in building applications to employ latent transformations that allow the thermal levels to be reduced. Thus, improving First and Second law efficiencies. This section provides a comprehensive review of PCMs, their application in buildings, thermal energy storage units, and solar thermal technologies.

The final part of the chapter presents briefly the technology that was used as the case study of the present thesis. The detailed focus on this specific system is demanded to Chapter 3 and Chapter 4.

Some portions of the present Chapter were already published in the following scientific papers:

• Design of a low-temperature solar heating system based on a slurry Phase Change Material (PCS). Authors: G Serale, E Fabrizio, M Perino. Journal: Energy and Buildings 106, 44-58 [144];

- Numerical model and simulation of a solar thermal collector with slurry Phase Change Material (PCM) as the heat transfer fluid. Authors: G Serale, F Goia, M Perino. Journal: Solar Energy 134, 429-444 [145];
- Potentialities of a Low Temperature Solar Heating System Based on Slurry Phase Change Materials (PCS). Authors: G Serale, Y Cascone, A Capozzoli, E Fabrizio, M Perino. Journal: Energy Procedia 62, 355-263 [148].

2.1 Solar thermal collectors

Solar thermal collectors are the most common devices used for the conversion of solar energy into heat [1]. The annual report carried out by the Solar Heating and Cooling program of the International Energy Agency at the end of 2017 [2], has reported that the worldwide installed heating capacity produced using solar thermal collectors was about 436 GW_{th}, which corresponded to an estimated total of $6.23 \cdot 10^8$ m^2 of collector area in operation. These installed power led to estimated annual energy savings of 357 GW_{th} worldwide, corresponding to a reduction of $1.24 \cdot 10^8$ emitted tons of CO_2 or $3.84 \cdot 10^7$ equivalent tons of oil consumption. In 2015 only, 40.2 GW_{th} of solar thermal systems were installed (64 % of those were new systems, 36 % refurbishment of existing systems). China is the leading country in the installation of new systems with about the 75 % of the market in 2015 and a total of $4.42 \cdot 10^8$ m^2 of collector area in operation. *Figure 1*(a) shows the trends of the overall installed heating capacity worldwide during the last years (referring to the data yearly outlined by the annual report of the Solar Heating and Cooling program of the International Energy Agency). *Figure 1*(b) reports the market shares of different world regions in 2015.

Focusing on Italy, a report of Assolterm [3] – the Italian Association of Solar Thermal Energy – dating back to 2014, described the Italian market as constituted by around $4 \cdot 10^5$ m^2 of panels installed each year, and a total installed power capacity of solar thermal systems that exceeded 1 GW_{th}. These numbers showed that, compared to the European countries most advanced in this sector, Italy is behind with respect to both the total installed power capacity per capita (i.e., 18 kW_{th} per 1000 inhabitants, compared to the 270 kW_{th} per 1000 inhabitants of Austria), and the annual market (i.e., an installed capacity of 5 kW_{th} per 1000 inhabitants, compared to the 29 kW_{th} per 1000 inhabitants of Austria).

The thermal energy produced by solar thermal systems can be used to satisfy:

• the domestic hot water demand;
• the space heating demand;
• the combined production of domestic hot water and space heating (combi-system).

The exploitation of solar energy for space heating alone can provide substantial energy savings under certain conditions, which depend on the location, and the energy demand profile [4,5]. The full profitability of this use is often limited to a great extent by the time mismatch between solar energy availability and building energy demand [6]. For instance, on the one hand, during winter time the limited solar irradiation that is available can barely cover the total energy demand for heating. On the other hand, the high solar radiation available in summertime far exceeds the energy demand for domestic hot water production, and no direct or fully profitable use for this excess can be found – unless large and expensive seasonal storages are adopted [7–9]. For this reason, solutions for

space-heating demand only and combi-systems are not very common in buildings. For example, in Italy 90 % of the installed collectors serve for the production of domestic hot water [3].

(a)

(b)
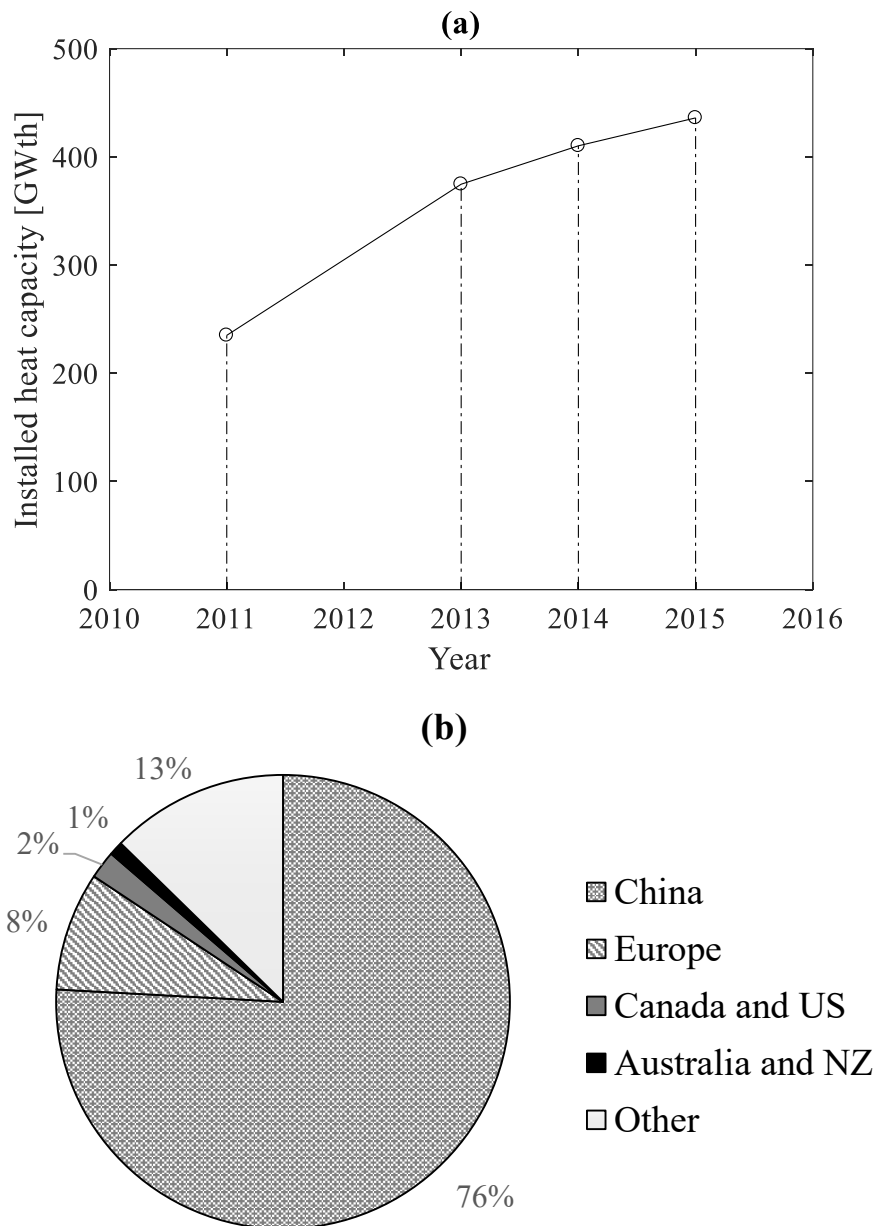
Figure 1. (a) Increasing trend of solar thermal system installed heat capacity worldwide. (b) Country distribution of solar thermal system installed in 2015. Data were retrieved from [2].

Conventional collectors use water and an additive (usually glycol, which acts as antifreeze) as a heat transfer fluid. The selection of the heat transfer fluid plays a very significant role in a solar thermal system because it is used to transfer the energy absorbed in the collector to the heat exchanger placed inside the storage tank. For water-based system typical range of working temperatures is 50 - 60 °C. This range is required firstly to provide heat terminal units with a sufficiently

large enthalpy flux and reasonable flow rates; secondly to ensure the use of sufficiently small thermal energy storage systems. This relatively high heat transfer fluid temperature range causes two different sets of problems:

• The first set of problems is related to the considerable thermal energy losses that occur in all of the system components. These are due to the high-temperature difference between the heat transfer fluid and the environment. For this reason, an increase in this temperature difference corresponds to a decrease in the instantaneous system efficiency as well as in the seasonal system efficiency. Higher efficiencies are only reached for a fixed heat transfer fluid temperature when the environment temperature rises. Once again, in winter time, when the temperature and irradiance are lower, the capability of the solar thermal system to exploit solar energy is reduced. Even in those winter days when there is high irradiation, the water-based heat transfer fluid undergoes a consistent increase in temperature to exploit the solar energy, and the inefficiency of the process also increases due to the enhanced heat dissipation towards the outside.
• The second set of problems is related to the time variation of the short periods of time during which the solar thermal system can be exploited to produce heat. The higher the heat transfer fluid temperature, the higher the minimum irradiation required to produce a useful heat gain [10].

2.1.1 Brief scientific literature overview about researches about solar thermal collectors

Solar thermal systems have been widely investigated since the '40s [11] and nowadays constitute a mature technology that is applied at a large scale and is spreading significantly. Shukla et al. have provided a complete review of solar thermal system developments that are still adopted in this technology and their limitations [12]. The present thesis is focused on solar thermal systems applied at building scale. Furthermore, the attention is focused on systems that consider solar thermal collector and thermal energy storage as separate elements with circulation guaranteed with mechanical pumps. Thus, other applications (e.g., solution for industrial or district heating purposes, compact systems integrating collector and storage, natural convection systems) are not particularly deepened. Eventually, flat plate collectors resulted more attractive for building applications compared to evacuated tube collectors. Indeed, even if evacuated collectors better perform in producing fluid at high temperatures, they are not competitive because of higher initial installation costs. Thus, they are mostly used for industrial [13], district-heating assisted [14], or solar-cooling [15] applications, where the process temperature required are higher and the panel efficiency can positively intervene in a cost-optimal assessment. Therefore, even if evacuated tube collectors are the most common technology for solar energy conversion in thermal power (due to their massive application in the industrial and district heating sectors in China),

they occupy only a small share of the market of building applications. Furthermore, in Italy 86.5 % of the installed solar collectors are of the flat plate type, and vacuum tube collectors represent only the remaining 13.5 %. *Table 1* reports the 2015 data of total heat power capacity installed in the various country for different collector technologies and different heat carrier fluids [2].

Table 1. Total heat power capacity installed in various country for different collector technologies and different heat carrier fluids.

Country	Flat plate collectors				Evacuated tube collectors
	Water Unglazed	Water Glazed	Air Unglazed	Air Glazed	
	[MW$_{th}$]	[MW$_{th}$]	[MW$_{th}$]	[MW$_{th}$]	[MW$_{th}$]
Australia	3605	2308	210	6	110
Italy	31	2527	/	/	395
Canada	560	49	280	34	32
China	/	24,885	/	/	285,585
United States	15,283	1921	73	36	102
New Zealand	5	100	/	/	7

Over the years, several developments have been made in order to improve the overall performance of solar thermal panels and their efficiency, and many activities are still underway. These studies can be divided into two macro-categories: those related to the collector as a component and those related to the investigation of novel heat transfer fluids instead of water-based solutions.

2.1.1.1 Studies regarding the collector technologies:

The solar thermal collector is the element used for harvesting solar energy. In the flat plate panel configuration, the collector is composed of the following different parts (highlighted in *Figure 2*):

- a transparent single (or double) glazing cover to reduce top heat-losses;
- a selectively coated a flat-plate absorber plate;
- pipes for the flow of the heat transfer fluid;
- thermal insulation to reduce heat losses from edge and back of the collector;
- a protective casing to ensure the components are free from dust and moisture.

Several researchers have worked on the design and development of flat plate collectors, mainly focusing on the first three elements that most influence the

overall collector performance and whose design can be optimised.

The most widely-used transparent cover material in solar collectors is the single glass configuration, due to its high solar transmittance and low cost. In recent years, plastic thin films, plastic sheets, polymeric materials or transparent honeycomb compounds are also considered as upper transparent cover material in solar collectors [12,16,17]. In the case of the glass cover, studies investigated the overall increase of the system efficiency achievable either by applying anti-reflected coatings to increase the solar transmittance [18] or by the adoption of multiple glass layers with air gaps to increase the thermal insulation [19]. A thermotropic layer may be added to the transparent cover (as well as over the absorber plate) to mitigate stagnation risk [20].
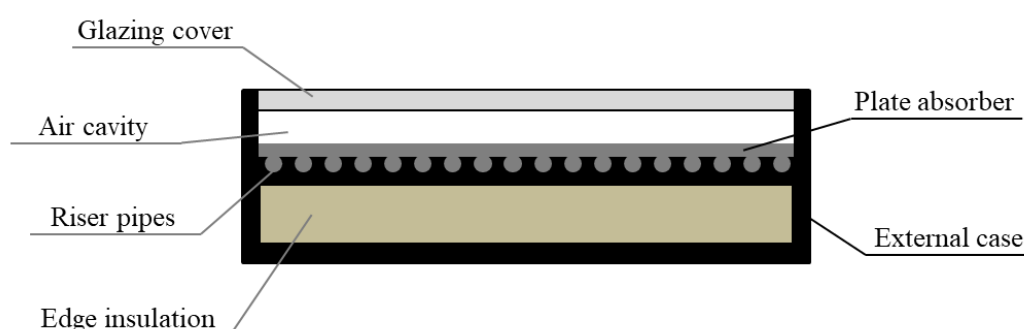
Figure 2. Schematic of the parts composing a flat-plate solar thermal collector.

The absorber plate is considered the most crucial parameter in the design of a solar thermal collector [21]. Its thermal performance is influenced by the absorber shape, material and coating. For easiness in the fabrication process, the most common absorber shape is the flat plate, which follows the collector shape. However, studies on parabolic, trapezoidal or variable thickness rectangular shapes were carried out, showing promising results in terms of improvement of the heat exchange. The traditional absorber material is generally a metal (i.e., aluminium or copper) for the requirement of high thermal conductivity to enhances the solar energy harvesting. However, nowadays polymer-based absorption plates are becoming more and more common because they are cheaper, more resistant to corrosion, lighter and easier to integrate into the collector [21]. This solution is the result of decades of research and development that led to realising polymeric material whose performance is comparable to one of the metal absorbers. Eventually, the black coating is the most traditional solution for absorber plates. However, for the sake of architectural requirements, panels with coloured plates were also developed and tested. Both theoretical and experimental results confirmed that coloured absorbers had efficiencies close to the black absorbers, if dark tone colour paintings are adopted [22].

The most common technological solutions concerning collector pipes are parallel pipes (risers) and serpentine pipes collectors. Serpentine pipes are more efficient due to a more uniform temperature distribution over the absorbed plate

surface, but at the same time they result more expensive. Other geometric designs include either two orders of pipes connected in parallel [23], rectangular pipes [24], fin-and-tube solutions [25] or conjugation with closed-end oscillating heat pipes [26].

The integration of solar thermal collector directly into building elements (e.g., in sloped roofs or façade panels) represents a further topic of investigation. It results particularly interesting from the architectural point of view. Furthermore, the overall benefits of such technologies should be carefully investigated considering both the effects in term of active envelope elements and effective renewable energy conversion. Maurer et al. provided extensive reviews about solar integration system technologies and strategies [27] and simplified models to assess the performance of such systems [28].

2.1.1.2 Studies regarding the heat transfer fluids adopted in the solar thermal systems:

As aforementioned, solar thermal collectors still suffer from efficiency drawbacks due to the relatively high working temperatures of the heat transfer fluid. An interesting concept that can be introduced to overcome the limitations mentioned above and to extend the operational time of solar thermal systems is represented by the adoption of a heat transfer fluid that exploits latent heat instead of (or together with) sensible heat. By making use of the (isobaric) phase change within the heat transfer fluid, which occurs at an almost constant temperature, a far greater amount of heat can be exploited in the process at lower temperature levels. High temperature-related inefficiencies can thus be reduced. This approach, which is based on the harvesting of energy with a low-exergy content, can be particularly suitable when used in combination with low-temperature HVAC equipment, such as radiant heating systems. On the other hand, domestic hot water production probably requires a slightly higher exergy content, and therefore needs to be achieved by coupling such a solar thermal system with other energy conversion systems that can increase the exergy level (for example, a heat pump).

In recent years, several research projects, involving a two-phase heat transfer process [12], have been conducted to study the effectiveness of solar thermal systems. In this way, the isobaric phase change process within the heat transfer fluid occurs at an almost constant temperature, without compromising the ability of the system to store thermal energy. Therefore, solar energy is exploited at lower thermal levels, and the previously described problems, due to a relatively high-temperature range, are also reduced. The use of refrigerant-filled solar collectors, whose application dates back to the '70s, has been investigated by many researchers. In these studies, heat pumps, integrated with solar collectors, were used to exploit the phase change of the refrigerants that were used as the heat transfer fluids. Many kinds of refrigerants - such as Chloro Fluoro Carbons and Hydro Fluoro Carbons [29,30] - or other natural fluids – such as propane or

carbon dioxide – have been used successfully [31,32]. When operating in a transcritical condition, the efficiency of these solar thermal systems is much higher than that of traditional water-based collectors. Nevertheless, these technologies are not so widely diffused due to the presence of substances that are harmful to the environment and the complexity of the system.

All these past attempts, which took advantage of the latent heat of the heat transfer fluid, were based on the exploitation of liquid-to-gas transition. However, it is also possible to exploit the solid-to-liquid transition latent heat. This solution can be obtained through the introduction of Phase Change Materials (PCMs) into the solar thermal system.

2.2 Phase Change Materials (PCMs)

The term Phase Change Materials (PCMs) is referred to industrial products which - at atmospheric pressure - undergo a phase transition (in general solid-liquid and vice versa) at a specific utilisation temperature. The nominal phase transition temperature should be chosen to match with the requirements of the specific application where the PCMs are used. PCMs store (during fusion) and release (during solidification) large amounts of thermal energy at an almost constant temperature. This fact is due to the exploitation of material latent heat of fusion/solidification. Specific latent heat capacities of fusion/solidification of PCMs are relatively high. PCMs are used to store excess energy, which would be otherwise wasted, and to match the demand and supply when they do not coincide in time [33,34]. In this process, PCMs act like an almost isothermal heat reservoir (*Figure 3*), due to the significant amount of heat they store or release during their phase transition. Thus, PCMs can be very useful in applications where the temperature control is essential.
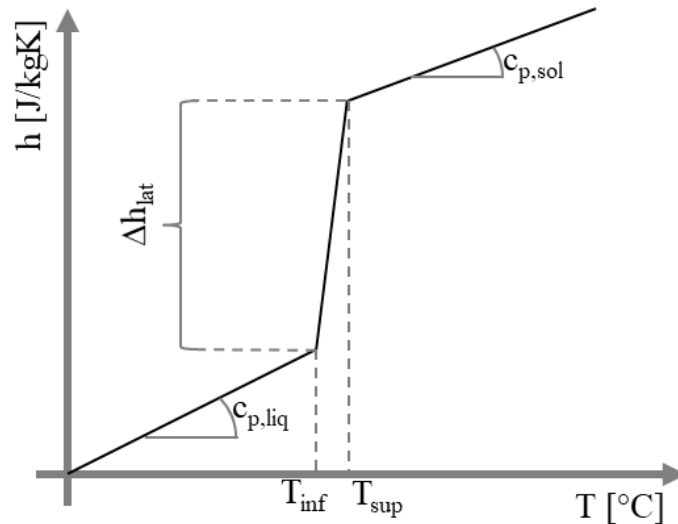
Figure 3. The PCMs allows a significant amount of thermal energy to be stored in an almost isothermal process.

2.2.1 Phase Change Materials features

Many characteristics of thermo-physical, chemical, kinetic, environmental and economic nature should be considered to evaluate the performance of a PCM [35–38]. In general, to satisfy the requirements of heat storage capability the following properties should be maximised (the higher the value, the better):

- specific latent heat capacity of fusion/solidification;
- specific sensible heat capacity;
- density (to maximise the heat storable per unit of volume).

Moreover, the density variation (hence volume change) between solid and liquid phases should be minimised. Otherwise, the container holding the material should be oversized to fit with the maximum volume reachable when the material is at the maximum expansion (generally during the liquid phase) [33].

PCMs should present long-term stability. It means that the thermo-physical properties of the PCM should remain constant regardless of the number of fusion/solidification cycles. Various laboratory ageing tests showed that the most of the materials satisfy this peculiarity.

For safety reasons, a PCM should be non-toxic and non-flammable at the operating temperatures. Chemical compatibility with the container holding the material is also required. In particular, corrosion should be avoided to avoid any possible leakage of the PCM in a liquid state. In case of encapsulated PCM (see 2.2.4 for details), process pressures should be maintained as low as possible to avoid the risk of encapsulating material ruptures.

Similarly to other products, the PCM environmental impact can be evaluated through a Life Cycle Assessment (LCA) associated with all the stages of product life [39]. Life Cycle Assessment allows both the embodied energy (i.e., the energy required from the extraction of raw materials to the final product assembly) and the operational energy (i.e., the overall energy required during the product expected lifetime) to be evaluated. Life Cycle Assessment evaluations found in the literature showed that applications of PCM in buildings mostly have a positive environmental impact [40–42]. Generally, the use of PCM is most favourable in locations with similar weather conditions throughout the year. Furthermore, to maximise the operational energy consumption a proper optimisation of the PCM features and integration should be performed.

Several authors investigated the economic feasibility of PCM applications in buildings [43]. Contrasting results were found according to different boundary conditions, in particular material costs and energy prices [44]. On the one hand, [45–47] found acceptable payback periods (between two and ten years). On the other hand, [48,49] found that PCMs are not economically beneficial. However, it should be considered that nowadays PCMs are mainly adopted in applications related to research investigations. Accordingly, prices are higher than the ones that would be expected in a scenario where PCMs broadly penetrate the market.

2.2.2 Main drawbacks of Phase Change Materials

According to the type of the PCM, problems such as low thermal conductivity, phase segregation, phase separation, hysteresis and supercooling may arise. In particular, phase segregation and supercooling are considered possible sources of poor stability, which may cause a reduced capability to store latent heat, or a significant variation in the phase change temperature [33,50]. The scientific literature proposed also several solutions to overcome the drawbacks. The adoption of a solution rather than another depends on the specific application.

2.2.2.1 Low thermal diffusivity

Since the PCM are mainly used to store energy when available, the thermal diffusivity is an essential factor to take into account when evaluating the performance of such materials. Indeed, thermal diffusivity strongly affects the homogeneity of the temperature distribution in the material, and this influences the level of exploitation of material heat storage capability. Since low thermal conductivities characterise many PCMs – values ranging around 0.2 and 0.5 W/(mK) – and high specific latent heat capacities (in particular when phase change occur), the thermal diffusivity is mostly mediocre. This feature causes problems in the fusion/solidification process that can occur only in the volumes closer to the heat sources (e.g., the heat exchanger in a thermal energy storage unit). Many studies investigated possible solutions to this problem recurring to material science solutions (e.g., mixing of PCMs with additives or surfactants) or to the adoption of arrays or structures, which enhances the heat transfer involving the PCM layer as a whole.

2.2.2.2 Phase segregation

Phase segregation takes place when solidification process occurs at a fast cooling rate for incongruent transformations. In these cases, the diffusion heat exchange – that is a prolonged process in the solid state of the material - is not sufficient itself to homogenise the composition, and non-equilibrium solidification takes place. This phenomenon causes the formation of layered grains; whose average composition is not a homogeneous equilibrium composition but a structure that differs from the core to the boundary. The solidification completes at a lower temperature, once the average composition of the solid matches that of the original mixture. Since phase segregation depends on the cooling rate, this drawback can be overcame selecting an appropriate heat transfer process speed rate. Nevertheless, this solution is consistently related to the degree of freedom offer by the specific application to the system designer, i.e. in some cases it would not be possible to intervene on the heat transfer process speed rate.

2.2.2.3 Phase separation

Phase separation is the conversion from a single-phase to a multi-phase system. Indeed, when a substance is formed by two or more components, according to its composition, it may separate in layers characterised by different phases. It is mainly due to gravitation effect caused by differences in density. For instance, in salt hydrates in the liquid state, sedimentation of the salt component in the lower layer of the mixture may occur. This fact is due to the salt density that is greater than the water one. Similarly, specific mixtures of micro-encapsulated PCM and water (see Section 2.2.5) show a phenomenon - named creaming effect

– where the lighter PCM floats on the more massive water matrix, establishing a more concentrated PCM layer in the upper part of the mixture. Both phenomena lead to a biphasic system with local component concentrations that differs from the initial and design conditions. Thus, the global properties of the mixture may vary due to this change in concentration, and the behaviour is not homogenous. Mechanical mixing can be used in storages to solve phase separation, but it would not be a solution at the material level. Another option is the adoption of surfactants and additives, which form a three-dimensional network capable of holding the PCM together at a microscopic scale or increasing the viscosity of the material.

2.2.2.4 Hysteresis

Hysteresis occurs when the PCM performs differently in case of heating or cooling. Hysteresis may cause different transition temperatures and specific latent heat capacities upon fusion or solidification process. Hysteresis can be caused by a low rate of crystal formation during solidification, a slow diffusion in the solid phase, or the formation of a different solid phase concerning the beginning of the melting process. Particular attention should be paid to the measurement process to avoid apparent hysteresis caused by non-isothermal conditions in the sample. The discussion concerning the possible solutions to overcome hysteresis is similar to the one figured out for coping with PCM phase segregation. Indeed, both drawbacks are due to the speed rate of the heat transfer process and can be handled reducing the heating/cooling rate applied to the PCM. Again this solution is dependent on to the degree of freedom offer by the specific application to the system designer.

2.2.2.5 Supercooling

Supercooling is the phenomenon for which a PCM remains in the liquid phase even when its temperature is lower than the solidification temperature, as shown in *Figure 4*. The solidification process is driven by the nucleation process that consists in the formation of first solid crystals (named nuclei). The capability to produce nuclei during the time is called nucleation rate. Solidification effectively starts only when nuclei with a sufficiently large radius are present. If nucleation does not occur or the nucleation rate is too low, the PCM remains liquid even at temperatures below its solidification temperature. Since the phase change is not activated correctly, this supercooling process involves sensible heat only. Afterwards, when the transition process is activated, the temperature suddenly rises again to the phase change temperature and remains there until the completion of the phase change transformation. Supercooling can be solved - or reduced - employing the addition of solid PCM particles to the supercooling liquid or

surfactants capable of acting as nucleators. Supercooling can also be considered a local form of hysteresis.
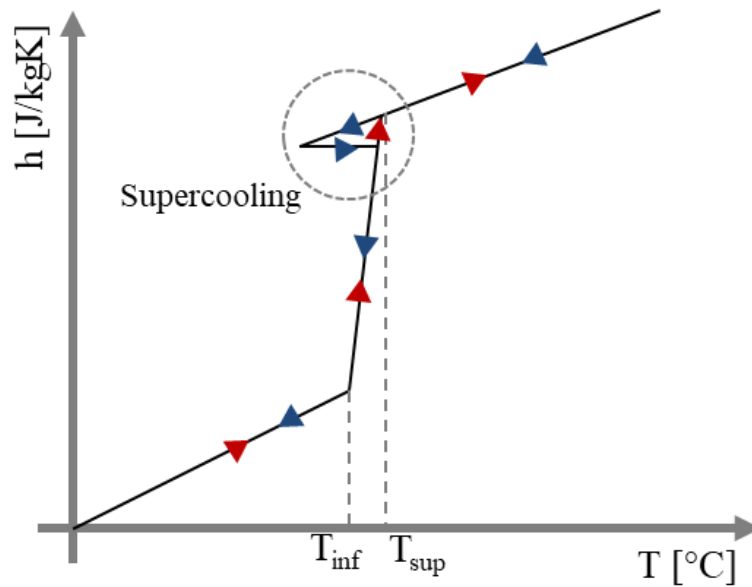
Figure 4. The supercooling drawback. This figure was adapted from [33].

2.2.3 Classification of Phase Change Materials

As shown in *Figure 5*, the substances used as PCMs can be classified as organic (e.g., paraffin and non-paraffin, such as fatty acids, esters and glycols), or inorganic (e.g., salt hydrate solutions and metals), or eutectic mixtures [51,52]. All these substances show a single melting temperature when they are pure, and a melting range when they are mixtures [53]. Nevertheless, since pure materials are costly, industrial materials are usually mixtures. Thus the phase change occurs in a temperature range.
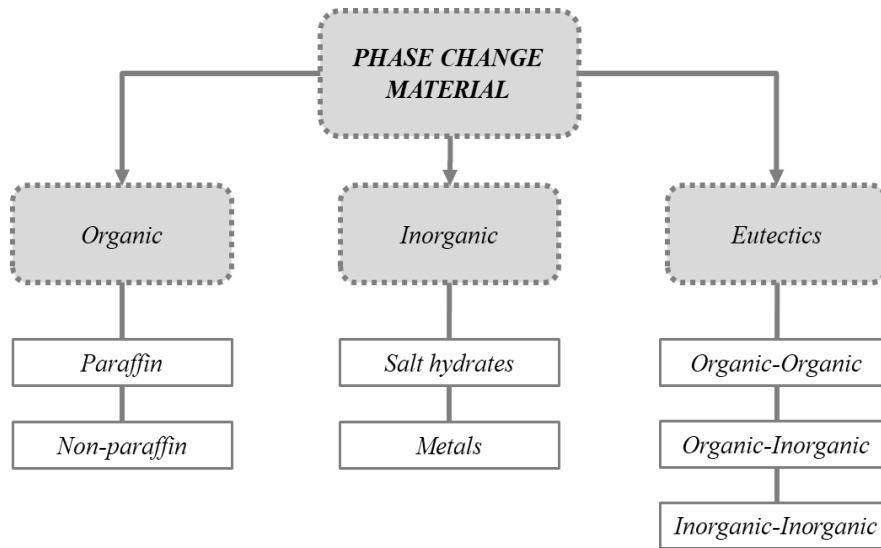
Figure 5. Classification of PCMs.

2.2.3.1 Organic Phase Change Materials

Organic PCMs can be further divided in paraffin or non-paraffin materials. On the one side, organic PCMs present no phase segregation, are chemically stable and have a high specific latent heat capacity of fusion/solidification. On the other side, organic PCM density is lower than the one of inorganic PCMs. Organic PCMs can be flammable, show a low thermal conductivity (around 0.2 W/(mK)) that reduces the heat diffusion and thus storage capability. Furthermore, they are characterised by high volume variations during phase transition, which can be not compatible with plastic containers. A broad literature review and extensive information on the main features of organic PCMs can be found in [33,36,50,52]. Typical paraffin materials are hydrocarbons (alkanes), whose general formula is C_nH_{2n+2}. The melting temperature increases accordingly to the number of carbon atoms in the molecular chain. Thus in the preparation process, the number of carbon atoms is the primary process controlled to suit the application requirements. Among the non-paraffin PCMs are fatty acids, esters and glycols. Non-paraffin materials are less adopted than paraffin material because more expensive and can be corrosive [51].

2.2.3.2 Inorganic Phase Change Materials

Inorganic PCMs can be further divided into salt hydrates or metals. Salt hydrates are inorganic salts which retain a definite number of water molecules within their crystal structure. The phase change in salt hydrates consists of the hydration or dehydration reaction - either total or partial - of the salt. Positive features of inorganic PCMs are the lower cost compared to other PCMs, the non-flammability, the relatively high specific latent heat capacity of fusion/solidification and thermal conductivity, around 0.5 W/(mK). Furthermore,

salt hydrates have lower embodied energy than other material, thus should be preferred in a Life Cycle Assessment perspective. On the contrary, salt hydrates present some negative properties such as a critical supercooling effect (see Section 2.2.2), a high volume change during phase transition, phase separation, and salt hydrates are corrosive towards metals. Extensive information on the main features of salt hydrate solutions can be found in [33,51].

2.2.3.3 Eutectics mixtures

Eutectics PCMs are mixtures of specific ratios of two (or more) components which do not usually chemically interact. The mixture forms a new compound, which undergoes a congruent melting with the simultaneous formation of two separate solid phases at a lower temperature than that of every single component. Eutectics mixtures have a sharp melting point similar to pure substances. Their adoption in building application is very limited and only a few data on their thermo-physical properties are available in the literature [36].

2.2.4 Incorporation methods

The PCMs are characterised by the occurrence of periods in which the material is in the liquid state. Liquid materials have more kinetic energy than solids, so their particles are less rigid and can slide around one another causing the fact that liquids have no a definite shape. Thus the need for a container that incorporates the PCM arises to give the liquid PCMs the possibility to take the shape of the container. In case of application of PCMs for active thermal energy storage, the storage tank can behave itself as the liquid material container. Otherwise (e.g., for the application of PCMs in the building envelope), various incorporation methods are viable, such as direct incorporation, immersion in porous materials and shape stabilisation, micro-encapsulation, and macro-encapsulation [43,54–56]. *Figure 6* summarises the incorporation methods for PCMs. Incorporation methods are also useful for the formation of those PCM slurries in which a separation between PCM and carrier fluid is required (see Section 2.2.5).
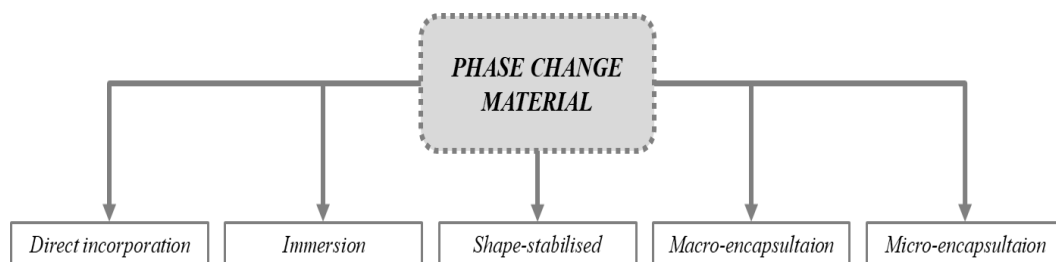
Figure 6. Incorporation methods for PCMs.

2.2.4.1 Direct incorporation and immersion

Direct incorporation and immersion methods are the most straightforward and cheapest methods to incorporate PCMs. Direct incorporation consists in directly mixing the liquid or powdered PCM into porous material matrices (e.g., gypsum, bricks, concrete or plaster in case of building applications) during their production. In the immersion method, the porous material matrices – in the form of final products (e.g., concrete blocks, gypsum boards) - are immersed in a high-temperature liquid PCM, which is absorbed by capillarity. Once the PCM cools down, it solidifies within the matrix pores and remains incorporated into the material. However, in the case of direct incorporation problems of leakage and degradation of the mechanical resistance of the porous material due to materials interaction may occur. Also in the case of immersion stability problems may arise due to PCM evaporation or material interactions.

2.2.4.2 Shape-stabilised Phase Change Materials

Shape-stabilised PCMs are compounds prepared by mixing melted PCM and support material (e.g., styrene-butadiene-styrene copolymer, density polyethylene, etc.). The solidified support material is characterised by a porous network that absorbs the liquid PCM avoiding leakage, and it provides structural rigidity, which is required to maintain the shape unchanged whether the PCM is in the liquid or solid state. The resulting mixture of shape-stabilised PCMs is a material with a homogeneous aspect. The percentage of PCM can be up to 80 %, so the amount of energy that can be stored is comparable to that of traditional PCMs. An exhaustive literature overview about shape-stabilised PCMs can be found in [57,58].

2.2.4.3 Macro-encapsulation

Macro-encapsulation is the process of packing PCMs in relatively big size containers, usually larger than 1 cm [59]. According to the type of application, these containers can have various shapes, such as panels, pouches, spheres or tubes. Containers should be designed appropriately to deal with possible volume expansions due to PCM density variation between solid and liquid state. The container should be optimised to enhance the heat transfer rate during the phase change processes. Coupling macro-encapsulated PCMs with materials characterised by high thermal conductivity values (e.g., water or metal matrices) allows enhancing the material storage capability through the attenuation of the PCM drawback related to its low thermal diffusivity. However, the thermal conductivity remains lower than micro-encapsulated solutions (see the following paragraph), and the thermal diffusivity of the PCM within the macro-capsule in the solid phase may remain poor. Eventually, macro-encapsulation can help to

overcome the flammability problems of some PCMs. PCM leakage due to perforation or capsule rupture should be avoided by a correct design of the capsules allowing the mechanical stress to be tolerated.

2.2.4.4 Micro-encapsulation

Micro-encapsulation is the process of packing solid particles or liquid droplets of a PCM by surrounding them with a coating of another substance (named *shell*). The central capsule part containing the micro-encapsulated PCM (referred as mPCM) is called capsule *core*.

The resulting microcapsules have a diameter that ranges approximately from 0.05 μm to 5000 μm. Micro-encapsulation can be obtained by means either of physical or chemical processes. Extensive literature reviews on the microencapsulation methods can be found in [60–62]. Micro-encapsulation processes were developed above all by pharmaceutical industries. Various micro-encapsulation methods are available, such as in-situ polymerisation and interfacial poly-condensation [63]. The purposes of micro-encapsulation are to protect PCMs from harmful interaction with the environment, to provide structural stability, and to make materials easier and/or safer to handle. Furthermore, the thermal diffusivity is enhanced by increasing the heat transfer surface and allowing the material to be easily mixed or included in matrices of other conductive materials (e.g., water or metal matrices), thus increasing the global thermal conductivity. In buildings, mPCM can also be used by mixing them with other traditional materials allowing the thermal capacity of the final mixture to be increased without the stability problems occurring in direct incorporation or immersion. The main disadvantages of mPCM are related to the microcapsules' shells. Firstly, the mass fraction of PCM - and hence the total heat storage capacity - is limited by the shell's thickness, which has to provide mechanical strength to avoid rupture of the capsules. Secondly, the shell materials (usually polymeric films or silica) are characterised by reduced thermal conductivity and severely affect the overall performance of the material.
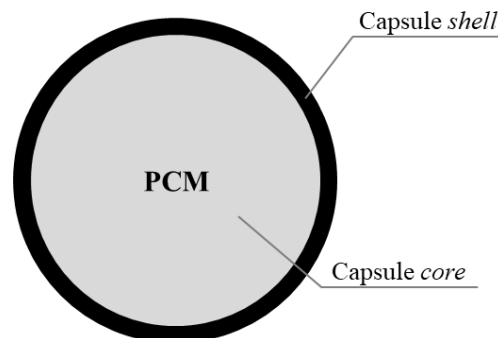
Figure 7. Overview of a micro-encapsulated PCM.

2.2.5 Phase Change Material slurries

In the last decade, a new technique of PCM usage has been proposed, tested, and adopted. It consists of forming a two-phase fluid, from the mixture of a carrier fluid and a dispersed PCM. Water (or water with antifreeze, such as glycol) is generally used as the carrier fluid. This choice is due to water high thermal conductivity, considerable specific heat, compatibility with PCMs, easiness in handles, cheapness and safety for the environment [64]. The resulting two-phase fluid is called PCM slurry. The main advantage of PCM slurries is to conserve the high thermal inertia of PCMs, combining it with higher thermal diffusivity, due to convection phenomena into the carrier fluid. Furthermore, phase segregation and subcooling phenomena are reduced. Thus the resulting two-phase fluid has features that match with the requirement of different applications and in particular the adoption in active systems, such as latent heat thermal energy storage system, heat exchangers and thermal control systems.

The following five types of PCM slurries were listed in the scientific literature [65] and summarised in *Figure 8*:

- *ice slurries*: in which ice particles are dispersed into a water carrier fluid;
- *PCM micro-emulsion*s: in which the PCM is dispersed in water through an emulsifying agent forming a homogenous mixture of PCM and carrier fluid;
- *mPCM slurries*: where mPCM capsules are dispersed into a carrier fluid (generally water);
- *clathrate hydrate PCM slurries*: where the clathrate hydrates are composed of water molecules (host molecule) forming a weaved structure where the molecules of the other substance (guest molecule) are accommodated;
- *shape-stabilised PCM slurries*: mixtures based on shape-stabilised PCM.
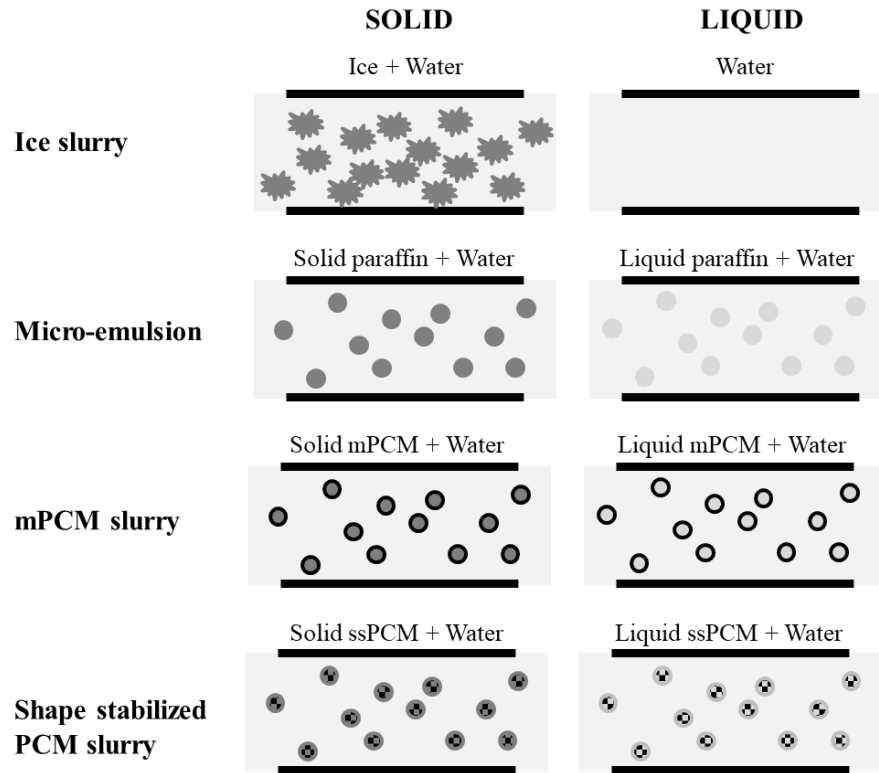
Figure 8. Schematic drawing of the different types of PCM slurries. This figure was adapted from [65].

Two-phase slurries have almost constant rheological properties, which are not concerned about the phase change occurrence. Therefore, PCM slurries always remain liquid, although with a high viscosity, and they can be pumped regardless of the state of the PCM component of the mixture. For this reason, PCM slurries can be used either as static thermal storage materials or pumped heat transfer fluids. Refs. [65] and [66] highlighted possible advantages offered by PCM slurries compared to similar solutions:

- high storage capability thanks to the latent heat exploitation;
- higher thermal diffusivity compared to traditional PCMs, due to the exploitation of the higher conductivity of the carrier fluid;
- possibility to use the same medium either to store energy and as heat transfer fluid, reducing in this way heat transfer losses due to heat exchanges temperature differences;
- when used as heat transfer fluid, possibility to realise processes at an approximately constant temperature and reduction of mass flow-rates due to higher heat capacity;
- high heat transfer rate due to the elevated ratio surface/volume.

Furthermore, the thermal energy storage capability is similar to the one of traditional pure PCM thanks to a commonly higher material density. Indeed, traditional PCMs in the solid state are characterised by high porosity in the container (a value that rises to 65 % in some instances [67]) that causes an

increase of the volume of the container per unit of energy stored. In the case of slurries, the porosity is filled by the carrier fluid that allows the global thermal energy storage density to be increased. Furthermore, conventional tanks designed for containing fluids can be easily adapted for PCM slurries [65].

The literature offers numerous extensive and comprehensive reviews regarding PCM slurries. These works cover all the various aspects concerning these materials from material preparation methods to the definition of thermal and rheological properties [64,65,68–70].

Since the present dissertation deals with the application of a mPCM slurry as the heat transfer fluid of a solar thermal system, a significant emphasis on mPCM slurries has been undertaken.

The advantages of using micro-encapsulated PCM (mPCM) slurries in the different thermal application were evident since the late '90s. The microencapsulation prevents the leakage of PCM in the liquid phase, and the slurry can be easily pumped, reducing clogging risk and pressure drops. Moreover, mPCM slurries have a higher surface to volume ratio than other PCM slurries, which maximises the heat exchanged. The market offers various mPCM solutions to prepare slurries characterised by different phase change transition temperature, which should be accurately selected accordingly with the application requirements. Formulations to describe mPCM slurry thermal, heat-exchange and rheological behaviour are available in the literature and are extensively discussed in the following parts of the thesis. The stability of mPCM slurry should be investigated from the thermal, structural and physical point of view. No particular drawbacks related to the thermal stability were pointed out for typical PCM slurry operating temperatures (some problems may arise at very high temperatures). Structural stability mainly concerns the potential rupture of the micro-capsules, which can be caused by mechanical shear forces. In case of mPCM used as heat transfer fluid the primary cause of shear forces is the pumping power. Different studies highlighted how the potential structural and mechanical drawbacks could be avoided employing the adoption of low-speed pumps (e.g., peristaltic or centrifugal pumps), as well as the adoption of small-sized mPCM or particles characterised by large shell thickness. Eventually, the physical stability strongly influences the overall heat transfer and thermal energy store properties. In case of mPCM slurry physical stability mainly concerns the possible stratification of the material (the creaming or sedimentation phenomena, which are caused by the density difference between the dispersed mPCM and carrier fluid). During the last few years, most of these problems have been studied extensively, and different solutions have been proposed to solve these drawbacks [71].

2.3 Applications of Phase Change Materials in buildings

The use of PCMs has rapidly been increasing in recent years in various building applications [72–75]. In general, PCMs are used to increase the thermal inertia of building components to reduce heating/cooling peak loads [76–78] or reducing temperature swings within the indoor environment. PCMs can be applied both as passive strategies when integrated within the building structure or envelope (e.g., either in the transparent or in the opaque components), and as active strategies, when integrated within the HVAC system. In HVAC systems the PCMs are used as a storage medium for renewable energy integration, including components of solar thermal systems. For passive application PCMs have been proven, by means of both experimental and numerical studies, to be beneficial especially in lightweight buildings.

In both cases, effective use of PCM in buildings requires an appropriate selection of PCMs thermo-physical properties, quantity and position according to the intended application and to the building location. Therefore, to guarantee the proper functioning of the PCM and ensure economic feasibility, optimisation of the PCM use can be advisable. In particular, the PCM should be accurately selected to have a melting temperature range that perfectly suits the requirements and the temperature ranges involved in the specific application. In this selection process, all the external disturbances affecting the building thermal behaviour (e.g., ambient temperature, solar radiation, wind velocity profiles, occupancy and endogenous heat load patterns, etc.) must be carefully taken into account. A broad melting temperature range could improve the adaptability of PCMs to the temperature variations, but the best achievable energy performance may be compromised. Under certain conditions, the adoption of two (or more than two) different PCMs with dissimilar phase change ranges may be favourable to improve the energy efficiency of buildings during the whole year (e.g., a PCM is activated during the cooling season and the other during the heating season) [79,80].

Peak load reduction strategies through PCMs are performed by the exploitation of the intrinsic high storage capabilities of the materials. This led to almost isothermal charging (fusion) and discharging (solidification) cycles. For instance, during summer periods, melting the PCM during daytime helps to avoid (or reduce) overheating risk [36]. Afterwards, the stored heat is realised during night time, when conditioning strategies are more efficient (e.g., free cooling or night ventilation). If the building location climate is suitable, this process can be performed utilising passive strategies only [81]. For winter applications, PCM integration in passive buildings was proposed especially within the floor. Therefore, the sunlit floor surface can store solar energy during the day and release it during the night [82,83].

Furthermore, peak load reductions can be related to the variation of energy prices during the time and the implementation of effective load shifting control strategies [51,84]. These are mainly interesting for cooling applications where the electricity is the primary energy vector, and it is price can vary sharply during the

time (e.g., real-time tariffs or demand response incentives or grids characterised by high penetration rates of renewable energy sources). According to the climate, the energy saving in peak loads may be more pronounced than the annual energy savings.

2.3.1 Phase Change Materials integration in building envelope components

PCM can be integrated in building envelope and structures both in opaque [50,56] and transparent components, as well as in shutters [85] or even in furniture [86].

2.3.1.1 Phase Change Materials in opaque components

PCMs can be incorporated into opaque components using macro-encapsulation (such as inside masonry blocks or sealed in thin polymeric pouches), or shape-stabilised panels. Moreover, PCM can be embedded through direct incorporation, immersion, or micro-encapsulation in traditional construction materials, such as plasters, gypsum boards, PCM-mortar bricks or concrete blocks. Since in most of these cases the PCMs are directly integrated into other building materials, the construction process does not significantly differ compared to traditional buildings [36].

Several experimental tests were carried out, gathering measurement both in laboratory and in-field, to investigate the effects of PCMs integration in the opaque envelope both at a component and whole building scale.

It was demonstrated that the integration of PCMs in roofs may have a positive effect in improving thermal comfort and reducing cooling loads (particularly when coupled with cool coatings) [79,87–89]. However, PCM roof applications have received less attention than wall and façade applications [36].

Generally, thin PCM layers showed higher PCM potentialities exploitation and cost benefits than thicker layers. The coupling of PCMs with ventilated façades was extensively examined by numerical and experimental studies [90,91]. Some authors also investigated the potential benefits achievable by the integration of PCMs to enhance the performance of thermal insulation components [92–94]. However, the most common integration of PCMs in buildings opaque envelope is achieved by the adoption of PCM to enhance wallboards or lightweight components properties (e.g., PCM-gypsum panels) [95]. Commonly the PCM layer is placed on the interior side of the building envelope [36]. The PCM activation in internal wallboards is strongly dependent on the convective heat transfer taking place with the indoor air, and natural convection heat exchanges are considered too low for effective exploitation of the PCMs potential. Possible solutions to enhance the convective heat transfer were investigated adopting

narrow cavities where ambient air can circulate [96]. Eventually, for passive cooling load reduction in tropical climates, PCMs were found to overperform when placed on the external surfaces of the façades [97,98].

It was found that the application of PCMs in the opaque envelope is particularly favourable in case of retrofitting buildings characterised by low thermal inertia [44]. In these cases, wallboards integrating PCM are often used, due to their low thickness and ease of installation. These PCM-based wallboards can either replace the existing interior finishing or can be placed over it [81].

2.3.1.2 Phase Change Materials in transparent components

As well as opaque building components, the PCMs can also be integrated into windows and glazing components [85]. In this approach, the interaction with the solar radiation represents the most critical driver of the energy storage/exchange process and the PCMs act both as a solar shading device and as a heat storage medium. The main scope of PCMs integration in glazing systems is the improvement of glazing system heat capacity, thus its thermal inertial behaviour. This fact leads to smooth the indoor surface temperature of the glazing system and provides peak load shifting at a component level. The simultaneous use of a thermotropic double glazing unit coupled with a PCM layer filled in the air gap showed over performing capabilities in managing the charging/discharging cycles of the PCM.

Several experimental [76,99–101] and numerical [102,103] studies investigated the performance of PCM-enhanced glazing components, and they were effectively resumed in the review paper [85]. Visual and optical properties play a fundamental role in the performance assessment of a transparent and translucent component. Nevertheless, PCM-filled glazing units badly influence the optical behaviour of such kind of system, being opaque when in solid state and translucent when in the liquid state.

2.3.2 Phase Change Materials integration in active thermal energy storage technologies

PCMs have been applied in buildings principally to enhance their thermal energy storage capabilities. As a consequence, they have found their most substantial diffusion in active thermal energy storage units coupled with the HVAC system. In the last decades, latent heat thermal energy storages have attracted considerable attention due to their proven effectiveness and superiority compared to other solutions [104]. In detail, PCM based storages compared to sensible heat storages allow higher stored energy densities to be pursued, reducing both storage volume and weight. Furthermore, they are less sophisticated and more cost-effective than alternative thermochemical solutions. Since PCM active

storage solutions have been in the spotlight for years, the scientific literature offers numerous review papers about this topic [33,38,54,58,59,105].

Applications of active latent heat thermal energy storage can be focused on the maximisation of renewable energy integration, the reduction of HVAC system peak loads and the integration of storage units to enhance free-cooling opportunities [51,104,106]. Previous works have covered many topics: from understanding the mathematical formulations that describe the behaviour of PCMs in the storage unit to assessing the actual influence of an active thermal energy storage unit on the entire building and HVAC system. Studies have been both theoretical (e.g., investigating the storage behaviour through simulations performed using computational fluid dynamic or simplified numerical models) and experimental.

To date, in market applications, the direct use of PCMs for energy storage has been still limited principally for the low thermal diffusivity of most PCMs, which requires additional efforts to charge/discharge the storage unit. This fact is particularly true when PCMs solidify on the heat transfer surface. To solve this issue, different solutions were proposed. On the one side, many studies investigated the development of optimised solutions for the storage tank. For example, PCMs were coupled with traditional storage systems by their insertion in dedicated units (e.g., PCM bricks, shell and tube, macro-encapsulated PCM). The improvement of PCM features with additives or surfactants was investigated, as well as the adoption of PCM slurries with higher thermal conductivity. Furthermore, particular heat exchangers were designed and optimised to enhance the heat transfer and heat diffusivity in the storage unit [107–109]. Particularly promising are the recent solutions that exploit the potentialities offered by additive manufacturing to perform topology optimisation [110].

2.3.3 Phase Change Materials integration with solar thermal systems

In the past few years, the use of PCMs has been tested in several different types of solar thermal systems. The presence of a PCM leads to an overall annual increase in the solar fraction, a higher efficiency of the system and significant storage heat capacity. In particular, three different methods have been proposed to incorporate PCMs into the systems: the integration of a PCM directly in a layer of the solar collectors, the addition of PCM nodes to the primary heat transfer fluid solar loop pipes and the addition of PCM elements to the inside of a storage tank [111]. A review of this topic has been published by Wang et al. [105].

In the first kind of proposed collectors – as shown in *Figure 9*(a) – the PCM is integrated directly into the panel as a layer with storage function. In the most common configuration, the PCM-integrated solar collector eliminates the need for conventional storage tanks, thus reducing costs and space. For example, in [112], the solar energy is stored in a salt-hydrate PCM layer held in the collector and is

discharged to cold water flowing through a surface heat exchanger located in an upper layer. A similar concept, which proposes a different kind of PCM and layer organisation to obtain better energy storage in the collector, has recently been introduced in [113,114]. A thermal solar system with PCM slurry storage integrated into the collector has also been studied in [115]. The storage-collector was filled with different concentrations of PCM with a 60 °C phase transition temperature. On the other hand, in [116], a PCM layer has been incorporated in a collector which combines photovoltaic electricity generation and solar thermal production. This solution is principally adopted to improve the inertia of the system and limit the temperature peaks and increase the photovoltaic efficiency without wasting energy [117].
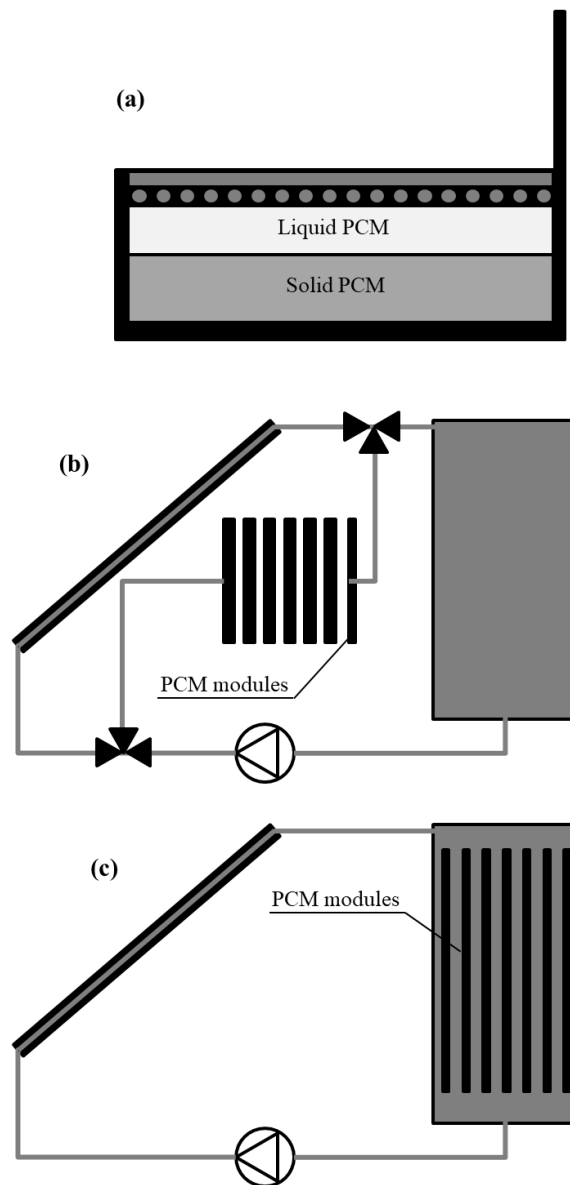
Figure 9. Examples of PCM integration into solar thermal systems. (a) PCM integrated into the storage tank. (b) PCM node between the collector and the storage tank. (c) PCM integrated into the solar thermal collector. This figure was adapted from [144].

A new system configuration – as shown in *Figure 9*(b) – has been proposed in references [107] and [118]. It has been called SDHW–PCM, and it includes a PCM node in the heat transfer fluid primary solar loop of the system. The node is combined with a traditional water storage tank, and it represents an additional storage unit. It is a compact heat exchanger made of four plates surrounded by storage composite material composed of compressed expanded graphite and paraffin. The authors showed that, compared to a traditional water-based solar thermal system, this configuration leads to increases in the solar fraction (i.e., the time during which the solar thermal system can be exploited to produce heat) in summer and winter of 8 % and 4 %, respectively.

The third kind of proposed solar thermal systems – as shown in *Figure 9*(c) – are those that use PCMs directly in the storage tank (see Section 2.3.2). A study on the enhancement of solar system performance using sodium thiosulfate pentahydrate as the PCM in the storage tank has been made by [119]. They found that the storage time was approximately 2.59 – 3.45 times greater than that of conventional water-heating systems. Experiments that involved the inclusion of a water tank and a PCM module in a complete solar water heating system have been conducted in [111] and [120]. In this case, the PCM was placed on several cylinders at the top of the water tank. Huang et al. have proposed a storage tank for solar water heating with a floor that houses capillary plates and a macro-packaged PCM layer [121]. Moreover, several studies can be found in literature about the introduction and heat transfer optimisation of PCM modules located inside a storage tank [122–125].

2.3.4 Application of Phase Change Material slurries in buildings and solar thermal applications

Most of the aforementioned solutions have only considered the improvement of a single static component of the solar thermal system. Indeed, these technologies used water or water-glycol as the heat transfer fluid in the primary loop of the solar collector. However, the heat transfer fluid plays a very significant role in a solar thermal system. It absorbs energy in the collector and transfers it to the storage tank and the end users' terminal units. If heat exchangers are used, this strategy implies fixed temperature differences between the heat transfer fluid flowing inside the solar collector loop and the PCM storage, as well as between the storage and the heat transfer fluid flowing to the terminal units. These heat exchanges introduce irreversibility and energy-losses. Moreover, in recent years, the thermal capacity of heat transfer fluid – that is the amount of heat transported by a unit of flow rate of heat transfer fluid – has also been considered a critical problem. Many thermal-energy systems have long piping sections to convey the heat transfer fluids from the source to the sink heat exchangers. In such conventional systems, thermal energy is transferred as the sensible heat of

the heat transfer fluid, and it is proportional to the difference between the source and the sink temperatures. If the temperature difference is small (as in the case of many renewable energy sources), the single-phase fluid must be pumped at high-volume flow rates. As a result, the system consumes a significant amount of pumping power.

During the '80s, the aforementioned problems led Kasza and Chen [126] to propose a system that directly uses Phase Change Material slurries as heat transfer fluids capable of exploiting the advantages offered by isothermal latent heat exchange. PCM slurries could be used for this purpose as an enhanced heat transfer fluid in the primary loop of solar collector systems. Nevertheless, during the '80s, some technological limitations arose, due to the possible solidification of the slurry in the pipes during its phase transition. Currently, due to the advancements in PCM slurry technologies, an alternative solution could be conceived.

In particular, mPCM slurries are those seems to be more promising for a broad application and market penetration. The advantages of using mPCM slurries in different thermal applications have been evident since the late '90s [127,128]. They showed reduced problems of clogging in the pipes and reduced production costs of the material [111,127].

Different experimental tests and models were carried out to investigate mPCM slurries behaviour and achievable advantages [64,65,68]. A mPCM slurry was used as turbo-chiller integrated storage to mitigate the decreased energy capacity due to refrigerant substitution in Narita Airport of Tokyo [129]. The mPCM slurries were also involved as heat transfer fluid in active building cooling system through chilled ceilings [130].

As previously discussed, the primary benefit of mPCM slurries is the increased heat transfer rate compared to traditional PCM technologies. Indeed, the mPCM slurry enhances the heat transfer capacity of the PCM and still retains the characteristic of high-energy storage density over a small temperature range. This led mPCM slurries to be considered suitable heat storage media in static storage technologies. The recent review paper [131] showed how the adoption of mPCM in thermal energy storages is a topic that has generated an increased interest in the last decade [132–135]. For instance, in [136,137] mPCM slurries were used as media for cold energy storages. In [115,138], a mPCM slurry thermal energy storage was coupled with a residential solar heating energy system.

A second significant benefit of mPCM slurries is the fact that they always guarantee the circulation of the mPCM slurry in pipes. Indeed, the two-phase fluid has almost constant rheological properties, and the phase-change only takes place inside the core of the microcapsules. A mPCM slurry always remains liquid, even though it has a high viscosity, and it can be pumped regardless of the state of aggregation of the microcapsule core. For this reason, the same mPCM slurry medium can be used to both transport and store energy, hence reducing the exergy and heat transfer losses due to the irreversibility of energy exchanges.

However, the use of mPCM slurries also involves some drawbacks. In the first instance - depending on the mPCM concentration in the mixture - the

viscosity of the mPCM slurry may be higher than that of water [139]. In particular, viscosity could become much higher than water for high concentration suspensions, and an increase in the pressure drops could occur [63]. Secondly, the mPCM slurry might not remain physically stable under certain conditions. For example, some creaming phenomena could occur if the material is not moved continuously (e.g., in the thermal energy storage tank) and the pipes could be affected by clogging problems [132,140]. Eventually, thermal cycles and mechanical stress, (e.g., shear solicitation due to circulating pumps) could eventually damage the micro-capsule shells, and the PCM could leak outside the micro-capsule.

This thesis – with the publication of its preliminary works in international scientific journals and conferences [144-148] - opens up a new research path in this field. Indeed, this work aims to investigate the advantages (as well as the disadvantages) achievable by the adoption of a mPCM slurry both as the heat transfer fluid and storage media in solar thermal systems installed for building applications. Up to now, the previous literature analysis has revealed a lack of extensive studies in this field. Fulfil this literature gap has been one of the primary goals of the present thesis. For this purpose, a mPCM slurry - a mixture of water and micro-encapsulated PCM – was investigated. The material is shown in *Figure 10(a)*. First of all, this thesis aimed at understanding the material properties to correctly design and build a full-scale prototype aiming at investigating the system performance. The prototype was named "Solar Heating with Phase Change Materials", with acronym "SolHe-PCM" and it is shown in *Figure 10(b)*.
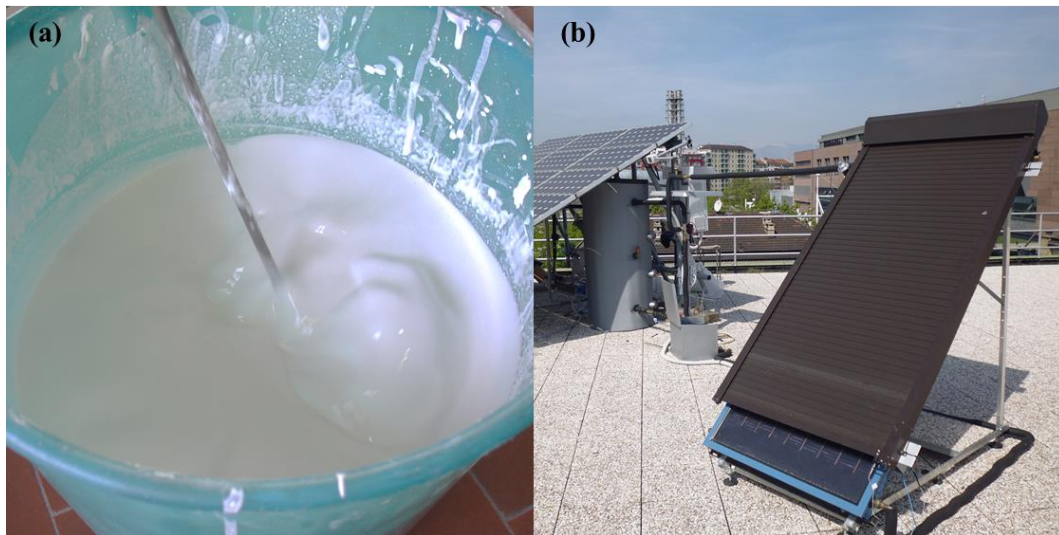
Figure 10. (a) Preparation of the n-eicosane mPCM slurry. (b) the solar thermal system (collector + thermal energy storage unit) named SolHe-PCM.

The work undertaken during the thesis can be somehow compared with the recent works of Qiu et al. [141,142] and Liu et al. [143]. Both these studies investigated the development of models and prototypes for combined photovoltaic and solar thermal (PV/T) system exploiting mPCM slurry as cooling fluid. On the one side, Qiu et al. investigations are divided into two papers: the first one

presented the theoretical concepts of a mPCM slurry based PV/T collector and a 1-D numerical model to describe its physical behaviour under different boundary conditions. The second paper described the experimental validation of the numerical model and the performance assessment of the proposed technology. From the author point of view, this numerical model was affected by several drawbacks (e.g., it is not clear to me how the Hottel-Willier model was adapted for considering the latent heat exchanges occurring in the mPCM slurry; many dimensionless parameters – such as the Nusselt coefficients – were referred to water as heat transfer fluid; etc.). Experimental evidence showed how the model always underestimated the performance of the PV/T system both regarding overall efficiency and useful heat produced, even for low mPCM concentrations. On the other side, Liu and al. developed a 2-D CFD simulation model to describe the behaviour of a PV/T collector exploiting mPCM slurry as heat transfer fluid. Simulation results showed an increase in the net efficiency of about 2 %. For the real implementation authors were concerned about the durability of the material and possible capsule leakages.

Despite these studies, the aim of obtaining more detailed knowledge and understanding of such a technology, required to develop numerical models and experimental prototypes of a solar thermal system based on mPCM slurry heat transfer fluid. All these aspects are extensively discussed in the next chapters of the present work.

2.4 Key-findings of the present chapter

The primary scope of the present chapter has been to provide to the reader a state-of-the-art review and summary of recent development in the solar thermal system and phase change material. From this survey has emerged that the two topics can be related. Indeed, the intermittency of the solar power source and the inefficiencies related to relatively high process temperature represent two of the main limitations to the solar thermal technology. The adoption of efficient thermal energy storage solutions and the reduction of process temperatures are required to handle these limitations and enhance the energy-saving opportunities. PCMs have demonstrated to be capable of dealing with both these aspects effectively. In the present chapter, firstly the primary characteristics and features of PCMs were introduced. Secondly, several applications of PCMs to buildings or buildings elements and systems were presented and discussed. PCM-based technologies proved to be effectively applied both to the building envelope and to the storage units of the HVAC systems. Afterwards, the chapter was focused on the integration of PCM solutions into solar thermal systems at a building scale. Generally, this is the case of the application of a PCM-based element for energy storage purposes either into the solar collector directly, into the primary heat transfer fluid loop or into the thermal energy storage unit. However, thanks to the recent advances in the material science a new configuration can be considered. Slurry PCMs are innovative heat transfer fluids that exploit the liquid to solid phase transition to enhance latent heat exchange processes without affecting the fluid rheological properties. The primary features of slurry PCM were analysed in this chapter. Afterwards, the section briefly presented a potential application of PCM slurries into a solar thermal system conceived to exploit the latent heat exchange directly within the heat transfer fluid. This system is studied in deep in the following chapters.

References

[1]   Duffie JA, Beckman WA. Solar Engineering of thermal processes. 4th Editio. New York, New York, USA: Wiley; 2013.

[2]   Weiss W, Spörk-Dür M, Mauthner F. Solar Heat Worldwide Global Market Development and Trends in 2016. SHC Rep 2017:86.

[3]   Verga V. Prospettive di sviluppo del solare termico: quali sfide al 2030? 2012;Available. www.assolterm.it.

[4]   Marcos JD, Izquierdo M, Parra D. Solar space heating and cooling for Spanish housing: Potential energy savings and emissions reduction. Sol Energy 2011;85:2622–41. doi:10.1016/j.solener.2011.08.006.

[5]   Fiorentini M, Cooper P, Ma Z. Development and optimization of an innovative HVAC system with integrated PVT and PCM thermal storage for a net-zero energy retrofitted house. Energy Build 2015;94:21–32. doi:10.1016/j.enbuild.2015.02.018.

[6]   Raffenel Y, Fabrizio E, Virgone J, Blanco E, Filippi M. Integrated solar heating systems: From initial sizing procedure to dynamic simulation. Sol Energy 2009;83:657–63. doi:10.1016/j.solener.2008.10.021.

[7]   Pinel P, Cruickshank C a., Beausoleil-Morrison I, Wills A. A review of available methods for seasonal storage of solar thermal energy in residential applications. Renew Sustain Energy Rev 2011;15:3341–59. doi:10.1016/j.rser.2011.04.013.

[8]   Guadalfajara M, Lozano M a., Serra LM. Simple calculation tool for central solar heating plants with seasonal storage. Sol Energy 2015;120:72–86. doi:10.1016/j.solener.2015.06.011.

[9]   Tao T, Zhang F, Zhang W, Wan P, Shen X, Li H. Low Cost and Marketable Operational Experiences for a Solar Heating System with Seasonal Thermal Energy Storage (SHSSTES) in Hebei (China). Energy Procedia 2015;70:267–74. doi:10.1016/j.egypro.2015.02.123.

[10]   Harrison J. The Effects Of Irradiance Level On Thermal Performance Tests Of Solar Collectors. Intersol Eighty FIve 1986:1269–73.

[11]   Hottel, Woertz. Performance of flat-plate solar-heat collectors. Trans ASME 1942;64:1942.

[12]   Shukla R, Sumathy K, Erickson P, Gong J. Recent advances in the solar water heating systems: A review. Renew Sustain Energy Rev 2013;19:173–90. doi:10.1016/j.rser.2012.10.048.

[13]   Baniassadi A, Momen M, Amidpour M, Pourali O. Modeling and design of solar heat integration in process industries with heat storage. J Clean Prod 2018;170:522–34. doi:10.1016/j.jclepro.2017.09.183.

[14]   Winterscheid C, Dalenbäck J-O, Holler S. Integration of solar thermal systems in existing district heating systems. Energy 2017;137:0–6. doi:10.1016/j.energy.2017.04.159.

[15]   Simonetti M, Gentile V, Fracastoro GV, Freni A, Calabrese L, Chiesa G. Experimental testing of the buoyant functioning of a coil coated with SAPO34 zeolite, designed for solar DEC (Desiccant Evaporative Cooling) systems of buildings with natural ventilation. Appl Therm Eng 2016;103:781–9. doi:10.1016/j.applthermaleng.2016.02.072.

[16]   Kalogirou SA. Solar thermal collectors and applications. vol. 30. 2004.

doi:10.1016/j.pecs.2004.02.001.

[17] Abdullah AH, Abou-Ziyan HZ, Ghoneim AA. Thermal performance of flat plate solar collector using various arrangements of compound honeycomb. Energy Convers Manag 2003;44:3093–112. doi:10.1016/S0196-8904(03)00013-X.

[18] Furbo S, Jivan Shah L. Thermal advantages for solar heating systems with a glass cover with antireflection surfaces. Sol Energy 2003;74:513–23. doi:10.1016/S0038-092X(03)00186-5.

[19] Akhtar N, Mullick SC. Computation of glass-cover temperatures and top heat loss coefficient of flat-plate solar collectors with double glazing. Energy 2007;32:1067–74. doi:10.1016/j.energy.2006.07.007.

[20] Wallner GM, Resch K, Hausner R. Property and performance requirements for thermotropic layers to prevent overheating in an all polymeric flat-plate collector. Sol Energy Mater Sol Cells 2008;92:614–20. doi:10.1016/j.solmat.2007.12.005.

[21] Hellstrom B, Adsten M, Nostell P, Karlsson B, Wackelgard E. The impact of optical and thermal properties on the performance of flat plate solar collectors. Renew Energy 2003;28:331–44. doi:10.1016/S0960-1481(02)00040-X.

[22] Tripanagnostopoulos Y, Souliotis M, Nousia T. Solar collectors with colored absorbers. Sol Energy 2000;68:343–56. doi:10.1016/S0038-092X(00)00031-1.

[23] Matrawy KK, Farkas I. Comparison study for three types of solar collectors for water heating. Energy Convers Mgmt 1997;38:861–9. doi:10.1016/S0196-8904(96)00089-1.

[24] Rommel M, Moock W. Collector efficiency factor F' for absorbers with rectangular fluid ducts contacting the entire surface. Sol Energy 1997;60:199–207. doi:10.1016/S0038-092X(97)00006-6.

[25] Alvarez A, Cabeza O, Muñiz MC, Varela LM. Experimental and numerical investigation of a flat-plate solar collector. Energy 2010;35:3707–16. doi:10.1016/j.energy.2010.05.016.

[26] Rittidech S, Wannapakne S. Experimental study of the performance of a solar collector by closed-end oscillating heat pipe (CEOHP). Appl Therm Eng 2007;27:1978–85. doi:10.1016/j.applthermaleng.2006.12.005.

[27] Maurer C, Cappel C, Kuhn TE. Progress in building-integrated solar thermal systems. Sol Energy 2017;154:158–86. doi:10.1016/j.solener.2017.05.065.

[28] Maurer C, Cappel C, Kuhn TE. Simple models for building-integrated solar thermal systems. Energy Build 2015;103:118–23. doi:10.1016/j.enbuild.2015.05.047.

[29] Soin RS, Sangameswar K, Rao DP, Rao KS. Performance of flate plane solar collector with fluid undergoing phase chance. Sol Energy 1979;23:69–73.

[30] Fanney AH, Terlizzi CP. Testing of refrigerant-charged solar domestic hot water systems. Sol Energy 1985;35:353–66.

[31] Charters WWS, Megler VR, Urma I, Aye L. Propane as working fluid in domestic heat pumps. Refrig. Clim. Control Energy Conversat., Melbourne: 1996, p. 11–4.

[32] White SD, Yarrall MG, Cleland DJ, Hedley RA. Modelling the performance of a transcritical CO_2 heat pump for high temperature heating ´ lisation de la performance d ' une pompe a ` chaleur au Mode ` haute CO

2 transcritique en application chauffage d ' eau a ´ rature tempe 2002;25:479–86.

[33] Mehling H, Cabeza LF. Heat and cold storage with PCM. Handbook. Springler; 2008.

[34] Huang M, Eames P, Hewitt N. The application of a validated numerical model to predict the energy conservation potential of using phase change materials in the fabric of a building. Sol Energy Mater Sol Cells 2006;90:1951–60. doi:10.1016/j.solmat.2006.02.002.

[35] Osterman E, Tyagi VV, Butala V, Rahim N a., Stritih U. Review of PCM based cooling technologies for buildings. Energy Build 2012;49:37–49. doi:10.1016/j.enbuild.2012.03.022.

[36] Kalnæs SE, Jelle BP. Phase change materials and products for building applications: A state-of-the-art review and future research opportunities. Energy Build 2015;94:150–76. doi:10.1016/j.enbuild.2015.02.023.

[37] Souayfane F, Fardoun F, Biwole PH. Phase change materials (PCM) for cooling applications in buildings: A review. Energy Build 2016;129:396–431. doi:10.1016/j.enbuild.2016.04.006.

[38] Tyagi VV, Buddhi D. PCM thermal storage in buildings: A state of art. Renew Sustain Energy Rev 2007;11:1146–66. doi:10.1016/j.rser.2005.10.002.

[39] ISO14040/44:2006, Environmental Management - Life Cycle Assessment, Standardization, International Organization for 2006.

[40] Menoufi K, Castell A, Farid MM, Boer D, Cabeza LF. Life Cycle Assessment of experimental cubicles including PCM manufactured from natural resources (esters): A theoretical study. Renew Energy 2013;51:398–403. doi:10.1016/j.renene.2012.10.010.

[41] De Gracia A, Rincón L, Castell A, Jiménez M, Boer D, Medrano M, et al. Life Cycle Assessment of the inclusion of phase change materials (PCM) in experimental buildings. Energy Build 2010;42:1517–23. doi:10.1016/j.enbuild.2010.03.022.

[42] Carbonaro C, Cascone Y, Fantucci S, Serra V, Perino M, Dutto M. Energy assessment of a PCM-embedded plaster: Embodied energy versus operational energy. Energy Procedia 2015;78:3210–5. doi:10.1016/j.egypro.2015.11.782.

[43] Soares N, Costa JJ, Gaspar a. R, Santos P. Review of passive PCM latent heat thermal energy storage systems towards buildings' energy efficiency. Energy Build 2013;59:82–103. doi:10.1016/j.enbuild.2012.12.042.

[44] Cascone Y, Capozzoli A, Perino M. Optimisation analysis of PCM-enhanced opaque building envelope components for the energy retrofitting of office buildings in Mediterranean climates. Appl Energy 2018;211:929–53. doi:10.1016/j.apenergy.2017.11.081.

[45] Sun X, Zhang Q, Medina MA, Lee KO. Energy and economic analysis of a building enclosure outfitted with a phase change material board (PCMB). Energy Convers Manag 2014;83:73–8. doi:10.1016/j.enconman.2014.03.035.

[46] Saffari M, De Gracia A, Ushak S, Cabeza LF. Economic impact of integrating PCM as passive system in buildings using Fanger comfort model. Energy Build 2016;112:159–72. doi:10.1016/j.enbuild.2015.12.006.

[47] Yantong L, Quan Z, Xiaoqin S, Yaxing D, Shuguang L. Optimization on Performance of the Latent Heat Storage Unit (LHSU) in Telecommunications Base Stations (TBSs) in China. Energy Procedia

2015;75:2119–24. doi:10.1016/j.egypro.2015.07.338.

[48] Lu S, Chen Y, Liu S, Kong X. Experimental research on a novel energy efficiency roof coupled with PCM and cool materials. Energy Build 2016;127:159–69. doi:10.1016/j.enbuild.2016.05.080.

[49] Lei J, Kumarasamy K, Zingre KT, Yang J, Wan MP, Yang EH. Cool colored coating and phase change materials as complementary cooling strategies for building cooling load reduction in tropics. Appl Energy 2017;190:57–63. doi:10.1016/j.apenergy.2016.12.114.

[50] Kuznik F, David D, Johannes K, Roux JJ. A review on phase change materials integrated in building walls. Renew Sustain Energy Rev 2011;15:379–91. doi:10.1016/j.rser.2010.08.019.

[51] Akeiber H, Nejat P, Majid MZA, Wahid MA, Jomehzadeh F, Zeynali Famileh I, et al. A review on phase change material (PCM) for sustainable passive cooling in building envelopes. Renew Sustain Energy Rev 2016;60:1470–97. doi:10.1016/j.rser.2016.03.036.

[52] Zalba B, Marín JM, Cabeza LF, Mehling H. Review on thermal energy storage with phase change : materials , heat transfer analysis and applications. Appl Therm Eng 2003;23:251–83.

[53] Yamagishi Y. Characteristics of Microencapsulated PCM Slurry as a Heat-Transfer Fluid. Al Chem Eng J 1999;45.

[54] Zhou D, Zhao CY, Tian Y. Review on thermal energy storage with phase change materials (PCMs) in building applications. Appl Energy 2012;92:593–605. doi:10.1016/j.apenergy.2011.08.025.

[55] Lecompte T, Le Bideau P, Glouannec P, Nortershauser D, Le Masson S. Mechanical and thermo-physical behaviour of concretes and mortars containing phase change material. Energy Build 2015;94:52–60. doi:10.1016/j.enbuild.2015.02.044.

[56] Memon SA. Phase change materials integrated in building walls: A state of the art review. Renew Sustain Energy Rev 2014;31:870–906. doi:10.1016/j.rser.2013.12.042.

[57] Zhang P, Xiao X, Ma ZW. A review of the composite phase change materials: Fabrication, characterization, mathematical modeling and application to performance enhancement. Appl Energy 2016;165:472–510. doi:10.1016/j.apenergy.2015.12.043.

[58] Kenisarin MM, Kenisarina KM. Form-stable phase change materials for thermal energy storage. Renew Sustain Energy Rev 2012;16:1999–2040. doi:10.1016/j.rser.2012.01.015.

[59] Cabeza LF, Castell a., Barreneche C, de Gracia a., Fernández a. I. Materials used as PCM in thermal energy storage in buildings: A review. Renew Sustain Energy Rev 2011;15:1675–95. doi:10.1016/j.rser.2010.11.018.

[60] Tyagi V V., Kaushik SC, Tyagi SK, Akiyama T. Development of phase change materials based microencapsulated technology for buildings: A review. Renew Sustain Energy Rev 2011;15:1373–91. doi:10.1016/j.rser.2010.10.006.

[61] Konuklu Y, Ostry M, Paksoy HO, Charvat P. Review on using microencapsulated phase change materials (PCM) in building applications. Energy Build 2015;106:134–55. doi:10.1016/j.enbuild.2015.07.019.

[62] Milián YE, Gutiérrez A, Grágeda M, Ushak S. A review on encapsulation techniques for inorganic phase change materials and the influence on their thermophysical properties. Renew Sustain Energy Rev 2017;73:983–99.

doi:10.1016/j.rser.2017.01.159.

[63] Youssef Z, Delahaye A, Huang L, Trinquet F, Fournaison L, Pollerberg C, et al. State of the art on phase change material slurries. Energy Convers Manag 2013;65:120–32. doi:10.1016/j.enconman.2012.07.004.

[64] Jurkowska M, Szczygiel I. Review on properties of microencapsulated phase change materials slurries (mPCMS). Appl Therm Eng 2016;98:365–73. doi:10.1016/j.applthermaleng.2015.12.051.

[65] Delgado M, Lázaro A, Mazo J, Zalba B. Review on phase change material emulsions and microencapsulated phase change material slurries: Materials, heat transfer studies and applications. Renew Sustain Energy Rev 2012;16:253–73. doi:10.1016/j.rser.2011.07.152.

[66] Royon L. Forced convection heat transfer with slurry of phase change material in circular ducts : A phenomenological approach. Energy Convers Manag 2008;49:928–32. doi:10.1016/j.enconman.2007.10.016.

[67] Chen S-L, Chen C-L, Tin C-C, Lee T-S, Ke M-C. An experimental investigation of cold storage in an encapsulated thermal storage tank. Exp Therm Fluid Sci 2000;23:133–44. doi:10.1016/S0894-1777(00)00045-5.

[68] Qiu Z, Ma X, Li P, Zhao X, Wright A. Micro-encapsulated phase change material (MPCM) slurries: Characterization and building applications. Renew Sustain Energy Rev 2017;77:246–62. doi:10.1016/j.rser.2017.04.001.

[69] Niedermaier S, Biedenbach M, Gschwander S. Characterisation and Enhancement of Phase Change Slurries. Energy Procedia 2016;99:64–71. doi:10.1016/j.egypro.2016.10.098.

[70] Zhang P, Ma ZW, Bai ZY, Ye J. Rheological and energy transport characteristics of a phase change material slurry. Energy 2016;106:63–72. doi:10.1016/j.energy.2016.03.025.

[71] Inaba H. New challenge in advanced thermal energy transportation using functionally thermal fluids. Int J Therm Sci 2000;729:991–1003.

[72] Nithyanandam K, Pitchumani R. Optimization of an encapsulated phase change material thermal energy storage system. Sol Energy 2014;107:770–88. doi:10.1016/j.solener.2014.06.011.

[73] Pomianowski M, Heiselberg P, Zhang Y. Review of thermal energy storage technologies based on PCM application in buildings. Energy Build 2013;67:56–69. doi:10.1016/j.enbuild.2013.08.006.

[74] Kasaeian A, bahrami L, Pourfayaz F, Khodabandeh E, Yan WM. Experimental studies on the applications of PCMs and nano-PCMs in buildings: A critical review. Energy Build 2017;154:96–112. doi:10.1016/j.enbuild.2017.08.037.

[75] Song M, Niu F, Mao N, Hu Y, Deng S. Review on building energy performance improvement using phase change materials. Energy Build 2018;158:776–93. doi:10.1016/j.enbuild.2017.10.066.

[76] Goia F, Perino M, Serra V. Experimental analysis of the energy performance of a full-scale PCM glazing prototype. Sol Energy 2014;100:217–33. doi:10.1016/j.solener.2013.12.002.

[77] Evola G, Marletta L, Sicurella F. A methodology for investigating the effectiveness of PCM wallboards for summer thermal comfort in buildings. Build Environ 2013;59:517–27. doi:10.1016/j.buildenv.2012.09.021.

[78] Favoino F, Goia F, Perino M, Serra V. Experimental assessment of the energy performance of an advanced responsive multifunctional façade module. Energy Build 2014;68:647–59. doi:10.1016/j.enbuild.2013.08.066.

[79] Pasupathy A, Velraj R. Effect of double layer phase change material in building roof for year round thermal management. Energy Build 2008;40:193–203. doi:10.1016/j.enbuild.2007.02.016.

[80] Buonomano A, De Luca G, Montanaro U, Palombo A. Innovative technologies for NZEBs: An energy and economic analysis tool and a case study of a non-residential building for the Mediterranean climate. Energy Build 2016;121:318–43. doi:10.1016/j.enbuild.2015.08.037.

[81] Rodriguez-Ubinas E, Arranz BA, Sánchez SV, González FJN. Influence of the use of PCM drywall and the fenestration in building retrofitting. Energy Build 2013;65:464–76. doi:10.1016/j.enbuild.2013.06.023.

[82] Xu X, Zhang Y, Lin K, Di H, Yang R. Modeling and simulation on the thermal performance of shape-stabilized phase change material floor used in passive solar buildings. Energy Build 2005;37:1084–91. doi:10.1016/j.enbuild.2004.12.016.

[83] Ye H, Long L, Zhang H, Zou R. The performance evaluation of shape-stabilized phase change materials in building applications using energy saving index. Appl Energy 2014;113:1118–26. doi:10.1016/j.apenergy.2013.08.067.

[84] Sun Y, Wang S, Xiao F, Gao D. Peak load shifting control using different cold thermal energy storage facilities in commercial buildings: A review. Energy Convers Manag 2013;71:101–14. doi:10.1016/j.enconman.2013.03.026.

[85] Silva T, Vicente R, Rodrigues F. Literature review on the use of phase change materials in glazing and shading solutions. Renew Sustain Energy Rev 2016;53:515–35. doi:10.1016/j.rser.2015.07.201.

[86] Johra H, Heiselberg P. Influence of internal thermal mass on the indoor thermal dynamics and integration of phase change materials in furniture for building energy storage : A review. Renew Sustain Energy Rev 2017;69:19–32. doi:10.1016/j.rser.2016.11.145.

[87] Alawadhi EM, Alqallaf HJ. Building roof with conical holes containing PCM to reduce the cooling load: Numerical study. Energy Convers Manag 2011;52:2958–64. doi:10.1016/j.enconman.2011.04.004.

[88] Li D, Zheng Y, Liu C, Wu G. Numerical analysis on thermal performance of roof contained PCM of a single residential building. Energy Convers Manag 2015;100:147–56. doi:10.1016/j.enconman.2015.05.014.

[89] Pasupathy A, Athanasius L, Velraj R, Seeniraj R V. Experimental investigation and numerical simulation analysis on the thermal performance of a building roof incorporating phase change material (PCM) for thermal management. Appl Therm Eng 2008;28:556–65. doi:10.1016/j.applthermaleng.2007.04.016.

[90] de Gracia A, Navarro L, Castell A, Cabeza LF. Energy performance of a ventilated double skin facade with PCM under different climates. Energy Build 2015;91:37–42. doi:10.1016/j.enbuild.2015.01.011.

[91] Diarce G, Campos-Celador Á, Martin K, Urresti A, García-Romero A, Sala JM. A comparative study of the CFD modeling of a ventilated active façade including phase change materials. Appl Energy 2014;126:307–17. doi:10.1016/j.apenergy.2014.03.080.

[92] Kośny J, Fallahi A, Shukla N, Kossecka E, Ahbari R. Thermal load mitigation and passive cooling in residential attics containing PCM-enhanced insulations. Sol Energy 2014;108:164–77. doi:10.1016/j.solener.2014.05.007.

[93]   Biswas K, Abhari R. Low-cost phase change material as an energy storage medium in building envelopes: Experimental and numerical analyses. Energy Convers Manag 2014;88:1020–31. doi:10.1016/j.enconman.2014.09.003.

[94]   El Omari K, Le Guer Y, Bruel P. Analysis of micro-dispersed PCM-composite boards behavior in a building's wall for different seasons. J Build Eng 2016;7:361–71. doi:10.1016/j.jobe.2016.07.013.

[95]   Zhou G, Zhang Y, Wang X, Lin K, Xiao W. An assessment of mixed type PCM-gypsum and shape-stabilized PCM plates in a building for passive solar heating. Sol Energy 2007;81:1351–60. doi:10.1016/j.solener.2007.01.014.

[96]   Evola G, Marletta L, Sicurella F. Simulation of a ventilated cavity to enhance the effectiveness of PCM wallboards for summer thermal comfort in buildings. Energy Build 2014;70:480–9. doi:10.1016/j.enbuild.2013.11.089.

[97]   Lei J, Yang J, Yang EH. Energy performance of building envelopes integrated with phase change materials for cooling load reduction in tropical Singapore. Appl Energy 2016;162:207–17. doi:10.1016/j.apenergy.2015.10.031.

[98]   Kuznik F, Virgone J, Johannes K. Development and validation of a new TRNSYS type for the simulation of external building walls containing PCM. Energy Build 2010;42:1004–9. doi:10.1016/j.enbuild.2010.01.012.

[99]   Gowreesunker BL, Stankovic SB, Tassou SA, Kyriacou PA. Experimental and numerical investigations of the optical and thermal aspects of a PCM-glazed unit. Energy Build 2013;61:239–49. doi:10.1016/j.enbuild.2013.02.032.

[100]   Bianco L, Cascone Y, Goia F, Perino M, Serra V. Responsive glazing systems: Characterisation methods, summer performance and implications on thermal comfort. Sol Energy 2017;158:819–36. doi:10.1016/j.solener.2017.09.050.

[101]   Bianco L, Cascone Y, Goia F, Perino M, Serra V. Responsive glazing systems: Characterisation methods, summer performance and implications on thermal comfort. Sol Energy 2017;158:819–36. doi:10.1016/j.solener.2017.09.050.

[102]   Goia F, Perino M, Haase M. A numerical model to evaluate the thermal behaviour of PCM glazing system configurations. Energy Build 2012;54:141–53. doi:10.1016/j.enbuild.2012.07.036.

[103]   Li D, Li Z, Zheng Y, Liu C, Hussein AK, Liu X. Thermal performance of a PCM-filled double-glazing unit with different thermophysical parameters of PCM. Sol Energy 2016;133:207–20. doi:10.1016/j.solener.2016.03.039.

[104]   Zeinelabdein R, Omer S, Gan G. Critical review of latent heat storage systems for free cooling in buildings. Renew Sustain Energy Rev 2017:0–1. doi:10.1016/j.rser.2017.10.046.

[105]   Wang Z, Qiu F, Yang W, Zhao X. Applications of solar water heating system with phase change material. Renew Sustain Energy Rev 2015;52:645–52. doi:10.1016/j.rser.2015.07.184.

[106]   Waqas A, Ud Din Z. Phase change material (PCM) storage for free cooling of buildings - A review. Renew Sustain Energy Rev 2013;18:607–25. doi:10.1016/j.rser.2012.10.034.

[107]   Haillot D, Franquet E, Gibout S, Bédécarrats J-P. Optimization of solar DHW system including PCM media. Appl Energy 2013;109:470–5.

doi:10.1016/j.apenergy.2012.09.062.

[108] Padovan R, Manzan M. Genetic optimization of a PCM enhanced storage tank for Solar Domestic Hot Water Systems. Sol Energy 2014;103:563–73. doi:10.1016/j.solener.2013.12.034.

[109] Xiao W, Wang X, Zhang Y. Analytical optimization of interior PCM for energy storage in a lightweight passive solar room. Appl Energy 2009;86:2013–8. doi:10.1016/j.apenergy.2008.12.011.

[110] Pizzolato A, Sharma A, Maute K, Sciacovelli A, Verda V. Design of effective fins for fast PCM melting and solidification in shell-and-tube latent heat thermal energy storage through topology optimization. Appl Energy 2017;208:210–27. doi:10.1016/j.apenergy.2017.10.050.

[111] Kousksou T, Bruel P, Cherreau G, Leoussoff V, El Rhafiki T. PCM storage for solar DHW: From an unfulfilled promise to a real benefit. Sol Energy 2011;85:2033–40. doi:10.1016/j.solener.2011.05.012.

[112] Rabin Y, Bar-Niv I, Korin E, B. M. Integrated solar collector storage system based on a salt hydrate phase-change material. Sol Energy 1995;55:435–44.

[113] Mettawee E, Assassa G. Experimental study of a compact PCM solar collector. Energy 2006;31:2958–68. doi:10.1016/j.energy.2005.11.019.

[114] Sharma A, Chen CR. Solar Water Heating System with Phase Change Materials. Int Rev Chem Eng 2009;1:297–307.

[115] Eames PC, Griffiths PW. Thermal behaviour of integrated solar collector/storage unit with 65°C phase change material. Energy Convers Manag 2006;47:3611–8. doi:10.1016/j.enconman.2006.02.029.

[116] Malvi CS, Dixon-Hardy DW, Crook R. Energy balance model of combined photovoltaic solar-thermal system incorporating phase change material. Sol Energy 2011;85:1440–6. doi:10.1016/j.solener.2011.03.027.

[117] Ciulla G, Brano V Lo, Cellura M, Franzitta V, Milone D. A Finite Difference Model of a PV-PCM System. Energy Procedia 2012;30:198–206. doi:10.1016/j.egypro.2012.11.024.

[118] Haillot D, Goetz V, Py X, Benabdelkarim M. High performance storage composite for the enhancement of solar domestic hot water systems. Sol Energy 2011;85:1021–7. doi:10.1016/j.solener.2011.02.016.

[119] Canbazoğlu S, Şahinaslan A, Ekmekyapar A, Aksoy ÝG, Akarsu F. Enhancement of solar thermal energy storage performance using sodium thiosulfate pentahydrate of a conventional solar water-heating system. Energy Build 2005;37:235–42. doi:10.1016/j.enbuild.2004.06.016.

[120] Cabeza LF, Ibáñez M, Solé C, Roca J, Nogués M. Experimentation with a water tank including a PCM module. Sol Energy Mater Sol Cells 2006;90:1273–82. doi:10.1016/j.solmat.2005.08.002.

[121] Huang K, Feng G, Zhang J. Experimental and numerical study on phase change material floor in solar water heating system with a new design. Sol Energy 2014;105:126–38. doi:10.1016/j.solener.2014.03.009.

[122] Sharma A, Tyagi VV, Chen CR, Buddhi D. Review on thermal energy storage with phase change materials and applications. Renew Sustain Energy Rev 2009;13:318–45. doi:10.1016/j.rser.2007.10.005.

[123] Li Z, Wu Z-G. Analysis of HTFs, PCMs and fins effects on the thermal performance of shell–tube thermal energy storage units. Sol Energy 2015;122:382–95. doi:10.1016/j.solener.2015.09.019.

[124] Padovan R, Manzan M. Genetic optimization of a PCM enhanced storage tank for Solar Domestic Hot Water Systems. Sol Energy 2014.

doi:10.1016/j.solener.2013.12.034.

[125] Khalifa AJN, Suffer KH, Mahmoud MS. A storage domestic solar hot water system with a back layer of phase change material. Exp Therm Fluid Sci 2013;44:174–81. doi:10.1016/j.expthermflusci.2012.05.017.

[126] Kasza KE, Chen MM. Improvement of the performance of solar enery or waste heat utilization system by using a phase-change slurry as an enhanced heat-transfer storage fluid. J Sol Energy Eng 1985;August:229–36.

[127] Yamagishi Y, Takeuchi H, Pyatenko AT, Kayukawa N. Characteristics of microencapsulated PCM slurry as a heat-transfer fluid. AIChE J 1999;45:696–707. doi:10.1002/aic.690450405.

[128] Royon L, P. P, G. G, S. F. Physical properties and thermorheological behaviour of a dispersion having cold latent heat-storage material. Energy Convers Manag 1998;39:1529–35.

[129] Shibutani S. PCM-micro Capsule Slurry Thermal Storage System for Cooling in Narita Airport. 3rd Work. IEA ECES IA Annex, 2002, p. 2002.

[130] Griffiths PW, Eames PC. Performance of chilled ceiling panels using phase change material slurries as the heat transport medium. Appl Therm Eng 2007;27:1756–60. doi:10.1016/j.applthermaleng.2006.07.009.

[131] Giro-Paloma J, Martínez M, Cabeza LF, Fernández AI. Types, methods, techniques, and applications for microencapsulated phase change materials (MPCM): A review. Renew Sustain Energy Rev 2016;53:1059–75. doi:10.1016/j.rser.2015.09.040.

[132] Delgado M, Lázaro A, Mazo J, Marín JM, Zalba B. Experimental analysis of a microencapsulated PCM slurry as thermal storage system and as heat transfer fluid in laminar flow. Appl Therm Eng 2012;36:370–7. doi:10.1016/j.applthermaleng.2011.10.050.

[133] Siao YH, Yan WM, Lai CM. Transient characteristics of thermal energy storage in an enclosure packed with MEPCM particles. Appl Therm Eng 2014;88:47–53. doi:10.1016/j.applthermaleng.2014.11.059.

[134] Zhang S, Niu J. Two performance indices of TES apparatus: Comparison of MPCM slurry vs. stratified water storage tank. Energy Build 2016;127:512–20. doi:10.1016/j.enbuild.2016.05.085.

[135] Liu L, Alva G, Jia Y, Huang X, Fang G. Dynamic thermal characteristics analysis of microencapsulated phase change suspensions flowing through rectangular mini-channels for thermal energy storage. Energy Build 2017;134:37–51. doi:10.1016/j.enbuild.2016.11.021.

[136] Zhang S, Niu J. Experimental investigation of effects of supercooling on microencapsulated phase-change material (MPCM) slurry thermal storage capacities. Sol Energy Mater Sol Cells 2010;94:1038–48. doi:10.1016/j.solmat.2010.02.022.

[137] Wang X, Niu J. Performance of cooled-ceiling operating with MPCM slurry. Energy Convers Manag 2009;50:583–91. doi:10.1016/j.enconman.2008.10.021.

[138] Huang MJ, Eames PC, McCormack S, Griffiths P, Hewitt NJ. Microencapsulated phase change slurries for thermal energy storage in a residential solar energy system. Renew Energy 2011;36:2932–9. doi:10.1016/j.renene.2011.04.004.

[139] Chen Z, Fang G. Preparation and heat transfer characteristics of microencapsulated phase change material slurry: A review. Renew Sustain Energy Rev 2011;15:4624–32. doi:10.1016/j.rser.2011.07.090.

[140] Delgado M, Lázaro A, Peñalosa C, Mazo J, Zalba B. Analysis of the physical stability of PCM slurries. Int J Refrig 2013;36:1648–56. doi:10.1016/j.ijrefrig.2013.04.020.

[141] Qiu Z, Ma X, Zhao X, Li P, Ali S. Experimental investigation of the energy performance of a novel Micro-encapsulated Phase Change Material (MPCM) slurry based PV/T system. Appl Energy 2016;165:260–71. doi:10.1016/j.apenergy.2015.11.053.

[142] Qiu Z, Zhao X, Li P, Zhang X, Ali S, Tan J. Theoretical investigation of the energy performance of a novel MPCM (Microencapsulated Phase Change Material) slurry based PV/T module. Energy 2015;87:686–98. doi:10.1016/j.energy.2015.05.040.

[143] Liu L, Jia Y, Lin Y, Alva G, Fang G. Performance evaluation of a novel solar photovoltaic–thermal collector with dual channel using microencapsulated phase change slurry as cooling fluid. Energy Convers Manag 2017;145:30–40. doi:10.1016/j.enconman.2017.04.089.

[144] Serale G, Fabrizio E, Perino M. Design of a low-temperature solar heating system based on a slurry Phase Change Material (PCS). Energy Build 2015;106:44–58. doi:10.1016/j.enbuild.2015.06.063.

[145] Serale G, Goia F, Perino M. Numerical model and simulation of a solar thermal collector with slurry Phase Change Material (PCM) as the heat transfer fluid. Sol Energy 2016;134:429–44. doi:10.1016/j.solener.2016.04.030.

[146] Buttitta G, Serale G, Cascone Y. Enthalpy-temperature evaluation of slurry phase change materials with T-history method. Energy Procedia, vol. 78, 2015. doi:10.1016/j.egypro.2015.11.352.

[147] Fan X, Serale G, Capozzoli A, Perino M. Experimental measurement and numerical modeling of the creaming of mPCM slurry. Energy Procedia, vol. 78, 2015. doi:10.1016/j.egypro.2015.11.192.

[148] Serale G, Cascone Y, Capozzoli A, Fabrizio E, Perino M. Potentialities of a low temperature solar heating system based on slurry phase change materials (PCS). Energy Procedia, vol. *62*, 2015:355-363. doi:10.1016/j.egypro.2014.12.397.

Chapter 3

Solar heating with Phase Change Material slurry as the primary heat transfer fluid and energy storage media (the Sol-He PCM project): materials, prototype and numerical models

The primary goal of this part is describing the steps undertaken in the development of a solar thermal system that adopts PCM slurry as heat transfer fluid and storage media.

Section 3.1 identifies the primary goals of this technology and the concepts that are at the basis of its conceiving and design.

Section 3.2 firstly defines the PCM slurry requirements in terms of physical, rheological and thermal features. The end of this part coincided with the selection of the PCM slurry considered most suitable for the specific needs of a solar thermal system Secondly it reports an experimental and parametrical investigation of the actual properties of the PCM slurry chosen for the specific application. On the one hand, the results of this part were necessary to design the full-scale prototype described in Section 3.3 properly. On the other hand, the material features herewith measured and estimated allowed the numerical models developed in Section 3.4 to be tailored to in the particular technology.

Section 3.3 pinpoints the steps that were necessary design and construction of a full-scale prototype for the technology. It describes in detail not only the primary features of each system element but also the regulation logic adopted within the embedded controller of the innovative solar technology.

Eventually, Section 3.4 reports the development of a mathematical model capable of describing the physical behaviour of a flat-plate solar thermal collector and a thermal energy storage unit capable of exploiting latent heat exchanges.

The results of experimental investigations concerning the PCM slurry properties are presented within the present Chapter 3. While the following Chapter 4 describes the data gathered during the experimental tests carried out on the full-scale prototype and the simulation results obtained through the numerical models herewith described.

Some portions of the present Chapter were already published in the following scientific papers:

- Design of a low-temperature solar heating system based on a slurry Phase Change Material (PCS). Authors: G Serale, E Fabrizio, M Perino. Journal: Energy and Buildings 106, 44-58 [1];
- Numerical model and simulation of a solar thermal collector with slurry Phase Change Material (PCM) as the heat transfer fluid. Authors: G Serale, F Goia, M Perino. Journal: Solar Energy 134, 429-444 [2];
- Enthalpy-temperature evaluation of slurry phase change materials with T-history method. Authors: G Buttitta, G Serale, Y Cascone. Journal: Energy Procedia 78, 1877-1882 [3];
- Experimental measurement and numerical modeling of the creaming of mPCM slurry. Authors: X Fan, G Serale, A Capozzoli, M Perino. Journal: Energy Procedia 78, 2010-2015 [4];
- Potentialities of a Low Temperature Solar Heating System Based on Slurry Phase Change Materials (PCS). Authors: G Serale, Y Cascone, A Capozzoli, E Fabrizio, M Perino. Journal: Energy Procedia 62, 355-263 [34].

3.1 The concepts behind the SolHe-PCM project

The previous review of the scientific literature has revealed a lack of evidence concerning the advantages (and disadvantages) of the exploitation of solid-to-liquid latent heat transition in direct combination with solar collectors for any application, and in particular for building-related applications. Therefore, a dedicated investigation has been set up, and it is currently ongoing, with the aim of obtaining more detailed information and understanding of such a technology. The research activity has been developed along various paths, ranging from the conception and design of a novel solar thermal system to the construction of a full-scale prototype; from the theoretical and experimental investigation of PCM slurry properties to the development of mathematical numerical models capable of describing the thermos-physical behaviour of such a technology.

A new system solution, based on PCM slurry, has been conceived, designed and prototyped to overcome the drawbacks of traditional solar thermal systems. The basic idea was to create a system that would be able to directly use a mPCM slurry as a heat carrier fluid and as an energy storage medium. The use of the mPCM slurry as the heat transfer fluid, instead of traditional aqueous solutions, makes it possible to exploit the effect of latent heat, to improve the flexibility of the solar thermal system, and to thus increase the efficiency of solar collectors and energy storage systems. Compared to other PCM-based solutions that are already available on the market the proposed configuration would in principle allow greater flexibility, in relation to variations in the boundary conditions or energy demand profiles. Furthermore, it would allow the heat transfer inefficiencies between the various components to be limited (thus improving the overall energy efficiency of the system). This system enables to optimise the heat transfer as well as similar systems that exploit latent heat exchanges (e.g., solar assisted heat pumps or heat pipe collectors). Moreover, compared to solutions that operate the liquid to vapour phase change, the proposed solution allows energy to be stored effectively without a fixed temperature difference.

In the proposed solution, the mPCM slurry has the characteristic of being able to remain in motion, regardless of the state of the PCM (solid/liquid). This feature makes it possible to store thermal energy directly in the fluid and, therefore, to utilise the entire mass of the fluid in the pipes and not only in the thermal energy storage tank. The proposed technology, compared to the existing solutions on the market, differs as far as the following aspects are concerned:

- it offers the ability to operate at low thermal levels with satisfactory efficiencies (thus improving the manufacturability of the panels);
- it results in a reduction in heat losses due to transmission toward the ambient, thanks to the lower temperature differences;
- it offers the possibility of using analogous or very similar components to those of traditional water systems;
- it provides the opportunity for relatively small costs of the fluids (in comparison to other methods) and easy maintainability;

- it offers the possibility of adapting the system for summer cooling.

The investigated system has been named "Solar Heating with Phase Change Material" and identified with the acronym SolHe-PCM. It was developed in the framework defined by the International Energy Agency's Energy in Buildings and Communities (IEA-EBC) Annex 59 "High-temperature cooling and low-temperature heating in buildings" [5]. The system has been conceived to cope with relatively low-temperature radiative systems in buildings that deliver energy for space heating purposes (e.g., radiant panels, Thermal Activated Building Structures).

In general, two possible system configurations can be adopted for the technology SolHe-PCM. The first one, which is represented in *Figure 1*(a), consists of a two open-loop circuit filled with PCM slurry. In this case, both the primary solar loop and the space heating secondary loop use PCM slurry as the heat transfer fluid. The complete absence of fixed temperature differences between the two circuits guarantees the maximum theoretical thermal efficiency from an exergetic point of view. The main drawback of this configuration concerns the difficulties that arise, from a technological point of view. The PCM slurry is the heat transfer fluid which has different rheological properties from water, and it requires particular attention during pumping, especially at the users' side.
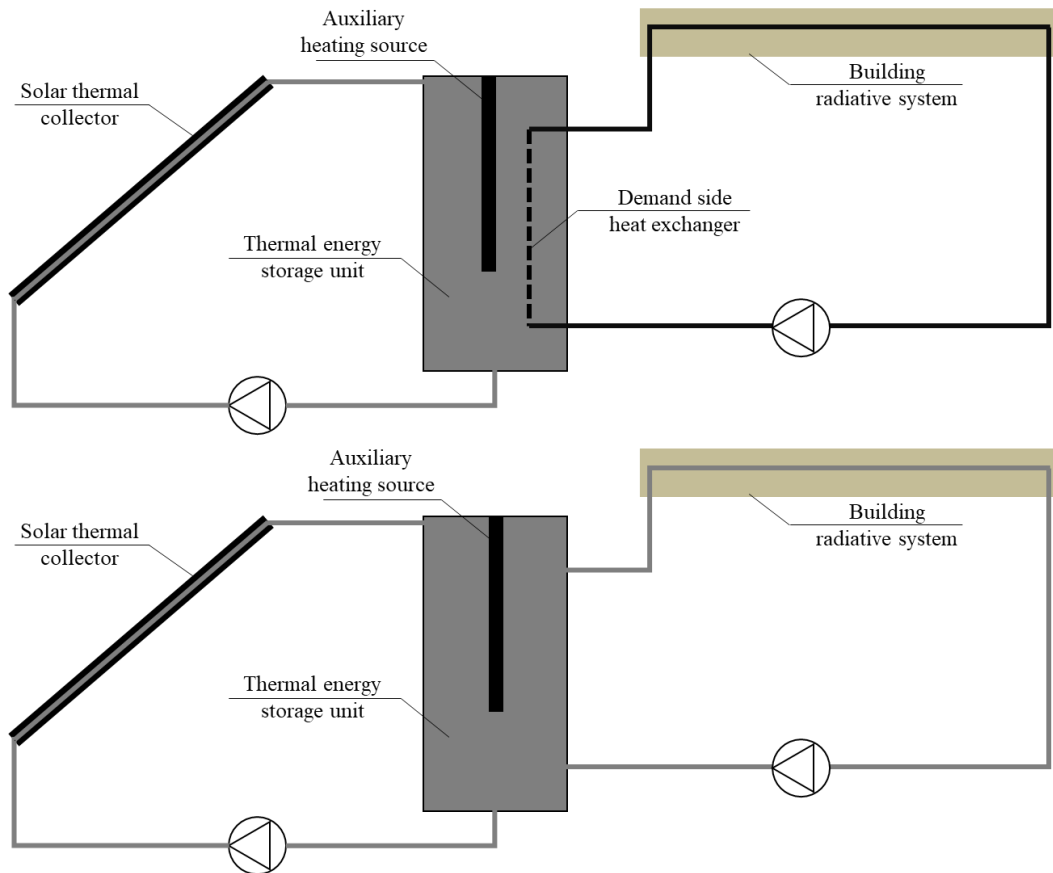
Figure 1. Schematics of the possible configurations of the SolHe-PCM technology: (a) two open-loop circuit filled with PCM slurry. (b) an open-loop circuit filled with PCM slurry and a closed-loop circuit filled with water.

The system described in *Figure 1*(b) solves some of these problems by reducing the length of the pipes in which the mPCM slurry flows. It consists of a primary solar loop filled with a mPCM slurry, coupled with a closed heating system secondary loop filled with water. As in the previous solution, the storage tank contains a mPCM slurry, and it allows large amounts of energy to be stored. However, the temperature difference between the storage tank and secondary water loop leads to a slight reduction in efficiency. On the other hand, this system guarantees easier technological implementation, and it allows a better evaluation of the behaviour of the solar system filled by mPCM slurry only. For these reasons, the solution outlined in *Figure 1*(b) was adopted by the authors as the most suitable to set up a full-scale prototype to preliminary test the technology.

Further system configurations can be conceived starting from these two preliminary solutions. For instance, it is possible to employ two different typologies of PCM slurries in the different loops served by the same energy storage unit. In this case, the transition temperature ranges for the two PCMs employed can differ. This fact allows the PCM transition temperature to be suitably selected according to the specific requirements of the heat exchange application (e.g., slightly higher in the primary collector loop, while slightly lower in the building supply loops). Nevertheless, for a sake of conciseness, the investigation of these additional configurations has been left to future studies, and the present thesis has been focused on the schematic outlined in *Figure1(b)*.

3.2 Features of the Phase Change Material slurry

A PCM slurry is a mixture of a carrier fluid and a dispersed PCM material. The PCM slurry can be used both the as heat transfer fluid in the primary loop of the solar circuit and as the storage media in the thermal energy storage unit. Some essential features are required to be suitable for the specific SolHe-PCM solar thermal application. Some of these requirements interest every fluid used as heat transfer fluid or storage media (e.g., high specific heat capacity, high thermal diffusivity, adoption of non-toxic and non-flammable materials, avoidance of fluid freezing, chemical compatibility with the container and pipes, etc.). Other features are more specific to a PCM slurry used as heat transfer fluid. The latter are those most influenced the selection of the particular PCM used in the slurry when the system was conceived and designed.

3.2.1 Requirements of the phase change transition range

The phase change transition should occur in a temperature range suitable for the specific application. In order to select the most appropriate transition interval, it was necessary to consider that the PCM slurry had to satisfy three primary goals:

- Convert solar energy into useful thermal energy;
- Store thermal energy in the thermal energy storage unit;
- Deliver thermal energy to the secondary heat exchanger serving the building space heating system.

When traditional fluids are used the sensible heat only is exploited. Therefore, the specific heat capacity and the fluid density are the main features to be considered dealing with the heat transfer fluid used this process. Instead, when PCM slurries are adopted most of the heat exchanges involve the latent heat, so the phase transition becomes the key-point in the fluid selection. Phase transition must occur in a temperature range that is suitable and advantageous for the specific SolHe-PCM application.

In general, for the First law of thermodynamics, the lower the heat transfer fluid temperature, the higher the energy amount that can be extracted by the system, and therefore its efficiency [6]. Since the phase transition temperature influences the overall temperatures involved in the process, the lower the phase change occurs, the higher the performance of the system. Nevertheless, when exergy issues are considered, temperature ranges higher enough to ensure all the heat transfer processes are required. This fact introduces some limitations to the minimum phase transition temperature allowable in the process. Indeed, to deliver thermal energy to the building, the temperature of the storage media must be higher than the supply temperature of the heat transfer fluid used in the secondary space heating circuit. In detail, if the Sol-He PCM system would be coupled with a low-temperature

radiative system (e.g., radiant panels or Thermally Activated Building Structures) the minimum supply temperature of the secondary circuit can be considered around 33 – 34 °C. Considering additional 2 °C of temperature difference due to heat exchange inefficiency, the minimum allowable phase transition temperature is in the range 35 – 36 °C. For this reason, the n-eicosane paraffin – whose nominal transition temperature of the pure material is indicated by the scientific literature equal to 37 °C – was chosen as the most suitable material for this purpose. *Figure 2* shows a schematic of the temperatures involved in the process of heat exchange in the secondary loop that delivers useful heat to the building.
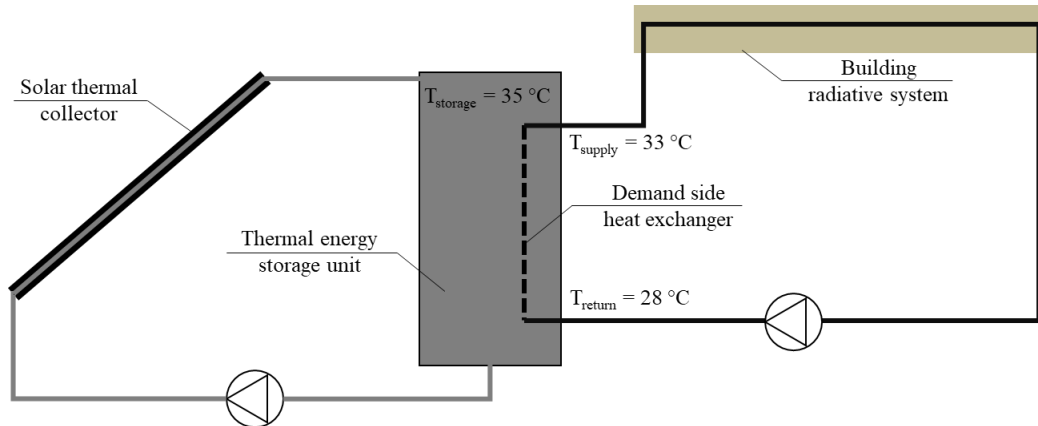
Figure 2. Schematic of the temperatures involved in the process.

3.2.2 Fluid rheological requirements

The PCM slurry had to be selected considering that it should ensure constant rheological properties, avoidance of pipes clogging and pump rupture. The PCM slurry has to be used either as the thermal storage media and as the heat transfer fluid in the primary loop of the solar thermal collector. In general, PCM slurries have almost constant rheological properties, which are not concerned about the phase change occurrence. Therefore, PCM slurries always remain liquid, although with a high viscosity, and they can be pumped regardless of the state of the PCM component of the mixture.
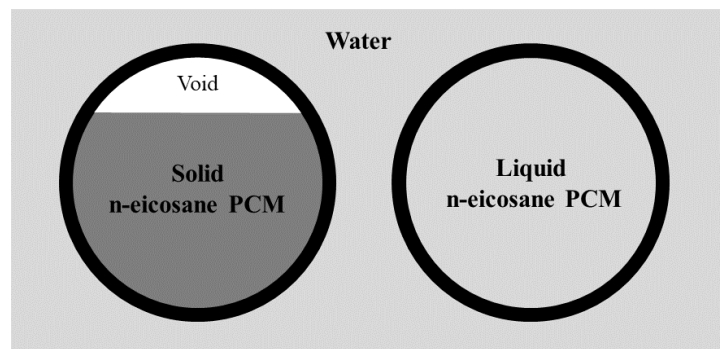
Figure 3. The phase transition occurs inside the capsule core, not affecting the whole fluid mixture rheological properties.

The mPCM slurries, based on micro-encapsulated PCM, were considered the most suitable solution for ensuring this property. Indeed, the micro-capsule *shell* represents a physical barrier that separates the capsule *core* – where the phase transition occurs – from the carrier fluid, which is in charge of ensuring fluid rheological properties (see *Figure 3*). Moreover, the micro-encapsulation prevents the leakage of PCM in the liquid phase, and the slurry can be easily pumped, reducing clogging risk and pressure drops. For this reason, the micro-encapsulation form of the n-eicosane paraffin was chosen as the mPCM dispersed in the slurry mixture.

3.2.3 Properties of the micro-encapsulated Phase Change Material slurry based on n-eicosane paraffin

As a consequence, the mPCM slurry used in the SolHe-PCM solar thermal application is a mixture of two components:

- A *carrier fluid*, which ensures the ability of the liquid to be pumped, enhances the thermal diffusivity and has antifreeze properties. A solution of water and glycol was selected for this purpose;
- A *dispersed mPCM*: which ensures latent heat exchanges without compromising the rheological properties of the whole mixture. A micro-encapsulated n-eicosane PCM was chosen for this purpose.

The overall mPCM slurry properties (e.g., thermal, rheological and physical stability properties) are a function of:

- The features of the carrier fluid;
- The features of the dispersed mPCM;
- The ratio of the dispersed material to the carrier fluid, generally referred as the concentration of mPCM capsules in the mixture. In general, this concentration is evaluated in weight total (w.t.).

Technical datasheets retrieved from material producers and data available from the scientific literature can provide information about the features of each pure material. Furthermore, the previous list highlighted how the overall properties of the mPCM slurry are also functions of the relative concentrations of its components. Indeed, the concentration of dispersed material influences both the thermophysical and rheological properties of the mPCM slurry. The latter shows highly non-linear dependence on the concentration. On the one hand, a high concentration of mPCM improves the heat storage capabilities of the mPCM slurry. On the other hand, it also increases the viscosity of the fluid, thus the pumping energy demand. A compromise between these two characteristics should be reached. This compromise is a tricky trade-off, since improving one feature may deteriorate the other one.

However, it must be taken into account that a higher thermal storage capacity also implies a lower flow rate and hence a reduction in the electric energy demand from the pump [7]. Once the optimised concentration has been chosen, the properties of the whole suspension can be or experimentally evaluated or calculated using formulations available in the scientific literature [8,9]. In this thesis, both the experimental approach and the theoretical approach were undertaken. The properties that mostly influence the solar thermal system behaviour (e.g., temperature versus enthalpy curves, specific heat capacities, rheological properties and physical stability of the mPCM slurry) were investigated with experimental tests; while other features (e.g., thermal conductivity, density, etc.) where calculated from the characteristic of each pure material in the mixture.

3.2.3.1 Reference properties of the carrier fluid: water and glycol

The carrier fluid is a mixture of water and glycol, used as antifreeze. The mass percentage of glycol is related to the climate conditions of the location where the collector is installed. In this work, a 40 % concentration of glycol was adopted in the glycol-water solution for all the simulations. This concentration is the typical mean value adopted for traditional panels installed in Central Europe area (2500-3000 Heating Degree Days).

Table 1 shows the primary data of the carrier fluid used in the PCM slurry.

Table 1. Details of the water and glycol mixture: carrier fluid.

Specification	Symbol	Value	m.u.
Water density	ρ_{H2O}	1000	kg m^{-3}
Glycol density	ρ_{gl}	1110	kg m^{-3}
Mass percentage of glycol	a_{gl}	40.0	%
Carrier fluid (water+glycol) density	ρ_{H2O+gl}	1044	kg m^{-3}
Carrier fluid (water+glycol) specific heat	$c_{p,\,H2O+gl}$	3600	J kg^{-1} K^{-1}
Carrier fluid (water+glycol) conductivity	λ_{H2O+gl}	0.369	W m^{-1} K^{-1}
Carrier fluid (water+glycol) dynamic viscosity @20°C	μ_{H2O+gl}	4.7·10^{-3}	Pa s
Carrier fluid (water+glycol) dynamic viscosity @40°C	μ_{H2O+gl}	2.4·10^{-3}	Pa s
Carrier fluid (water+glycol) dynamic viscosity @60°C	μ_{H2O+gl}	1.5·10^{-3}	Pa s

3.2.3.2 Reference properties of the dispersed mPCM: n-eicosane

The suspended material in the PCM slurry is a micro-encapsulated PCM based on the paraffin n-eicosane. The two main concerns when it comes to the choice of this component are the melting temperature and the latent heat of fusion. The temperature range of the phase-change process for n-eicosane is 36 ° - 38 °C. Data on this material are available in the literature, and other data have been provided by the technical datasheets of the manufacturer [10,11]. The manufacturer of the n-eicosane mPCM used in this application was the Microtek Laboratories. Wherever different values of the same property were found in literature, and their mean value was adopted. Table 2 summarises the main thermophysical properties of the n-eicosane adopted in the SolHe-PCM solar thermal system. These features refer to the bulk material contained in the core of the micro-capsules.

Table 2. Thermophysical properties of the chosen mPCM: n-eicosane.

Specification	Symbol	Value	m.u.
Mass percentage of the core	a_{core}	87.5	%
Core density (solid/liquid)	ρ_{core}	815/780	kg m^{-3}
Shell density	ρ_{shell}	1190	kg m^{-3}
Micro-capsule density(solid/liquid)	ρ_{mPCM}	861/831	kg m^{-3}
Average particle diameter	D_{mPCM}	17-20·10^{-6}	m
Conductivity (solid/liquid)	λ_{mPCM}	0.23/0.15	W m^{-1} K^{-1}
Specific heat (solid/liquid)	c_{p_mPCM}	1.92/2.46·10^3	kJ kg^{-1} K^{-1}
Latent heat	$\Delta h_{lat,mPCM}$	1.95·10^5	kJ kg^{-1}
Nominal phase change temperature	θ_{n_mPCM}	37	°C
Nominal phase change temperature range	θ_{inf_mPCM}-θ_{sup_mPCM}	35-37	°C

The properties of the mPCM are a function of the characteristic of the PCM contained in the micro-capsule *core*, the material used as micro-capsule *shell* and the ratio of mass percentage of the core. Values of the overall microcapsule can be experimentally evaluated or calculated by means of the equations proposed by [8,9,12–14]:

$$\rho_{mPCM} = a_{mPCM,co} \cdot \rho_{mPCM,co} + \left(1 - a_{mPCM,co}\right) \cdot \rho_{mPCM,sh} \qquad (3.1)$$

$$c_{p,mPCM} = \frac{\left(c_{p,mPCM,co} + a_{mPCM,co} \cdot c_{p,mPCM,co}\right) \cdot \rho_{mPCM,co} \cdot \rho_{mPCM,sh}}{\left(\rho_{mPCM,co} \cdot a_{mPCM,co} + \rho_{mPCM,sh}\right) \cdot \rho_{mPCM}} \qquad (3.2)$$

$$\lambda_{mPCM} = \frac{1}{D_{mPCM}} \cdot \left(\frac{1}{\lambda_{mPCM,co} \cdot D_{mPCM,co}} + \frac{D_{mPCM} - D_{mPCM,co}}{\lambda_{mPCM,co} \cdot \lambda_{mPCM,sh} \cdot D_{mPCM}}\right) \qquad (3.3)$$

Where: $a_{mPCM,co}$ is the mass percentage of the core material; ρ is the density; c_p is the specific heat capacity; λ is the thermal conductivity; and D is the diameter. The subscript *mPCM,co* and *mPCM,sh* refer to the micro-capsule core and shell respectively; while *mPCM* refers to the overall micro-capsule. The values of specific heat capacity and thermal conductivity reported in *Table* 2 were derived from the literature data, while the mPCM liquid/solid densities were calculated.

3.2.4 Experimental determination of temperature versus specific enthalpy curves of the n-eicosane mPCM slurry

The first significant step for experimentally evaluate the n-eicosane mPCM slurry was the determination of the relation interworking between temperature and specific enthalpy. These curves allow the heat storage capability of PCMs to be determined as a function of its temperature. Indeed, specific enthalpy is a property of great importance to accurately predict the behaviour of the material and its storage capabilities. The dependency of the storage capacity on temperature can be described in terms of specific heat capacity, $c_p(\theta)$, or concerning specific enthalpy variation, $h(\theta)$. The relationship between these two quantities is:

$$h(\theta) = \int_{\theta_1}^{\theta_2} c_p(\theta) \cdot d\theta \qquad (3.4)$$

$$c_p(\theta) = \frac{dh(\theta)}{d\theta} \qquad (3.5)$$

For this purpose, several experimental procedures can be performed, such as Differential Scanning Calorimetry [15], Differential Thermal Analysis, T-history method [16], Thermal Gravimetric Analyser [17,18] direct or inverse approaches [19], and others [20]. Thermal Gravimetric Analyser is seldom used. Differential Scanning Calorimetry and Differential Thermal Analysis are similar methods, even though Differential Thermal Analysis is mostly used for qualitative measurements. The most appropriate techniques to investigate the enthalpy-temperature curves are Differential Scanning Calorimetry and T-History. Both experiments require careful preparation and data post-processing. The sample has to be representative of the material under investigation, and the specific boundary conditions of the experiment should be taken into account when the monitored data are post-

processed. Gschwander et al. [13] developed general guidelines for referring the experiments of PCM characterisation to standard conditions.

For the mPCM slurry under investigation, experimental tests based on T-History method were preferred for several reasons. First of all, the simplicity of the requested experimental setup. This simplicity is especially useful when the thermal properties are not entirely provided by the manufacturer, and the customer company do not hold the necessary instrumentation for carrying out sophisticated thermal analyses. T-History represents an optimum compromise between the data reliability and the lower cost of the experimental set up compared to other methods. Secondly, T-History allows samples with a broader volume than different ways to be analysed. Indeed, the T-History method is the technique most widely adopted to investigate the thermal behaviour of large PCM samples. This fact is particularly advantageous for PCM slurries because the representative volume of the sample should be comprehensive enough to guarantee the correct mixing of the two substances. Furthermore, specific heat capacity in the solid and liquid state, melting temperature and latent heat of fusion of several PCM samples can be simultaneously measured. Eventually, supercooling can be well characterised with T-History. The T-History was proposed by Zhang and Jiang [21] in 1999 as an alternative method to Differential Scanning Calorimetry or Differential Thermal Analysis and several contributions were subsequently published to improve it [22]. Afterwards, many examples where the T-History method was adopted to characterise PCMs and PCM slurries can be found in the scientific literature [22].

3.2.4.1 T-History: methodology

At least two tubes are required to perform a T-history test. At least one tube must be filled with the material under investigation, and one must be filled with reference material. The reference material should be a substance with well-known thermal properties, such as distilled water. Since the T-history method is based on the lumped capacitance model, the characteristics of the tubes should guarantee a sufficiently small Biot number (below 0.1) in order to ensure a slight temperature gradient within the test material. The Biot number is calculated as follow:

$$Bi = \frac{h_c \cdot r}{2\lambda} \qquad (3.6)$$

Where h_c is the heat transfer film coefficient of the sample tubes with the external environment, r is the radius of the sample tubes, and λ is the thermal conductivity. The tubes are preheated above the PCM melting temperature ($\theta_{pre\text{-}heat}$ > θ_m) and afterwards they are cooled down by exposing them to air at ambient temperature. During the cooling process, the curves of temperature versus time are recorded. Thermal properties can be determined by comparing these curves for the PCM and the reference material.

A horizontal setup should be preferred over a vertical installation to improve the measurement accuracy. Indeed, during the experiment, the effect of creaming

of the mPCM slurry might be non-negligible. A horizontal setup was also found to reduce the discrepancies between freezing and melting enthalpy-temperature curves. During our experimental tests, the horizontal setup improved the accuracy of the results up to 18 % compared to the vertical position.

The original T-history method proposed by Zhang et al. was developed for pure materials or eutectics. In the following years, several contributions were suggested to improve both its mathematical basis and its measuring process. In detail, some adjustments were necessary for those materials whose phase change occurs in a temperature range – likewise the mPCM slurry under investigation. Marin et al. proposed an improved T-History method that is more suitable for this kind of materials. In this updated method, the thermal balance of the tube filled with PCM and that of the tube with distilled water are determined.

The formulations of Marin et al. allow the data gathered during T-history experiments to be used to determine the specific enthalpy versus temperature curves at different mPCM concentrations. Distilled water was used as the reference fluid. Under the hypothesis of equal convection heat transfer coefficient for both tubes, the correlations are the following:

$$\Delta h_{PCM}(\theta_i) = \left(\frac{m_{H2O} \cdot c_{p,H2O}(\theta_i) + m_t \cdot c_{p,t}(\theta_i)}{m_{PCM}} \right) \cdot \frac{A_i}{A'_i} \cdot \Delta\theta_i - \frac{m_t}{m_{PCM}} \cdot c_{p,t}(\theta_i) \cdot \Delta\theta_i \qquad (3.7)$$

$$A_i = \int_{\tau_0}^{\tau_i} \left(\theta_{PCM,i} - \theta_{a,i} \right) \cdot d\tau \qquad (3.8)$$

$$A'_i = \int_{\tau_0}^{\tau_i} \left(\theta_{H2O,i} - \theta_{a,i} \right) \cdot d\tau \qquad (3.9)$$

$$h_{PCM}(\theta_i) = \sum_{i=1}^{n} \Delta h_{PCM}(\theta_i) + h_{H2O} \qquad (3.10)$$

Where h is the specific enthalpy, m is the mass, c_p is the specific heat capacity, θ is the monitored fluid temperature, τ is the time, A' is the integral of the temperature difference between the reference fluid and the ambient temperature, and A is the integral of the temperature difference between the PCM slurry fluid and the ambient temperature. Both the integrals refer to a period ranging from the beginning of the experiment till the end of the phase change transition. The subscript H_2O indicates the distilled water used as reference fluid, t indicates the tube of the sampler, PCM the micro-capsule of PCM, a is the external ambient in which the tubes are cooled down, and i is the generic i-th sampling time instant.

Afterwards, the calculation of the specific heat capacity was possible since it is defined as the derivative of the specific enthalpy versus temperature curve. The trend of the specific heat can be described as the combination of two Gaussian curves, one for the liquid part and the other one for the solid part.

$$c_p = \begin{cases} c_{p,s} + \left(c_{p,m} - c_{p,s}\right) \cdot e^{-\left(\frac{\theta_m - \theta}{\omega_s}\right)^2} & \theta \le \theta_m \\[2mm] c_{p,l} + \left(c_{p,m} - c_{p,l}\right) \cdot e^{-\left(\frac{\theta_m - \theta}{\omega_l}\right)^2} & \theta > \theta_m \end{cases} \qquad (3.11)$$

In which ω are the width coefficients of the Gaussian curves. While the subscribe s refers to the solid state, l to the liquid state, and m to the peak value.

Thus, starting from the approximation obtained for deriving the specific heat capacity of the material, the final equation for an approximated temperature versus enthalpy curve results in the following formulation.

$$h = \begin{cases} c_{p,s} \cdot \left(\theta - \theta_{mPCM,inf}\right) - \left(c_{p,m} - c_{p,s}\right) \cdot \frac{\sqrt{\pi}}{2} \cdot A & \theta \le T_p \\[2mm] c_{p,l} \cdot \theta - \left(c_{p,m} - c_{p,l}\right) \cdot \frac{\sqrt{\pi}}{2} \cdot B - c_{p,s} \cdot \theta_{mPCM,inf} + \theta_m \cdot \left(c_{p,s} - c_{p,l}\right) & \theta > T_p \\[2mm] A = \omega_s \cdot \left[\text{erf}\left(\frac{\theta_m - \theta}{\omega_s}\right) - \text{erf}\left(\frac{\theta_m - \theta_{mPCM,inf}}{\omega_s}\right)\right] \\[2mm] B = \omega_l \cdot \text{erf}\left(\frac{\theta_m - \theta}{\omega_l}\right) + \omega_s \cdot \text{erf}\left(\frac{\theta_m - \theta_{mPCM,inf}}{\omega_s}\right) \end{cases} \qquad (3.12)$$

3.2.4.2 T-History: material and method

The material under investigation was the n-eicosane mPCM slurry obtained by a mixture of water and micro-encapsulated n-eicosane. Since mPCM slurry thermophysical properties are strictly related to the mass concentration of the PCM in the mixture, different weight concentrations must be investigated to determine material features. Two sets of experimental tests were carried out. The first set of measurements examined higher mPCM mass concentrations performing tests at nominal values of 20 % w.t., 30 % w.t., 40 % w.t., and 50 % w.t concentration. The second set of measures considered lower mPCM mass concentrations, performing tests at nominal values of 5 % w.t., 10 % w.t., and 15 % w.t. concentration. The other mPCM characteristics necessary for the experimentation were derived from the previous analysis of manufacturer datasheets and data available in the scientific literature.

The experimental setup consisted of:

- Distilled water, used as reference material, with a specific heat capacity of 4186 J/(kgK);
- Scale for sample weighting (sensibility of 0.01 g);
- 5 Falcon low-density polyethylene tubes with 15 mm diameter, with a specific heat capacity of 2300 J/(kgK);
- 7 T-type thermocouples, previously calibrated using a Pt-100 as a reference;
- DT85 data-logger with support for multiple SDI-12 sensor networks and 12V regulated output to power sensors;
- Haake F3 thermostatic bath for sample heating (temperature accuracy of 0.02 °C, operative range of -20/150 °C);

- Insulated thermostatic chamber for sample cooling (1 °C internal temperature control accuracy);
- Ventilated oven and a webcam as auxiliary devices.

The mPCM slurry was obtained by accurately mixing distilled water and micro-encapsulated n-eicosane. The concentration was verified during sample preparation and after the experiment. First, samples at different concentration were prepared by weighing the material samples on the scale. Afterwards, a gravimetric test was performed drying the samples in the oven until constant weight to double check the mass concentration of the samples. The samples were labelled according to their theoretical mass concentration from preparation on the scale. However, the concentrations resulting from the gravimetric tests slightly differ. *Table 3* reports these values.

Table 3. Sample weight concentration resulting from gravimetric tests.

Sample label	Actual mass concentration	Standard deviation
PCM slurry 5 % w.t. mPCM concentration	4.9 % w.t.	± 0.1 % w.t.
PCM slurry 10 % w.t. mPCM concentration	9.2 % w.t.	± 0.2 % w.t.
PCM slurry 15 % w.t. mPCM concentration	14.8 % w.t.	± 0.5 % w.t.
PCM slurry 20 % w.t. mPCM concentration	20.1 % w.t.	± 0.7 % w.t.
PCM slurry 30 % w.t. mPCM concentration	29.2 % w.t.	± 1.0 % w.t.
PCM slurry 40 % w.t. mPCM concentration	39.5 % w.t.	± 1.1 % w.t.
PCM slurry 50 % w.t. mPCM concentration	49.1 % w.t.	± 0.9 % w.t.

For each concentration, four tubes were filled with the PCM slurry sample, and a fifth tube was filled with distilled water. The thermocouples were stably fixed in the middle of each tube. After sample preparation, all the tubes were placed in the thermostatic bath (*Figure 4*). Two additional thermocouples further monitor edits temperatures. The bath temperature was set at 60 °C, which is a higher temperature than the nominal melting temperature of the PCM slurry. When the thermodynamic equilibrium was reached, the tubes were moved into the thermostatic chamber (*Figure 5*). The temperature of the thermostatic chamber was set at a constant value of 18 °C to cool the samples below their melting temperature. The thermocouples

previously used for measuring the water temperature in the thermostatic bath were used to measure the air temperature within the chamber. The data were recorded by the data logger every 5 seconds. The preliminary temperature versus time curves were obtained in this phase. A webcam programmed with Matlab snapped a picture every 15 minutes to monitor how the experiment was progressing and the effects of the creaming phenomenon on the samples.

Figure 4. The thermostatic bath used to heat up to 60 °C the samples.
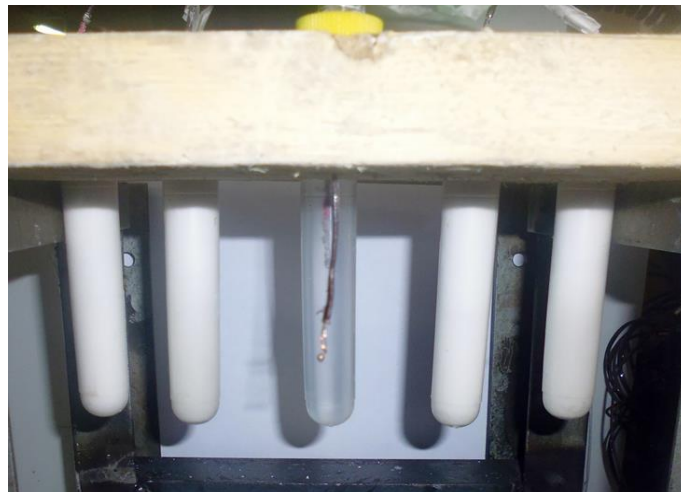
Figure 5. The samples cooled down in the thermostatic chamber and monitored with thermocouples in the centre of the tube

3.2.4.3 T-History: results and discussion

The elaboration of the results can be roughly divided into three steps. The first one is plotting the raw acquired data of temperature versus time. The second step is the application of the Marin et al. correlations to define the enthalpy versus temperature curves from the gathered data. Eventually, the third step consists in the derivation the specific heat capacities from the enthalpy data. Within the phase

transition range, the specific heat capacities assume fictitious values, which merge the effects of specific heat capacity and latent heat capacity.

Figure 6 reports two example of curves obtained with raw data of temperature versus time. In detail data of 20 % w.t. concentration is shown in *Figure 6*(a), while data of 50 % w.t. in *Figure 6*(b). In this stage, it was possible to understand if there is one or more sample affected by errors (e.g., whose data are not comparable with the one of other samples at the same concentration). In case of a single sample diverging, its data were discarded, while in case of recurrent errors the tests were repeated for the concentration affected by this drawback. It can be observed that the temperature data reported in *Figure 6* were comparable for both experiments within all the fours samples.
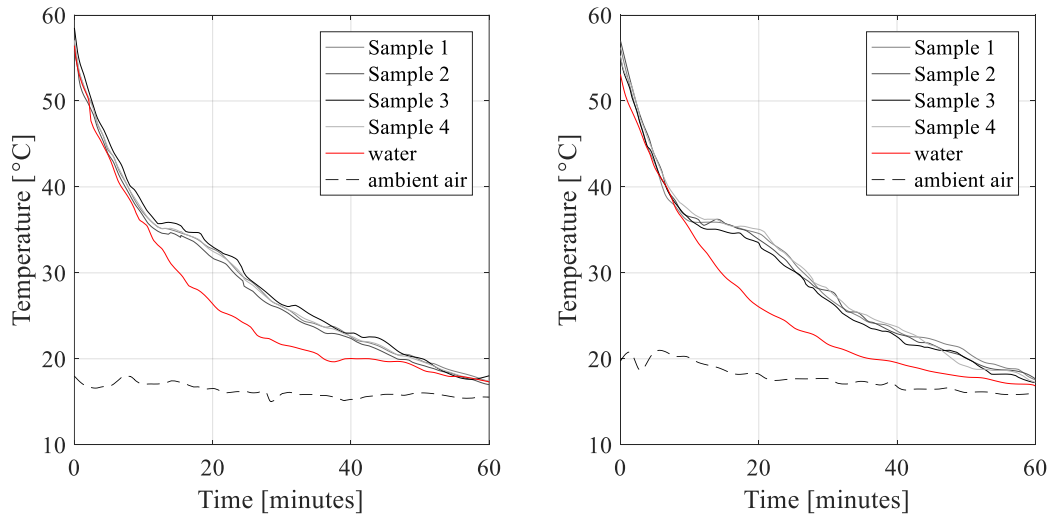
Figure 6. T-History raw data: time versus temperature versus time curves.
(left) 20 % w.t. mass concentration. (right) 20 % w.t. mass concentration.

First of all, the enthalpy values were calculated for each sample employing Marin et al. correlations. The temperature 28 °C was chosen as the reference value to set the 0 kJ/kg for calculating the enthalpy differences. The choice of this value is completely arbitrary and does not completely affect the final results. Secondly, average enthalpy values were calculated for each concentration. *Figure* 7 and *Figure 8* show the average enthalpy versus temperature curves that resulted from these elaborations of the measured data. The two figures refer to the two sets of measurements that were carried out. In the first one the concentrations at 20 %, 30 %, 40 %, and 50 % w.t. were investigated (*Figure* 7), while in the second set the concentrations at 5 %, 10 %, and 15 % w.t. were considered (*Figure 8*).

Considering that the latent heat involved in the transition process is lower for small mPCM concentrations, *Figure 8* shows a smaller temperature range (0.1 °C against 0.2 °C) compared to *Figure* 7 in order to better highlight the effects of PCM latent heat exchanges. It can be inferred from both figures that the transition process occurs in a temperature range that was slightly shifted to lower values (around 34 – 36 °C) compared to the nominal range values (35 – 37 °C). This fact was probably

due to hysteresis of the material since the melting temperature was provided by the manufacturer whereas the T-history measured the solidification temperature. Furthermore, a small amount of phase change enthalpy, which is due to rotator-crystal transition [11], appeared in the temperature interval below 30 °C (not shown in the figure). As it was expected, the latent heat related to higher concentrations was significantly higher than the one of lower concentrations.
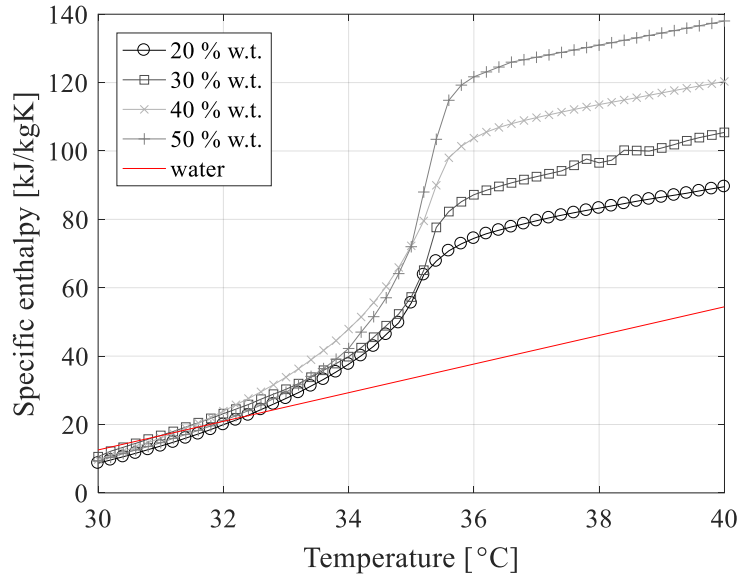
Figure 7. Enthalpy versus temperature curves for 20 %, 30 %, 40 %, and 50 % w.t.
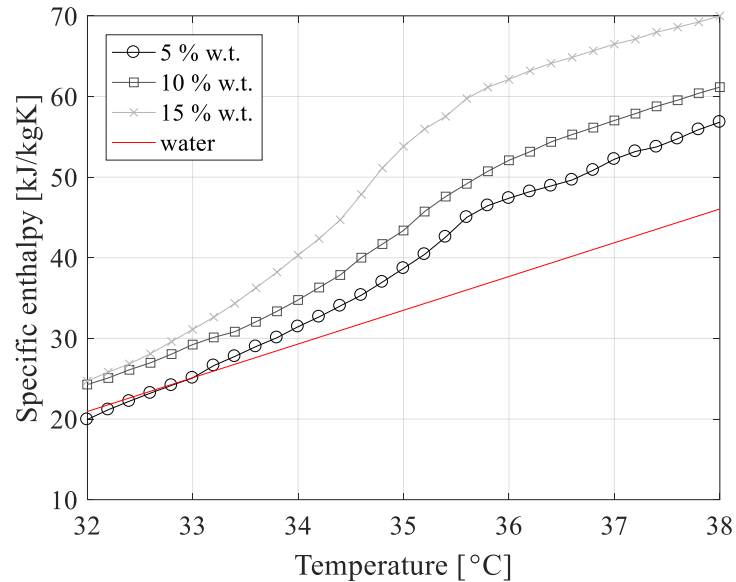
Figure 8. Enthalpy versus temperature curves for 5 %, 10 %, and 15 % w.t.

The measured values were compared with the theoretical ones to determine the reliability of the test results. The latter were obtained by applying the Equations 3.18 and 3.19 described in Section 3.2.7 with the micro-encapsulated n-eicosane thermal properties reported in *Table 2*. In particular, the experimental and theoretical values of the specific enthalpy difference in the range 30 °C – 40 °C

were evaluated. The Mean Absolute Percentage Error (MAPE) was used to assess the prediction accuracy of the experimental method.

$$MAPE = \frac{100}{n} \cdot \sum \left| \frac{\Delta h_{experimental} - \Delta h_{theoretical}}{\Delta h_{experimental}} \right| \qquad (3.13)$$

Where n is the number of samplings in the considered range and Δh is the specific enthalpy difference. *Table 4* reports the results of this comparison of theoretical and experimental results. These results are in accordance with the theoretical values, and the discrepancy between the values is included in the uncertainty typically observed in T-History experiments. Lower concentrations were affected by the higher uncertainty of the results. This discrepancy is mainly attributable to the accuracy of the experimental setup. Indeed, the lower the concentration the lower the magnitude of the measured variables (e.g., sample weight, enthalpy difference). So that, even if the absolute error due to experimental apparatus uncertainty is the same, lower concentrations are more sensitive to the relative error, likewise MAPE.

Table 4. Comparison between theoretical end experimental specific enthalpy differences in the range 30 – 40 °C of the mPCM slurry for various concentrations of mPCM in the mixture.

Concentration w.t.	Theoretical specific enthalpy difference [kJ/kg]	Experimental specific enthalpy difference [kJ/kg]	MAPE [%]
5 %	50.5	57.1	9.9
10 %	59.1	54.2	9.1
15 %	67.8	61.6	9.9
20 %	76.4	80.9	5.5
30 %	95.0	94.8	1.3
40 %	110.7	110.1	0.6
50 %	132.4	128.7	2.9

The instability of the PCM slurry due to creaming (see Section 3.2.5) could partially affect the results of the T-History tests. Indeed, the variation of concentration gradient during time could due to the creaming strongly affect the local thermophysical properties of the PCM slurry and thus the reliability of the temperature data monitored by the thermocouple placed inside the samples. For this reason, PCM sedimentation was observed during the experiments through a webcam. No visible separation between water and mPCM occurred within the duration of the tests (about one hour). Preliminary results show that creaming

becomes to be visible after three hours. Experimental tests showed how the lower the concentration, the sooner the creaming appearance, thus worst MAPE values for lower concentrations can be partially explained by the occurrence of actual concentration variation within the samples.
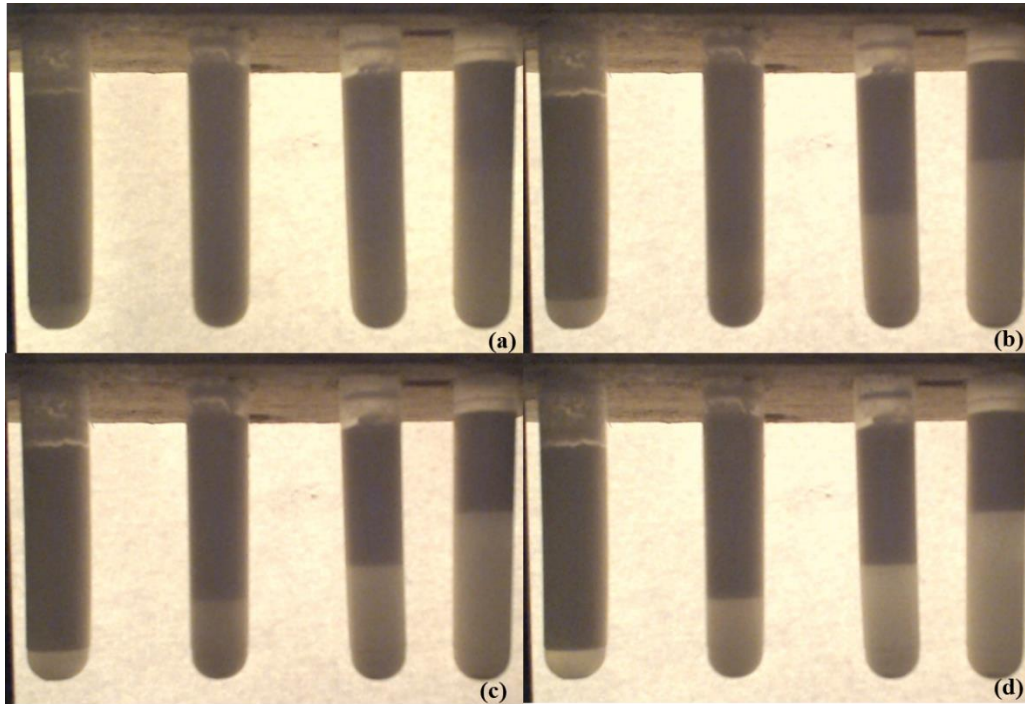
Figure 9. Creaming monitoring through web-cam during the T-History tests. (a) samples after 3 hours; (b) samples after 6 hours; (c) samples after 9 hours; (d) samples after 12 hours.

3.2.5 Investigation of n-eicosane rheological properties

It is fundamental to assess the rheological properties in order to evaluate the performance of a heat transfer fluid. Indeed, the rheological properties – and the viscosity in particular – affect the shear rate of the fluid. Thus the pumping power needed to ensure the flow-rates required by a system. In detail, before proceeding with the design and construction of the solar thermal prototype based on an innovative heat transfer fluid, it was necessary to assess:

- If the mPCM slurry causes clogging or other drawbacks, when pumped in pipes of the same type of those used in solar thermal collectors and systems;
- The additional pressure drops, compared to traditional heat transfer fluids based on water and glycol, due to the increased viscosity of the mPCM slurry.

In detail, several tests of pressure drop have been carried out using different concentrations of mPCM before the real scale prototype system was set up. The primary concern was understanding the rheological behaviour of the mPCM slurry

in pipes of real systems. Dedicated experimental setup and experimental tests were necessary for this purpose.

3.2.5.1 Investigation of rheological properties: material

The experimental setup consisted of:

- The pipe circuit shown in *Figure 10*, used to perform the tests. This scale circuit was made up of similar copper pipes to those used in flat-plate solar collectors. The inner diameter of the pipes was 8 mm, and the external diameter is 10 mm. The circuit was composed of two straight pipe sections and two 90° curves. The height difference between the upper and the lower part of the circuit was 0.5 m. Four transparent piezometer pipes (named A, B, C, and D) were placed in the circuit to monitor the pressure drops. The difference of fluid height between piezometers A and B or C and D was used to determine the distributed pressure drops. The distance between these piezometers is 6 m. The difference of fluid height between piezometers B and C was used to calculate the concentrated pressure drops due to the two 90° curves;
- A programmable Verderflex Scientific AU UV 3000 HD peristaltic pump, whose main features are summarised in *Table 10*;
- Two plastic buckets;
- A scale for measuring the fluid flown in the circuit (thus the flow-rate) with a sensibility of 10 g and a measuring range between 0 and 5 kg;
- A precision scale for sample weighing (sensitivity of 0.01 g) and a ventilated oven. They were used for the gravimetric tests to determine the exact mixture concentration;
- The heat transfer fluids to be tested: water and glycol, and mPCM slurry.

Figure 10. The pressure drops testing circuit.

The samples of mPCM slurry were obtained by accurately mixing water and glycol with micro-encapsulated n-eicosane. Six different concentrations were tested

according to *Table 5*. The concentration was verified during sample preparation and after the experiment. First, samples at different concentration were prepared by weighing the materials on the scale. Afterwards, a gravimetric test was performed drying the samples in the oven until constant weight to double check the mass concentration of the samples. The samples were labelled according to their theoretical mass concentration from preparation on the scale.

Table 5. Sample concentrations during the various tests.

Test 1	Test 2	Test 3	Test 4	Test 5	Test 6
Water + glycol	mPCM slurry 25 % w.t.	mPCM slurry 30 % w.t.	mPCM slurry 35 % w.t.	mPCM slurry 40 % w.t.	mPCM slurry 48 % w.t.

3.2.5.2 Investigation of rheological properties: method

A schematic of the experimental procedure is shown in *Figure 11*. The heat transfer fluid was pumped from a plastic bucket to the testing circuit through the peristaltic pump. The pressure drops were measured reading the height differences of the fluid within the various piezometers. At the end of the circuit, the fluid flowed into the second plastic bucket, which was placed on a scale. Measuring the second plastic bucket weight variation over a time span (fixed equal to 1 min) allowed the flow-rate passing in the circuit to be evaluated (in kilograms per minute). Buckets and piezometers were preferred to digital devices for various reasons. First of all, one of the scopes of the investigation of the rheological properties was the verification of the capability of the PCM slurry to flow in circuits. For this reason, electronic sensors placed within the pipes were eluded to avoid any potential pipe clogging due to their presence. Secondly, since the PCM slurry is a bi-component fluid – with solid particle suspended – it was not clear to the author if sensor designed for measuring traditional fluids (like water) would be able to provide reliable measures. Finally, the adoption of the weighing buckets method allowed the mass flowing in the circuit to be measured directly, without passing through a measurement of volumetric flow rate and a density.

Firstly, the circuit was tested using water with glycol to simulate the typical heat transfer fluid used in solar thermal systems. Secondly, the tests were performed with various mPCM slurry concentrations according to *Table 5*.
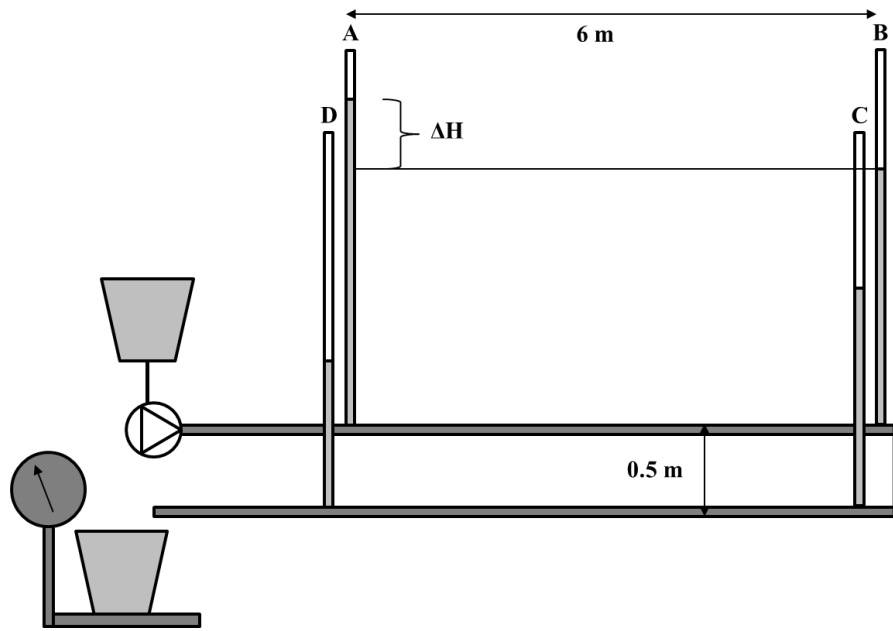
Figure 11. Schematic of the experimental procedure.

3.2.5.3 Investigation of rheological properties: results

Figure 12, Figure 13 and *Figure 14* show the outcomes of distributed and concentrated pressure drop tests respectively. Experiments were carried out for different volume flow-rates and concentrations of mPCM in the slurry. The results obtained for the pressure drop of the water and glycol fluid were equal to reference literature values. It is possible to infer from the figures how the pressure drops showed a linear increase with the flow-rate and a non-linear increase with the concentration. In particular, concentrations over 35 % w.t. are characterised by a non-Newtonian behaviour that causes further non-linearities. It was not possible to pump the mPCM slurry for higher concentrations than 50 % w.t., while the mPCM slurry pressure drops resulted in being similar to those of water for mPCM concentrations lower than 30 % w.t.
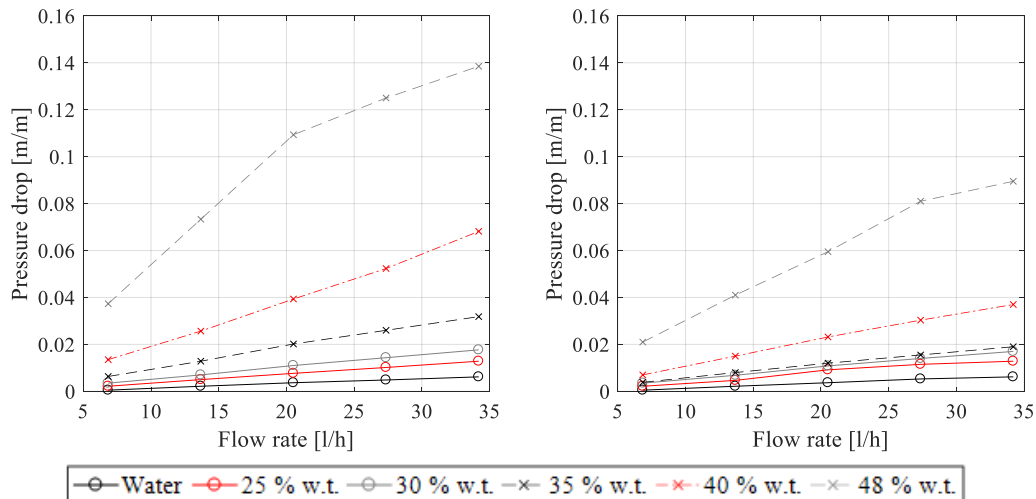
Figure 13. Distributed pressure drops measured on the test-bed circuit. (left) Pressure drop versus concentration at various flow-rates in weight total for the "clean" circuit. (right) Pressure drop versus concentration at various flow-rates in weight total for the "dirty" circuit.
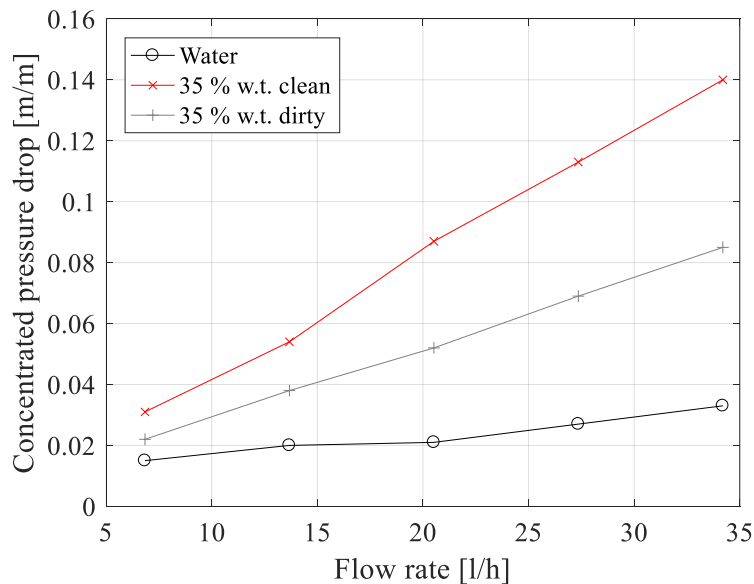
Figure 14. Concentrated pressure drops measured on the test-bed circuit for the concentration 35 % w.t. of mPCM.

An interesting outcome from these tests was that the monitored pressure drop varies in time. In fact, after 12 hours of continuous monitoring, the material showed a completely different behaviour compared to initial tests, with less noticeable

pressure drops. This fact led to distinguish the two configurations highlighted in *Figure 12* and *Figure 13*. "Clean" circuit indicates the measurements carried out at the beginning of the tests, while "dirty" circuit the measurements after 12 hours of monitoring. The higher the mPCM concentration in the slurry, the more significant this phenomenon. This behaviour was principally due to the appearance of the creaming effect even within pipes. Creaming caused the division in layers of the mPCM slurry with different micro-capsules concentrations.

It was possible to derive an apparent viscosity of the fluid starting from the pressure drop measurements. First of all, it was necessary to convert the pressure drops from differences of height (metres of water column per meters of pipe) to differences of pressure (Pascal per meter of pipe). This calculation was possible with the formulation:

$$\Delta p = \Delta H \cdot g \cdot \rho \tag{3.14}$$

Where ΔH is the difference of fluid height in two subsequent piezometers; g is the standard acceleration due to gravity assumed equal to 9.81 m/s^2; and ρ is the fluid density (see Section 3.2.6 for the calculation of mPCM slurry density at various concentrations). Secondly, it was possible to derive the apparent fluid viscosity according to the following expression:

$$\Delta p = \frac{\Delta p \cdot \pi \cdot D_i{}^4}{8 \cdot \dot{V}} \tag{3.15}$$

Where D_i is the inner diameter of the circuit pipes, equal to 0.008 m; and V is the volumetric flow-rate. *Figure 15* reports the results of these viscosity calculations. Since the viscosity is a property of the material itself, it is not influenced by the flow-rate variation. An exception was made for higher concentrations where the non-Newtonian properties of the material influenced its shear rate, showing a pseudo-plastic behaviour (the higher the solicitation, the lower the apparent viscosity). The average apparent viscosities were plotted for each concentration in *Figure 16*.
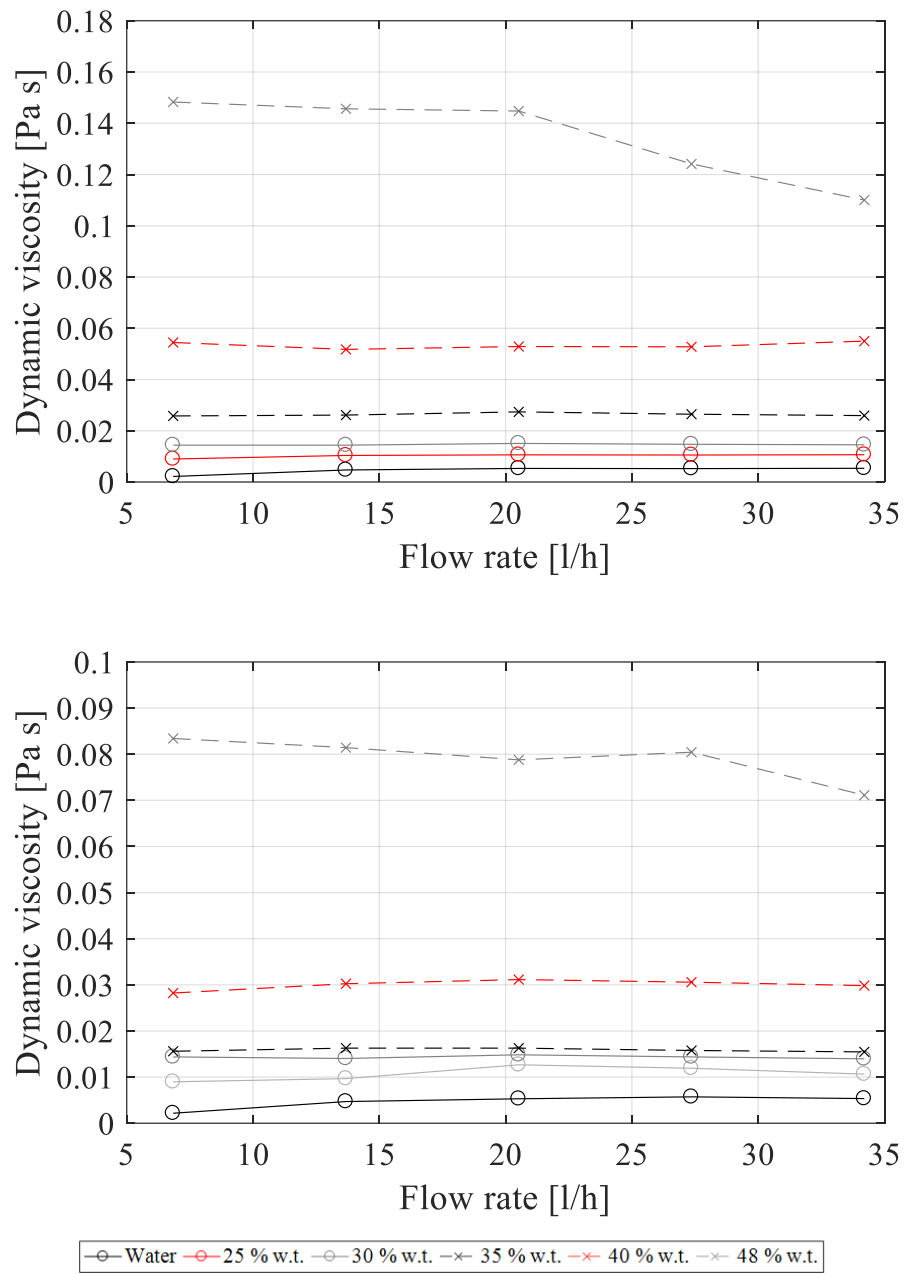
Figure 15. Dynamic viscosity versus flow-rate. (top) "clean" circuit. (bottom) "dirty" circuit.
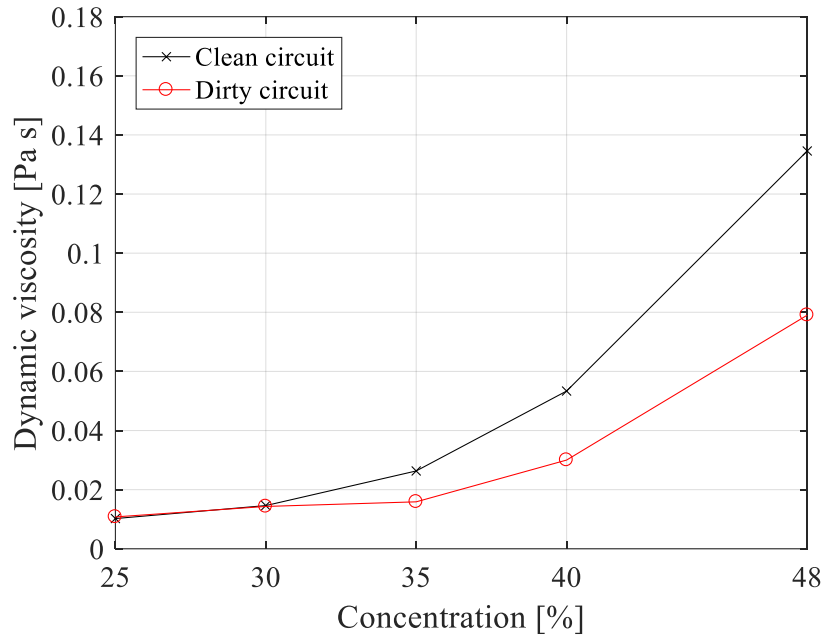
Figure 16. Dynamic viscosity variation at various mPCM concentrations.

3.2.6 Investigation of n-eicosane creaming phenomenon

One of the possible drawbacks related to the adoption of PCM slurries is the creaming phenomenon [23], which caused by the density differences between the suspended mPCM and the water and glycol carrier fluid. The creaming is the movement of the suspended particles towards the superior part of the suspension as a result of gravity [24,25]. After a period of tie depending on the material, the two phases of the PCM slurry are likely to show separation. This kind of process is quite common in mPCM slurries, and it usually takes hours or even days to overcome. In the case of the n-eicosane mPCM slurry, a layer of more concentred mPCM layer appears in upper part of the mixture.

As discussed in the following Sections, the creaming drawback can strongly affect the performance of the material in the SolHe-PCM prototype. Indeed, the creaming phenomenon occurs whenever the fluid is not kept in motion – for example when the mPCS slurry is in the thermal energy storage tank or pipes during the off periods. This phenomenon can cause severe problems in the functioning of the prototype. The stratification in the storage tank causes on the one side non-homogenous energy storage, on the other side it affects the concentration of the material pumped in the primary loop of the solar thermal system. Furthermore, the occurrence of creaming in the pipes can cause severe clogging.

However, very few studies on this phenomenon are available in the literature. Up to now, no quantitative analysis about it has been done. A detailed qualitative investigation on the physical stability of PCM slurries was carried out by Delgado et al. [23]. In general, creaming can be solved by reducing the mPCM capsule size or by adding surfactants [25]. Al-Shannaq et al. [26] increased the stability of a PCM slurry with a polymethyl methacrylate shell using mixed surfactants, such as sodium dodecyl sulphate and ploy vinyl acrylate. Zhang & Zhao [27] dealt with the

problem of mPCM slurry creaming by adding multi-walled carbon nanotubes. The mPCM slurry showed excellent stability and no visible creaming or sedimentation were observed two months after the addition of the nanotubes. A study on a mPCM slurry conducted at the Fraunhofer Institute for Solar Energy Systems has been reported in [26]. In this case, a thickener was added to the mixture, and this slowed down the separation speed.

The goal of the experimental tests herewith reported was to carry out quantitative results aiming at better understanding the creaming phenomenon. In particular, it was possible to define a physical law, which reproduces the dynamical evolution during the time of the creaming phenomenon.

3.2.6.1 Investigation of creaming phenomenon: material

The mPCM slurry was tested at different concentrations to investigate how the presence of mPCM in the mixture affects the creaming phenomenon. Table 6 reports the volumetric and mass concentrations of the sampled used in these experimental tests. The samples were obtained by accurately mixing distilled water and micro-encapsulated n-eicosane. The concentration was verified during sample preparation and after the experiment. First, samples at different concentration were prepared by weighing the materials on the scale. Afterwards, a gravimetric test was performed drying the samples in the oven until constant weight to double check the mass concentration of the samples. The samples were labelled according to their theoretical mass concentration from preparation on the scale.

Table 6. Mass and volumetric concentrations of the samples used for the investigation of the creaming phenomenon.

Sample	Mass Concentration	Volumetric Concentration
A	25 % w.t.	28.0 %
B	30 % w.t.	33.4 %
C	35 % w.t.	38.6 %
D	40 % w.t.	43.8 %

The experimental setup consisted of:

- Four 50mL conical Falcon tubes of low-density polyethylene were used to hold as many samples of the different concentrations;
- A metallic support was selected to carry the tubes, keeping them vertically without interfering in the visual field;
- A webcam was placed 50 cm in front of the samples. It was programmed with Matlab to snap a picture every 5 minutes for monitoring how the creaming phenomenon evolved;

- A 40 x 12 cm OLED was put back the samples to maintain a constant apparent illuminance to use as a reference in post-processing elaborations.

Figure 17 shows a schematic diagram of this experimental setup. All these devices were placed inside an insulated thermostatic chamber (1°C internal temperature control accuracy) to maintain the samples at a constant temperature (20° C). This fact avoids that the temperature variations influence on the system. An electronic scale (sensibility of 0.01 g) and a ventilated oven were used as an auxiliary device to determine the exact sample concentration.
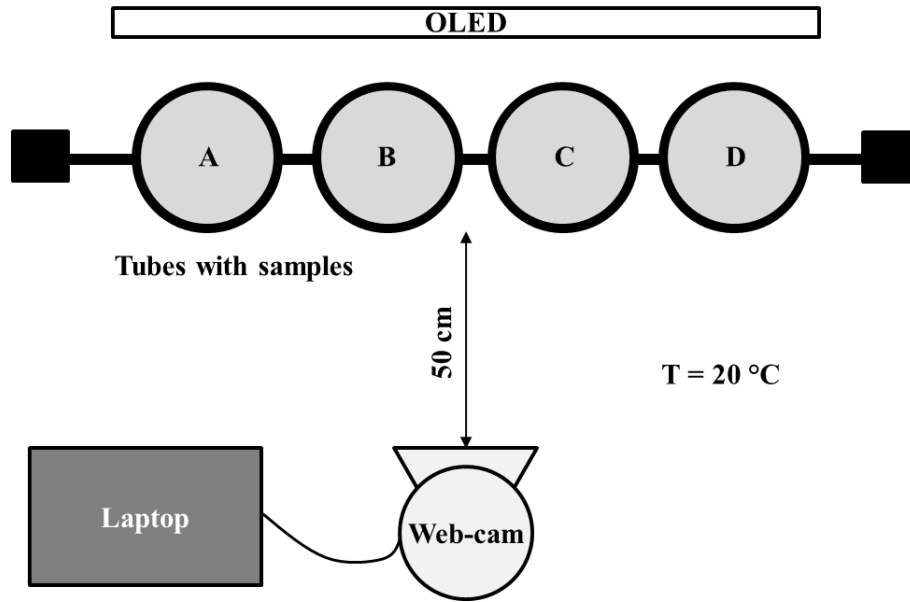
Figure 17. Experimental setup for investigation of the creaming phenomenon.

3.2.6.2 Investigation of creaming phenomenon: method

The method used for investigating the creaming phenomenon was straightforward. It consists of continuously monitoring the creaming event in some tubes filled with samples of the mPCM slurry at different concentrations. The continuous monitoring was possible by snapping pictures with a webcam every 5 minutes for a global period of 2800 minutes.

3.2.6.3 Investigation of creaming phenomenon: results

The photos shown in represent the results of the continuous monitoring through the webcam. From the time sequence, it can be inferred the evolution of the creaming of the mPCM slurry two components. In particular, it was found that the material concentration is directly related to the illuminance of the background transmitted through the tubes and the samples within contained. On the one hand, the water is almost transparent to the light radiation, while on the other hand, the PCM slurry becomes opaque. For this reason, the higher the illuminance passing

through the samples, the lower the mPCM concentration. The amount of light radiation flux through the samples varies at different height during the time, according to the concentration changes due to the creaming phenomenon. It is clear to observe that after almost 1000 minutes the process reaches a quasi-steady state and seemingly the conditions remain practically constant until the end of the experiment. The correlation between background light and concentration allows the data to be automatically processed through Matlab Image Processing Toolbox.

As shown in *Figure 19*, the creaming process was reduced to a one dimensional advection-diffusion problem in a cylinder with a variable cross-sectional area $A_{tube}(z)$, and the mPCM concentration a_{mPCM} was considered as constant across each horizontal cross-section, (i.e., it varies according the tube height and time $a_{mPCM} = a_{mPCM}(z, \tau)$). Using the model similar to Refs. [28,29], the equation which describes the creaming is given by:

$$
\frac{\partial a_{mPCM}}{\partial \tau} + \frac{1}{A_{tube}(z)} \cdot \frac{\partial}{\partial z} [A_{tube}(z) \cdot u_0 \cdot a_{mPCM} \cdot (1 - a_{mPCM})^C]
$$
$$
= \frac{1}{A_{tube}(z)} \cdot \left\{ \frac{\partial}{\partial z} \left[A_{tube}(z) \cdot D_0 \cdot (1 - a_{mPCM})^C \cdot \frac{\partial a_{mPCM}}{\partial z} \right] \right\}
$$

(3.16)

Where u_0 is the terminal velocity of a single particle of mPCM, C is the Richardson and Zaki index, z is the tube height coordinate, A_{tube} is the cross-sectional area of the sample tube, a_{mPCM} is the concentration of micro-capsules in the mixture, and D_0 is the diffusion coefficient [30]. The parameters used in the model relative to the mPCM slurry are listed in *Table 7*. In this model, the initial and boundary conditions were set equal to:

- $a_{mPCM}(z, 0) = a_{mPCM,0}$;
- $0 \leq z \leq h$ (where h is the maximum height of the tube);
- zero-flux boundary conditions at two tube conclusions.

The generalised upwind finite volume method is used to solve the previous equation and simulate the dynamical evolution of the system during the time. The simulation results are shown in *Figure 20*. Results are strongly in accordance with the experimental data. The creaming phenomenon reaches a quasi-steady state after 1000 minutes regardless of different initial concentrations.

Table 7. Parameters used in the model and numerical simulations.

Water density	Acceleration of gravity	Diffusion coefficient	Richardson and Zaki index	Terminal velocity of single mPCM particle
ρ_{H2O}	g	D_0	C	U_0
kg/m^3	m/s	m^2/s	-	-
1000	9.81	10^{-8}	4.65	$g \cdot (\rho_{mPCM} - \rho_{H2O}) \cdot D_{mPCM}^2 / (18 \cdot \mu)$
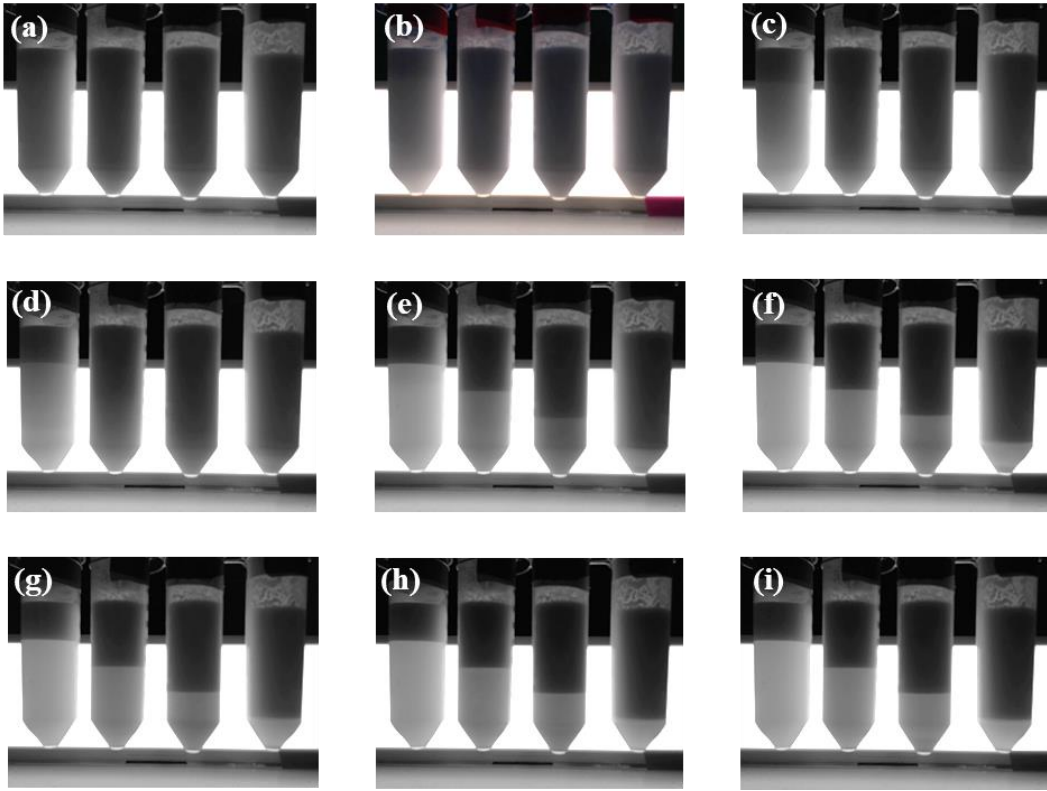
Figure 18. Photos of the evolution of the creaming phenomenon in samples of PCS with different concentrations, from 0 minute to 2800 minute. (a) 0 minutes; (b) 50 minutes; (c) 100 minutes; (d) 200 minutes; (e) 500 minutes; (f) 1000 minutes; (g) 1500 minutes; (h)2000 minutes; (i) 2800 minutes.
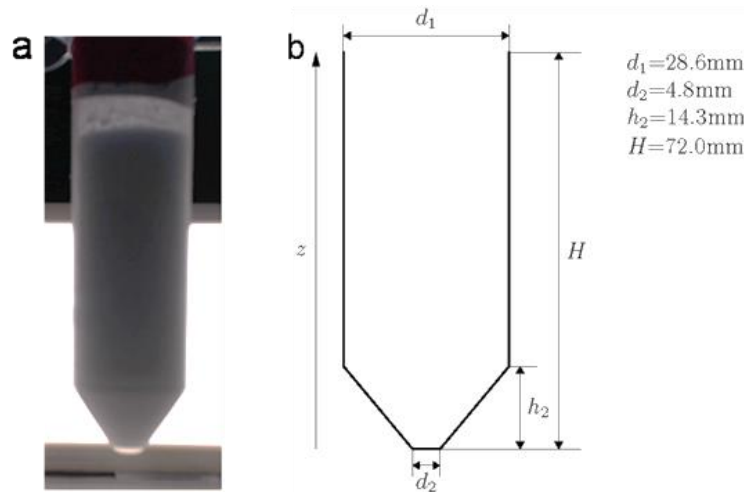
Figure 19. (a) Photo of a tube containing mPCM slurry; (b) Diagram for the reduction of the problem to a one-dimensional numerical model.
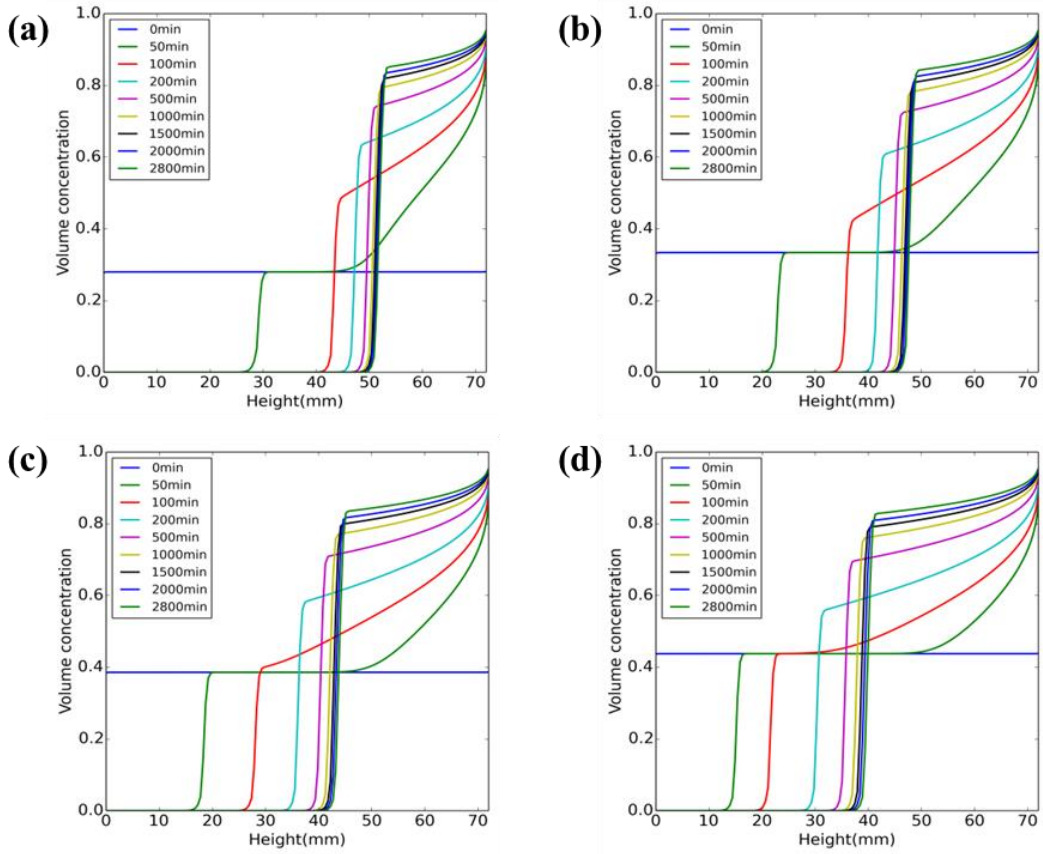
Figure 20. The simulated volume concentration of mPCM slurry at different height and time-steps. (a) 20 % w.t. sample; (b) 25 % w.t. sample; (c) 30 % w.t. sample; (d) 40 % w.t. sample.
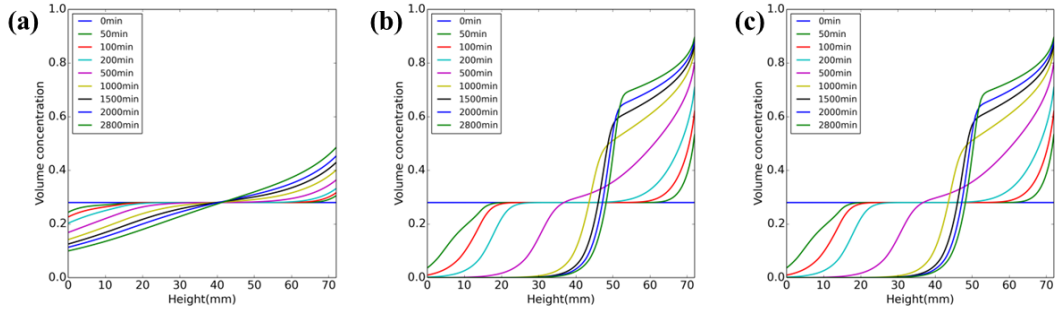
Figure 21. Simulated volume concentration of different scenario to reduce the creaming effect. (a) 10 % of current micro-particle mean size; (b)1000% of current viscosity; (c) 10% of current density difference.

The creaming of mPCM slurry is undesirable, therefore it is important to reduce or slow down its occurrence. Since the previously presented model has been validated with data of the experimental tests, it was possible to use it as a tool to evaluate possible solutions to reduce the creaming phenomenon. Numerical simulation of three different scenarios were conducted to this purpose. The first one analysed the effect of reduction of the mPCM micro-particles size to 10 % of its current size. The second scenario investigated the increasing of the carrier fluid

viscosity to 1000 % of the actual water viscosity. Eventually the last scenario is to decrease the density difference of mPCM and carrier fluid to 10 % of the current value. The simulated results are shown in *Figure 21*. It is easy to observe that decreasing the mean micro-particle size, increasing the viscosity of the carrier fluid and decreasing the density difference between the two parts of the mixture can reduce the creaming. In detail, decreasing the mean micro-particle size is the more effective of all the three methods. These investigated scenarios give a theoretical guide for manufacturing the mPCM in the future.

3.2.7 Features of n-eicosane based mPCM slurry at different mPCM concentration

The overall mPCM slurry properties are a function of the features of the water and glycol used as the carrier fluid, the features of the dispersed mPCM, and the concentration of mPCM capsules in the mixture evaluated in weight total (w.t.). Therefore, the assessment of the overall mPCM slurry features requires a set of suitable auxiliary equations that consider all the properties of the various components and the concentration of the mPCM.

The properties of the mPCM slurry suspension have been calculated employing the following equations [8,9,12–14]:

$$\rho_{mPCMs} = a_{mPCM} \cdot \rho_{mPCM} + (1 - a_{mPCM}) \cdot \rho_{H2O} \tag{3.17}$$

$$c_{p,mPCMs} = \frac{c_{p,mPCM} \cdot a_{mPCM} \cdot \rho_{mPCM} + (1 - a_{mPCM}) \cdot \rho_{H2O} \cdot c_{p,H2O}}{\rho_{mPCMs}} \tag{3.18}$$

$$\Delta h'_{lat,PCMs} = \Delta h_{lat,mPCM} \cdot a_{mPCM} + c_{p,H2O} \cdot (\theta_{sup,mPCM} - \theta_{inf,mPCM}) \cdot (1 - a_{mPCM}) \tag{3.19}$$

Where a_{mPCM} is the concentration in weight total of the mPCM in the mixture; ρ is the density; c_p is the specific heat capacity $\Delta h_{lat,mPCM}$ is the specific latent heat capacity of phase change; and $\theta_{sup,mPCM}$ and $\theta_{inf,mPCM}$ are the higher and the lower temperature limits of the phase change range respectively. The subscripts *mPCM* and *H₂O* refer to the mPCM and the carrier fluid (water and glycol) respectively; while *mPCMs* is related to the overall mPCM slurry. Different density and specific heat capacity values were calculated for solid and liquid mPCM. It can be inferred that *Δh'lat,mPCS* is a fictitious latent heat, which includes the mPCM latent heat and the sensible heat of the water-glycol carrier, in the phase change temperature range. A parametric analysis can be performed to assess the variation of each feature at the various concentrations under investigation. Since the T-History tests showed small differences between experimental data and data retrieved by the scientific literature and datasheets, the latter were considered reliable and used in this parametric analysis. Table 8 summarises the results obtained considering the values defined in *Table 1* and *Table 2* within the previous equations.

Table 8. mPCM slurry density, specific heat capacity and fictitious latent heat capacities (solid and liquid mPCM) at various mPCM concentrations in weight total.

Material concentration	ρ_{mPCMs} liquid mPCM	ρ_{mPCMs} solid mPCM	$c_{p,mPCMs}$ liquid mPCM	$c_{p,mPCMs}$ solid mPCM	$\Delta h'_{lat,mPCS}$
[-]	[kg/m^3]	[kg/m^3]	[kJ/(kg·K)]	[kJ/(kg·K)]	[kJ/kg]
5 %	1033	1035	3.55	3.53	16.95
10 %	1023	1026	3.51	3.46	26.70
15 %	1012	1017	3.46	3.39	36.45
20 %	1001	1008	3.41	3.31	46.20
30 %	980	989	3.31	3.16	65.70
40 %	959	971	3.20	3.00	85.20
50 %	937	953	3.09	2.84	104.70

The results summarised in *Table 8* are also shown in *Figure 22*. It can be inferred that the higher the mPCM concentration, the higher the reduction of both the mPCM slurry density and the mPCM slurry specific heat capacity. This fact affects the mPCM slurry capacity to store sensible heat. Indeed, this feature is strongly influenced by the product of these two variables (the so-called $\rho \cdot c_p$ product). *Figure 22*(d) compares this feature with the water one (assumed at a fixed value of 4186 kJ/m^{3}K). It is possible to understand from the figure that the specific heat capacity reduction can be up to 73 % respect to the water one. Therefore, it becomes crucial to make sure that the mPCM slurry operates mainly in the transition range where it can store up to 10 times the thermal energy of water.

The mPCM slurry dynamic viscosity is influenced by the heat transfer fluid temperature and the volumetric concentration of mPCM in the mixture. The Vand's model [31] is used to calculate this property, which considers that the temperature dependence influences the carrier fluid only. The Vand's equations are formulated as follows:

$$\mu_{mPCMs} = \mu_{H2O}(T) \cdot (1 + \varphi + A \cdot \varphi^2)^{2.5} \qquad (3.20)$$

$$\varphi = a_{mPCM} \cdot \frac{\rho_{mPCMs}}{\rho_{mPCM}} \qquad (3.21)$$
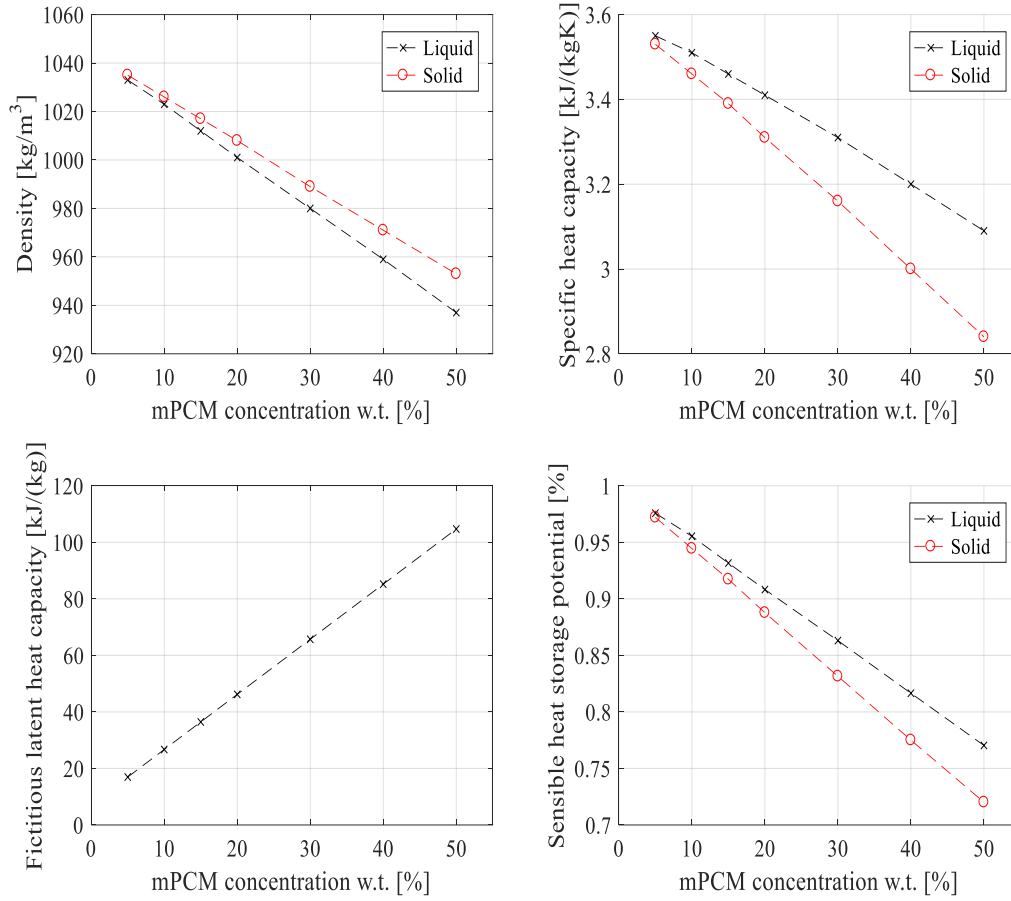
Figure 22. Parametrical analysis of mPCM features versus concentration. (top-left) Density at various concentrations. (top-right) Specific heat capacity. (bottom-left) Fictitious specific latent heat capacity. (bottom-right) Reduction of sensible heat storage capability ($\rho \cdot c_p$ product).
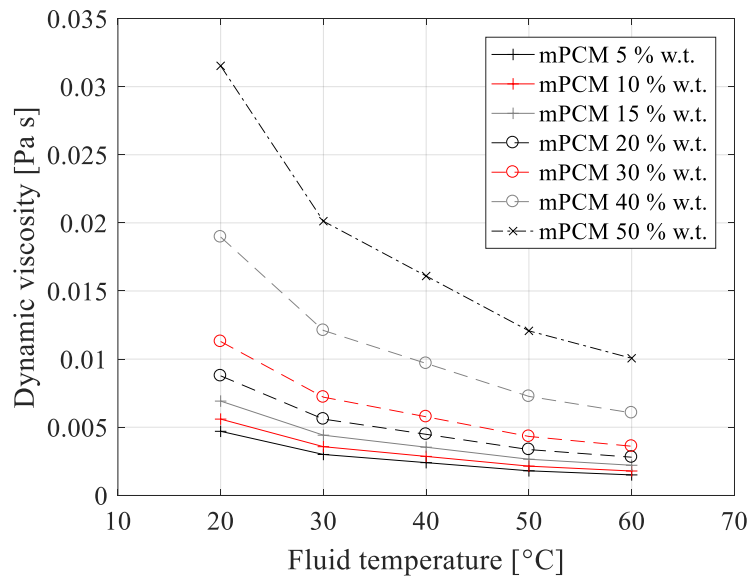
Figure 23. Dynamic viscosity as a function of mPCM concentration and mixture temperature.

Where $\mu_{H2O}(T)$ is the carrier fluid dynamic viscosity that varies according to the temperature (see *Table 1* for details); φ is the volumetric concentration of the mPCM calculated in function of the material density and mass concentration; and *A* is a coefficient influenced by particle diameter (equal to 3.4 for particle size around 17-20 μm [31]). Nevertheless, Vand's correlations do not take into account the non-linearities due to the onset of non-Newtonian behaviour at higher mPCM concentrations. For this reason, it can be considered reliable up to 30 % w.t. concentration. *Figure 23* reports the results of the calculation of the mPCM slurry dynamic viscosities at different mPCM concentrations and different mixture temperatures.

The thermal conductivity of the mPCM slurry varies in case of stationary material (e.g., the fluid used as storage media in the thermal energy storage unit) or flowing material (e.g., the mPCM slurry flowing in the primary collector loop of the solar thermal system). In the case of a stationary fluid, the thermal conductivity $\lambda_{mPCMs,st}$ of the mPCM slurry can be calculated as a function of the features of the two components of the mixture and their concentration with the following Maxwell's relation:

$$\lambda_{mPCMs,st} = \lambda_{H2O} \cdot \frac{2 + \frac{\lambda_{mPCM}}{\lambda_{H2O}} + 2 \cdot \varphi \cdot \left(\frac{\lambda_{mPCM}}{\lambda_{H2O}} - 1\right)}{2 + \frac{\lambda_{mPCM}}{\lambda_{H2O}} - \varphi \cdot \left(\frac{\lambda_{mPCM}}{\lambda_{H2O}} - 1\right)} \tag{3.22}$$

In the case of flowing mPCM slurry an increase in the thermal conductivity must be considered due to the interaction of the mPCM micro-capsules with the carrier fluid. The increase of thermal conductivity is function of the mPCM volumetric concentration and the Peclet number and can be expressed as follows:

$$\lambda_{mPCMs,fl} = \lambda_{mPCMs,st} \cdot (1 + B \cdot \varphi \cdot Pe^m) \tag{3.23}$$
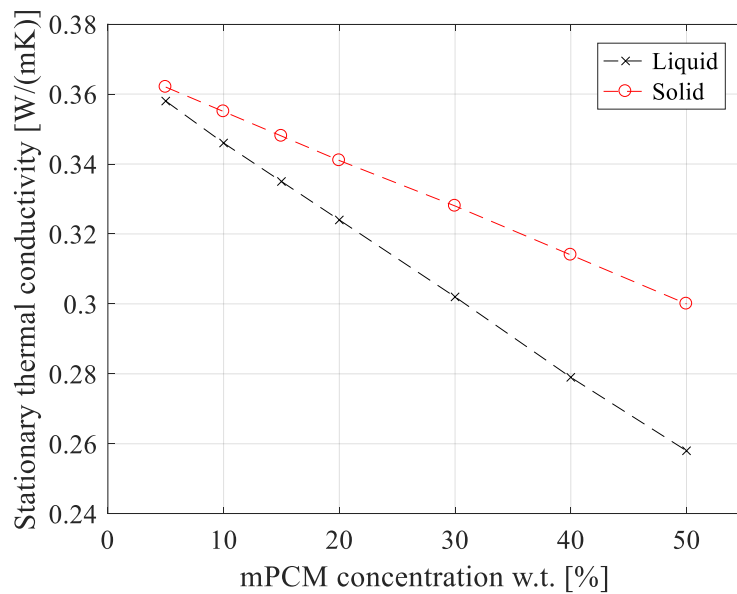
Figure 24. mPCM slurry thermal conductivity in stationary conditions according to the variation of mPCM concentration.

In this equation, the coefficient B and the exponent m are functions of the Peclet number. They are equal to 3 and 1.5, respectively, when the Peclet number is lower than 0.63, and are equal to 1.8 and 0.18 when the Peclet number is in the 0.63 to 250 range, while they are equal to 3 and 0.09 for Peclet numbers higher than 250. Considering circular pipes involved in the heat exchanges the actual Peclet number assumes different values at different polar coordinates r due to the fluid velocity variation along the radius $v(r)$:

$$Pe(r) = \frac{16 \cdot r \cdot v_{mPCMs}(r) \cdot R_{mPCM}^2}{\alpha_{H2O} \cdot R_{pipes}^2} \qquad (3.24)$$

Where r is the polar coordinate; R_{mPCM} is the average radius of the mPCM micro-capsules (assumed equal to 10 μm); α_{H2O} is the thermal diffusivity of the carrier fluid (water and glycol); and R_{pipes} is the internal radius of the pipes in which the mPCM slurry is flowing (that is 1/2" for the pipes of the primary collector loop of the solar thermal system). This formulation can be appropriately integrated to obtain an average Peclet number, which is assumed constant in the whole section.

$$\overline{Pe} = \frac{8 \cdot \bar{v}_{mPCMs} \cdot R_{mPCM}^2}{\alpha_{H2O} \cdot R_{pipes}} = \frac{8 \cdot \dot{m}_{mPCMs} \cdot c_{p,H2O} \cdot R_{mPCM}^2}{\pi \cdot \lambda_{H2O} \cdot R_{pipes}^3} \qquad (3.25)$$

Where $c_{p,H2O}$ and λ_{H2O} are the water specific heat capacity and thermal conductivity respectively. Their values are assumed constant and are shown in *Table 1*. The $\dot{m}_{mPCMs}$ is the mass flow rate of the mPCM slurry and varies during time according to the control logic implemented. The mass flow rate assumes values in the range 0 – 120 kg/h for the entire primary loop circuit and in the range 0 – 15 kg/h within the riser pipes of the solar thermal collector.

Eventually, the stationary mPCM slurry thermal diffusivity, α_{mPCMs}, can be calculated for various mPCM concentrations. This parameter is particularly important to enhance the thermal energy storage capabilities. *Figure 26* reports the variation of the stationary thermal diffusivity of solid and liquid PCM according to the concentration variation. From *Figure 26* it can be inferred that the thermal diffusivity – at temperatures out of the phase transition range – remains in the range ± 10 % of the water and glycol thermal diffusivity.

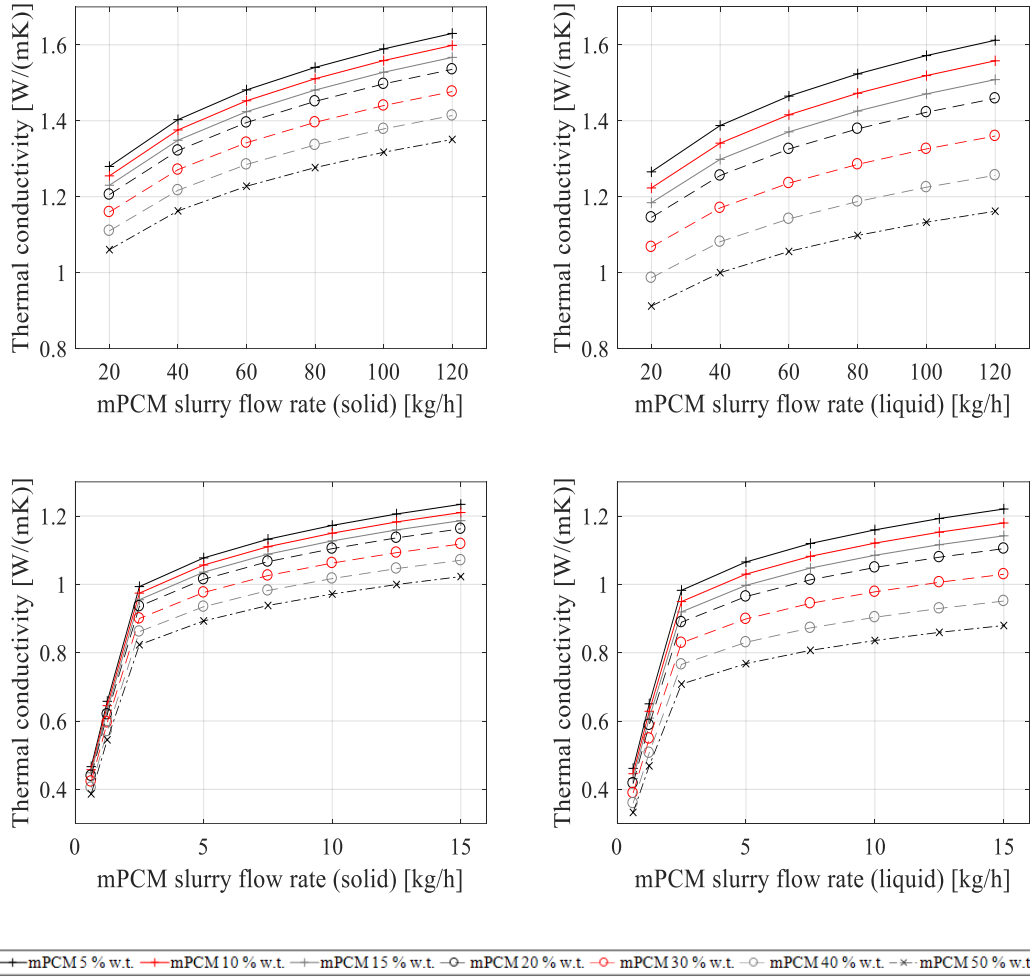$$\alpha_{mPCMs} = \frac{\lambda_{mPCMs,st}}{c_{p,mPCMs} \cdot \rho_{mPCMs}} \qquad (3.26)$$

Figure 25. Thermal conductivity of the flowing slurry mPCM at various flow rates. (top-left) Solid PCM - main system pipes. (top-right) Liquid PCM - main system pipes. (bottom-left) Solid PCM - collector pipes. (bottom-right) Liquid PCM - collector pipes.
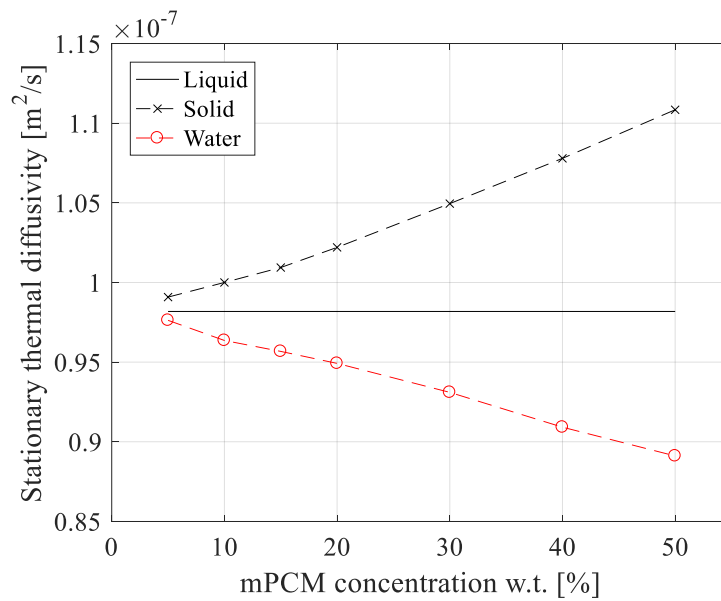

Figure 26. Stationary thermal diffusivity of mPCM slurry at various concentrations.

3.2.8 Lesson learned from the evaluation of the slurry mPCM material properties

A preliminary investigation of the material properties was necessary to better understand the suitability of the mPCM slurry for being used as heat transfer fluid and storage media within solar thermal systems. This investigation followed the indications pinpointed from the scientific literature review undertaken in Chapter 2. The three main mPCM slurry features that affect the system performance are:

- Rheological properties (e.g., viscosity, pipe clogging, etc.);
- Thermal properties (e.g., specific heat capacity, latent heat capacity, thermal conductivity, heat storage capability, etc.);
- Physical stability (e.g., the occurrence of creaming phenomenon).

In detail, the primary concern when the SolHe-PCM project was conceived was the issue "*can the slurry mPCM flow in the pipes of a solar thermal system?*". The primary result of the rheological tests was a qualitative answer to this issue. The material, at weight concentration up to 45 %, can be straightforwardly used in the solar thermal system without particular pumping problems. For higher concentrations, problems may arise due to a stronger non-Newtonian behaviour and increased viscosity of the slurry. The pressure drop tests allowed quantitative results to be carried out and used for more detailed evaluations. In particular, the parametrical analysis undertaken in Section 3.2.6 showed how the maximum dynamic viscosity increase (occurring at 50 % w.t. concentration and 20 °C) do not overcome 10 times the dynamic viscosity of water and glycol (and it is less than 3.5 times the water one). Moreover, higher temperatures further reduce this difference.

Regarding the thermal properties, the T-History tests allowed to measure the specific and latent heat capacity of the mPCM slurry as a whole. The results were used to calibrate further parametrical analysis. This studies highlighted how the material significantly overperform the water within the phase change range, while the density and specific heat capacity reduction can negatively affect the mPCM slurry performance out of this range (with a decrease of the material storage potential up to 27 %). This fact highlights how – when a phase change is involved – it is crucial to correctly design the system (and its controller) in order to work mainly at operative temperatures contained in the transition range. Eventually, the material showed a certain physical instability due to the occurrence of creaming. This phenomenon was studied qualitatively and quantitatively. From the very first tests, the creaming appearance seems to be the most annoying drawbacks of the system because it can affect storage uniformity and cause pipe clogging. Several configurations of the system were tested (and are described in Section 3.3) to deal with this material shortcoming.

3.3 Design and construction of a full scale prototype of solar thermal system adopting micro-encapsulated Phase Change Material slurry as heat transfer fluid and thermal energy storage media

Since the most suitable mPCM slurry to be used as the heat transfer fluid was identified and its properties investigated, it was possible to properly define and build a full-scale prototype to test the proposed technology. Starting from the schematics and concepts outlined in Section 3.1, various steps were necessary to design and build the system correctly. Firstly, each component of the system (i.e., solar collector, piping and pumping system, thermal energy storage unit) must be adequately defined. Secondly, a monitoring system must be devised to gather the data necessary to assess the system performance and automatically regulate its functioning Finally, to be able to test the system under realistic operative conditions, a heating demand-side simulator was conceived and built.

The present Section is focused on the description of the various features of each component constituting the SolHe-PCM solar thermal system. Furthermore, control logic to manage the innovative PCM slurry based technologies is herewith presented. The hydraulic components were developed with the aid of the company Teknoenergy, an Italian producer of solar thermal systems. While the monitoring and control system was devised using LabView programming language on an embedded controller developed with the aid of the company Teseo, an Italia company dealing with automatic industrial regulation and control systems. An overall schematic of the prototype and its monitoring control system is outlined in *Figure 27*. *Figure 28* shows the Visual Interface (VI) of the LabView code used to monitor and regulate the system.
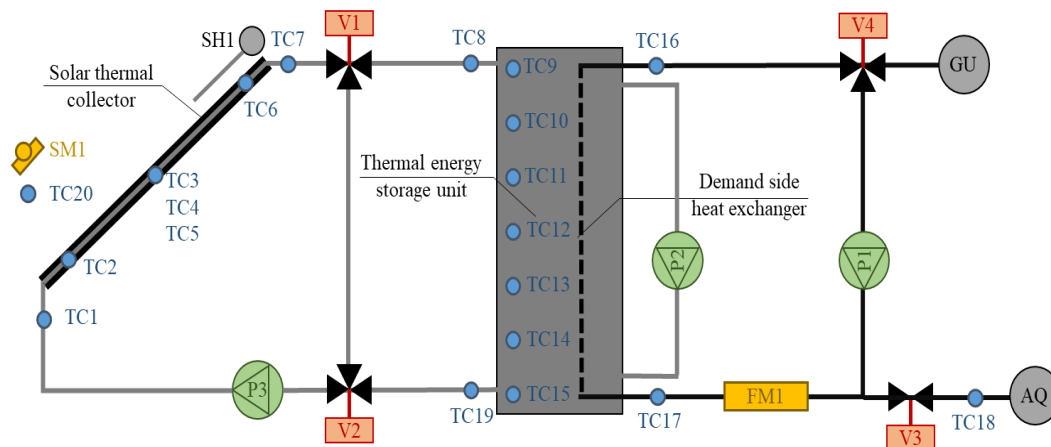
Figure 27. Schematic of the SolHe-PCM prototype.
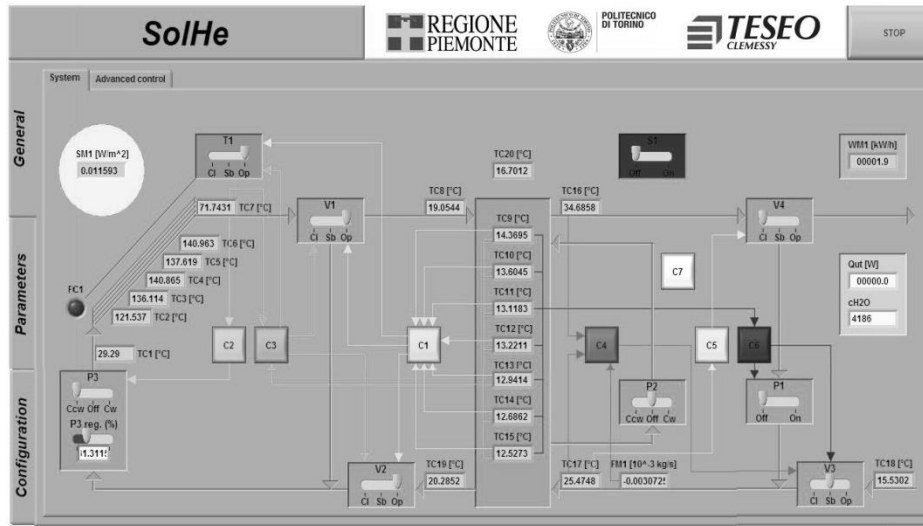
Figure 28. LabView Visual Interface of the monitored and controlled prototype.

3.3.1 The solar thermal collector

The specifications of the panel were chosen after the rheology tests, which demonstrated that the mPCM slurry could flow in the pipes of flat-plate solar collectors up to a specific viscosity. In future development of the system, the optimisation of the hydraulic circuits could be considered. At present, thanks to the fact that the rheological properties of the fluid used for the prototype are not so different from those of a typical glycol-water solution, a commercial solar thermal collector has been adopted for the measurement campaign. The collector is equipped with a curtain (or shutter) that can shade the absorber plate to avoid overheating processes. The curtain is controlled by a stepper motor that can be manually operated by the electric cabinet or automatically regulated. In case of automatic control, two possible states only were considered (δ_i: shutter fully opened, and δ_{ii}: shutter fully closed), as shown in *Figure 29*.

Figure 29. The solar thermal collector used in the full-scale prototype.

The main features of the chosen collector are summarised in *Table 9*:

Table 9. Specification of the solar thermal collector.

Specification	Symbol	Value	m.u.
Panel length	L	2.1	m
Panel width	l	1.1	m
Panel thickness	s	0.20	m
Number of heat exchanger pipes	N_{pipes}	8	-
Distance between heat exchanger pipes	W_{pipes}	0.13	m
External diameter of pipes	$D_{ex,pipes}$	$8 \cdot 10^{-3}$	m
Inner diameter of pipes	$D_{in,pipes}$	$7.6 \cdot 10^{-3}$	m
Plate thickness	s_{plate}	$2 \cdot 10^{-4}$	m
Plate absorbing coefficient	α_{plate}	0.95	-
Plate emissivity	ε_{plate}	0.05	-
Plate conductivity	λ_{plate}	385	$W\,m^{-1}\,K^{-1}$
Bond width	l_{bond}	$2 \cdot 10^{-4}$	m
Cavity thickness	s_{cavity}	0.025	m
Cover thickness	s_{caover}	$4 \cdot 10^{-3}$	m
Cover extinction coefficient	K_{caover}	16.10	m^{-1}
Air refraction index	n_1	1	-
Cover refraction index	n_2	1.526	-
Cover emissivity	ε_{cover}	0.8	-
Thickness of the bottom insulation	s_{ins_bot}	0.05	m
Thickness of the edge insulation	s_{ins_edg}	0.02	m
Insulation conductivity	λ_{ins}	0.04	$W\,m^{-1}\,K^{-1}$

3.3.2 Thermal energy storage unit

Many examples of PCMs based thermal energy storage tanks for solar systems can be found in the literature (see Section 2.3.2). As it can be inferred from *Figure 27*, the thermal energy storage unit is characterised by a primary open loop with the heat transfer fluid (the mPCM slurry) that is used both flowing in the solar thermal collector and as storage media. The secondary loop, which aims to deliver the space heating to the end users, is connected with the thermal energy storage unit with a spiral heat exchanger made by a copper pipe (the so-called demand-side heat exchanger in *Figure 27*). The volume of the storage tank was selected in accordance with the collector size and the space heating requirements. Two different thermal energy storage units were used during the present thesis. The first design was not able to mitigate the mPCM slurry creaming occurrence. Thus the storage tank was substituted during Summer 2017.

3.3.2.1 Thermal energy storage unit: version 1

The primary thermal energy storage unit adopted was a steel made inertial tank with an internal volume of 200 l and a maximum operating pressure of 3 bar. The thermal dispersions of the storage tank were limited to an insulation layer of 8 cm realised with fibreglass. The thermal energy storage unit is shown in
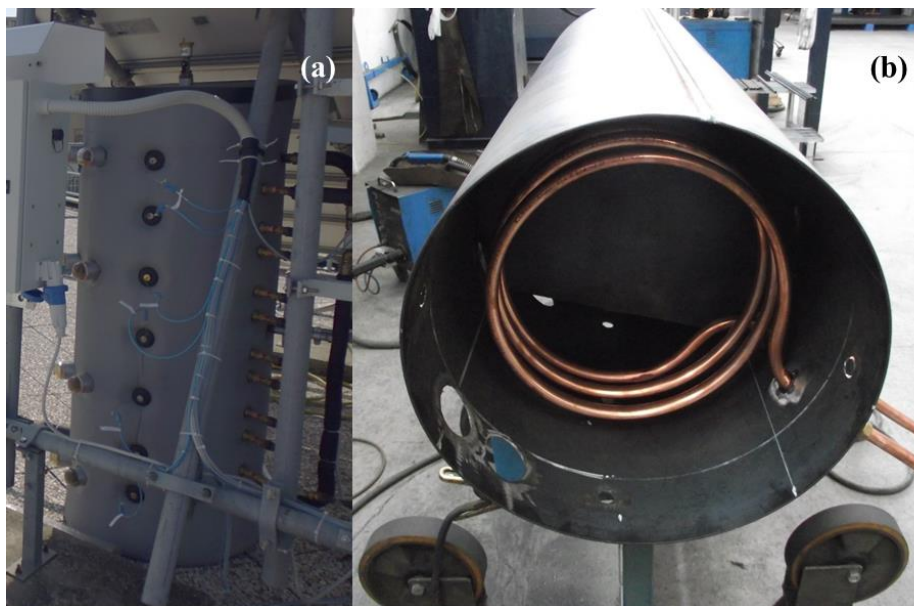
Figure 30. (a) Overall view of the thermal energy storage unit installed in the full-scale prototype of the solar thermal system. (b) Overview of the interior of the thermal energy storage tank (with a focus on the copper heat exchanger and the internal partitions).

In this configuration, the demand-side heat exchanger has many by-pass possibilities to choose the heat exchange surface (whole storage tank, upper part,

lower part). Specific measures concerning the geometric optimisation of the tank may be adopted in the future.

As aforementioned the central issue regarding the PCM slurry based solar thermal system is the occurrence of instability and stratification of the material due to the creaming effect. This aspect is particularly true when the material is not moved, likewise in thermal energy storage unit. Twelve transparent inspection openings were made in the thermal energy storage tank at different heights to have visual control of this phenomenon. Moreover, the mPCM slurry was continuously kept in motion in the storage tank, even during the off periods. This feature was made possible through the use of partitions in the storage tank - which can be seen in *Figure 30*(b). Furthermore, a bypass circuit, with a secondary peristaltic pump, is switched on when the main pump of the primary loop is stopped. This process causes additional energy consumption and makes the pumping system more complicated. Furthermore, if the mPCM slurry is mixed continuously, the heat transfer fluid in the storage tank cannot stratify, and the heat transfer to the secondary loop becomes worst. However, at this stage, the adoption of a bypass circuit was chosen because it was the easiest and cheapest way to overcome the creaming phenomenon. Indeed, it would have been possible to find a chemical-physical solution for the creaming problem. Nevertheless, such a study was beyond the scope of this work, although it may be dealt with in the future before the system is pushed on the market. Furthermore, it should be noted that, on the one hand, the electric energy consumption of the auxiliary recirculation pumps is expected to be very low (as the speed of the fluid is kept quite low to avoid the creaming process). On the other, the control strategies of the system will be aimed at optimising the exploitation of the latent heat of the system. Therefore, for most of the time, the fluid will be roughly isothermal, and stratification in the storage tank will not take place.

Nevertheless, the measures adopted to monitor and contrast the creaming phenomenon proved to be insufficient. In detail:

- Since the internal layer of the tank was not realised in stainless steel, rust appeared affecting both the composition of the heat transfer fluid used as storage media and the clearness of the twelve inspection openings used to monitor the creaming phenomenon;
- The experimental tests undertaken during the Winter season 2016-2017 demonstrated that the flow rates in the thermal energy storage unit guaranteed by the secondary peristaltic pump and the tank partitions were not sufficient to oppose the creaming phenomenon. Indeed, the mPCM slurry was mixed slower than the creaming occurrence. This problem caused significant uncertainty in the results due to a gradient in the concentration of the heat transfer fluid.

3.3.2.2 Thermal energy storage unit: version 2

A new version of the thermal energy storage tank was designed to overcome the previously mentioned drawbacks. In detail, was chosen a solution with the following characteristics:

- Envelope material composed of a material that does not cause rust formation and has chemical compatibility with the mPCM slurry;
- Envelope material transparent or translucent to enhance the visual inspection possibilities;
- Presence of a mechanical mixer of adequate power to contrast the creaming occurrence.

To address these specifications a new thermal energy storage unit was installed. In detail, it consisted of a plastic tank of 300 l volume made by high molecular density polyethylene. The variation in volume – compared to the previous 200 l version – was due to manufacturer product availability. The envelope colour is translucent white, which allows visual inspections to be undertaken effectively. The plastic tank is equipped with a vertical mixer of thermoplastic material. An electronic inverter and an external timer activate the mixer at constant time intervals, in order to mix the mPCM slurry and contrast the creaming phenomenon. A spiral 2.5 kW copper-made heat exchanger was inserted in the tank as the demand-side simulator. The tank cover was appropriately drilled with holes that allow various thermocouples to be added at different heights of the storage unit. The same fibreglass layer adopted for the previous version of the storage tank can be additionally used as envelope insulation. It is worth to mention that are still valid the considerations discussed in the prior storage version, concerning the drawbacks caused by the additional energy consumption due to the mixing system and the absence of storage media stratification.
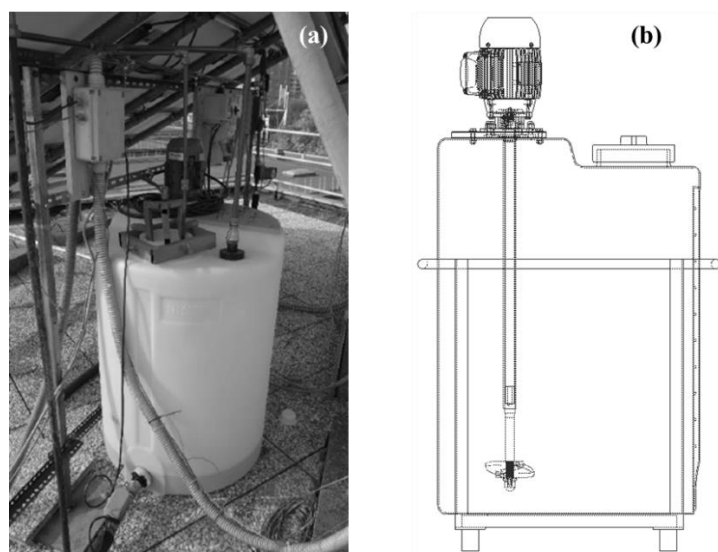
Figure 31. (a) The second version of the thermal energy storage unit installed in the SolHe-PCM full-scale prototype. (b) A blueprint of the thermal energy storage tank and its mechanical mixer.

3.3.3 Pumps, valves and pipes

As well as for the solar collector, the rheological tests demonstrated that the mPCM slurry could smoothly flow in traditional piping systems used for hydraulic purposes. For this reason, copper pipes with a diameter of 1" were selected for the primary loop of the solar thermal collector.

Rupture of the mPCM microcapsules can cause several problems to the system. In particular, leakage of the PCM from the capsule could induce clogging of the pipes and a change in the thermal properties of the heat transfer fluid. Damage and cracking of the capsules are usually due to mechanical stress induced by the pumps [32] or the valves.

Valves were necessary for the primary loop of the solar thermal system to realise the by-pass tee highlighted in *Figure 32*. This measure was appropriate to contrast the creaming phenomenon. Indeed, when there is not sufficient solar radiation, and the mPCM slurry should not be flowing in the primary collector loop, the creaming can occur even in the pipes of the primary loop causing the appearance of mPCM high concentration rates in the upper part of the piping system, which leads to clogging the pipes. For this reason, the material must be continuously kept in motion by the primary pump also in the primary collector loop. However, to avoid heat dispersions toward the ambient, this recirculation must be separated from the one interesting the material contained in the storage (with higher exergy content). Therefore, solenoid valves were chosen to by-pass the thermal energy storage unit when necessary (in *Figure 27* and following schematics, these valves are indicated with the acronyms V1 and V2). Ball solenoid valves were adopted for this purpose since producers ensured that this valve typology causes lower mechanical stress on the fluid compared to other typologies (e.g., piston solenoid valves). The valves V1 and V2 have only two operating modes: (δ_i) fully allow the heat transfer fluid to flow in the thermal energy storage tank; (δ_{ii}) by-pass mode.
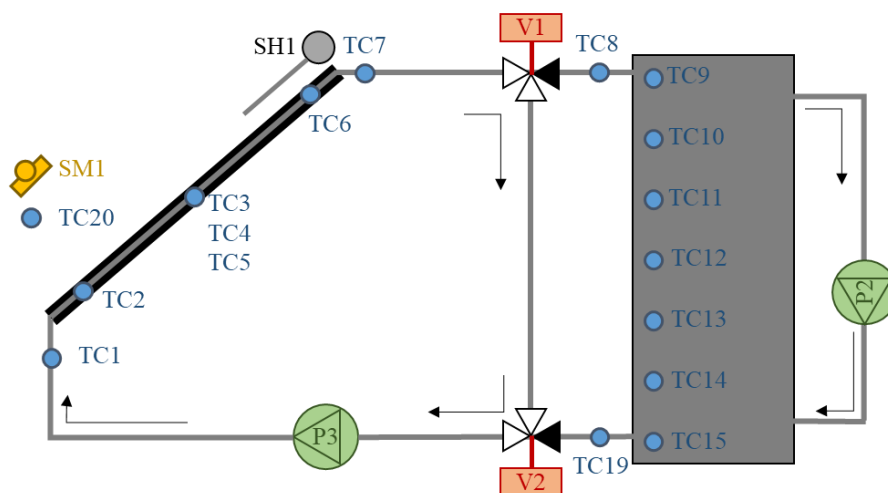
Figure 32. Recirculation of the mPCM slurry. The by-pass tee allows the fluid in the primary collector loop to be recirculated by the primary pump; while the secondary pump (or the mixer) recirculates the material in the storage unit.

A consequence of this configuration – with a bypass tee where the fluid is continuously kept in motion – is an additional energy demand due to the pumping power. However, this extra-consumption has to be considered proper of the prototype only and not attributable to the final SolHe-PCM technology. Indeed, the recirculation of the fluid in the primary loop is an attempt of attenuating the creaming phenomenon occurring in the storage tank. The scientific literature has shown various possible solutions to overcome this shortcoming (see Section 2.2.5) mainly with the use of surfactants in the mixture. It is expected that the creaming problem will be solved in the final version of the SolHe-PCM technology. However, this research topic involves mainly material science studies, and they are not included among the scopes of the present thesis. For this reason, additional speculations on this topic have been neglected and are left to future works.

Centrifugal pumps do not induce capsule rupture, and only a small number of microcapsule shells has been damaged or destroyed during long-term operations [64, 65]. However, peristaltic pumps were adopted to further reduce the possible risks due to such problems. These pumps offer the advantage of not having any moveable parts in direct contact with the fluid that flows inside the pipe. Therefore, there are fewer mechanical actions than in any other kind of pump. The main pump of the primary loop – which is a programmable Verderflex Scientific AU UV 3000 HD, whose main features are summarised in *Table 10* – is shown in Figure 7. In the schematic of *Figure 27*, this pump is indicated with the acronym P3.

Table 10. Specifications of the Verderflex Scientific AU UV 3000 HD pump.

Specification	Value	m.u.
Power consumption	5-55	W
Protection rating	IP66	-
Speed control	4-20	mA
	0-10	V
Speed range	10-250	RPM
Standard tube material	verderprene	-
Standard tube inner diameter size	$8 \cdot 10^{-3}$	M
Standard tube inner diameter thickness	$3.2 \cdot 10^{-3}$	M
Nominal flow rates	5.82-145.50	l/h
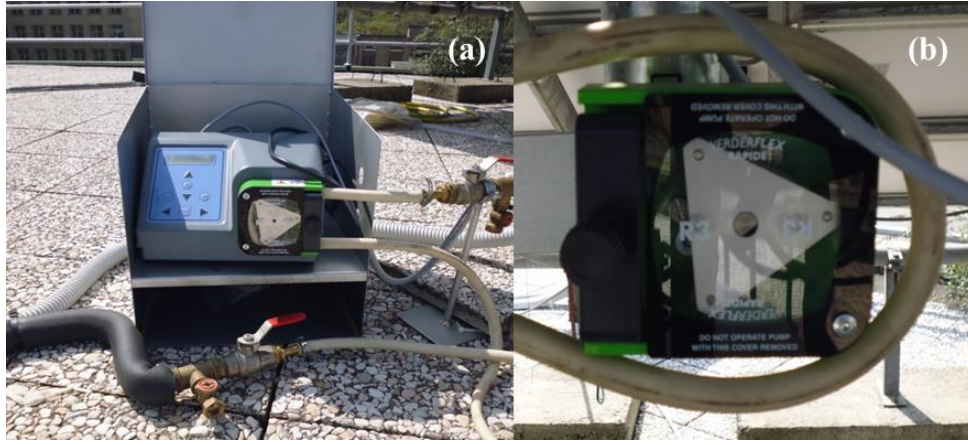
Figure 33. (a) The peristaltic pump that regulates the primary loop of the solar thermal system. (b) the peristaltic recirculation pump that was present in the initial version of the thermal energy storage tank.

The main characteristics of the recirculation pump of the storage bypass loop, which is a Verderflex OEM M3000, are summarised in *Table 11*. In *Figure 27* this pump is indicated with the acronym P2. The recirculation pump was removed when the initial version of the storage tank was substituted with the secondary version that integrates a vertical mixer.

Table 11. Specifications of the Verderflex OEM M3000 pump.

Specification	Value	M.u.
Power consumption	55	W
Protection rating	IP66	-
Speed control	set	-
Speed possibilities	55 or 125 or 240	RPM
Standard tube material	verderprene	-
Standard tube inner diameter sizeFigure 27	$9.6 \cdot 10^{-3}$	M
Standard tube inner diameter thickness	$3.2 \cdot 10^{-3}$	M
Nominal flow rates	46.9 or 106.5 or 204.5	l/h

3.3.4 Demand-side simulator

A suitable demand-side simulator was designed to be able to test the prototype under realistic boundary conditions. The demand-side simulator consists of a 2.5 kW spiral heat exchanger made of copper and in the actuators necessary to modulate

the space heating demand. Indeed, a controlled water flow rate is used in the spiral heat exchanger to extract, at a controllable rate, the thermal energy stored in the tank. Aqueduct water was used as heat transfer fluid in the demand-side simulator. The aqueduct water was preheated by mixing with the warm water supplied by the thermal energy storage unit. This configuration was adopted to be able to extract the desired thermal energy from the storage tank with a water flow rate whose temperature is similar to the return temperature of a real radiant panel heating system. The control logic necessary to adequately control the demand-side simulator is described in Section 3.3.6, while *Figure 34* shows the actuators used to implement this control logic. In detail:

- The solenoid 2-way valve V3 controls the water flow rate, to meet the required heating demand. V3 allows a proportional regulation through Pulse Width Modulation (PWM).
- The solenoid 3-way valve V4 adjusts the water temperature at the storage inlet (TC17) to simulate the return temperature of a real radiative space heating system operating at low temperatures. V4 allows a proportional regulation through Pulse Width Modulation.
- The pump P1 compensate the pressure drops occurring in the demand-side simulator piping circuit to enable the recirculation of the water supplied by the thermal energy storage unit.
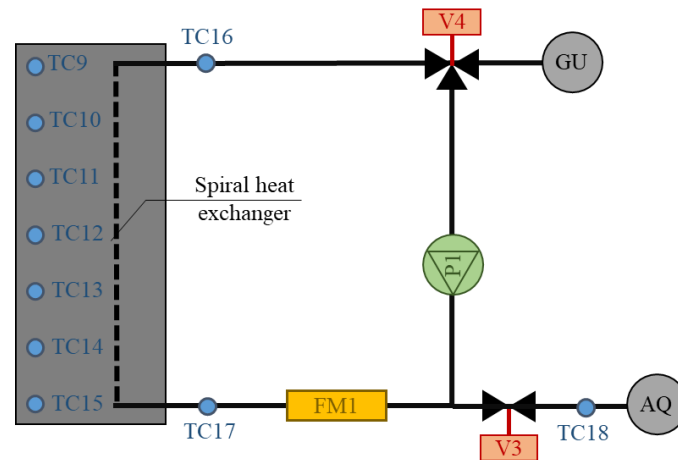
Figure 34. Schematic of the demand-side simulator used to extract energy from the thermal energy storage unit, thus simulate typical profiles of space heating demand with low-temperature radiative systems.

3.3.5 Data gathering system

The core of the monitoring and control system is a National Instrument compactRIO (or cRIO). It is a real-time embedded industrial controller, whose

configuration can be easily custom made with the addition of reconfigurable I/O modules (e.g., thermocouple module, voltage or current I/O module), communication modules (e.g., Ethernet output) or data storage modules (e.g., SD card module). *Figure 35* shows the electrical cabinet hosting the embedded controller that regulates the SolHe-PCM full-scale prototype.

The National Instrument compactRIO allows both the control of the system and the monitoring of the system parameters. The controller was programmed employing LabVIEW and can be accessed with a Visual Interface through an Ethernet cable. The users can set the data acquisition time according to their specific requirements. Even if this kind of controller allows minimal frequency rate of acquisition to be established, in general for thermodynamic processes dynamics are relatively slow and the acquisition time can be higher than 1 min. Data are stored on an SD card embedded in a module of the controller. Data gathering is made possible by the use of specific sensors:

Figure 35. The electrical cabinet designed and installed to control the full-scale prototype.

- An IME static wattmeter in the electric cabinet. This component is used to measure the electrical power absorbed by the circulation pumps in the PP1 and PP2 primary loops. It has an accuracy of "cl.1", according to the EN/IEC 62053-21 standard, with a resolution of 0.1 kWh. The acquisition frequency is 50 Hz, and it communicates with the rest of the control system using an M-Bus.
- Twenty armoured TERSID MTS-15101-T-300 thermocouples. These are T type copper/constantan thermocouples, which are used to monitor and control the temperatures in the different loops of the system. The thermocouples are

highlighted in *Figure 27* with the acronym TC and follow a progressive enumeration from 1 to 20.

- A SITRANS FC flow-meter. This element is a Coriolis flow-meter composed of a flow-rate sensor (MASS 2100) and an electronic transmitter (MASS 6000IP67). This sensor is used to monitor the water mass flow rate in the demand-side simulator. The advantage of using a Coriolis flow meter is that it directly returns a mass flow rate, and it allows the uncertainty pertaining to the density to be neglected. The nominal declared sensitivity is better than 0.1% of the mass flow rate, and the accuracy of the density is equal to $5 \cdot 10^{-4}$ gcm^{-3}. The MASS 6000IP67 transmitter is combined with the sensor, and it delivers exact multi-parameter measurements (i.e., mass flow, volume flow, density, temperature and fraction). The flow-meter is highlighted in *Figure 27* with the acronym FM1.
- A Campbell Scientific LP02 pyranometer. This component was placed next to the panel with the same tilt, in order to monitor the solar incident radiation on the tilted surface. The spectral selectivity is from 305 nm to 2000 nm (+/- 5 %), and the sensitivity is 10-40 $\mu VW^{-1}m^{-2}$. The pyranometer is highlighted in *Figure 27* with the acronym SM1.

3.3.6 Development of control logic for the solar thermal system

The real-scale prototype needs to be controlled using appropriate strategies. Two sets of control logic have been identified:

- Control 1 (or alternatively Control 1'), Control 2, and Control 3 regulate the primary loop of the solar collector;
- Control 4, Control 5, and Control 6 manage the discharge of the energy stored in the storage tank, thus the demand-side simulator.

The overall control logic was uploaded on the compactRIO embedded controller and can be activated/deactivated individually through the Visual Interface of the controller.

The first set of control logic is a combination of Rule-Based Controllers (RBC) that regulates the primary loop of the solar collector. It deals with the pump P3 flow-rate regulation and complies with the physical or technological limitation of the system. As it can be inferred from the subsequent description, constraints and pump management are included in different control formulations (i.e., Control 1 regulates the pump, while Control 2 and 3 manage the system constraints). Furthermore, the set-point chosen for Control 1 were defined with the expertise accumulated over years of regulation of traditional solar thermal systems. Therefore, during the definition of this set of control logic regulating the primary loop of the solar system emerged the necessity of going further, looking for innovative control logic capable of completely enhance the benefits offered of such

new technology. This need led to investigate the model-based predictive controllers, described in Chapter 5 of the present thesis.

The latter set of control logic has the goal of regulating the demand-side simulator to analyse the performance of the overall solar system during actual operative conditions. It can be used or to remove a constant heat flux from the thermal energy storage unit or to reproduce the time profile of space heating demand. When a relatively high constant heat flux is removed (more than 2 kW) the amount of energy stored in the thermal energy storage unit is minimised; and the collector can be tested under almost steady boundary condition. Otherwise, a time-series vector of required heat fluxes can be used as input to simulate a typical space heating demand profile over time. This profile can be defined by means of dynamic thermo-energetics simulations (white-box methods) or derived from the analysis of real monitored data (inverse or data-driven methods).

The following *Table 12* summarises the control logic used to regulate the full-scale prototype of SolHe-PCM.

Table 12. Summary of the control logic of the SolHe-PCM system

Name	Input	Output	Typology	Scope
Control 1	SM	P3	RBC	Regulate flow rate
Control 1'	TC7	P3	PI	Regulate flow rate
Control 2	TC7	V1, V2	RBC	Contrast creaming
Control 3	storage temp.	V1, V2, SH1	RBC	Ensure safety
Control 4	TC17	V4, P1	RBC, PI	Regulate supply temp.
Control 5	TC16, TC17	V3	PI	Regulate flow rate
Control 6	TC16, storage temp.	V3	RBC	Regulate flow rate

3.3.6.1 Control 1 and Control 1'

This control logic represents the central controller for the primary loop that includes the solar collector. Two different versions of this controller were developed, and their schematics are reported in *Figure 36*.

Control 1 – defined in *Figure 36*(a) – is an open-loop controller on the solar radiation measured by the pyranometer SM1. It is based on the assumption that the higher the solar thermal radiation, the higher the collector production. The pump P1 is regulated consequently with more rounds per minute speed – thus flow-rates – when high solar radiation levels occur. This assumption was necessary to reduce the temperatures involved in the solar thermal collector heat exchanges. Nevertheless, since open-loop control does not ensure direct feedback on the

controlled variable, this solution is not recommended when closed-loop solutions can be implemented.

For this reason Control 1' – defined in *Figure 36*(b) – was developed with a closed-loop regulation. Control 1' uses feedback on the temperature at the outlet of the panel θ_{out}, which is monitored by the thermocouple TC7. The fundamental idea of this solar system is to exploit the latent heat as much as possible, in order to maximise the overall energy efficiency of the system. For this reason, the optimal working condition of the solar collector is the one in which the mPCM slurry concludes its transition phase precisely at the collector outlet. In this way, it is possible to maintain the lowest possible average operating temperature of the solar panel (thus minimising the losses) while still optimising the thermal energy storage (since the heat for the isothermal phase change is fully exploited). From a practical point of view, this situation occurs when the temperature of the heat transfer fluid at the outlet of the solar thermal collector is equal (or slightly above) to the higher temperature of the melting range.

$$\theta_{out} = \theta_{TC7} \cong \theta_{sup} \qquad (3.27)$$

Therefore, the logic that drives this controller is as follows: the temperature of the heat carrier fluid is detected at the outlet of the solar collector and is used as input in a Proportional Integral Derivative (PID) system that adjusts the rounds per minute speed of the peristaltic pump P1 in order to keep such a temperature as close as possible to the set point fixed. The set-point temperature was chosen equal to 40 °C (e.g., 3 °C higher than the nominal melting temperature of the mPCM) in the full-scale prototype. The user can adjust the set-point value using the Visual Interface of the controller. Since this control can be affected by *wind-up* drawbacks (mainly due to Integral error accumulation during night time when the set point cannot be tracked) anti wind-up filters had to be implemented. Otherwise, PD formulations, which neglect the Integral error term, resulted in over perform PID regulation. A further discussion of this Control 1' logic can be found in Section 3.4.3 where this controller is implemented in the Simulink numerical model of the solar thermal system.
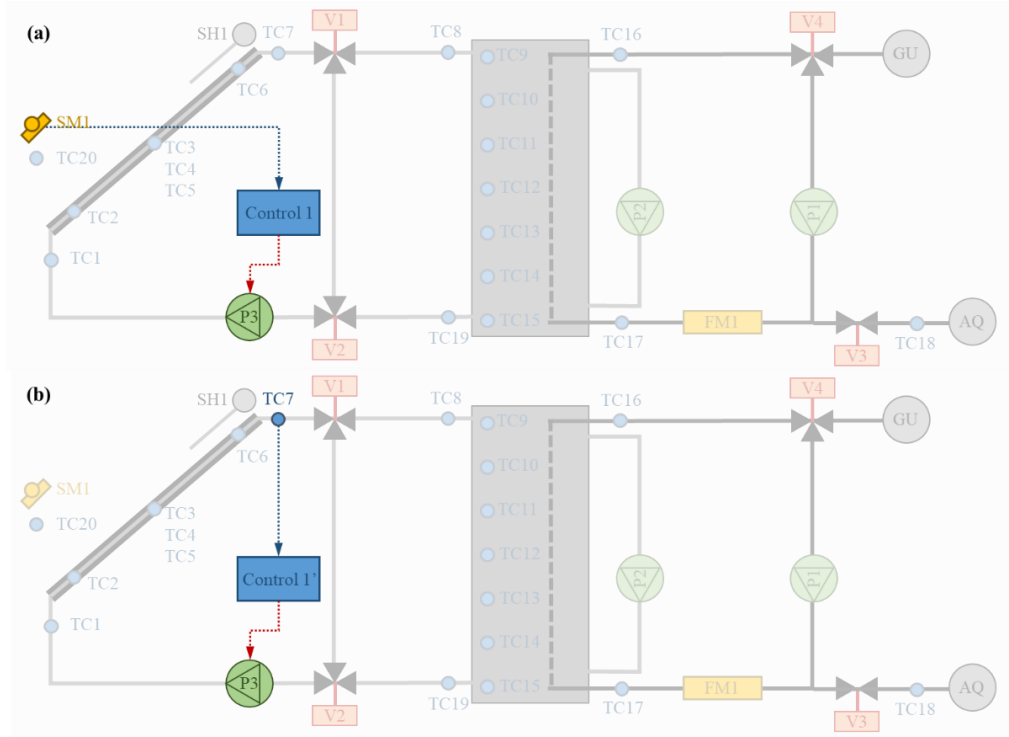
Figure 36. (a) Schematic of the sensors and actuators involved in the Control 1.
(b) Schematic of the sensors and actuators included in the Control 1'.

3.3.6.2 Control 2

This control logic it is used to manage the coupling between the solar collector and the thermal energy storage tank. It aims at achieving a physical constraint of the system. Specifically, it avoids the necessity of feeding the thermal energy storage unit with a heat transfer fluid that is colder than the storage media contained in the thermal energy storage unit. For this reason, the average temperature (θ_{st}) of the seven thermocouples located inside the storage unit (TC9, TC10, TC11, TC12, TC13, TC14 and TC15) is measured and compared with the temperature at the collector outlet, which is measured by TC7. If the average storage temperature is higher than the panel outlet temperature, the circulation between the collector and the thermal energy storage unit is stopped, and valves V1 and V2 are set in by-pass mode. A criterion must also be chosen to define the condition of return at the previous system state. In order to avoid excessively rapid switching between the by-pass and the normal mode, the circulation between the collector and the storage is only restored when $\theta_{out} \geq (\theta_{avg} + 5\ °C)$. The two criteria can be expressed with the following formulations:

$$if\ \theta_{out} = \theta_{TC7} < \overline{\theta_{st}}\ then\ (V1 = \sigma_{ii}\ and\ V2 = \sigma_{ii}) \tag{3.28}$$

$$if\ \theta_{out} = \theta_{TC7} > \overline{\theta_{st}} + 5\ then\ (V1 = \sigma_i\ and\ V2 = \sigma_i) \tag{3.29}$$

Figure 37. (a) Schematic of the sensors and actuators involved in the Control 2.
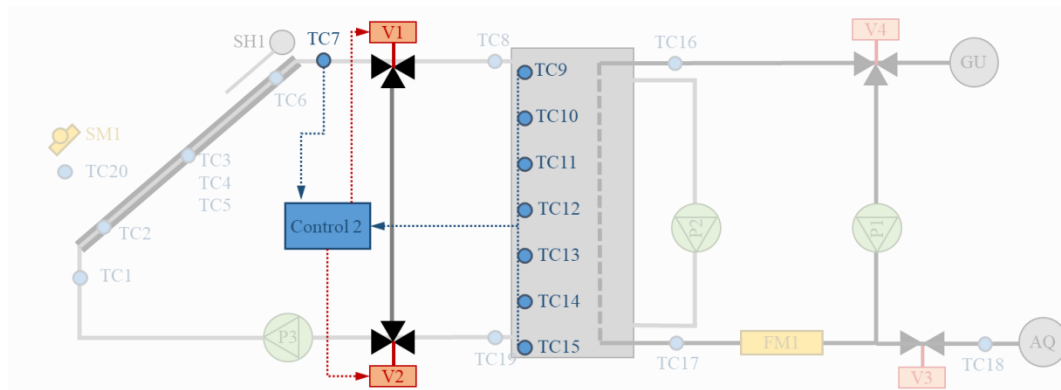
3.3.6.3 Control 3

This control logic pertains to a safety constraint for technological reasons. In order to avoid problems due to the decay of the material properties, the mPCM slurry must be kept at a temperature that does not exceed 65 - 70 °C. Moreover, some of the components of the storage tank are designed for a maximum temperature of about 65 °C. Therefore, the control C3 switches on if one of the seven thermocouples inside the storage tank (TC9, TC10, TC11, TC12, TC13, TC14 or TC15) reaches a temperature equal or above 65 °C. When C3 is activated, the curtain of the solar collector comes down and valves V1 and V2 are set in the by-pass mode. In this way, the hot heat transfer fluid no longer flows in the storage unit and the temperature in the storage tank decreases. The normal working conditions are restored when all the temperatures recorded by the thermocouples inside the storage tank are lower than a safety value of 60 °C. The two criteria can be expressed with the following formulations:

$$if \ \max|\theta_{st}| \geq 65°C \ \ then \ (V1 = \sigma_{ii} \ and \ V2 = \sigma_{ii} \ and \ SH1 = \sigma_{ii}) \qquad (3.30)$$

$$if \ \ \max|\theta_{st}| \leq 60°C \ \ then \ (V1 = \sigma_{i} \ and \ V2 = \sigma_{i} and \ SH1 = \sigma_{i}) \qquad (3.31)$$

Figure 38. Schematic of the sensors and actuators involved in the Control 3.
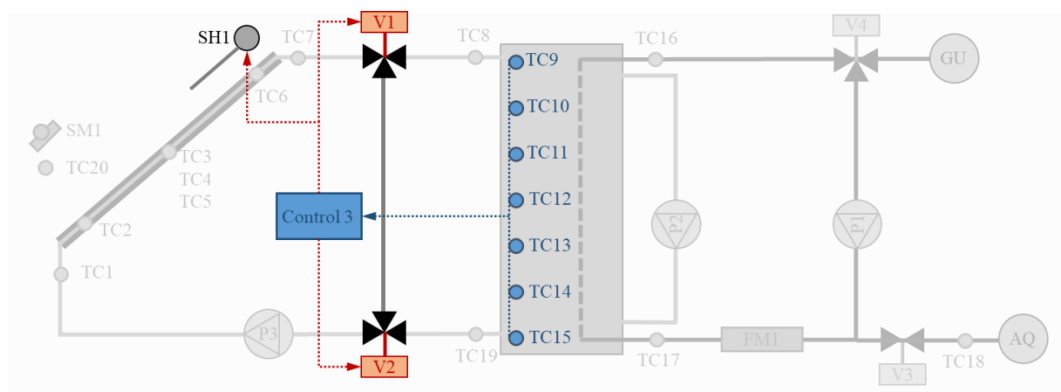
3.3.6.4 Control 4

This control logic is used to simulate the behaviour of the prototype under realistic conditions when the solar system is coupled to a heating system with radiant panels. In this context, Control 4 operates so to keep the water temperature at the inlet of the heat exchanger in the storage tank (the demand-side simulator) at a temperature of about 28 – 30 °C. This value is the typical return temperature of a real radiant panel heating system. In general, the temperature difference between the supply and return heat transfer fluid used in radiant panel systems is 5 °C. For this reason, the supply temperature at the inlet of the panel is almost 33 – 35 °C, a value that is entirely compatible with the solar energy system under investigation. Such control is implemented employing the proportional regulation of a three-way solenoid valve (V4), which allows a variable recirculation rate of the water at the outlet of the demand-side simulator. The PID regulates the position of valve V4. The goal is to keep the temperature of the water measured at the inlet of the storage tank (using the thermocouple TC17) at the set point value defined by the user through the Visual Interface of the controller (generally in the range 28 - 30 °C). The pump P1 is also activated when V4 allows the demand-side simulator fluid to fluid in the recirculation tee.
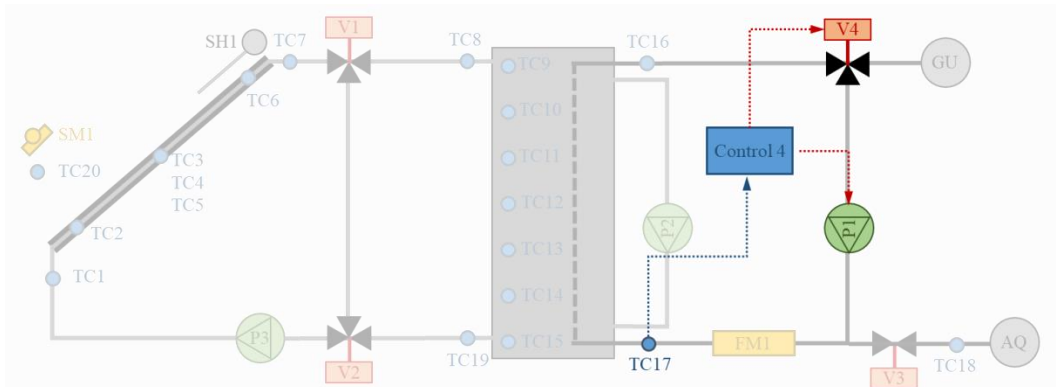
Figure 39. Schematic of the sensors and actuators involved in the Control 4.

3.3.6.5 Control 5

This control allows the time profile of the heating demand to be reproduced and acts on the demand-side simulator. The controlled variable is the enthalpy flux that is subtracted from the thermal energy storage tank from the spiral heat exchanger that simulates the space heating demand, $\dot{Q}_{need}$, and the control variable is the water mass flow rate, $\dot{m}_{H2O}$. The shape of the time profiles of the heating demand can be chosen freely by the user and implemented in the controller through the Visual Interface of the controller.

The inlet temperature in the thermal energy storage tank (monitored by the thermocouple TC17) is kept at a constant nominal value of 28 – 30 °C by means of the C4 control. Instead, control C5 adjusts the water mass flow rate in the following way:

- at each time step, the value of the $\dot{Q}_{need}$ that has to be removed from the storage tank is taken from a look-up table (that reproduces the user-defined heating demand profiles);
- based on the knowledge of $\dot{Q}_{need}$, the water mass flow rate $\dot{m}_{H2O}$ that has to flow in the demand-side simulator (to remove $\dot{Q}_{need}$) is caculated as:

$$\dot{m}_{H2O} = \frac{\dot{Q}_{need}}{c_{p,H2O} \cdot (\theta_{TC16} - \theta_{TC17})} \tag{3.32}$$

Where c_{pH2O} is the specific heat capacity of water assumed equal to 4186 J/(kgK); and θ_{TC16} and θ_{TC18} are the temperatures measured the thermocouples at the inlet of the thermal energy storage unit (TC17) and the outlet of the storage tank (TC16) respectively. The water mass flow rate $\dot{m}_{H2O}$ is then compared with the actual value measured through the Coriolis flowmeter; if an error is found, a PID control acts on the two-way solenoid valve V3 to try to rule out this difference.
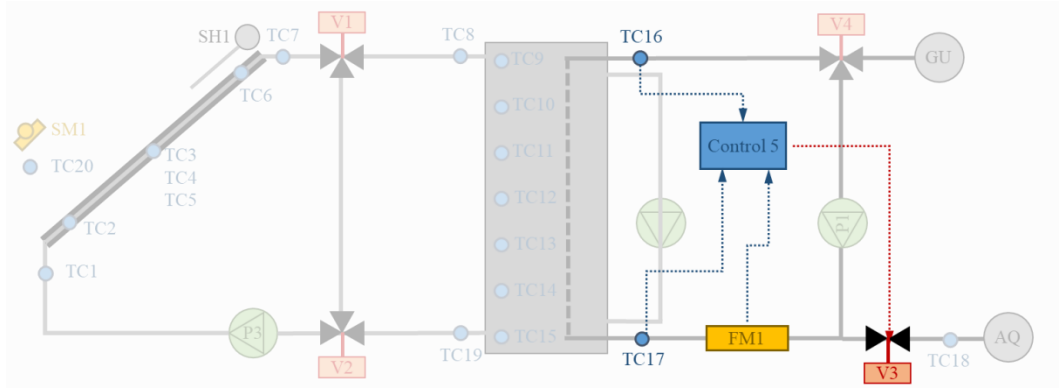
Figure 40. Schematic of the sensors and actuators involved in the Control 5.

3.3.6.6 Control 6

This control always ensures a positive energy extraction from the thermal energy storage tank and avoids cooling of the hot water of the demand-side simulator, instead of heating. For this purpose, it is necessary to be sure that the temperature of the mPCM slurry in the thermal energy storage tank is always higher than that water in the demand-side simulator loop. Control 6 has precisely this task. It calculates the average temperature (θ_{st}) of the seven thermocouples located inside the storage unit (TC9, TC10, TC11, TC12, TC13, TC14 and TC15) and compares it with the temperature of the demand-side simulator at the inlet of the storage tank (monitored by TC18). If the latter is equal or above the average storage temperature, the demand-side simulator loop is stopped.
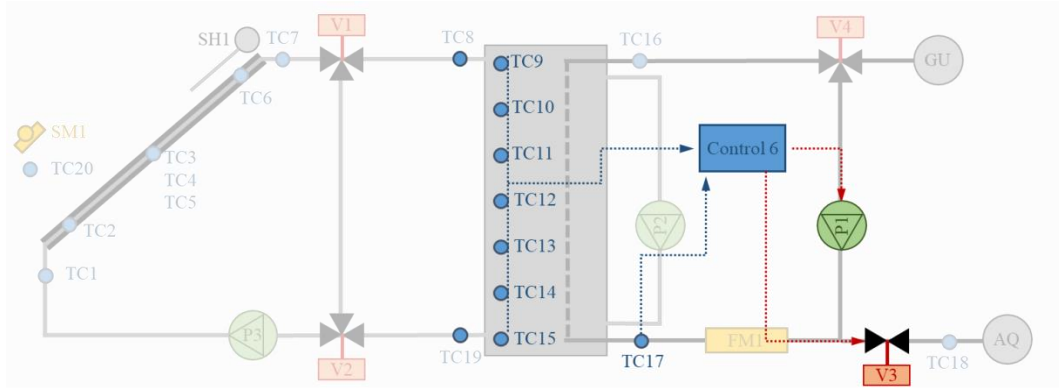
Figure 41. Schematic of the sensors and actuators involved in the Control 6.

The control completely closes the V3 valve and stops the circulating pump P1 of the demand-side simulator. When a reasonable temperature difference is again reached (e.g., a temperature difference of 5 °C between the two considered values), the Control 6 restores the normal operation mode. The two criteria can be expressed with the following formulations:

$$if\ \theta_{in,dss} = \theta_{TC17} < \overline{\theta_{st}}\ then\ (V3\ and\ P1 = stop) \tag{3.33}$$

$$if\ \theta_{in,dss} = \theta_{TC17} > \overline{\theta_{st}} - 5\ then\ (V3\ and\ P1 = stop) \tag{3.34}$$

3.4 Development of a physical mathematical model of the solar thermal system based on Phase Change Material slurry

A mathematical numerical model capable of describing the physical behaviour of the solar thermal systems based on PCM slurries was not present in the existing literature. For this reason, it was necessary to develop a physical-mathematical model capable to describe the dynamical evolution of the SolHe-PCM system. This numerical model had a two-fold aim: on one hand, it was used to support the design phase of the experimental test rig; on the other hand, it was used as a preliminary tool to analyse and test the profitability of the concept by means of comparative performance simulations against a conventional, water-based, reference solar thermal system.

Indeed, to better investigate the opportunities offered by the adoption of mPCM slurry in the solar thermal system, a numerical model was necessary to perform simulation and parametrical analysis. These allowed the system performance to be tested under different boundary conditions and climatic parameters. The numerical model had to be capable to describe both the sensible and the latent heat exchanges occurring in the system. In this way, both traditional water-based and innovative heat transfer fluid based on mPCM slurries were tested and the system performance compared.

The developed solar thermal system model is characterised by three key elements describing as many system elements:

•   the model for the solar thermal collector;
•   the model for the thermal energy storage unit;
•   the closed loop controller that regulates the pump speed, thus the flow rate flowing in the overall system.

Considering these three elements integrated into a complete model of the overall system allowed the performance of the solar thermal system based on mPCM slurry to be assessed. *Figure 42* reports a schematic of the mutual interaction of the three key elements composing the overall numerical model of the solar thermal system.

Both the collector model and the model of the thermal energy storage unit have been developed as simplified mathematical models. In particular, in the second version of the models, both the collector and the storage unit were identified as finite elements thermodynamic systems discretised in lumped nodes. Thus, the mathematical modelling is capable to describe the evolution in terms of internal energy storage and temperature profile for each node. The complete model has been entirely developed by means of Matlab scripts and Simulink flows. The complete model can be used to simulate both traditional water-based and solar thermal systems exploiting mPCM slurries, such as SolHe-PCM system. The switch

between the two options is possible by adopting different settings of the features of the heat transfer fluid and storage media.
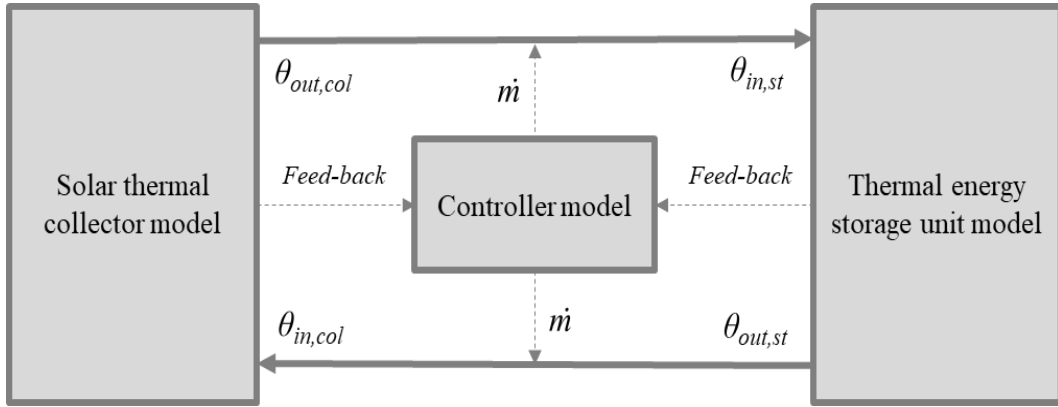
Figure 42. Schematic of the three key elements of the numerical model of the solar thermal system based on mPCM slurry.

The overall model considers the following assumptions:

- the temperature of the heat transfer fluid at the outlet of the solar thermal collector is, unless a negligible error, the temperature at the inlet of the thermal energy storage unit ($\theta_{out,col} = \theta_{in,st}$);
- vice versa, the temperature of the heat transfer fluid at the outlet of the thermal energy storage unit is, unless a negligible error, the temperature at the inlet of the solar thermal collector ($\theta_{in,col} = \theta_{out,st}$).

The external disturbances influencing the system are the external weather conditions and the space heating energy demand. The external weather conditions that mainly affect the system heat exchanges are:

- the ambient air temperature, θ_a;
- the total solar radiation, G_T (which can be further divided into the two components beam solar radiation, G_b, and diffuse solar radiation, G_d);
- the angle of incidence of the solar radiation on the collector, γ_{inc};
- the wind velocity, v_w;
- the radiative temperature of the sky, θ_{sky}.

The thermal energy storage model considers the ambient temperature as unique weather disturbance; while the solar thermal collector model is affected by all the previous parameters. The space heating energy demand affects the model of the thermal energy storage unit only. In particular, it is modelled as the following two parameters:

- the inlet temperature of the demand-side heat exchanger, $\theta_{hx,in}$;
- the thermal energy required by the demand-side heat exchanger, Q_{hx}.

Both the model of the collector and the storage unit have been released in two versions. The reasons behind this process were different.

In the case of the collector model the first version of the model was very detailed but affected by computational instability and slowness due to the use of iterative calculations to solve the thermal balances contained within the model. The second version represented the solution to these drawbacks. Furthermore, the opportunity to evaluate the temperature profile within the collector was implemented in the second release.

In the case of the model describing the behaviour of the thermal energy storage unit, the two version were required by the adoption of two different storage tank in the full-scale prototype. The first model version was developed and calibrated to fit the behaviour of the first storage tank, while the second model was representative of the second tank (the one equipped with a mechanical mixer).

3.4.1 The model for the flat-plate solar thermal collector based on the mPCM slurry

The proposed model of the solar thermal collector was based on the Hottel-Willier equations [33]. These equations were developed to describe the thermophysical behaviour of a flat-plate solar panel that makes use of a single-phase heat transfer fluid (e.g., a traditional water-based collector). For this reason, the model of a solar thermal collector exploiting phase change materials should be suitably modified to handle the heat exchange processes that involve the latent heat.

Two versions of the model describing the thermophysical behaviour of the PCM slurry based solar collector were carried out. The first one represents the preliminary approach to the problem and it was necessary to formulate the equations regulating the latent heat exchanges. Even if this version was accurate from the physical-mathematical point of view, when translated in the Matlab-Simulink programming language, it was affected by some computational drawbacks. These affected the model operative effectiveness. Indeed, this first version was based on recursive calculations of the length of panel segments involved in either sensible or latent heat exchanges. This process can be solved by the Simulink solver by numerical iterative calculations. However, on the one hand, this way to formulate the problem can strongly increase the computational time required to perform simulations. On the other hand, when singularities occur, the solutions can be affected by instabilities or result divergences. For this reason, a second version of the collector model was carried out. This second version represents an evolution of the preliminary attempt. It apriori discretises the collector in 10 (or more) segments of the same length and solves a finite element thermodynamic problem that assumes constant mPCM slurry properties for each segment.

3.4.1.1 General assumptions and modelling approach

Some assumptions and some simplifications were made in the Hottel-Willier model to make the physical-mathematical description of the components easier. The same assumptions are still valid in the numerical model herewith proposed:

- quasi-steady-state of the collector components (e.g., glazing cover, absorber plate, edge and back insulation casing);
- forcing parameters and boundary conditions updated at each calculation time-step;
- uniform external weather conditions over the whole collector;
- one-dimensional heat flux (from the top cover to the back insulation);
- heat losses towards the same heatsink, considered at the outdoor air temperature θ_a.

All these assumptions have also been adopted in the proposed new model for solar thermal collectors based on mPCM slurry. Furthermore, other simplifications related to the heat transfer fluid material properties have been taken into account. These were necessary to simplify the model and to reduce the number of input data. These main additional assumptions were:

- the phase change occurs completely in the nominal transition range of the mPCM, $\theta_{sup,mPCM} - \theta_{inf,mPCM}$;
- in the phase change range, the contribution of the sensible heat is due to the water-glycol portion of the mixture only and it is considered in the fictitious latent heat $\Delta h'_{lat,mPCS}$.

It is worth mentioning that the hypothesis of a quasi-steady state regime, adopted in the Hottel-Willier model, only applies to the elements that constitute the solar collector (i.e., the energy storage in the cover, plate and casing and in the back insulation of the collector is assumed negligible). Instead, as far as the heat transfer fluid is concerned, both latent and sensible heat are considered and the energy storage effects are taken into account.

3.4.1.2 First version

The basic equation of the Hottel-Willier model has been derived from the energy balance equation of the solar thermal collector, which relates the enthalpy flux of the heat transfer fluid to several parameters that depend on the environmental conditions and thermal panel features. The various heat transfer fluxes involved in this thermal balance are highlighted in the scheme shown in Figure 43 [2].
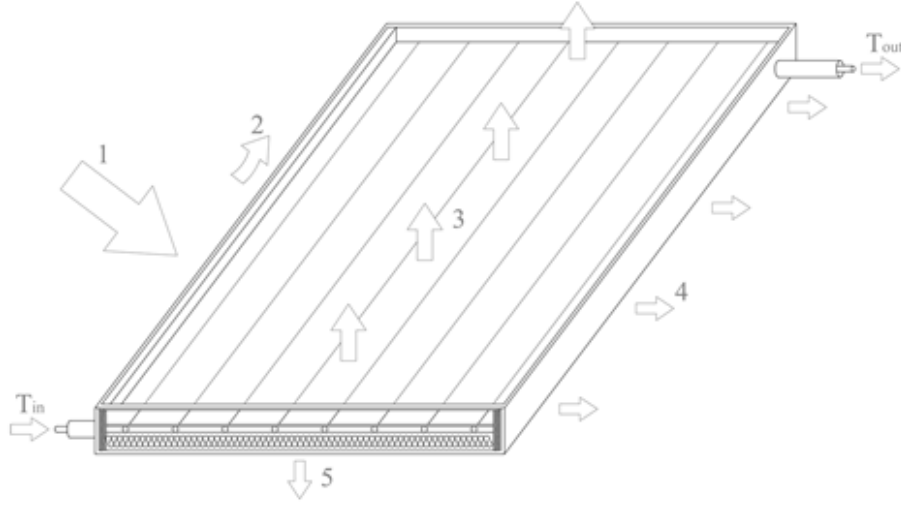
Figure 43. Schematic of the heat fluxes involved in a flat-plate solar thermal collector. 1. Solar radiation incident on the panel; 2. Optical losses; 3. Convective and radiative heat losses through the glass cover; 4. Convective heat losses through the edge casing; 5. Convective heat loss through the bottom.

$$\dot{m} \cdot c_{p,HTF} \cdot \left(\theta_{HTF,out} - \theta_{HTF,in}\right) = \dot{Q}_u \tag{3.35}$$

Where $\dot{m}$ is the heat transfer fluid flow rate in the solar thermal collector; $c_{p,HTF}$ is the specific heat capacity of the generic heat transfer fluid adopted in the collector (i.e., mPCM slurry in the case of the SolHe-PCM system); $\theta_{HTF,in}$ and $\theta_{HTF,out}$ are the temperature of the heat transfer fluid at the collector inlet and outlet, respectively. The right-hand side of the previous equation is the so-called useful heat flux, $\dot{Q}_u$, which can be written as:

$$\dot{Q}_u = A_{coll} \cdot F_R \cdot \left[G_T \cdot (\tau\alpha)_e - U_L \cdot \left(\theta_{HTF,in} - \theta_a\right)\right] \tag{3.36}$$

The previous equation establishes a balance between the incident solar radiation G_T, the optical losses (accounted for by means of the $(\tau\alpha)_e$ product) and the heat flux lost towards the outdoor environment $U_L \cdot (\theta_{HTF,in} - \theta_a)$; while A_{coll} is the collector area and F_R is the collector heat removal factor. This latter term takes into account the different temperatures along the panel surface. Such a temperature distribution is due to the so-called "fin effect" (evaluated with parameter F') and the "heat-exchanger effect".

The calculation of F' and U_L is not affected by the nature of the heat exchange (sensible or latent) that takes place in the heat transfer fluid, but their values are functions of the temperature levels at which the fluid operates. Therefore, in the proposed model, they have been assessed using the same equations as those used in the conventional Hottel-Willier model. On the contrary, changes were implemented in order to correctly take into consideration any phase changes that occur in the heat transfer fluid during the path of the fluid along the solar collector. In fact, these phase changes can determine a considerable modification of the temperature distribution over the plate, and can consequently influence the value of the F_R factor

(which not only depends on the inlet and outlet fluid temperatures but also on other parameters).

The proposed model is still based on the two previous equations to allow a simple comparison to be made with the traditional one.

In a collector that exploits mPCM slurries, the "temperature increase per unit of length" of the heat transfer fluid flowing along the panel pipes varies, according to whether only sensible heat or both sensible and latent heat are exploited. In general, the temperature gradient is much smaller when latent heat is used, in spite of the sensible heat.

If the mPCM slurry temperature is lower than the lowest temperature of the transition phase, $\theta_{inf,mPCM}$, or higher than the highest temperature of the transition phase, $\theta_{sup,mPCM}$, only sensible heat exploitation takes place. On the other hand, when the mPCM slurry temperature is in the $\theta_{inf,mPCM} - \theta_{sup,mPCM}$ range, a combination of latent/sensible heat is involved (the effect of this blend is evaluated by means of the fictitious latent heat, $\Delta h'_{lat,mPCS}$). For these reasons, in a solar thermal panel based on mPCM slurry the temperature distribution is very different from that of a traditional water-based collector.

As already mentioned, F_R is a function of the temperature distribution along the panel. Since only sensible heat is considered in the Hottel-Willier model, just one value is calculated for the overall panel surface. On the contrary, in the mPCM slurry based solar collector, the value of F_R varies over the panel surface, according to the state of aggregation of the mPCM slurry.

In the general case, the mPCM slurry enters the collector at a lower temperature (θ_{in}) than $\theta_{inf,mPCM}$. Therefore, the temperature of the fluid increases along the first part of its path inside the panel as it collects solar energy. After reaching the temperature level at which the phase change starts, $\theta_{inf,mPCM}$, the mPCM slurry starts exploiting its latent heat of fusion. When the phase change has been completed ($\theta_{mPCS} > \theta_{sup,mPCM}$), the mPCM slurry again starts to only exploit the sensible heat. The heat transfer fluid leaves the collector at a higher temperature than $\theta_{sup,mPCM}$, when and if the mPCM is in a complete liquid state. *Figure 44* shows the expected temperature profiles along the rising pipes of the collector.

As it can be inferred from Figure 44 the solar thermal collector can be divided into three virtual segments along the flow path (y-axis):

- Δy_1: is the panel segment between the collector inlet and the point at which the heat transfer fluid reaches a temperature equal to $\theta_{inf,mPCM}$;
- Δy_2: is the segment where the PCM inside the microcapsules undergoes the phase change and the mPCM slurry temperature rises from $\theta_{inf,mPCM}$ to $\theta_{sup,mPCM}$ (transition range);
- Δy_3: is the segment where the temperature of the mPCM slurry increases further, sensible heat is once again exploited, and the collector outlet temperature θ_{out} is reached.
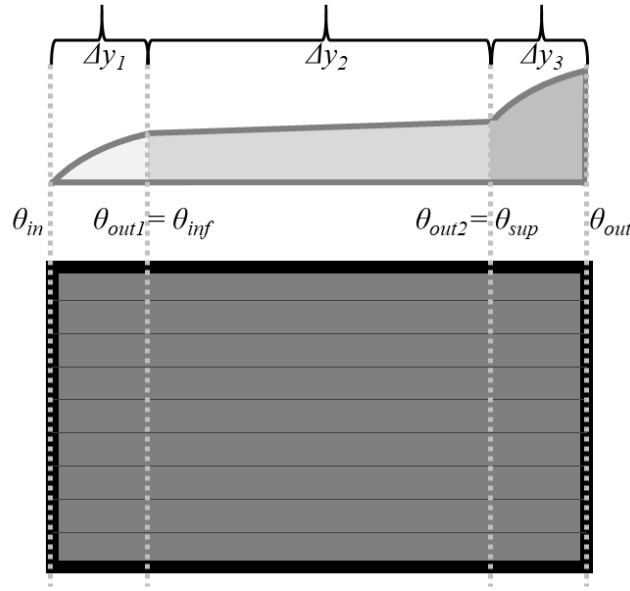
Figure 44. Schematic of the temperature profile along the rising pipes of the collector in the ideal functioning of a flat-plate solar thermal collector based on mPCM slurry.

The lengths of the three virtual segments along the y-axis can be obtained by solving the energy balance equations. The length of each segment at each time step is calculated using appropriate boundary conditions.

The length of Δy_1 can be obtained by solving the differential equation of the heat exchanger [33], reformulated by assuming $\theta_{out1} = \theta_{inf,mPCM}$ as a boundary condition. This leads to the following formulation:

$$\Delta y_1 = \frac{\dot{m} \cdot c_{p,mPCMs,sol}}{N \cdot W \cdot F' \cdot U_L} \cdot ln \left[\frac{\theta_{in} - \theta_a - \frac{G_T \cdot (\tau\alpha)_e}{U_L}}{\theta_{inf,mPCM} - \theta_a - \frac{G_T \cdot (\tau\alpha)_e}{U_L}} \right] \tag{3.37}$$

Where $c_{p,mPCMs,liq}$ is the mPCM slurry specific heat capacity in the solid phase; N is the number of rising pipes within the collector; W is the distance between two rising pipes; and θ_a is the ambient air temperature considered as the unique heat sink interesting the heat losses.

Similarly, Δy_2 can be calculated assuming that the mPCM slurry temperature at the end of this segment is $\theta_{out} = \theta_{sup,mPCM}$; the mPCM slurry temperature at the inlet of this segment is $\theta_{in,\Delta y2} = \theta_{inf,mPCM}$; and that the whole mass of the mPCM has melted. In this section, the mPCM slurry mainly exploits the phase change and its energy content can be assessed by means of the fictitious latent heat $\Delta h'_{lat,mPCMs}$. By introducing the mass ratio of the melted PCM over the total mass of PCM, β, it is possible to formulate the following equation for the Δy_2 segment in which the phase change occurs.

Therefore, it results that:

$$\frac{\dot{m}}{N} \cdot \Delta h'_{lat,mPCMs} \cdot d\beta = -W \cdot F' \cdot U_L \cdot \left(\theta_{y,mPCMs} - \theta^* \right) \cdot dy \tag{3.38}$$

In order to simplify the model, a constant mPCM slurry temperature has been considered in segment Δy_2, which is assumed to be equal to the mean value of the melting range (the smaller the melting range, the better the approximation). Furthermore, the boundary condition $\beta = 1$ can be imposed, which means that the mPCM slurry has melted completely at the end of the Δy_2 segment. Under these hypotheses, the previous differential equation can be expressed as:

$$\Delta y_2 = \frac{\dot{m} \cdot \Delta h'_{lat,mPCMs}}{N \cdot W \cdot F' \cdot U_L \cdot \left[\frac{\theta_{sup,mPCM} + \theta_{inf,mPCM}}{2} - \frac{G_T \cdot (\tau\alpha)_e}{U_L} - \theta_a \right]} \tag{3.39}$$

The length of the third collector segment, Δy_3, is obtained from the difference between the sum of the two previous segments and the total length of the panel:

$$\Delta y_3 = L_{coll} - \Delta y_1 - \Delta y_2 \tag{3.40}$$

After calculating the length of the three effective virtual segments, their related areas can be calculated as:

$$A_{coll,1} = A_{coll} \cdot \frac{\Delta y_1}{L_{coll}} \tag{3.41}$$

$$A_{coll,2} = A_{coll} \cdot \frac{\Delta y_2}{L_{coll}} \tag{3.42}$$

$$A_{coll,3} = A_{coll} \cdot \frac{\Delta y_3}{L_{coll}} \tag{3.43}$$

Each of these areas has a different collector heat removal factor, F_R, since the heat exchange occurs in temperature fields that have different temperature distributions. Therefore, it is necessary to calculate the useful heat flux delivered by each area of the collector separately.

The process in $A_{coll,1}$ and $A_{coll,3}$ only involves a sensible heat exchange, and the temperature of the mPCM slurry increases as in a normal, water-based collector. The equations are therefore similar to those of the Hottel-Willier model:

$$F_{R,1} = \frac{\dot{m} \cdot c_{p,mPCMs,sol}}{A_{coll,1} \cdot U_L} \cdot \left(1 - e^{\frac{A_{coll,1} \cdot U_L \cdot F'}{\dot{m} \cdot c_{p,mPCMs,sol}}} \right) \tag{3.44}$$

$$F_{R,3} = \frac{\dot{m} \cdot c_{p,mPCM,liq}}{A_{coll,3} \cdot U_L} \cdot \left(1 - e^{\frac{A_{coll,3} \cdot U_L \cdot F'}{\dot{m} \cdot c_{p,mPCM,liq}}} \right) \tag{3.45}$$

Substituting these values and the mPCM slurry temperature at the inlet of the Δy_1 and Δy_3 segments, on the right-hand side of the equation that expresses the useful heat produced as a function of the heat removal factor, one obtains:

$$\dot{Q}_{u,1} = A_{coll,1} \cdot F_{R,1} \cdot [G_T \cdot (\tau\alpha)_e - U_L \cdot (\theta_{in} - \theta_a)] \qquad (3.46)$$

$$\dot{Q}_{u,3} = A_{coll,3} \cdot F_{R,3} \cdot \left[G_T \cdot (\tau\alpha)_e - U_L \cdot \left(\theta_{sup,mPCM} - \theta_a\right)\right] \qquad (3.47)$$

The mPCM slurry instead shows a rather moderate temperature rise over the $A_{coll,2}$ area. Therefore, in the proposed model, due to this fairly small variation, its value has been assumed to be constant and equal to the average value of the melting range.

Adopting such an approximation, the $F_{R,2}$ parameter becomes equal to F'. Moreover, since complete melting of the mPCM occurs, $\dot{Q}_{u,2}$ can be simply calculated according to:

$$\dot{Q}_{u,2} = \dot{m} \cdot \Delta h'_{lat,mPCMs} \qquad (3.48)$$

Eventually, the total useful heat flux delivered by the whole solar thermal panel, is obtained as the sum of the contributions from each area of the collector:

$$\dot{Q}_u = \dot{Q}_{u,1} + \dot{Q}_{u,2} + \dot{Q}_{u,3} \qquad (3.49)$$

Once the useful heat flux is known, the efficiency η of the solar thermal collector is calculated from the ratio of the useful heat flux delivered by the collector and the solar irradiation on the collector cover:

$$\eta = \frac{\int \dot{Q}_u \cdot dt}{A_{coll} \cdot \int G_T \cdot dt} \qquad (3.50)$$

The previously presented equations represent the most general behaviour of a solar thermal panel capable of exploiting the latent heat of the mPCM slurry. It is worth mentioning that the previous discussion refers to the most general behaviour of the system – as shown in *Figure 44* – but five other particular cases are also possible:

- *Case A:* The mPCM slurry enters the panel at a lower temperature than the minimum value of the melting range: $\theta_{in} < \theta_{inf,mPCM}$, and the absorbed heat is not enough to reach the PCM melting range. Therefore, no phase change occurs along the path inside the collector, as shown in *Figure 45*(a). In this case, the PCM remains always solid and the panel only exploits sensible heat and works as a traditional collector.
- *Case B*: The mPCM slurry enters the panel at a higher temperature than the maximum value of the melting range: $\theta_{in} \geq \theta_{sup,mPCM}$. In this case, the PCM

remains always in a liquid state and the panel only exploits sensible heat and works as a traditional collector, as shown in *Figure 45*(a).

- *Case C*: The mPCM slurry enters the panel at a lower temperature than the minimum value of the melting range: $\theta_{in} < \theta_{inf,mPCM}$. The material then starts to melt, but the absorbed heat is not enough to complete the phase change or to fully exploit the PCM latent heat, as shown in *Figure 45*(b). In this case, the PCM is only partially melted ($\beta < 1$) at the panel outlet and the mPCM slurry reaches a temperature lower than the superior limit of the phase change range.

- *Case D*: The mPCM slurry enters the panel at a temperature that falls within the melting range $\theta_{inf,mPCM} < \theta_{in} < \theta_{sup,mPCM}$. For this reason, the PCM is partially melted at the collector inlet ($\beta > 0$), the phase change occurs completely and the sensible heat is exploited in segment Δy_3, as shown in *Figure 45*(c) .

- *Case E*: The mPCM slurry enters the panel at a temperature that falls within the melting range $\theta_{inf,mPCM} < \theta_{in} < \theta_{sup,mPCM}$. For this reason, the material is partially melted at the collector inlet ($\beta > 0$). Moreover, the absorbed useful heat is not enough to complete the phase change or to fully exploit the latent heat, as shown in *Figure 45*(d). The PCM slurry at the panel outlet is therefore only partially melted ($\beta < 1$) and the mPCM slurry reaches a temperature lower than the superior limit of the phase change range. The heat exchange in the collector occurs completely in the phase-change range.

In order to take these particular cases into due account, some additional equations need to be implemented in the model.

Where *Case A* or *Case B* occur, the mPCM slurry would not reach the lowest limit of the PCM phase change, $\theta_{inf,mPCM}$, before leaving the collector. In these circumstances, the real length of the solar thermal collector along the y-axis, L_{coll}, is shorter than the virtual segment Δy_1. Therefore, the effective length of $\Delta y_{1,eff}$ needs to be introduced to consider this situation:

$$\Delta y_{1,eff} = \min \begin{cases} \Delta y_{1,eff} \\ L_{coll} \end{cases} \tag{3.51}$$

In *Case C*, even though $\theta_{inf,mPCM}$ is reached, the mPCM slurry leaves the solar collector at a lower temperature than $\theta_{sup,mPCM}$. In this situation, a fraction of the mPCM remains in a solid state and the phase change does not involve the entire mass of the mPCM. For this condition, Δy_1 can be assessed by means of the traditional equation, Δy_3 is zero, and a suitable value, $\Delta y_{2,eff}$ has to be introduced in relation to the second segment:

$$\Delta y_{2,eff} = \min \begin{cases} \Delta y_2 \\ L_{coll} - \Delta y_{1,eff} \end{cases} \tag{3.52}$$
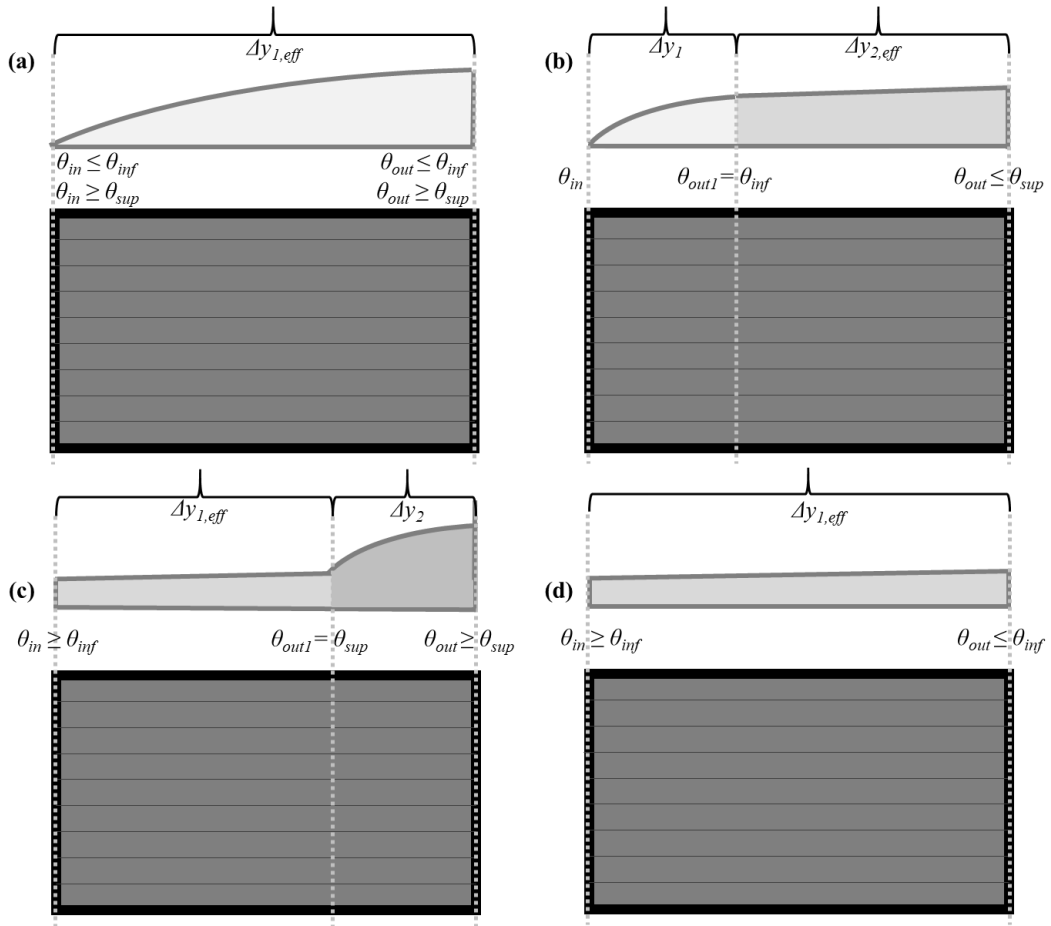
Figure 45. Schematic of the temperature profile along the rising pipes of the collector: possible cases considering different boundary conditions.

In this case, it is worth noting that the calculation also needs to be modified, since the latent heat of the PCM is not completely exploited. Firstly, the fraction of the PCM that has melted, β, (that is, the mass ratio of the melted PCM to the total mass of PCM) is assessed as follows:

$$\beta_{out} = \frac{\Delta y_{2,eff}}{\Delta y_2}$$
(3.53)

The exploited useful heat of the $\Delta y_{2,eff}$ segment can then be evaluated as:

$$\dot{Q}_{u,2} = \beta_{out} \cdot \dot{m}_{PCMs} \cdot \Delta h'_{lat,mPCMs}$$
(3.54)

In the condition of *Case E*, the lengths of the first and third segments are equal to zero: $\Delta y_1 = \Delta y_3 = 0$. The length of the second segment is equal to the total collector length: $\Delta y_2 = L_{coll}$.

However, the model needs a further input parameter: the mass fraction of the melted mPCM at the inlet of the panel. This value can be determined as follows:

$$\beta_{in} = \frac{\theta_{sup,mPCM} - \theta_{in}}{\theta_{sup,mPCM} - \theta_{inf,mPCM}} \tag{3.55}$$

In this case, the equation to calculate the useful heat produced by the segment that evaluates the latent heat exchanges becomes:

$$\dot{Q}_{u,2} = (\beta_{out} - \beta_{in}) \cdot \dot{m} \cdot \Delta h'_{lat,mPCS} \tag{3.56}$$

Case D can be solved by suitably combining the above equations.

The physical-mathematical model of the solar thermal collector based on mPCM slurry has been implemented in the Matlab-Simulink environment. A brief description of the Simulink model structure is provided hereafter for the sake of completeness. *Figure 46* shows the general scheme of the Matlab-Simulink blocks in which the sub-systems and the data flow have been highlighted. Diverse elements of the code are represented by different colours.

- Green: input variables of the model. They can be computed using a Matlab script, adopting scalars or vectors for parameters that change in time (assuming a mean hourly value). These inputs are fluid properties, solar thermal panel characteristics, climatic conditions and locations;
- Yellow: these are the different subsystems that implement the model equations. In particular:
  - S1: defines the direct incident radiation normal to the collector surface;
  - S2: calculates the $(\tau\alpha)_e$ product that represents the optical energy losses of the panel;
  - S3: determines the heat-transfer coefficients that can be used to calculate the energy loss the panel, and its outputs are the thermal resistance and the corresponding heat losses coefficient, U_L;
  - S4: describes the heat exchange between the panel and the heat transfer fluid;
  - S5: is the "core" of the model. It allows the following to be determined: the $F_{R,1}$, $F_{R,2}$ and $F_{R,3}$ parameters, the various lengths $\Delta y_{1,eff}$, $\Delta y_{2,eff}$, $\Delta y_{3,eff}$ that identify the various zones of the solar collector (see, for example, sections 2.3 and 2.4) and the temperature of the heat transfer fluid at the outlet of the panel;
  - S6: gives the cover temperature through an iterative calculation. Its output depends on the outputs of sub-systems S3 and S5;
  - S7: provides the main outputs of the model, that is: the useful heat flux, $\dot{Q}_u$ and the collector efficiency, η.
- Orange: outputs of the model. The most important ones are the useful heat flux and the instantaneous efficiency of the collector. Moreover, it is also possible to evaluate some additional information that may be useful for analysis of the system, such as the mean heat transfer fluid temperature and the temperature at

the outlet of the panel, the critical radiation and the stagnation temperature of the collector.
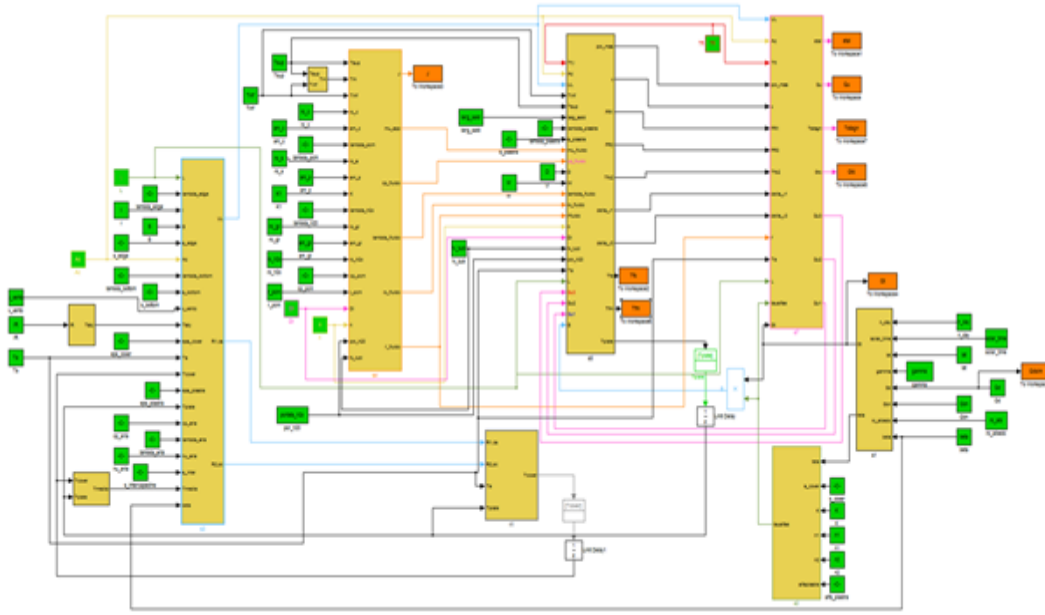
Figure 46. Matlab-Simulink model overview for the solar thermal system based on mPCM slurries

3.4.1.3 Second version

A second version of the model was developed to shorten the computational time required to simulate the behaviour of the system. In fact, the first version was based on an iterative numerical solution based on recursive calculations that affect the computational performance of the model. Furthermore, the first version did not allow the temperature profile over the panel length to be determined. Indeed, from this formulation, it was possible to derive only the panel segment length where the phase transition occurred and not a temperature distribution over the panel to be compared with experimental tests.

Firstly, to reduce the interactions required to solve the thermo-dynamical problem, an enthalpy approach, instead of a temperature one, was used to evaluate the internal energy of the system. In this way, the energy balance can be directly solved without determining the temperature of each panel component with a recursive calculation process. Afterwards, it is possible to derive the respective temperatures, by exploiting the enthalpy property of being a continuous and invertible function of the temperature, *h=h(θ)*. In this way, the problem can be readily formulated in Simulink, thanks to the adoption of specific enthalpy versus temperature curves defined using "Look-Up table" blocks (*Figure 47*). These "Look-Up table" blocks are based on the temperature versus enthalpy curves obtained in Section 3.2.2 with the T-History tests.
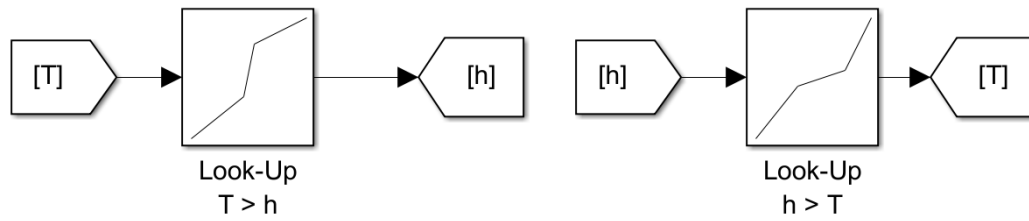
Figure 47. The Look-Up tables in Simulink used to convert temperature values in specific enthalpy values, and vice versa.

Secondly, in the second version of the numerical model, the collector has been apriori discretised in 10 segments of the same length to evaluate the temperature profile over the panel. Each segment represents a lumped node having constant thermodynamic properties (e.g., temperature, specific enthalpy, conductivity, etc.). For each segment, an energy balance can be formulated and computed, from the previously described modified Hottel-Willier model for solar thermal collectors that exploit latent heat exchanges. The outlet of a panel node – concerning heat transfer fluid temperature and enthalpy – is the inlet of the subsequent node. Shows a schematic of the Simulink formulation of the collector model, which is composed by 1 input node, 1 output node and 8 central nodes. In this way, it is possible not only to determine the useful heat produced by the panel but also to carry out the temperature and the heat fluxes involved in the process of each node [9]. Knowing the temperature of the 10 nodes allows the temperature profile of the collector to be approximated.
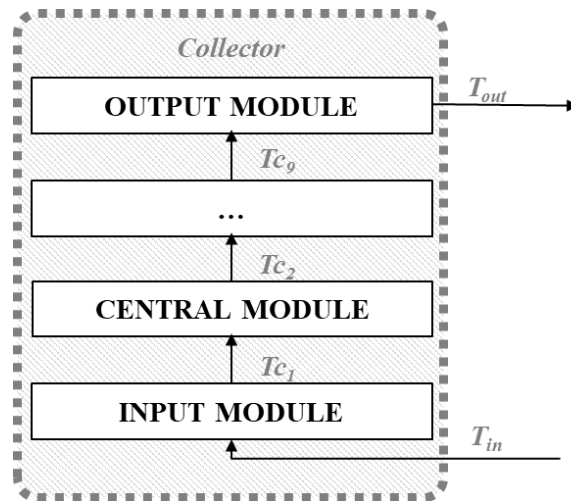
Figure 48. Schematic of the second version of the Simulink model of the flat-plate solar thermal collector discretised in 10 nodes.

3.4.2 Model of the thermal energy storage unit

There are three possible approaches to carry out a model of the physical behaviour of a thermal energy storage unit:

- The fluid-dynamic approach considers the heat exchanges within the fluid used as storage media utilising dimensionless parameters (such as the Reynolds number or the Grashof number);
- The exergetic or entropic approach, which is based on the Second Law and considers the maximum quantity of useful work that can be produced by the system according to a specific outdoor environment (exergy) and the internal disorder of the system (entropy).
- The energetic approach, which is based on the First Law and considers the energy exchanges and heat transfer of the storage unit with the external environment.

Since the numerical model under development is mainly devoted to estimating the useful heat production of the system, the energetic approach resulted as the most suitable. In detail, the energetic *multi-node* model – introduced by the Institute of Thermal Engineering within the Task 32 of the International Energy Agency Solar Heating and Cooling (IEA-SHC) – was chosen as a reference. This solution has revealed to be particularly suitable for traditional water-based storage units, storage units equipped with PCM modules and storage units exploiting PCM slurry as heat storage media.

In this case also, two versions of the numerical model of the storage unit were necessary. In this case the two versions were due to the change of the full-scale prototype of the storage tank during the experimentations. Indeed, since two different storage tanks were adopted, it was necessary to develop and implement in Matlab-Simulink two different numerical models.

- The first storage tank was divided into seven partitions and monitored with as many thermocouples. Thus the first version of the numerical model used seven lumped nodes to describe the behaviour of the storage unit;
- The heat transfer fluid within the second storage tank was continuously mixed employing the mechanical mixer. Thus a single lumped node model was sufficient to evaluate the average thermal energy storage temperature in the second version of the numerical model.

Equations developed in the first version of the multi-node model can be easily adapted to the second version with a single node.

3.4.2.1 General assumptions and modelling approach

Likewise the solar collector model, some assumptions and simplifications were have been necessary to make the physical-mathematical description of the thermal energy storage unit easier:

- Quasi-steady-state of the thermal energy storage unit components (e.g., tank, insulation layer);

- Forcing parameters and boundary conditions updated at each calculation time-step;
- Uniform boundary conditions over the whole thermal energy storage unit;
- One-dimensional mass flow-rate, from the top upper part (inlet) to the lower part (outlet) of the storage unit;
- Heat losses towards the same heatsink, considered at the outdoor air temperature θ_a;
- Since in the full-scale prototype the thermal energy storage unit is placed narrow to the solar thermal collector, the ambient air is considered at the same temperature for both the elements;
- Pressure drops within the thermal energy storage unit are assumed negligible;
- The heat storage fluid is considered perfectly mixed and characterised by uniform properties (e.g., temperature) within each lumped node of the storage unit;
- The phase change occurs entirely in the nominal transition range of the mPCM, $\theta_{sup,mPCM} - \theta_{inf,mPCM}$;
- In the phase change range, the contribution of the sensible heat is due to the water-glycol portion of the mixture only, and it is considered in the fictitious latent heat $\Delta h'_{lat,mPCS}$.

3.4.2.2 First version

In this version, the numerical model divides the thermal energy storage unit in seven nodes (one inlet, one outlet and five internal nodes). In the full-scale prototype, these nodes are represented by the interior partitions of the storage tank and the temperature of each node is monitored by a specific thermocouple (*Figure 49*).

Similarly to the second version of the collector model, an approach based on the enthalpy was adopted. In this approach, the specific enthalpy is considered as a continuous and reversible function of the temperature. For this reason, once the curves of temperature versus specific enthalpy of the storage media are known (see Section 3.2.2), the energy balance can be formulated for each node of the storage unit. Under this assumption, the evolution over time of the storage unit internal specific enthalpy can be easily related to its temperature evolution $h(\tau) \rightarrow \theta(\tau)$. Each *j-th* node of the thermal energy storage unit is an open system, and the energy balance of its control volume can be derived as follows:

$$\dot{Q}_{dp,j} + \dot{Q}_{hx,j} + \dot{Q}_{aux,j} + \dot{Q}_{cond,j} + \dot{Q}_{loss,j} = m_j \cdot \frac{h_j(k+1) - h_j(k)}{d\tau} \qquad (3.57)$$

Where $\dot{Q}_{dp,j}$ is the open system heat flux associated with the heat transfer fluid flowing in or out the control volume represented by the *j-th* node (this term is also known as *dual ports* heat flux); $\dot{Q}_{hx,j}$ is the heat flux due to a heat exchanger within the *j-th* node (e.g., the demand-side simulator heat exchanger); $\dot{Q}_{aux,j}$ is the heat flux due to an auxiliary heater within the *j-th* node; $\dot{Q}_{cond,j}$ is the heat flux exchanged

between two adjacent nodes (this term is also referred as *conduction* heat flux); $Q_{loss,j}$ are the heat losses toward the outdoor air heat sink of the *j-th* node; m_j is the mass of the storage media contained in the *j-th* node; and the last term describes the evolution over time of the specific enthalpy of the storage media included in the *j-th* node of the thermal energy storage unit.

The heat flux of *dual ports* is influenced by the PCM slurry flow rate flowing in the solar thermal system, $\dot{m}_{PCMs}$, and can be derived as follows:

$$\begin{cases} \dot{Q}_{dp,j} = \dot{m}_{PCMs} \cdot \left(h_{st,in} - h_j\right) & if\ j = 1 \\ \dot{Q}_{dp,j} = \dot{m}_{PCMs} \cdot \left(h_{j-1} - h_j\right) & if\ j \neq 1 \end{cases} \qquad (3.58)$$

The node j = 1 represents the storage inlet. The numerical model has been developed under the general assumption that "the temperature of the heat transfer fluid at the outlet of the solar thermal collector is, unless a negligible error, the temperature at the inlet of the thermal energy storage unit ($\theta_{out,col} = \theta_{in,st}$)" and the relation temperature versus specific enthalpy is reversible. Thus, the term $h_{st,in}$ is equal to the enthalpy derived from the temperature of the mPCM slurry at the outlet of the collector.
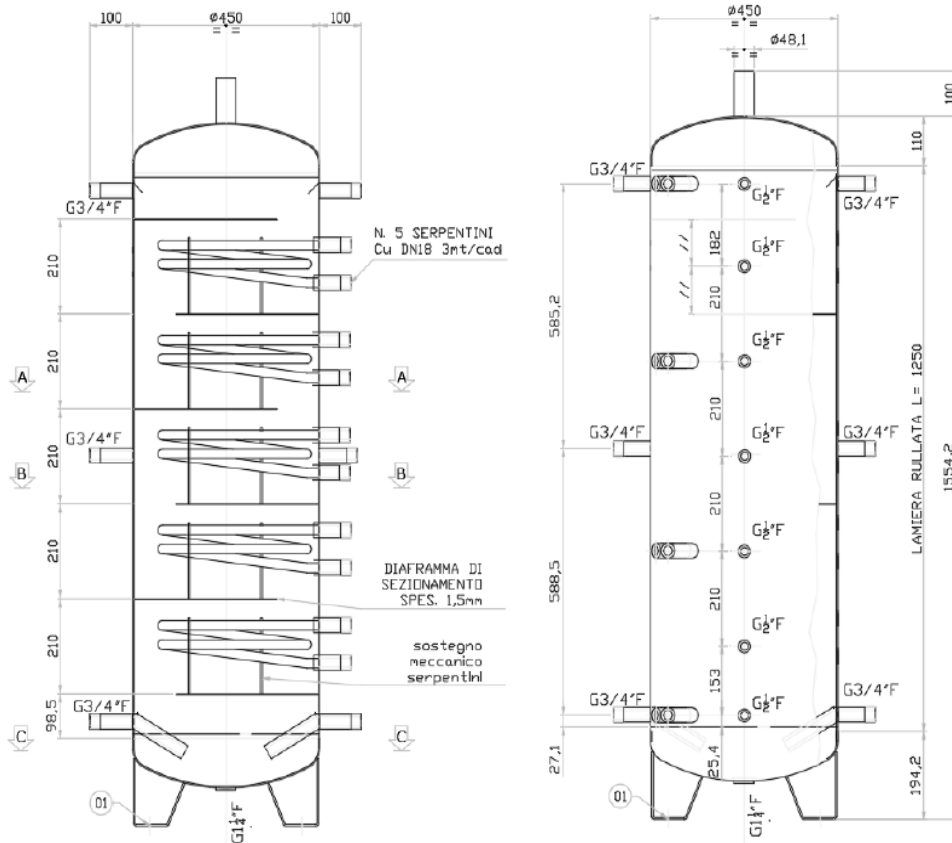

Figure 49. Technical blueprints of the first version of the thermal energy storage tank with highlighted the seven internal partitions.

The heat flux due to the demand-side simulator heat exchanger is assumed to be equal to the energy required for satisfying the space heating demand Q_{need}. In the considered storage unit configuration, the inlet (j = 1) and the outlet (j = 7) nodes are not interested in this kind of heat exchange. While the energy required for satisfying the space heating demand is assumed linearly distributed among the remaining nodes:

$$\begin{cases} \dot{Q}_{hx,j} = 0 & if\ j = 1,7 \\ \dot{Q}_{hx,j} = \dot{Q}_{need}/5 & if\ j \neq 1,7 \end{cases} \tag{3.59}$$

The temperature of the *j-th* node is influenced by the ones of the adjacent nodes. This fact influences the heat exchanges accounted for the conduction phenomenon:

$$\begin{cases} \dot{Q}_{cond,j} = \lambda_{eff} \cdot \dfrac{A_j}{\Delta z_j} \cdot \left(\theta_{j+1} - \theta_j\right) & if\ j = 1 \\[2ex] \dot{Q}_{cond,j} = \lambda_{eff} \cdot \dfrac{A_j}{\Delta z_j} \cdot \left(\theta_{j+1} - 2 \cdot \theta_j + \theta_{j-1}\right) & if\ j \neq 1,7 \\[2ex] \dot{Q}_{cond,j} = \lambda_{eff} \cdot \dfrac{A_j}{\Delta z_j} \cdot \left(\theta_{j-1} - \theta_j\right) & if\ j = 7 \end{cases} \tag{3.60}$$

Where A_j is the area of the horizontal section of the *j-th* node; Δz_j is the j-th node height; and λeff is the fictitious effective vertical thermal conductivity that considers the stratification phenomenon within the storage. Its value is assumed to be equal to 0.6 W/(mK) for thermal energy storage units without an internal heat exchanger, while it is in the range 1 – 1.5 W/(mK) for thermal energy storage units with an internal heat exchanger. In this specific case, 1 W/(mK) was assumed to consider the effect of interior partitions that allowed a further physical separation between the warm and the cold fluid.

Eventually, the losses toward the ambient air of the *j-th* node can be evaluated with the following expression:

$$\dot{Q}_{loss,j} = U_{st} \cdot A_{loss,j} \cdot \left(\theta_a - \theta_j\right) \tag{3.61}$$

Where U_{st} is the thermal transmittance of the storage unit; and $A_{loss,j}$ is the j-th node external area losing energy toward the outdoor environment.

Afterwards, the previous equations were implemented in the Matlab-Simulink environment to develop the multi-node energetic model of the thermal energy storage unit. As well as the second version of the collector model, the mutual correlations between heat transfer fluid temperature and specific enthalpy were determined through the use of the Look-Up tables assessed through the results of the T-History tests. Figure 50 shows the Simulink formulation of the generic *j-th* node.
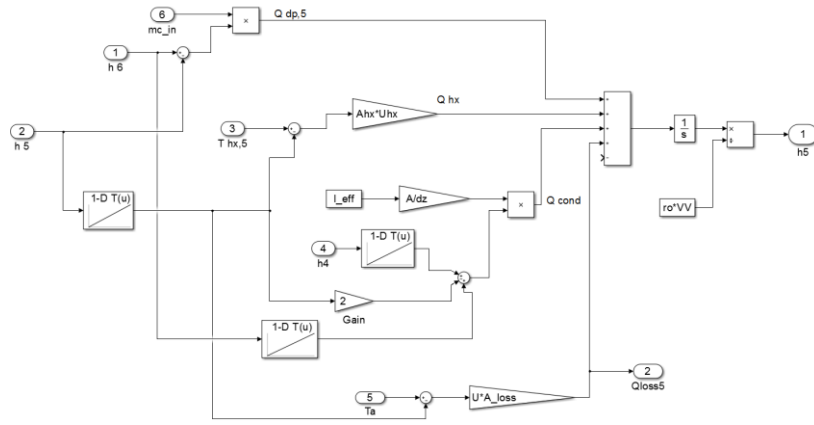
Figure 50. The generic j-th node as it appears in the Simulink environment.

3.4.2.3 Second version

The second version of the thermal energy storage unit numerical model was developed to simulate the behaviour of improved thermal energy storage tank with the internal mechanical mixer. It was reliable to consider a unique average temperature value characterised this storage unit. Indeed, the mechanical mixer continuously blends the storage media and does not allow the mPCM slurry stratification or creaming. For this reason, the model was simplified to a single lumped node, which can be described by the following equation:

$$\dot{Q}_{dp} + \dot{Q}_{hx} + \dot{Q}_{aux} + \dot{Q}_{loss} = m \cdot \frac{h(k+1) - h(k)}{d\tau} \tag{3.62}$$

Where Q_{dp} is the open system heat flux associated with the heat transfer fluid flowing in and out the thermal energy storage unit; Q_{hx} is the heat flux due to the secondary heat exchanger (e.g., the demand-side simulator heat exchanger) and it is equal to the energy need for space heating; Q_{aux} is the heat flux due to an auxiliary heater; Q_{loss} are the heat losses toward the outdoor air heat sink; m is the mass of the storage media included in the thermal energy storage unit; and the last term describes the evolution over time of the specific enthalpy of the storage media contained in the thermal energy storage unit.

The heat flux associated with the heat transfer fluid flowing in and out the thermal energy storage unit can be calculated as follows:

$$\dot{Q}_{dp} = \dot{m}_{PCMs} \cdot \left(h_{st,in} - h_{st,out} \right) \tag{3.63}$$

Eventually, the heat losses toward the outdoor air are evaluated as:

$$\dot{Q}_{loss,j} = U_{st} \cdot A_{loss,j} \cdot (\theta_a - \theta_{st}) \tag{3.64}$$

3.4.3 Model of the controllers

Once the flat-plate collector and the thermal energy storage unit models were developed, it was necessary to couple them to simulate the overall SolHe-PCM system performance. This fact was possible through the development of a model capable of replicating the control logic regulating the full-scale prototype (see Section 3.3.6). In detail, Control 1 or Control 1', Control 2, and Control 3 allow the regulation of the primary collector loop, thus the coupling of the panel with the thermal energy storage unit.

On the one hand, the Rule Base Controllers defined on thresholds (i.e., Control 1', Control 2, and Control 3) are programmed employing "if then else" rules or "Switch" blocks in Matlab-Simulink, using equalities or inequalities appropriately.

On the other hand, Control 1 is a PID (or a PI) closed-loop feedback controller. As illustrated in *Figure 51*, a closed-loop feedback controller acquires an input signal from the controlled plant (*system feedback*) and compares it with a reference value (*set-point*), calculating the *error* as the discrepancy between the two values. In the case of the numerical model of the SolHe-PCM system, the error is calculated for every discrete time instant *(k)* as the difference between reference set-point – equal to 40 °C – and the simulated outlet temperature of the panel:

$$e(k) = \theta_{set-point}(k) - \theta_{panel,outlet}(k) \qquad (3.65)$$
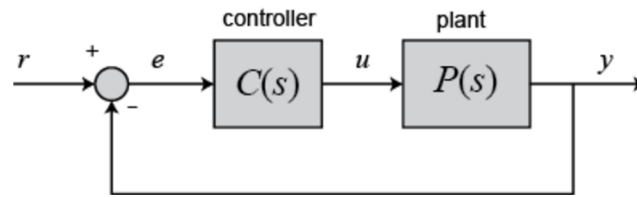
Figure 51. Schematic of a feedback controller.

From a mathematical point of view, the discrete PID controller processes the error signal as follow:

$$u(k) = K_p \cdot e(k) + K_i \cdot \int e(k) \cdot d\tau + K_d \cdot \frac{de}{d\tau} \qquad (3.66)$$

Where *u(k)* is the control signal (also referred as *system control input*), which is based on the summation of three terms:

- The first term is the Proportional term (P). This value is a function of the proportional coefficient K_p, and it is directly proportional to the error. It allows the time of reaching the set-point to be reduced, but it is not capable itself to eliminate the error when the steady state is reached (asymptotically convergence).
- The second term is the Integral term (I). This value is a function of the integral coefficient K_i, and it is directly proportional to the integral during the time of

the error. In this case, the controller is discrete. Thus the integral is approximated by a summation over time. When steady state is reached the Integral terms allows the error to be eliminated, but it increments the time required to achieve the steady state.

- The third term is the Derivative term (D). This value is a function of the derivative coefficient K_d, and it is directly proportional to the instantaneous derivative of the error. The Derivative term allows the error fluctuations to be anticipated, but it increments the control signal noise.

The second and the third term can be neglected by considering their coefficients K_i and K_d equal to 0. In this case, the feedback controller is referred as P, PI, or PD. Since physical actuator constraints exist (e.g., the minimum/maximum flow-rate of a pump), some saturation limits should be set to the control signal output. Furthermore, in general, limitations exist also on the minimum or maximum variation rate of the control signal (e.g., the minimum discrete interval of variation of the flow-rate of a pump).

The Control 1 of the SolHe-PCM system regulates the flow-rate of the primary collector loop. PID controllers used to regulate a flow-rate slightly differ from traditional closed-loop PID. Indeed, in case of flow-rate regulation, the PID output is not correlated directly with the actuator input, but with the variation rate of the control signal (also referred as *control effort*). For instance, when the error signal is equal to 0 (e.g., the temperature at the panel outlet has reached the required set-point), it means that the flow-rate has not to be changed ($\Delta u(k) = 0$, while the expression $u(k) = 0$ would not be correct). The controller saturation limits were fixed equal to the minimum and the maximum RPM allowed by the peristaltic pump P3 (see Section 3.3.3), 10 and 250 respectively. Moreover, the discrete interval of the control input variation rate was fixed equal to 1 RPM due to the physical limitations of the actuator. Eventually, the derivative coefficient K_d was set equal to 0, transforming the controller in the PI formulation that follows:

$$\Delta u(k) = K_p \cdot e(k) + K_i \cdot \int e(k) \cdot d\tau$$
$$\Delta u(k) = \max(\Delta u(k), 1)$$
$$u(k) = u(k-1) + \Delta u(k) \qquad\qquad (3.67)$$
$$u(k) = \min(u(k), 250)$$
$$u(k) = \max(u(k), 10)$$

Furthermore, the Integral term requires a mechanism to discharge its value when it reaches saturation. For instance, in the SolHe-PCM project, during night time, it is prevalent that the apparent outlet temperature of the collector (it is defined "apparent" because the heat transfer fluid is not in motion) sharply differs from the set-point. For this reason, the Integral term can accumulate a considerable summation error, which can severely influence the behaviour of the controller during the following day. A mechanism called anti-windup was applied to the PI controller to avoid this drawback. In detail, the *clamping method* was used. Clamping method interrupts the Integral term summation when a specific value is

reached. The Simulink flow programmed to model the PID controller that regulates the primary collector loop of the SolHe-PCM system (Control 1) assumes the form highlighted in *Figure 52*.
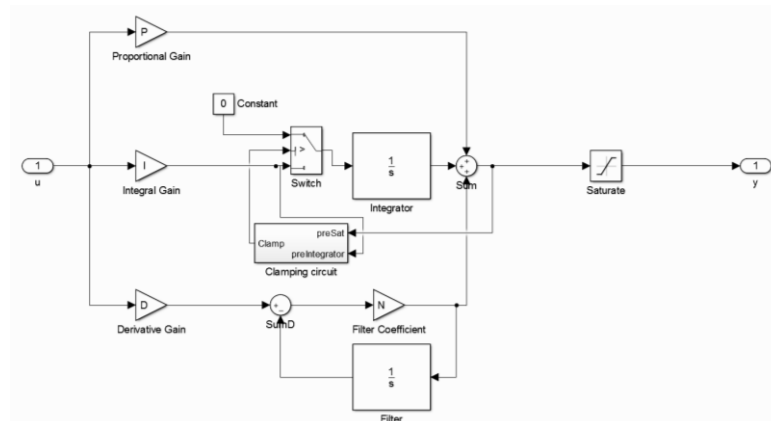
Figure 52. The Simulink flow used to simulate the PID Control 1, regulating the primary collector loop of the SolHe-PCM system.

3.5 Key-findings of the present chapter

The present chapter has introduced a solar thermal technology based on PCM slurry, named SolHe-PCM. The system uses the slurry as heat transfer fluid in the primary loop of the collector and as a storage medium in the thermal energy storage unit. The PCM slurry is based on micro-encapsulated n-eicosane, a paraffin characterised by a nominal melting temperature around 37 °C. The features of the slurry were investigated theoretically and experimentally. In detail, the T-History tests used to assess the thermal behaviour of the material have demonstrated its potentiality to overperform the storage capacity of traditional heat transfer fluids in the PCM phase transition temperature range. Rheological tests demonstrated that the material can be readily pumped up to 45 % w.t. concentration. Moreover, for the relatively lowest concentrations, the apparent viscosity of the slurry is very close to the one of traditional heat transfer fluids. Eventually, the physical stability of the suspension was tested, discovering the occurrence of a drawback called creaming phenomenon. This shortcoming was qualitatively and quantitatively studied. This test was necessary to define a system design configuration capable of coping with the additional challenges required to overcome the creaming occurrence.

Starting from the results of aforementioned investigations, the following of the present chapter deals with the design and the realisation of a full-scale prototype of the system. The various elements of the system are described in detail. Particular attention was given to the explanation of the control logic aiming at regulating the system. In fact, since the preliminary design steps, it has emerged that the controller of novel technology affects the overall system performance significantly. This research part is further discussed in Chapter 5.

Eventually, the present chapter reported the central assumptions and equations constituting a physical-mathematical model capable of describing the thermo-energetic behaviour of the solar thermal system. This model is divided into three sub-models (collector, thermal energy storage unit, and controllers), which were described in detail. The development of this model has been beneficial for the subsequent steps of the thesis. Indeed, on the one hand, in Chapter 4, the model – after calibration and validation – has been used to assess the performance of the innovative PCM-based solar thermal system according to several boundary conditions. On the other hand, in Chapter 5, these equations have been used as a control oriented model to device an innovative Model Predictive Control algorithm capable to further enhance the system efficiency.

References

[1]   Serale G, Fabrizio E, Perino M. Design of a low-temperature solar heating system based on a slurry Phase Change Material (PCS). Energy Build 2015;106:44–58. doi:10.1016/j.enbuild.2015.06.063.

[2]   Serale G, Goia F, Perino M. Numerical model and simulation of a solar thermal collector with slurry Phase Change Material (PCM) as the heat transfer fluid. Sol Energy 2016;134:429–44. doi:10.1016/j.solener.2016.04.030.

[3]   Buttitta G, Serale G, Cascone Y. Enthalpy-temperature evaluation of slurry phase change materials with T-history method. Energy Procedia, vol. 78, 2015. doi:10.1016/j.egypro.2015.11.352.

[4]   Fan X, Serale G, Capozzoli A, Perino M. Experimental measurement and numerical modeling of the creaming of mPCM slurry. Energy Procedia, vol. 78, 2015. doi:10.1016/j.egypro.2015.11.192.

[5]   Jiang Y, Liu X, Zhang L, Zhang T. High Temperature Cooling and Low Temperature Heating in Buildings. Energy Procedia 2015;78:2433–8. doi:10.1016/j.egypro.2015.11.222.

[6]   Koca A, Oztop HF, Koyun T, Varol Y. Energy and exergy analysis of a latent heat storage system with phase change material for a solar collector. Renew Energy 2008;33:567–74. doi:10.1016/j.renene.2007.03.012.

[7]   Serale G, Baronetto S, Goia F, Perino M. Characterization and Energy Performance of a Slurry PCM-based Solar Thermal Collector: A Numerical Analysis. Energy Procedia 2014;48:223–32. doi:10.1016/j.egypro.2014.02.027.

[8]   Goel M, S. R, S. S. Laminar forced convection heat transfer in microcapsulated phase change material suspensions. Int J Heat Mass Transf 1994;37:593–604.

[9]   Charunyakorn P, Sengupta S, Roy S. Forced convection heat transfer in microencapsulated phase change material slurries: flow in circular ducts. Int J Heat Mass Transf 1991;34:819–33.

[10]   Alkan C, Sarı A, Karaipekli A. Preparation, thermal properties and thermal reliability of microencapsulated n-eicosane as novel phase change material for thermal energy storage. Energy Convers Manag 2011;52:687–92. doi:10.1016/j.enconman.2010.07.047.

[11]   Genovese A, Amarasinghe G, Glewis M, Mainwaring D, Shanks RA. Crystallisation, melting, recrystallisation and polymorphism of n-eicosane for application as a phase change material. Thermochim Acta 2006;443:235–44. doi:10.1016/j.tca.2006.02.008.

[12]   Chen B, Wang X, Zeng R, Zhang Y, Wang X, Niu J, et al. An experimental study of convective heat transfer with microencapsulated phase change material suspension: Laminar flow in a circular tube under constant heat flux. Exp Therm Fluid Sci 2008;32:1638–46. doi:10.1016/j.expthermflusci.2008.05.008.

[13]   Gschwander S, Schossig P, Henning H. Micro-encapsulated paraffin in phase-change slurries. Sol Energy Mater Sol Cells 2005;89:307–15. doi:10.1016/j.solmat.2004.12.008.

[14]   Mehling H, Cabeza LF. Heat and cold storage with PCM. Handbook.

Springler; 2008.

[15] Sari A, Karaipekli A. Thermal conductivity and latent heat thermal energy storage characteristics of paraffin/expanded graphite composite as phase change material. Appl Therm Eng 2007;27:1271–7. doi:10.1016/j.applthermaleng.2006.11.004.

[16] Del Barrio EP, Dauvergne JL. A non-parametric method for estimating enthalpy-temperature functions of shape-stabilized phase change materials. Int J Heat Mass Transf 2011;54:1268–77. doi:10.1016/j.ijheatmasstransfer.2010.10.025.

[17] Alkan C, Sari A, Karaipekli A, Uzun O. Preparation, characterization, and thermal properties of microencapsulated phase change material for thermal energy storage. Sol Energy Mater Sol Cells 2009;93:143–7. doi:10.1016/j.solmat.2008.09.009.

[18] Lazaro A, Peñalosa C, Solé A, Diarce G, Haussmann T, Fois M, et al. Intercomparative tests on phase change materials characterisation with differential scanning calorimeter. Appl Energy 2013;109:415–20. doi:10.1016/j.apenergy.2012.11.045.

[19] Cascone Y, Perino M. Estimation of the thermal properties of PCMs through inverse modelling. Energy Procedia 2015;78:1714–9. doi:10.1016/j.egypro.2015.11.275.

[20] Cabeza LF, Barreneche C, Martorell I, Miró L, Sari-Bey S, Fois M, et al. Unconventional experimental technologies available for phase change materials (PCM) characterization. Part 1. Thermophysical properties. Renew Sustain Energy Rev 2015;43:1399–414. doi:10.1016/j.rser.2014.07.191.

[21] Yinping Z, Yi J, Yi J. A simple method, the -history method, of determining the heat of fusion, specific heat and thermal conductivity of phase-change materials. Meas Sci Technol 1999;10:201–5. doi:10.1088/0957-0233/10/3/015.

[22] Solé A, Miró L, Barreneche C, Martorell I, Cabeza LF. Review of the T-history method to determine thermophysical properties of phase change materials (PCM). Renew Sustain Energy Rev 2013;26:425–36. doi:10.1016/j.rser.2013.05.066.

[23] Delgado M, Lázaro A, Peñalosa C, Mazo J, Zalba B. Analysis of the physical stability of PCM slurries. Int J Refrig 2013;36:1648–56. doi:10.1016/j.ijrefrig.2013.04.020.

[24] Tadros T. Application of rheology for assessment and prediction of the long-term physical stability of emulsions. vol. 108–109. 2004. doi:10.1016/j.cis.2003.10.025.

[25] Delgado M, Lázaro A, Mazo J, Zalba B. Review on phase change material emulsions and microencapsulated phase change material slurries: Materials, heat transfer studies and applications. Renew Sustain Energy Rev 2012;16:253–73. doi:10.1016/j.rser.2011.07.152.

[26] Al-Shannaq R, Farid M, Al-Muhtaseb S, Kurdi J. Emulsion stability and cross-linking of PMMA microcapsules containing phase change materials. Sol Energy Mater Sol Cells 2015;132:311–8. doi:10.1016/j.solmat.2014.08.036.

[27] Zhang GH, Zhao CY. Thermal property investigation of aqueous suspensions of microencapsulated phase change material and carbon nanotubes as a novel heat transfer fluid. Renew Energy 2013;60:433–8. doi:10.1016/j.renene.2013.05.041.

[28] Bürger R, Damasceno JJR, Karlsen KH. A mathematical model for batch and

continuous thickening of flocculated suspensions in vessels with varying cross-section. Int J Miner Process 2004;73:183–208. doi:10.1016/S0301-7516(03)00073-5.

[29]   Abeynaike A, Sederman AJ, Khan Y, Johns ML, Davidson JF, Mackley MR. The experimental measurement and modelling of sedimentation and creaming for glycerol/biodiesel droplet dispersions. Chem Eng Sci 2012;79:125–37. doi:10.1016/j.ces.2012.05.036.

[30]   Richardson JF, Zaki W. Sedimentation and Fluidisation: Part I. Trans Inst Chem Eng 1954:35–53. doi:10.1098/rspa.1963.0204.

[31]   Vand V. Theory of viscosity of concentrated suspensions. Nature 1945:364–5.

[32]   Yamagishi Y, Takeuchi H, Pyatenko AT, Kayukawa N. Characteristics of microencapsulated PCM slurry as a heat-transfer fluid. AIChE J 1999;45:696–707. doi:10.1002/aic.690450405.

[33]   Duffie JA, Beckman WA. Solar Engineering of thermal processes. 4th Editio. New York, New York, USA: Wiley; 2013.

[34]   Serale G, Cascone Y, Capozzoli A, Fabrizio E, Perino M. Potentialities of a Low Temperature Solar Heating System Based on Slurry Phase Change Materials (PCS). Energy Procedia 2014, vol. 62, 355-263. doi: 10.1016/j.egypro.2014.12.397.

Chapter 4

Solar Heating with Phase Change Material slurry as the primary heat transfer fluid (Sol-He PCM project): results

The present chapter outlines the results obtained with the adoption of the models carried out in Chapter 3 and their integration with experimental data retrieved through the full-scale prototype. The chapter is organised as follows.

The first part (Section 4.1) shows the calibration procedure of the two models (collector and storage unit) with the data gathered during the experimental monitoring. The models were calibrated separately. Afterwards, a validation of the overall model operating in closed-loop was undertaken by a comparison with the monitored results. This procedure was concluded successfully. The Key Performance Indicators used to evaluate the worthiness of the method outlined a maximum discrepancy between experimental and simulated data lower than 12 %.

The second part (Section 4.2) compares the performance of the SolHe-PCM system with a traditional water-based system. Firstly, the analysis was undertaken using parametrical simulations, which evaluated how a single variable affected the overall system performance. Secondly, a long-term (year-long) performance evaluation was carried out for three localities characterised by different climatic conditions. The efficiency and useful heat produced by the collector were calculated with First law balances for water-based and PCM slurry based solar thermal systems. The performance of the storage unit in a closed-loop configuration was also evaluated with Second law considerations for the location of Turin. Compared to a traditional water-based system, the simulation results showed that the SolHe-PCM collector could improve the production of useful heat up to 7 % throughout the year and 19 % during the heating season. In terms of The second law analysis, simulation outcomes highlighted how the SolHe-PCM

system (collector and storage unit) could reduce the entropy generation rate up to 17 %.

The last part of the chapter (Section 4.3) describes the attempts of long-term monitoring of the technology. This parts strongly influenced also the previous Section 3.3 which describes the full-scale prototype design and construction. Indeed, the system performance was optimised with a trial-and-error procedure (typical of each new technology), which consisted in re-defining the design of a single system element when shortcomings show that better solution are necessary. This fact was particularly true for the thermal energy storage tank, where the physical instability – referred as creaming – affected the experimental campaign.

Some portions of the present Chapter were already published in the following scientific papers:

- Numerical model and simulation of a solar thermal collector with slurry Phase Change Material (PCM) as the heat transfer fluid. Authors: G Serale, F Goia, M Perino. Journal: Solar Energy 134, 429-444 [20];
- Characterization and energy performance of a slurry PCM-based solar thermal collector: a numerical analysis. Authors: G Serale, S Baronetto, F Goia, M Perino. Journal: Energy Procedia 48, 223-232 [21].

4.1 Preliminary monitoring campaign to calibrate the physical-mathematical model

In the first instance, it was necessary to calibrate the physical-mathematical numerical model. Indeed, on the one side, a calibrated numerical model allows reliable simulations to be performed. On the one side, these simulations can be used to tune the controller parameters in closed-loop scenarios (e.g., the tuning of the PID coefficients, the definition of the thresholds in RBC). On the other side, the simulation allows studying the performance of the systems also with different contexts and boundary conditions. These calibrated simulations lead to realise parametrical analyses and obtain performance results of more general validity.

The calibration process means to accurately identify the model parameters that allow simulated results to best-fit the actual performance of the monitored system prototype. This procedure is also often referred as system identification. The scientific literature is full of methods that can be adopted for calibration purposes [1–3]. In 2015, Fabrizio and Monetti for example stated that it is quite common to use "trial and error" methods to calibrate thermos-energetic models of buildings and their systems. Since these models can be very complex assumptions are necessary. For this reason, to handle the model complexity during calibration properly, the tuning process of the model parameters requires domain experts' knowledge [22]. Most commonly, the statistical methods based on regressions and Bayesian inference are used for this purpose. These methods are based on the fact that any physical model has some parameters that cannot be a-priori stetted, because their values are affected by inherent uncertainty (e.g., the liminar coefficients of a thermal models, the air change rates of indoor environments, etc.). These uncertain model parameters can be adjusted between some boundaries and under constraints of physical validity. This process can be driven by using a dataset of real monitored records. Section 5.2.5 analyses in details the system identification methods normally used for building application purposes.

4.1.1 Methodology used for calibration

In general, the calibration procedure aims to select the combination of model parameters that reduce the discrepancies between simulation results and the dataset of recorded data. This discrepancy is evaluated referring to a key performance indicator or a biased error. A model is considered calibrated when a selected key performance indicator or biased error underlies or overlies specific prefixed values (e.g., the error between real and simulated date must not exceed a fixed threshold). It is clear how optimization procedures and statistical analyses can positively intervene in this operation. There are several actors that have developed guidelines and methodologies to establish a measure of the accuracy of these models. In case on energy simulations referred to the whole building performance the most widely recognised – according to a study of Ruiz and

Bandera [23] – are ASHRAE Guidelines 14-2014 [24], the International Performance Measurement and Verification Protocol (IPMVP) [25], and the Federal Energy Management Program (FEMP) [26].

Since the system identification and the calibration procedure is not a primary concern of the present thesis, a simplified model calibration based on parametrical analyses was carried out. It consists of four steps:

- Individuate the parameter most affected by uncertainty in the numerical model through a sensitivity analysis;
- Define a set of possible (technologically and physically realistic) values that this parameter may assume;
- Compare the monitored data and the simulation results by varying the parameter affected by uncertainty through the entire set of possible values;
- Individuate the solution for which simulations best fit the recorded dataset, following a key performance indicator.

It was necessary to separate the effects related to the variation of the heat transfer fluid into the prototype from the calibration of the model itself. Indeed, since it is based on physical principles, the numerical model must be valid for both traditional heat transfer fluids (water and glycol), and each concentration of the innovative mPCM slurry. For this reason, it was chosen to calibrate the parameters referring to the system itself only, and not those related to the heat transfer fluid. Since under these hypotheses the calibration procedure is not fluid dependent, the calibration tests were undertaken using water and glycol (40 % w.t.) as heat transfer fluid and storage media. Thus the experimental tests with the mPCM slurry were used to validate the model performance afterward.

Furthermore, to avoid overfitting, the calibration procedure was undertaken separately for the solar thermal collector model and the thermal energy storage unit models. In this procedure the real data were gathered from the full-scale prototype that was operating normally in closed-loop. In the case of the collector model calibration, the inlet temperature of the panel was considered know and equal to its real measured value. In the case of the storage unit model calibration, the inlet temperature of the storage unit was considered know and equal to its real measured value. The two calibrated models have merged only afterwards, and the performance of the overall system model was evaluated and validated.

ASHRAE guidelines 14-2014 [24] defined calibration as the: "*process of reducing the uncertainty of a model by comparing the predicted output of the model under a specific set of conditions to the actual measured data for the same set of conditions.*" Three different key performance indicators were considered to evaluate the model calibration: Root Mean Square Error (RMSE), Mean Absolute Error (MAE) and Mean Absolute Percentage Error (MAPE) [4]. All these indices measure the distance between the model estimated values $\hat{y}_i$ and the actual recorded observations y_i. If the model results are all under the experimental evidence, the distance between these two values is equal to 0 and $\hat{y}_i = y_i$. It is a very unrealistic scenario since uncertainties (in the models or the measurements)

always affects the results. Each indicator is affected by pros and cons; thus their combination can be useful to understand the problem better [5,6]. The recent study of Ruiz and Bandera [23] highlighted the most common errors caused by a misinterpretation of the key performance indicators typically used in building energetics applications.

On the one hand, RMSE (also referred as Root Mean Square Deviation) is a simple distance function differentiable, symmetric, and quadratic (all these features are useful when optimal solution search is performed to define the solution that better calibrate the model). On the other hand, RMSE is very sensitive to outliers. Therefore, very few extreme values can ultimately affect its accuracy. After a discrete number n of i observations, the RMSE can be calculated as follows:

$$RMSE = \sqrt{\frac{\sum_i^n (\hat{y}_i - y_i)^2}{n}} \tag{4.1}$$

The MAE (also referred Normalised Mean Bias Error) as has a physical significance, and it represents the average discrepancy between real and simulated data by definitions. However, since this discrepancy is not normalised on the magnitude of the monitored data, it cannot be used to assess the effectiveness and the reliability of the estimation directly. MAE is defined as:

$$MAE = \frac{1}{n} \cdot \sum_i^n |\hat{y}_i - y_i| \tag{4.2}$$

Eventually, the MAPE (also referred as Mean Absolute Percentage Deviation) represents the error calculated by MAE, normalised on the recorded observation and multiplied per one hundred to obtain a percentage error:

$$MAPE = \frac{100}{n} \cdot \sum_i^n \left| \frac{\hat{y}_i - y_i}{y_i} \right| \tag{4.3}$$

The main drawback of the MAPE is its being biased. Indeed, it is bounded on the lower-end – the minimum error is 0 % – but is unbounded on the upper-end – the maximum percentage error can be infinite. This is a particular problem if the denominator is small or zero. For example, this condition happens when the model is attempting to forecast the power production of the collector when small or null solar radiation occurs.

4.1.2 Model calibration and validation

The model calibration and validation process lasted 5 days in total (from May 25th to May 30th). In this period the behaviour of the full-scale prototype was

continuously monitored under the variation of the climatic disturbances. Firstly, the solar thermal collector and the thermal energy storage were calibrated as stand-alone elements with separate procedures. To calibrate the panel model, the collector inlet temperature (influenced by the storage unit outlet temperature) was considered known and equal to the data gathered experimentally. To calibrate the storage unit model, the thermal energy storage unit inlet temperature (influenced by the collector outlet temperature) was considered known and equal to the data gathered experimentally. Afterwards, the two calibrated models were merged and validated through simulation of the closed-loop behaviour of the system. The following *Figure 1* highlights the profiles of solar radiation and ambient temperature during the calibration period.
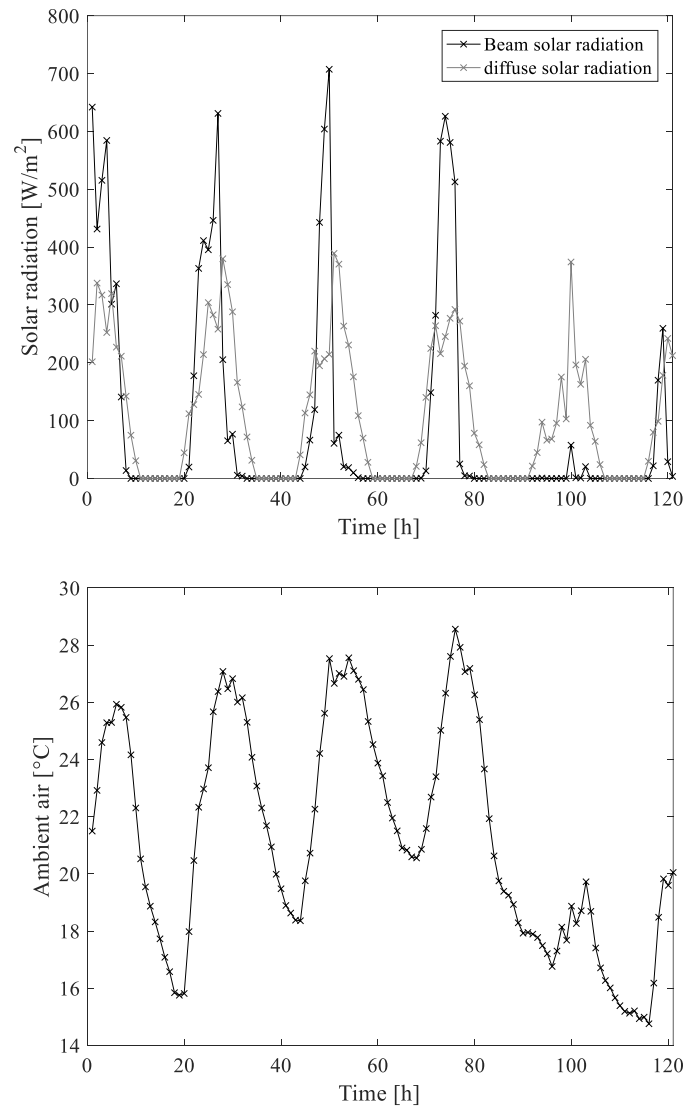
Figure 1. (top) Solar radiation. (bottom) Ambient air temperature.

It can be inferred from the figure how the very first three days and a half were sunny days, while the last two days were cloudy. The full-scale system under investigation was equipped with the first version of the thermal energy storage

unit (multi-partition thermal energy storage). For this reason, this calibration process refers to the first version of the numerical model of the thermal energy storage unit. Contrariwise, it was adopted the computationally more robust second version of the collector numerical model.

It was necessary to separate the effects due to the regulation of the system from its thermo-dynamical evolution. Thus, the calibration procedure was undertaken under constant control conditions. In particular:

- The set-point of primary peristaltic pump of the collector loop circuit (P3) was set equal to 70 RPM, corresponding to a flow-rate equal to about 55 l/h ($1.5 \cdot 10^{-2}$ kg/s);
- The demand side simulator was configured to cool down the thermal energy storage continuously, setting a constant flow-rate equal to 410 kg/h and an inlet temperature of 15 °C.

4.1.2.1 Calibration of the solar thermal collector numerical model

The calibration of the numerical model of the solar thermal collector was carried out under the assumptions previously mentioned. The real monitored weather conditions were used as solicitations of the Matlab-Simulink model. Furthermore, the collector inlet temperature was set equal to the actual temperature value recorded by the thermocouple TC1.

The collector outlet temperature was used to assess the reliability of the simulation results with the experimental data. Assumed known the flow-rate flowing in the panel and the collector inlet temperature, the uncertainty on this value is the one that affects the useful thermal power production of the system.

The parameter individuated to calibrate the panel is the optical/thermal transmission, and absorption coefficient of the glazing cover of the solar thermal collector. This parameter is generally identified with the expression $(\tau\alpha)_e$ *product*, introduced by Duffie and Beckman [7]. This value depends on the glazing cover typology, and it is influenced by the angle of incidence of the solar radiation, so its value varies during the daytime. The gazing cover used in the SolHe-PCM prototype is an extra-clear single glass. However, there were not experimental evidence or technical data-sheets to characterise its $(\tau\alpha)_e$ product property. For this reason, the $(\tau\alpha)_e$ product was affected by substantial uncertainty. To perform the simulations, $(\tau\alpha)_e$ was calculated starting from the curve of $(\tau\alpha)$ vs. the angle of incidence of the solar radiation, γ, provided by the *WINDOW| Windows and Daylighting* software of LBNL [8] for an extra-clear single glass.

To obtain the $(\tau\alpha)_e$ product from the abovementioned curve it was necessary to multiply these curves for a coefficient e that accounts the additional optical losses due to the accumulation of dirtiness on the panel cover. Moreover, for the specific SolHe-PCM prototype, the coefficient e has to consider also the further optical losses due to the metal frame of the panel curtain system. To perform the parametrical model calibration, it was supposed that the coefficient e does not affect the shape of the $(\tau\alpha)_e$ product curve. Thus, it assumes values constant for

each possible angle of incidence of the solar radiation, γ, and the expression of $(\tau\alpha)_e$ can be formulated as:

$$(\tau\alpha)_e = (1 - e) \cdot (\tau\alpha)(\gamma) \qquad (4.4)$$

The coefficient e is entirely empiric. Thus, it may assume any value in the range between 0 (no dirtiness/frame effects) and 1 (no radiation through the glazing system due to dirtiness/frame effects). The parametrical analysis for calibration purposes was performed with the values of the coefficient e ranging between 0 (used as a reference for a completely clear glazing cover) and 0.25. The following *Figure 2* shows the variation of $(\tau\alpha)_e$ curves according to the different parametric values of the coefficient e.
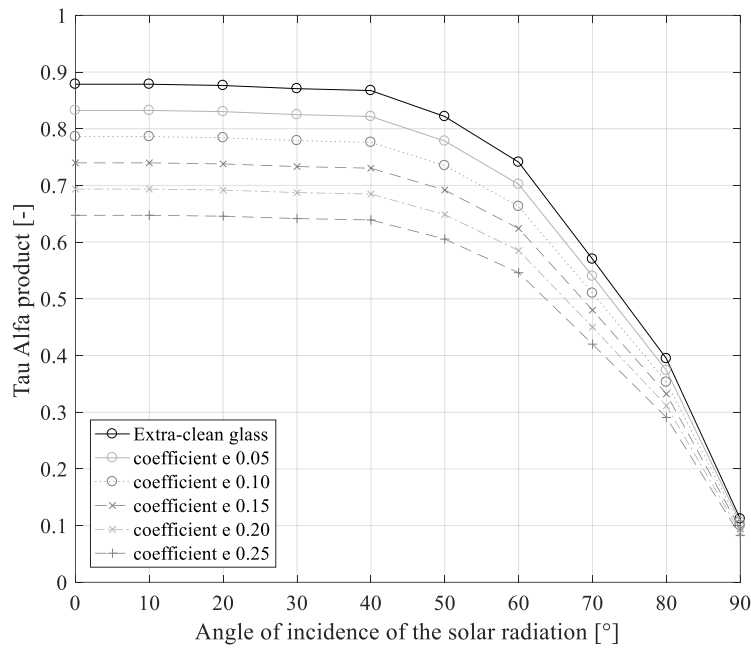
Figure 2. Variation of the $(\tau\alpha)_e$ curves according to different values of the coefficient e, that considers panel dirtiness and curtain frame shading.

Simulations were performed, parametrically varying the e coefficient. The difference between real and monitored values of the collector outlet temperature was used to evaluate the model effectiveness. Results concerning key performance indicators are reported in *Table 1*. From that table, it can be inferred as the most reliable results are those referring to the $(\tau\alpha)_e$ curve derived with e coefficient equal to 0.10. Indeed, they overperform the others according to every indicator used to evaluate the model reliability.

Figure 3 highlights the collector outlet temperature behaviour during one day of monitoring (red curve) and simulations (black and grey curves). It allows the discrepancies between the results obtained with different e coefficients to be also visually appreciated.

Table 1. Trends of the error indicators during the parametrical calibration.

	e = 0	e = 0.05	e = 0.10	e = 0.15	e = 0.20	e = 0.25
MAE	0.54 °C	0.41 °C	**0.39 °C**	0.53 °C	0.70 °C	0.89 °C
MAPE	2.37 %	1.95 %	**1.88 %**	2.31 %	2.87 %	3.48 %
RSME	0.71 °C	**0.50 °C**	**0.50** °C	0.71 °C	1.01 °C	1.35 °C

The following *Figure 3*, *Figure 4*, and *Figure 6* shows the comparison between simulated and recorded data along the weekdays of the calibration procedure. *Figure 4* refers to the collector outlet temperature, which is the most critical parameter since it is the one used to calculate the error indices for calibrating the model. *Figure 5* reports the overall temperature profiles along the 10 nodes in which the panel was discretised. Eventually, *Figure 6* shows the patterns of useful thermal power production.
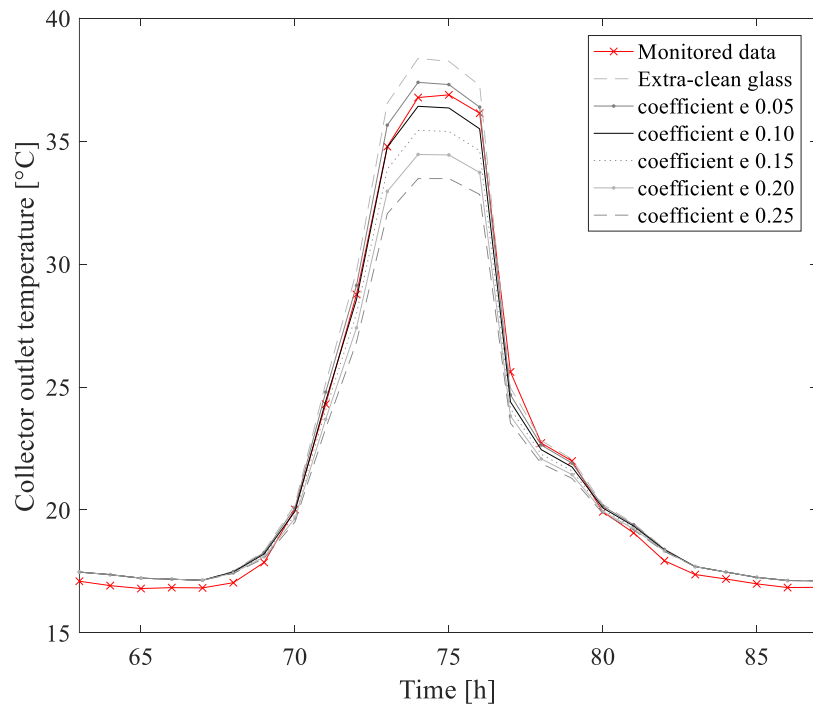
Figure 3. Comparison between the real monitored data and the simulated results, overview of a day for different (τα)ₑ curves relative to different e coefficients.

From *Figure 6*, it can be inferred how the significant discrepancies between real and monitored data occur only during night-time or when the useful thermal power production is shallow. Therefore, they can be considered negligible. These discrepancies can be explained with the following consideration. The model has been developed on the basis of the Hottel-Willier model that was tailored to capture the dynamics of a solar thermal collector producing useful heat. In this case, the primary variable influencing the system heat exchange is the Sun shortwave radiation. During the night time, the primary heat exchange dynamics

influencing the system are others, i.e., the ambient air and the longwave radiation towards the sky. The model is less sensitive to capture these dynamics and, for this reason, a slightly larger discrepancy between monitored and simulated data may occur.
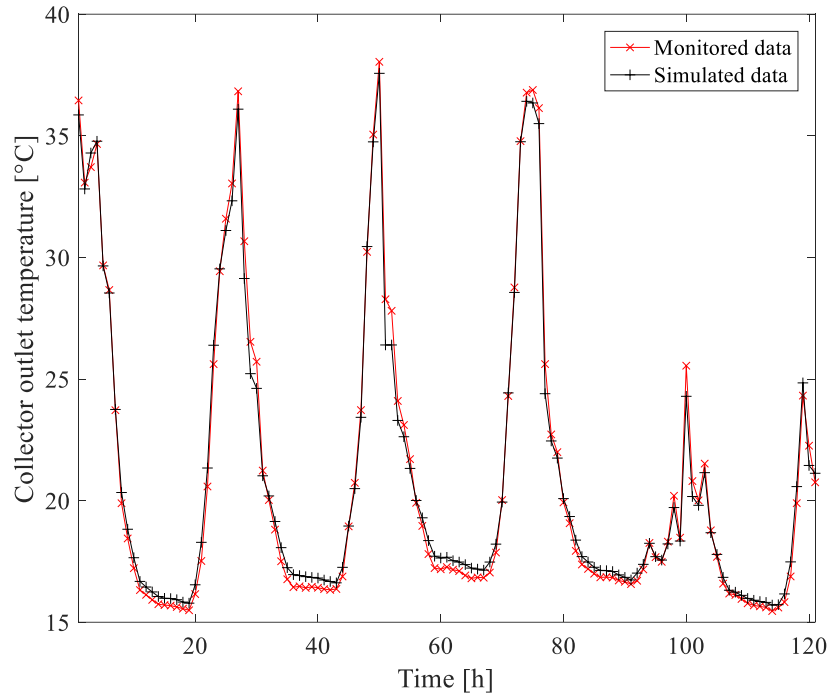
Figure 4. Comparison between the real monitored data and the simulated results of the collector outlet temperature, after the calibration of the model with the adoption of the (τα)ₑ curve relative to the coefficient e = 0.10.

Figure 5. Simulated results of the temperature profile of the heat transfer fluid over collector length, after the calibration of the model with the adoption of the (τα)ₑ curve relative to the coefficient e = 0.10.

Figure 6. Comparison between the real monitored data and the simulated results of the collector thermal power produced, after the calibration of the model with the adoption of the $(\tau\alpha)_e$ curve relative to the coefficient e = 0.10.

4.1.2.2 Calibration of the thermal energy storage unit numerical model

The thermal energy storage unit model was calibrated in the meanwhile of the solar collector model. The real monitored weather conditions were used as solicitations of the Matlab-Simulink model. Furthermore, the inlet temperature of the thermal energy storage unit was set equal to the actual temperature value recorded by the thermocouple TC8. Both the full-scale prototype and the model allows monitoring the trend of the temperature of the energy storage media in the seven partitions of the storage tank. Therefore, the experimentally recorded values of the thermocouples TC9, TC10, TC11, TC12, TC13, TC14, and TC15 were used to be compared with the simulation results data.

From a sensitivity analysis, the *U-value* of the thermal energy storage unit was individuated as the parameter affected by the uncertainty that most influences the reliability of the results. Indeed, this value is affected by the uncertainty due to the internal liminar coefficient (of the layer combining the storage fluid with the tank envelope) and the external liminar coefficient (of the layer combining the tank envelope with the ambient air). For this reason, the U-value of the thermal energy storage unit was varied parametrically and used to calibrate the numerical

model. The U-value of a cylindrical element – as the storage tank is – is defined as follows:

$$U_{st} = \left(\frac{1}{h_{int}} + \frac{R_{st,in}}{\lambda_{tank}} \cdot \ln\left(\frac{R_2}{R_{st,in}}\right) + \frac{R_{st,in}}{\lambda_{ins}} \cdot \ln\left(\frac{R_{st,est}}{R_2}\right) + \frac{R_{st,in}}{R_{st,est}} \cdot \frac{1}{h_{est}} \right)^{-1} \qquad (4.5)$$

Where h_{int} and h_{est} are the internal and external liminar coefficient respectively; $R_{st,int}$, $R_{st,est}$, and R_2 are the thermal energy storage unit inner radius, external radius, and radius of the layer in between tank envelope and the insulation layer (see *Figure 7* for details); and λ_{tank}, and λ_{ins} are the thermal conductivity of the tank envelope (iron) and the insulation layer (fiberglass) respectively. Except for the radii, all these features influencing the storage unit conductivity are affected by some uncertainty. Table 2 summarises the values assumed in first approximation for this features.
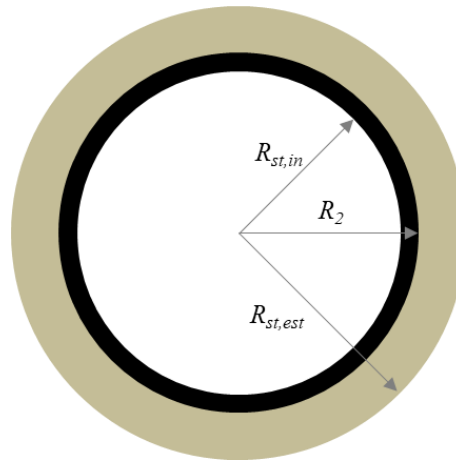
Figure 7. Radii characterising the thermal energy storage unit.
Table 2. Features of the thermal energy storage influencing its thermal conductivity.

Specification	Symbol	Value	m.u.
Inner radius	$R_{st,int}$	0.222	m
External radius	$R_{st,est}$	0.222	m
Tank-insulation radius	R_2	0.325	m
Tank conductivity (iron)	λ_{tank}	50	W m^{-1} K^{-1}
Insulation conductivity (fiberglass)	λ_{ins}	0.04	W m^{-1} K^{-1}
Internal liminar coefficient	h_{int}	500	W m^{-2} K^{-1}
External liminar coefficient	h_{est}	10	W m^{-2} K^{-1}

According to these features, the U-value of the thermal energy storage tank resulted equal to 0.47 W/(m^{2}K). This value was assumed as the first approximation for the parametrical calibration of the model. Afterwards, it was increased or decreased by a percentage value to calibrate the model parametrically. The following *Table 3* summarises the U-values considered in the parametrical calibration.

Table 3. Parametric variation of the thermal conductivity for calibration purposes. U-values are expressed in W/(m^{2}K).

-15%	-10 %	-5 %	-	+5%	+10 %	+15%
0.40	0.43	0.45	0.47	0.50	0.52	0.54

Simulations were performed, parametrically varying the U-value. The difference between real and monitored values of the collector outlet temperature was used to evaluate the model effectiveness. Results concerning key performance indicators are reported in *Table 4*. From that table, it can be inferred as the most reliable results are those referring to the U-value increased of 10 %.

From *Table 4* it is possible to infer that the variation of U-value only slightly affects the reliability of the model. Indeed, the heat losses toward the ambient air affect only marginally the dynamical evolution of the system, if compared to the magnitude of the heat exchanges occurring with the primary collector loop and the demand side simulator. Nevertheless, the accuracy and reliability of the model are still very high, as the low error indicators highlight.

Table 4. Trends of the error indicators during the parametrical calibration procedure. The results referring to the e coefficient 0.10 overperform the others according to every indicator used to evaluate the model reliability.

U-value [W/(m^{2}K)]	0.40	0.43	0.45	0.47	0.50	0.52	0.54
MAE	1.87 °C	1.86 °C	1.86 °C	1.86 °C	1.86 °C	**1.85 °C**	1.86 °C
MAPE	10.06%	10.05%	10.04%	10.05%	10.02%	**10.01%**	**10.01%**
RSME	1.66 °C	1.65 °C	1.64 °C	1.64 °C	1.64 °C	**1.63 °C**	1.64 °C

Figure 8 and *Figure 9* highlight for one day the resulting temperature profiles over the various storage unit partitions. They show the comparison between monitored (red curves) and simulated data (black curves). From these figures, it is possible to appreciate how the numerical model well estimates the temperature

trends of the upper partitions (*Figure 8*), while it tends to anticipate the temperature rising during daytime in the lower partitions (*Figure 9*). This time shift can be charged to the complex dynamics of the fluid flowing into the storage. Indeed, the simplified multimode lumped model could not be able to capture complex rheological phenomenon occurring between the partitions of the storage (e.g., vortex formation, interactions between convection dynamic and flow dynamics). However, these drawbacks caused a temperature difference between recorded and simulated data no more significant than 1.5 °C.
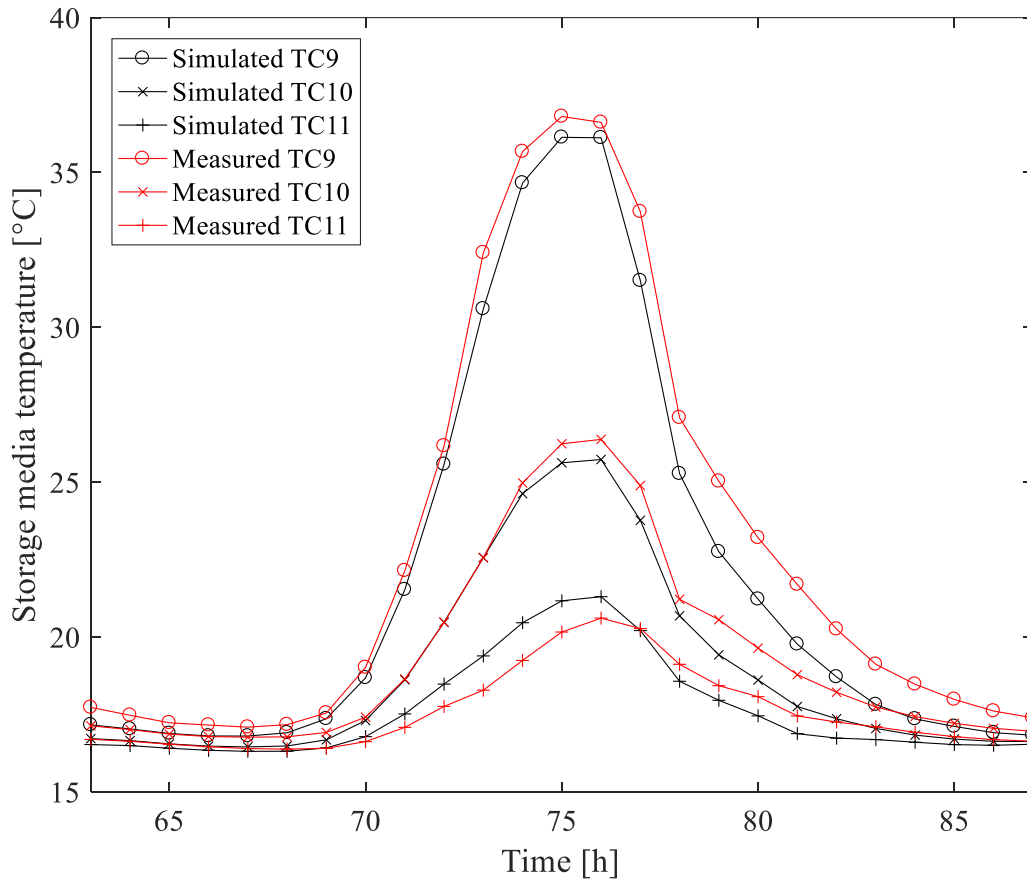
Figure 8. Daily profiles of the storage media internal temperature (upper partitions).

Eventually, *Figure 10* shows the temperature profiles of the various partitions for the entire week during which the calibration process was undertaken. The higher and the lower partitions are highlighted with black lines to indicate that are those mostly influence and are influenced by the primary loop of the collector.
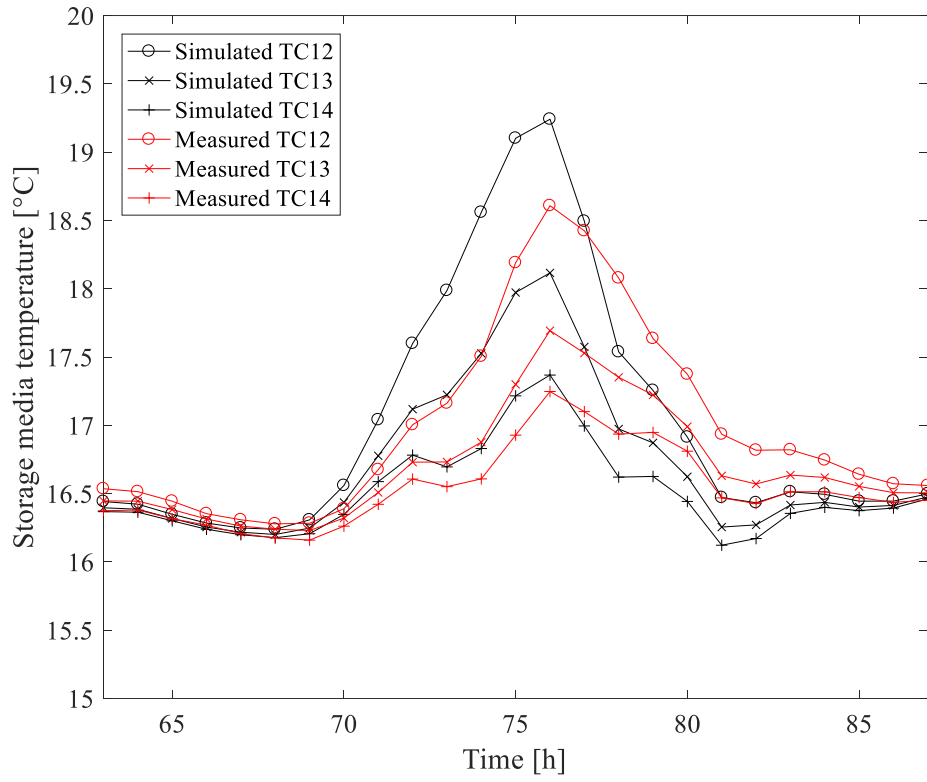
Figure 9. Daily profiles of the storage media internal temperature (lower partitions).
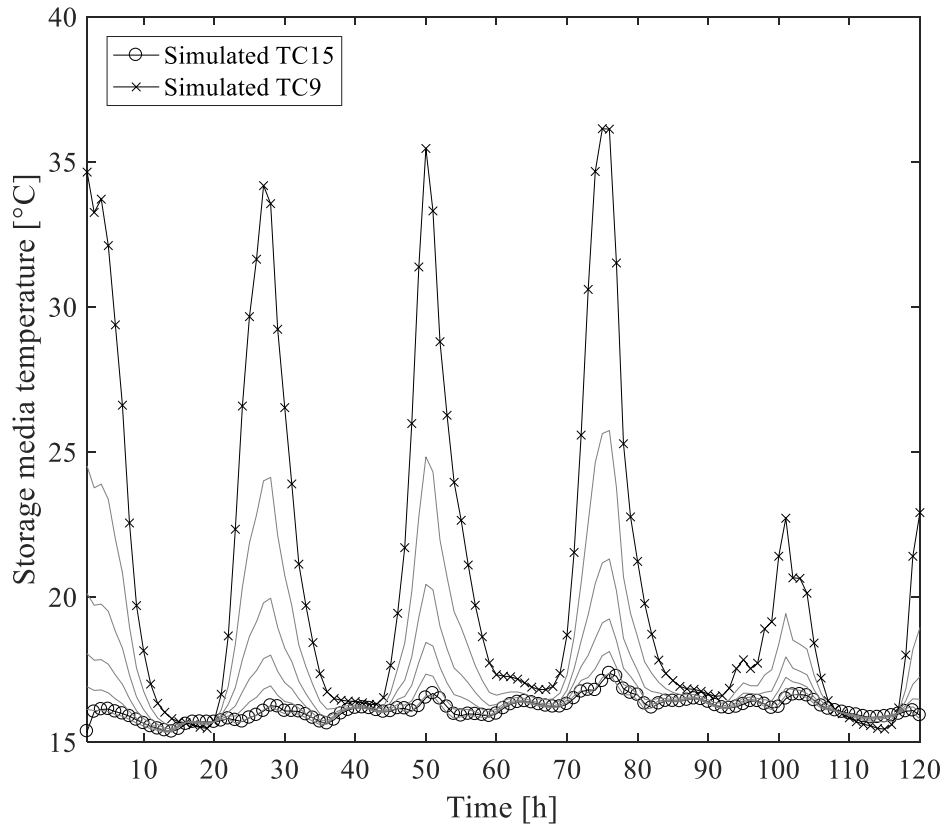
Figure 10. Weekly temperature profiles into the different thermal energy storage partitions resulting from the simulations after the calibration procedure.

4.1.2.3 Validation of the calibrated model by the comparison of the experimental and simulation results referring to the overall solar thermal system

In the calibration processes discussed above, the boundary conditions referring to the inlet temperatures of the storage or the collector were assumed known. They were set equal to the monitored data. In the case of closed-loop simulations this is not valid anymore. Indeed, the inlet temperature of the panel is the influenced by the outlet temperature of the storage. Vice versa, the inlet temperature of the storage is affected by the outlet temperature of the collector. For these reasons, the closed-loop validation introduces an increasing of the possible causes of error in both models. Nevertheless, error indicators obtained after the validation process in closed-loop simulations remained still small, as it can be observed in *Table 5*.

The goodness of the results – thus the reliability of the model – can be observed in the following *Figure 11*, *Figure 12*, *Figure 13*, and *Figure 14*.

Table 5. Error indicators obtained during the validation process in closed-loop simulations of the solar thermal system model.

	MAE	MAPE	RSME
Solar collector	2.19 °C	8.05 %	2.10 °C
Thermal storage	0.38 °C	11.79 %	0.83 °C
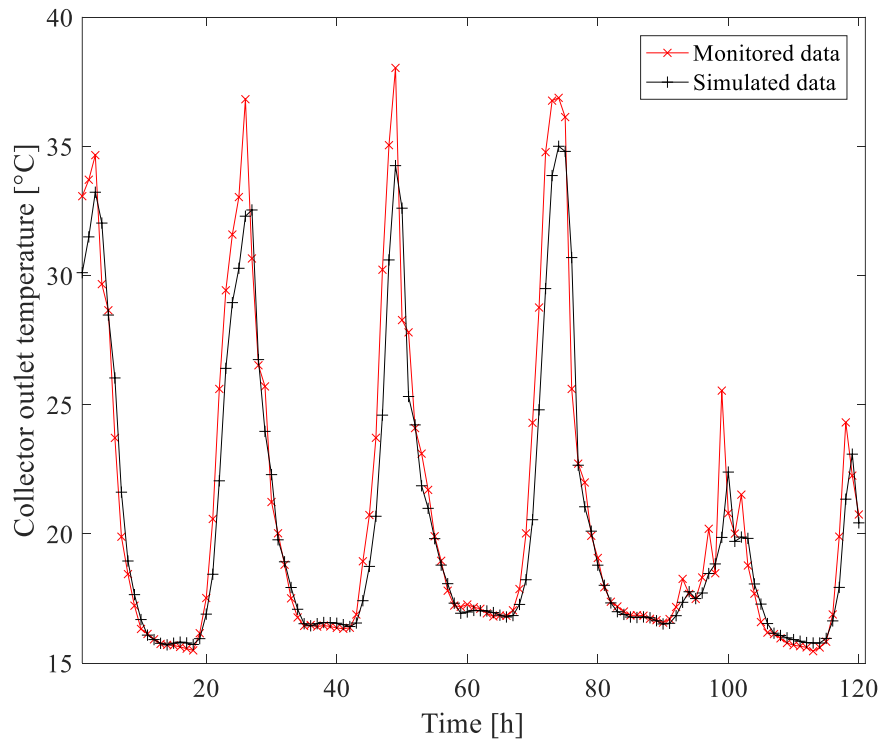
Figure 11. Validation in closed-loop simulations. Comparison between the real monitored data and the simulated results of the collector outlet temperature.
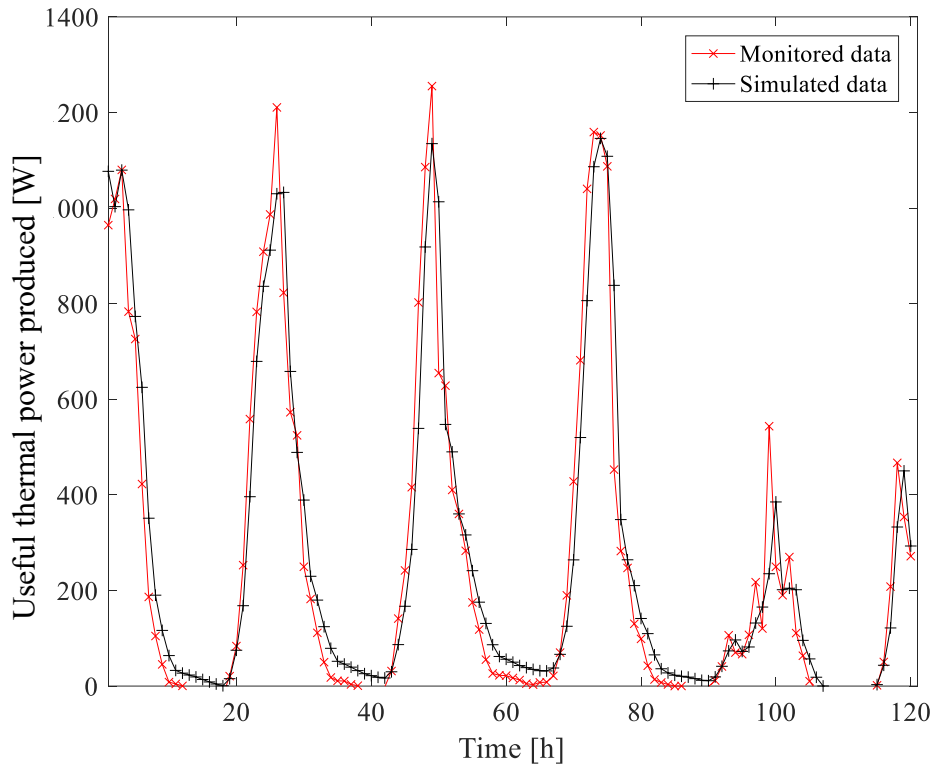
Figure 12. Validation in closed-loop simulations. Comparison between the real monitored data and the simulated results of the panel thermal power produced.
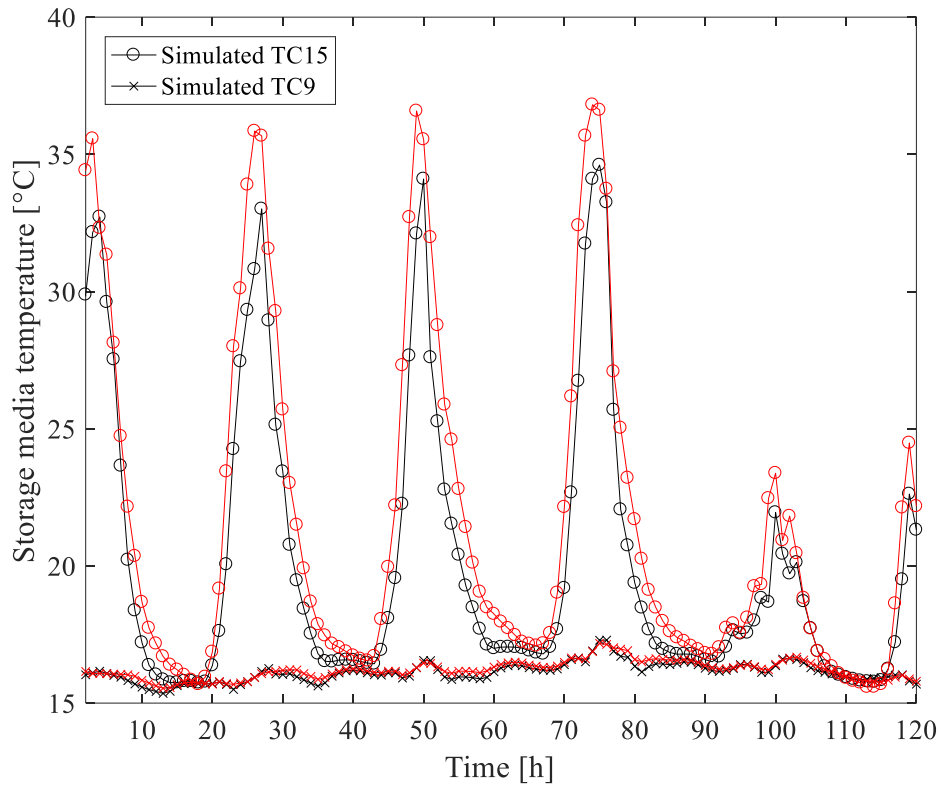
Figure 13. Validation in closed-loop simulations. Comparison between the real monitored data and the simulated results of the storage media temperature in the higher and the lower partitions.
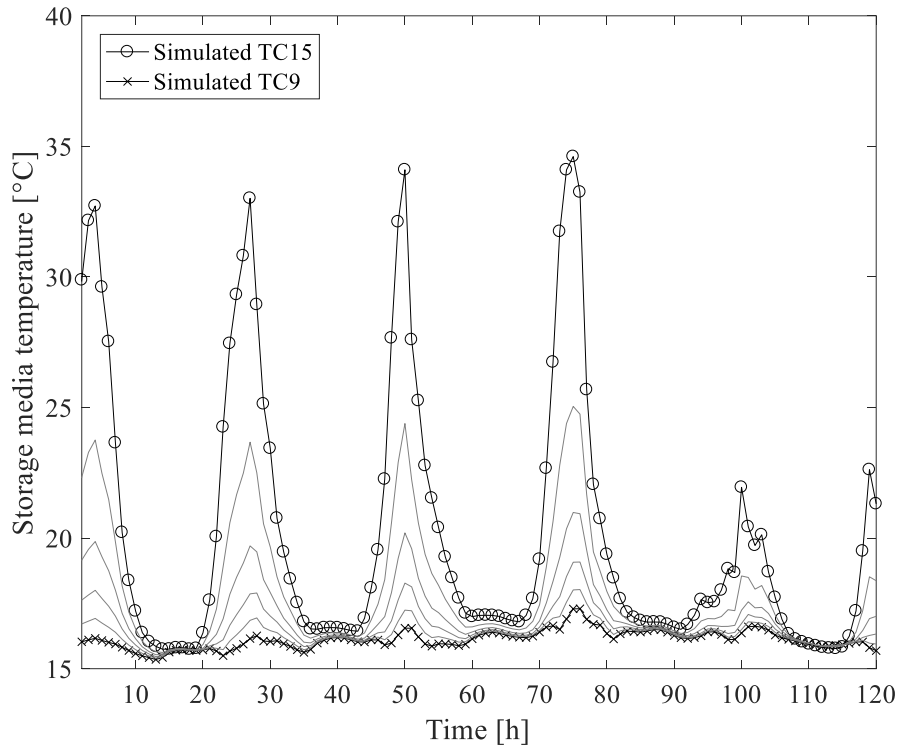
Figure 14. Validation in closed-loop simulations. Weekly temperature profiles into the different thermal energy storage partitions.

From the former *Figure 11*, *Figure 12*, *Figure 13* and Figure 14 it is possible to point out how the numerical model is able to effectively capture the dynamics of the system operating in closed-loop condition. This fact is also underlined by the worthy results obtained by the key performance indicators used to assess the reliability of the estimated results. The small discrepancies between simulated and monitored data show that the model slightly underestimates the actual values and there is a small time lag in the simulated data, particularly during the peak periods. The large part of this small shortcomings are attributable to the thermal inertia of the collector that has not been modelled in the Hottel-Willier equations. Since this thermal inertia is very small it does not affect the results dramatically but its influence is not negligible. Future works may include also this variable in the numerical model to further improve the worthiness of the simulation results.

4.2 Calibrated numerical model: simulation results

The validated numerical model was used to carry out simulation results. These outcomes led to investigate the benefits in terms of energy efficiency achievable by the adoption of the SolHe-PCM technology. The simulations were carried out for various boundary conditions (e.g., different weather conditions, various concentrations of mPCM in the mixture). A traditional solar thermal system using water and glycol as the heat transfer fluid and storage media was used as a baseline for comparisons reference.

The numerical simulations considered either the solar collector only or the overall solar thermal system (collector, storage and controller). Concerning the collector two different types of evaluation were performed:

• Parametrical evaluations, which tested how the variation of several boundary conditions affects the system performance;
• Year-long numerical simulations, which investigated the efficiency of the system set in three locations with various configurations.

The parametrical evaluations are a great tool to assess the instantaneous efficiency under different boundary condition. The instantaneous efficiency assumes a significant relevance in the case of the standalone collector element, where the influence of the thermal inertia on the component performance is negligible. Contrariwise, regarding the thermal energy storage unit, it is crucial to be focused on its dynamical evolution to assess its performance. In fact, in this case, the thermal inertia of the element plays an essential role. For this reason, only the year-long simulations were performed to estimate the performance of the overall system.

4.2.1 Parametrical evaluations of the performance of the solar thermal collector based on mPCM slurry

The instantaneous collector performance was parametrically investigated for various PCM concentrations in the mixture. In detail, concentrations of 10 % w.t., 20 % w.t., 30 % w.t., and 40 w.t. were considered. For the sake of briefness, results herewith reported referring to the 30 % w.t. concentration only. Indeed, a sensitivity analysis underlined that 30 % w.t. was the concentration that ensures the best trade-off between improvement of the material thermal features and worsening of the fluid viscosity. The collector was considered tilted at 45° for the entire simulation set.

Concerning weather disturbances, the Hottel-Willier model of the panel highlighted how ambient temperature and solar irradiance on the tilted surface are the two parameters that most influence the component performance. Particularly the latter is the variable that primary determines the useful thermal power

delivered by the collector. For this reason, the parametrical evaluations considered different levels of solar irradiance. In detail, simulations were performed assuming the global solar irradiance on the tilted surface (45°) equal to 200 W/m^2, 400 W/m^2, 600 W/m^2, and 800 W/m^2. The variation of the ambient temperature had to be investigated likewise. However, for providing reliable results, it might be statistically related to the solar irradiance. For this purpose, firstly, Turin was chosen as the reference location for instantaneous parametrical evaluations. This assumption is due to the fact that the numerical model was calibrated on the data gathered by the SolHe-PCM prototype installed in Turin. Secondly, the International Weather file for Energy Calculation (IWEC) for Turin was examined. The maximum and minimum temperature occurring in correspondence of o a certain range of average hourly global solar irradiance on the tilted were individuated processing the IWEC data of Turin. The irradiance ranges selected were the representative bounds of the parametrically investigated irradiance levels. *Table 6* reports these values.

Table 6. Individuation of the maximum and minimum temperatures recorded in the IWEC file for different solar radiation thresholds.

G$_T$ [W/m^2]	101-300	301-500	501-700	>701
Min [°C]	-3.0	0.7	4.1	12.0
Max [°C]	30.3	30.7	31.0	30.7

The following caption is valid for *Figure 15*, *Figure 16*, *Figure 17*, and *Figure 18*. Red lines refer to PCM at 30 % w.t., while black lines refer to water and glycol as the heat transfer fluid used in the collector.

The results of the first instantaneous parametrical simulations aimed at investigating how the flow-rate flowing in the collector affects the useful thermal power produced. The heat transfer fluid temperature at the collector inlet was considered equal to 35 °C (around the lower phase change limit of the material). The ambient temperature was set equal to either the minimum or the maximum temperature recorded in correspondence of each solar irradiance range listed in *Table 6*. Results are shown in *Figure 15* and *Figure 16* respectively.
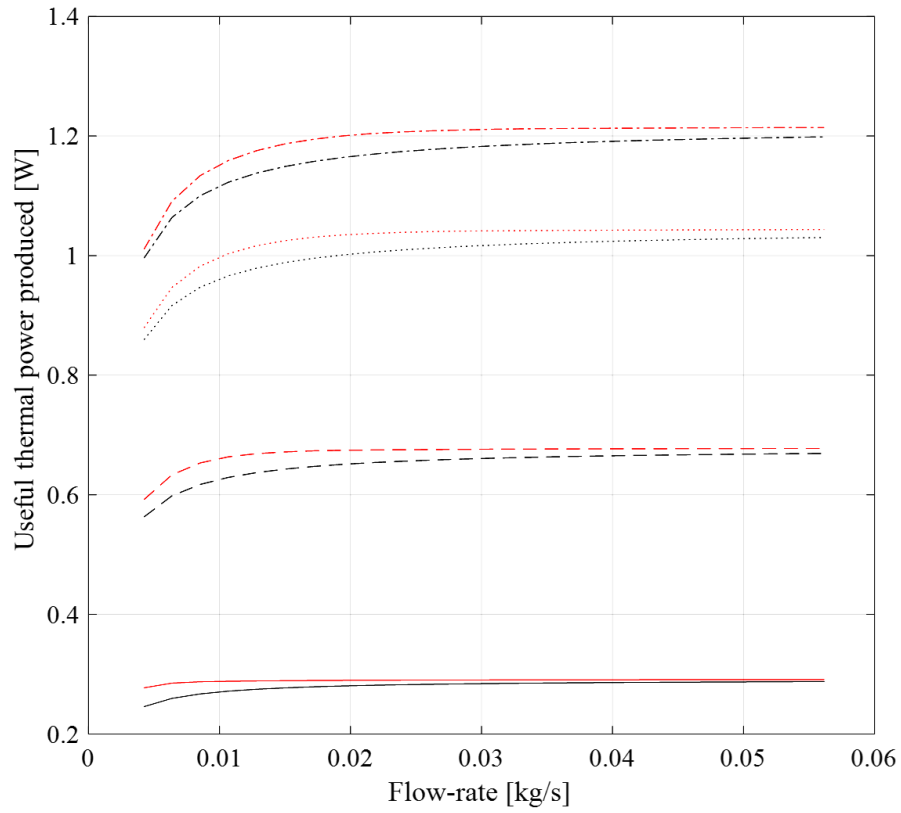
Figure 15. Instantaneous parametrical evaluations. Useful thermal power produced by the collector vs. heat transfer fluid flow-rate. Minimum ambient temperature.
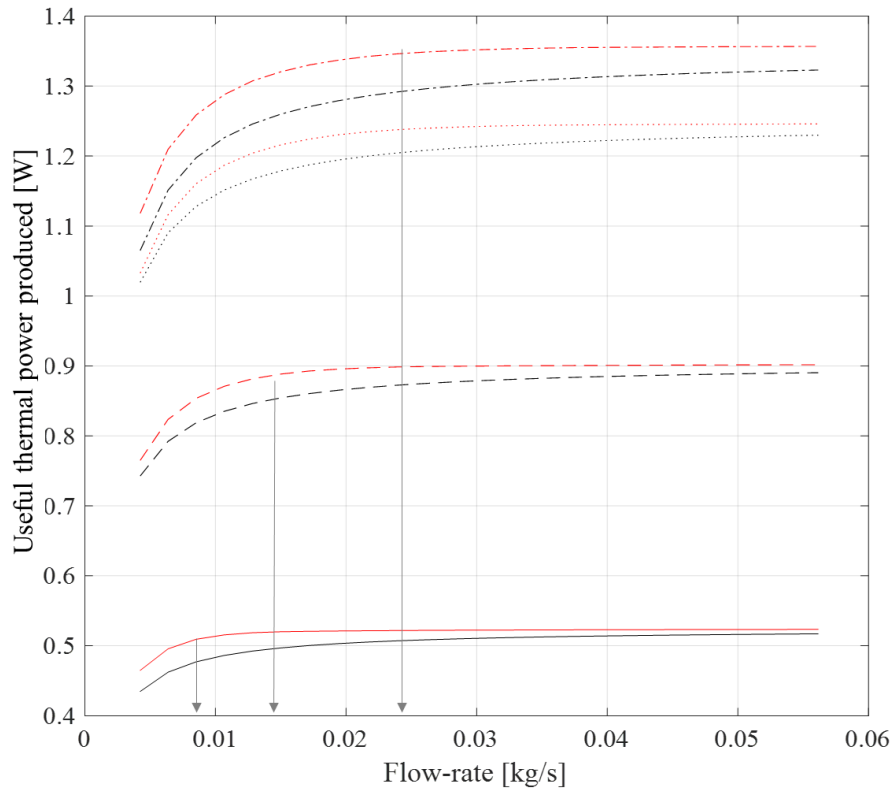
Figure 16. Instantaneous parametrical evaluations. Useful thermal power produced by the collector vs. heat transfer fluid flow-rate. Maximum ambient temperature.

152

From the results illustrated in *Figure 16,* it was possible to define the radiation thresholds used in the open-loop version of the controller (see Section *3.3.6.1*) regulating the flow-rate of the peristaltic pump P3. Indeed, this control logic is a Rule-Based Controller (RBC) that associates a certain flow-rate of the heat transfer fluid to a specific level of global solar irradiation monitored on the tilted plane of the solar thermal collector. *Table 7* summarises this RBC control logic.

Table 7. Pump flow-rates, baseline controller irradiance thresholds and related electric power consumptions.

Flow-rate		Irradiance thresholds	Power
[l/h]	[m^3/s]	[W/m^2]	[W]
0	0	0 - 50	0
10	$2.8 \cdot 10^{-6}$	50 - 225	5
60	$1.7 \cdot 10^{-5}$	225 - 500	25
90	$2.5 \cdot 10^{-5}$	> 500	55

The radiation thresholds of *Table 7* were used to define the flow-rates of the subsequent parametrical analyses. Findings of the following evaluation are reported in *Figure 17*. They correlated the panel instantaneous efficiency with the ambient temperature. The vertical black dashed lines reported in the figure indicate the reference ambient temperature for heating design calculations (-8.0 °C) and the yearly average ambient temperature (12.4 °C) in Turin. The vertical grey dashed lines indicate the lower temperature threshold in correspondence to a specific solar irradiance level (see *Table 6*). The lower the solar irradiance level, the more left the vertical grey dashed line. Also in this case, the collector inlet temperature was again assumed equal to 35 °C.

Figure 18 shows the outcomes of the parametrical evaluation about how the useful thermal power produced by the collector is affected by varying the collector inlet temperature. The ambient temperature was assumed constant and equal to the yearly average ambient temperature in Turin, 12.4 °C. The phase change transition range can be appreciated in the figure. Furthermore, the chart highlights once again as the control of the temperatures is crucial for a technology that exploits the latent heat. Indeed, as long as the collector inlet temperature is maintained equal or lower to the lower phase change temperature the collector based on mPCM slurry overperforms the traditional water-based one. Once the upper limit of phase change is exceeded, the lower specific heat capacity of the mPCM slurry negatively affects the behaviour of the heat transfer fluids. The performance of the panel drops consequently.
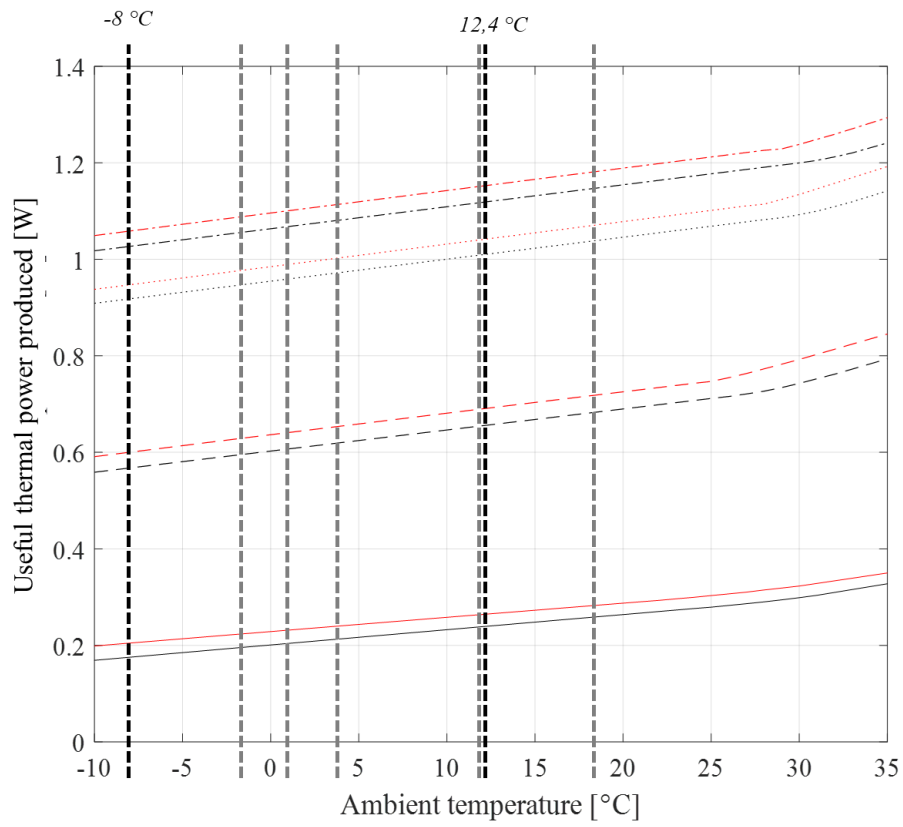
Figure 17. Instantaneous parametrical evaluations. Useful thermal power produced by the collector vs. ambient temperature.
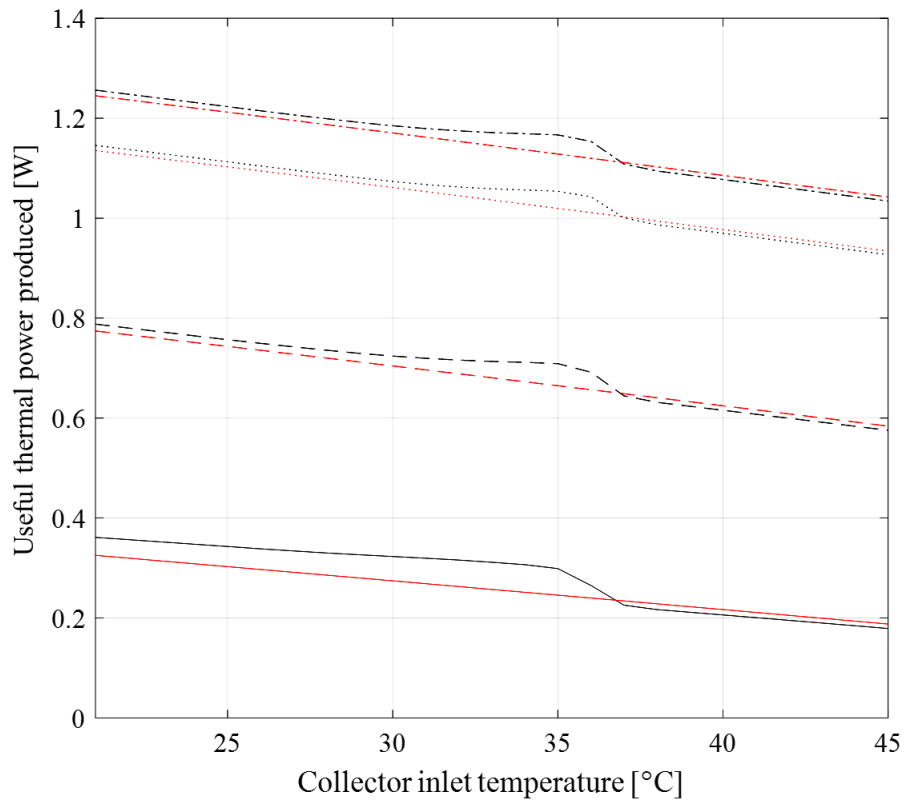
Figure 18. Instantaneous parametrical evaluations. Useful thermal power produced by the collector vs. collector inlet temperature.

4.2.2 Year-long numerical simulations

4.2.2.1 Definition of the boundary conditions

Climatic data were necessary to perform the simulations through the numerical model correctly. In detail, they were retrieved from the International Weather for Energy Calculation (IWEC) files of Department of Energy of United States. The performance of the solar thermal system based on mPCM slurry has been assessed for three different climates to understand the impact of different climatic conditions on the performance of the system. These three selected locations are representative of different climates and cover a large mid-latitude region. They are Turin (North Italy), Princeton-Trenton (United States), and Oslo (Norway). Data about the location and climate classifications are given in *Table 8*. A time step of 1 hour was selected for the simulations, according to availability of hourly climatic data of the IWEC datasets.

Table 8. Climate characteristics and optimal tilt angle for different locations.

Location	Latitude	Köppen climate classification	Annual solar global horizontal radiation	Heating degree days	Optimal tilt (for heating demand)
			[kWh/m^2]	[DD]	[°]
Turin	45° 04' N	Cfb	1294	2617	53
Trenton	40° 30' N	Cfa	1323	2859	48
Oslo	59° 57' N	Dfb	879	4714	68

While the panel azimuth (γ) was kept constant (south) for all the climates, the tilt (β) angle was changed in order to obtain the optimal performance in each latitude – (the energy output of the solar thermal panel is affected to a great extent by the tilt angle). Many investigations can be found in literature on the estimation of the optimal tilt angle for systems with different boundary conditions – e.g., Ref. [9] and Ref. [10]. Different "rules of thumb" have been suggested to design the tilt of panels but, in general, the values for the optimal tilt angle - for the entire year, for summer or for winter – are correlated to the latitude. For instance, Lewis [9] suggested to adopt the following rule:

$$\beta_{opt} = latitude \pm 8° \tag{4.6}$$

Where "+" stands for winter, and "-" for summer. In the simulations, a tilt angle equal to the latitude ($\beta = latitude$) was chosen to define more generic results, valid for the overall year productivity.

The climatic data listed in *Table 8* represent a first indication of the weather conditions characterising the different locations. Further information can be derived from the evaluation of ratio of the difference between the heat transfer fluid mean temperature (θ_f) and the ambient temperature (θ_a) to the incident solar radiation on the tilted surface (G_T). This index assumes great importance in the evaluation of the conventional panel efficiency according to the Italian and European standard UNI EN 12975 [11]. In formula:

$$\frac{\overline{\theta_f} - \theta_a}{G_T} \tag{4.7}$$

Referring to a heat transfer fluid mean temperature equal to the nominal melting temperature of the material, the frequency distribution of occurrence of this parameter was calculated for the three location under investigation. In *Figure 19* the value on the x-axis represents exactly the variable expressed by Equation 4.7 (where *dT* represents the temperature difference at the numerator, while *I* is the hourly solar irradiation, that is the hourly integration of the variable G_T at the denominator).
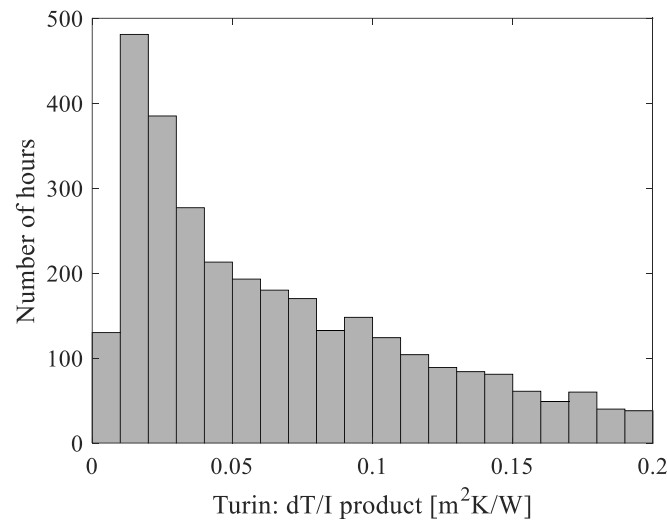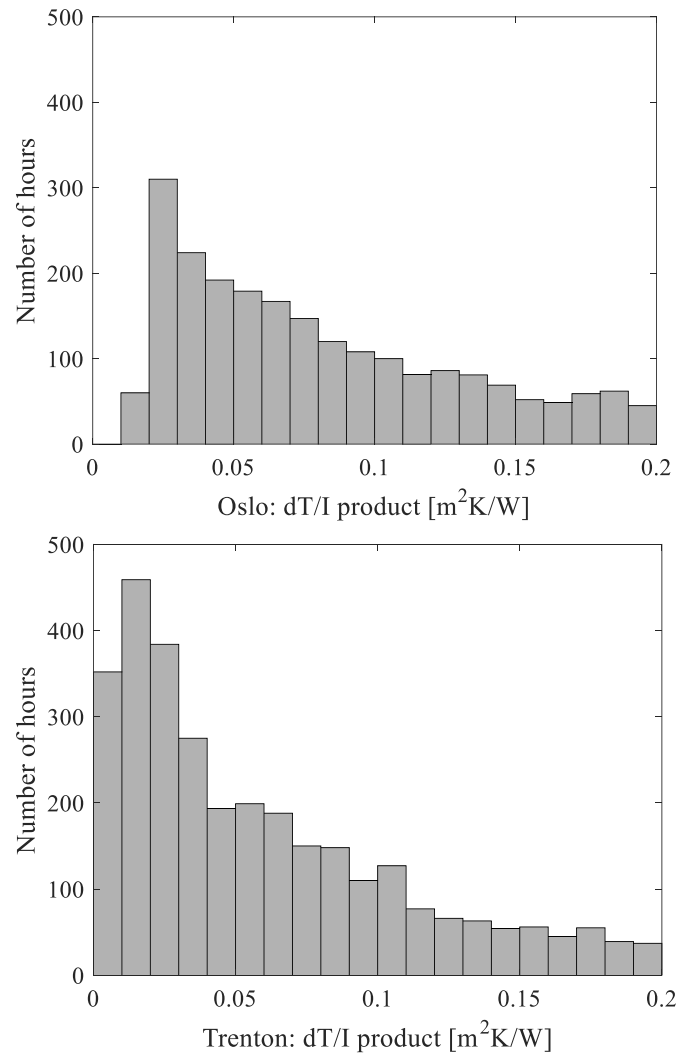
Figure 19. Frequency distribution of the parameter most influencing the performance of a solar thermal system for the three locations.

From *Figure 19*, it can be inferred how the outdoor climate can potentially influence the system in different ways for the three locations under investigation. On the one side, Turin and Trenton present a similar shape of the frequency distribution. However, the Trenton one is characterised by a more significant number of the smallest values (almost double than in Turin). This frequency difference can be referred to the moments in which the temperatures are low, but the solar radiation is high. Indeed, as can be derived from *Table 8* Trenton is characterised by a higher amount of solar radiation but a colder climate compared to Turin. On the other side, Oslo has a curve more flattened due to its stiffer climate and lower solar radiation levels.

Since the SolHe-PCM system was conceived for space heating production evaluations referring to the heating season only are significant. For instance, the conventional heating season of Turin lasts from November 15th to April 15th.

4.2.2.2 Solar thermal collector

Year-long simulations were performed to assess the performance of the proposed technology. The preliminary simulations regarded the solar thermal collector as a stand-alone element. The flow-rate was controlled with the open loop version of the *Control 1*, based on the thresholds individuated in *Table 7*. The temperature at the panel input was set equal to 35 °C. The simulations were performed for various concentrations of mPCM slurry (10 % w.t., 20 % w.t., 30 % w.t, and 40 % w.t.) and compared with the results obtained with a traditional water-based collector. Detailed results were reported for the 30 % w.t. concentration only.

Table 9. Results of the year-long simulation in terms of useful heat produced by the panel referring to mPCM slurry at 30 % w.t concentration.

	Turin		Oslo		Trenton	
	Water	mPCM	Water	mPCM	Water	mPCM
	[kWh]	[kWh]	[kWh]	[kWh]	[kWh]	[kWh]
Heating season	390	410	128	149	441	443
Year	1200	1240	718	751	1242	1315

Figure 20 reports the comparison between the results obtained in term of cumulated useful heat production increase with the various concentration of mPCM in the heat transfer fluid. A traditional water-based solar thermal system was used as the baseline. The performance increasing was evaluated with a percentage calculated as follow:

$$\Delta\eta = \frac{\sum \dot{Q}_{us\_water} - \sum \dot{Q}_{us\_water}}{\sum \dot{Q}_{us\_water}} \tag{4.8}$$

The summations were extended in one case to the entire year and in the other case to the heating season only. For all the locations the heating season was considered extended from November 15th to April 15th.

Several considerations can be carried out by observing the various scenarios defined by the results of the simulation and highlighted by the bars plots of *Figure 20*. First of all, as it was expected, the higher the concentration on mPCM the higher the efficiency of the collector. For all the locations, the efficiency increases more during the winter time. This is due mainly to the reduced operating temperatures of the innovative technology that improves the First law efficiency mostly when the ambient temperature is lower. This is particularly true for locations where the winter conditions are stiff, but characterised by elevated levels of solar radiation (e.g., in Trenton). Since the system was mainly conceived for space heating purposes, the improved efficiency during winter time was a desirable feature.

The effects of the collector inlet temperature on the panel performance were also investigated. In detail, for the location of Turin, year-long simulations were performed again considering an inlet temperature of 25 °C (versus an initial value of 35 °C). Results are reported in *Table 10.* It can be inferred how there is only a slight increase of the collector useful heat production by lowering the panel inlet temperature. This is mainly due to the reduction of the number of moments in which the heat transfer fluid in the collector overcomes the upper limits of phase change. Nevertheless, since the variation of results was small, the effects on the open-loop simulation of the collector inlet temperature were considered negligible.
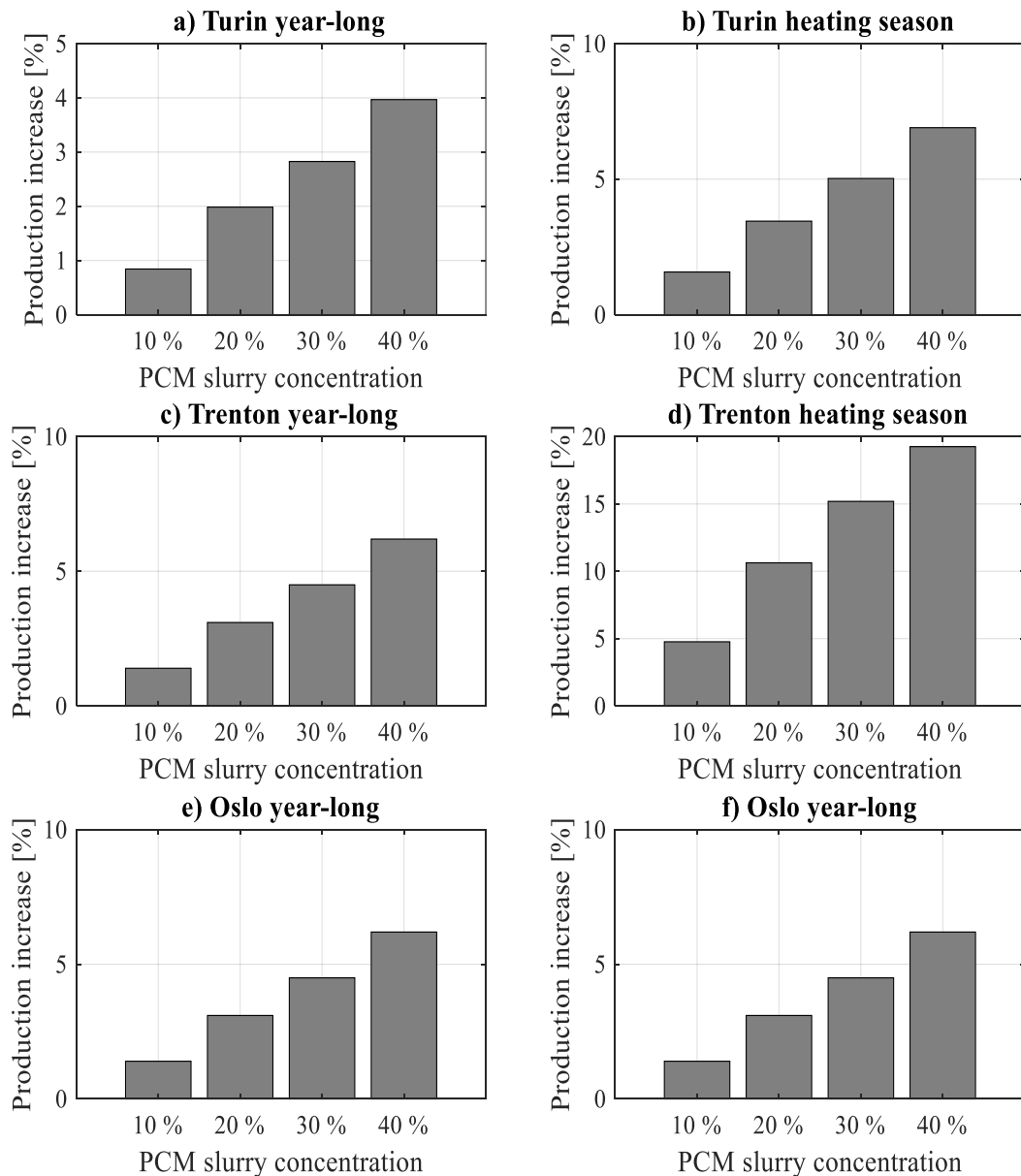
Figure 20. Increase of the useful heat produced by the solar thermal collector based on PCM slurry compared to water based collectors.

Table 10. Collector inlet temperature vs. increase in the useful heat produced.

		10 % w.t.	20 % w.t.	30 % w.t.	40 % w.t.
Heating season simulation	Tin = 25 °C	1.5 %	3.4 %	5.0 %	7.0 %
	Tin = 35 °C	1.5 %	3.4 %	4.9 %	6.9 %
Yearly simulations	Tin = 25 °C	0.9 %	2.0%	2.9 %	4.2 %
	Tin = 35 °C	0.8 %	1.9 %	2.8 %	4.0 %

Hourly distributions of the useful thermal power produced by the collector are reported in *Figure 21* for two typical winter days in Turin (February 7th and February 8th). The subsequent set of figures shows the energy delivered daily on a monthly basis for the collector exploiting the two different heat transfer fluid in Turin.

These figures further highlights how the system based on mPCM slurry improves the amount of useful heat produced mostly during the colder months. This is particularly desirable for a system designed for deliver space heating. Thus whose efficiency must be maximised during the winter period. The daily and hourly useful heat production distributions showed similar profiles also for the location of Trenton and Oslo. For a matter of conciseness, they were not reported in the present work.
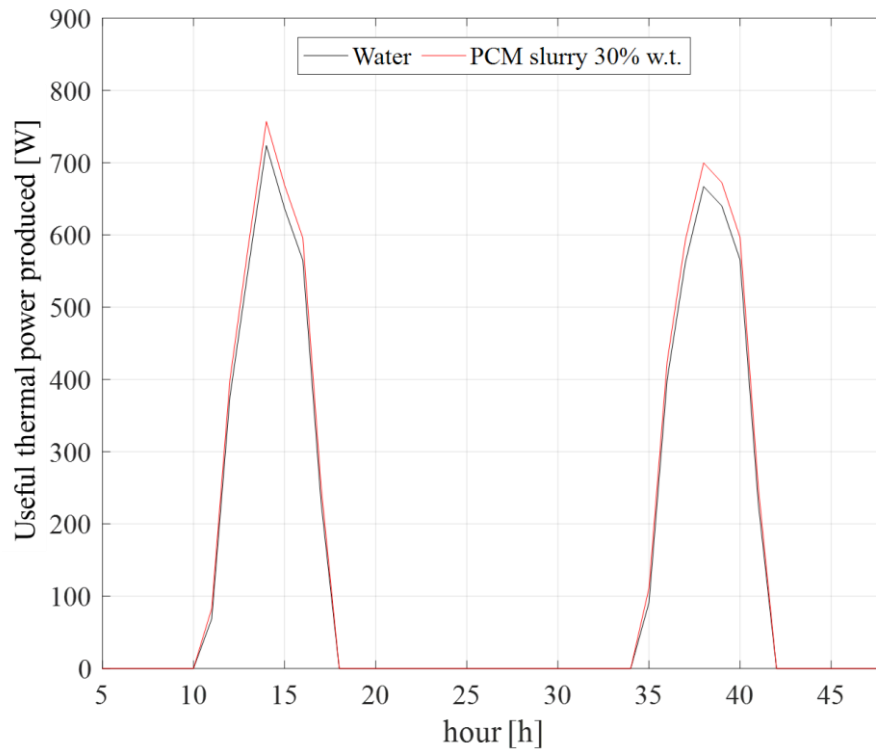
Figure 21. Two significance winter days (February 7th and February 8th) hourly profiles of useful thermal power produced by the panel. Simulations are referred to the location of Turin and constant panel inlet temperature of 35 °C.
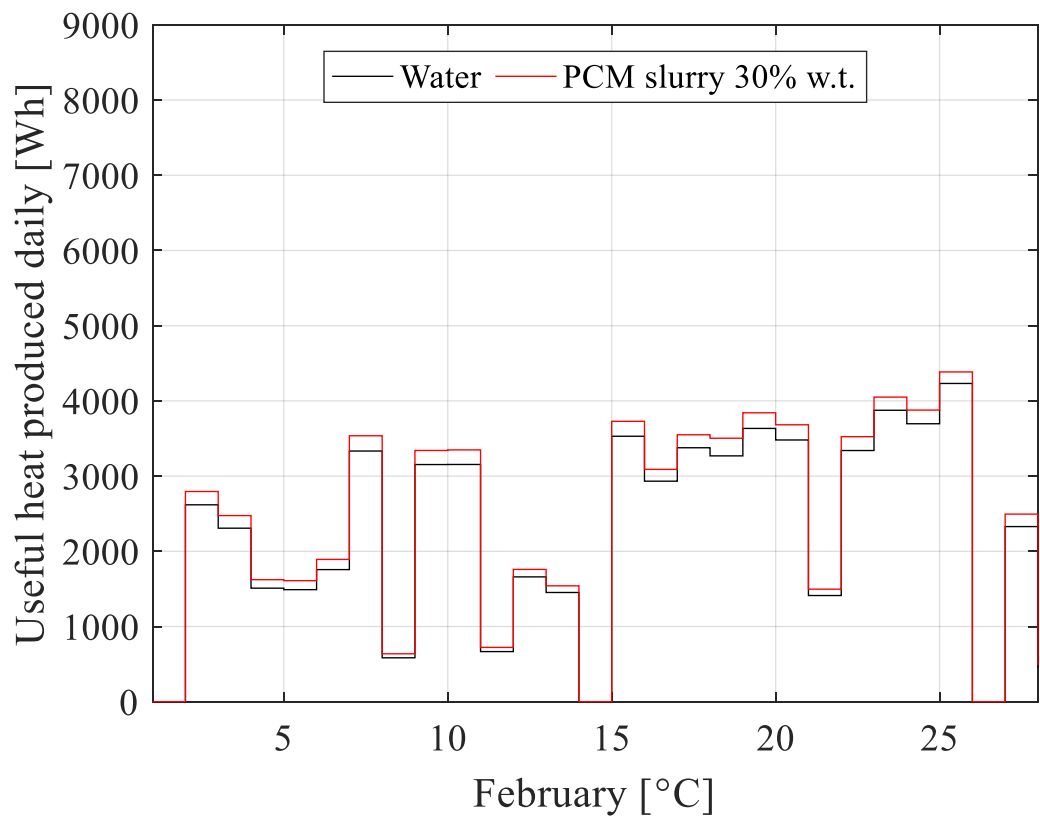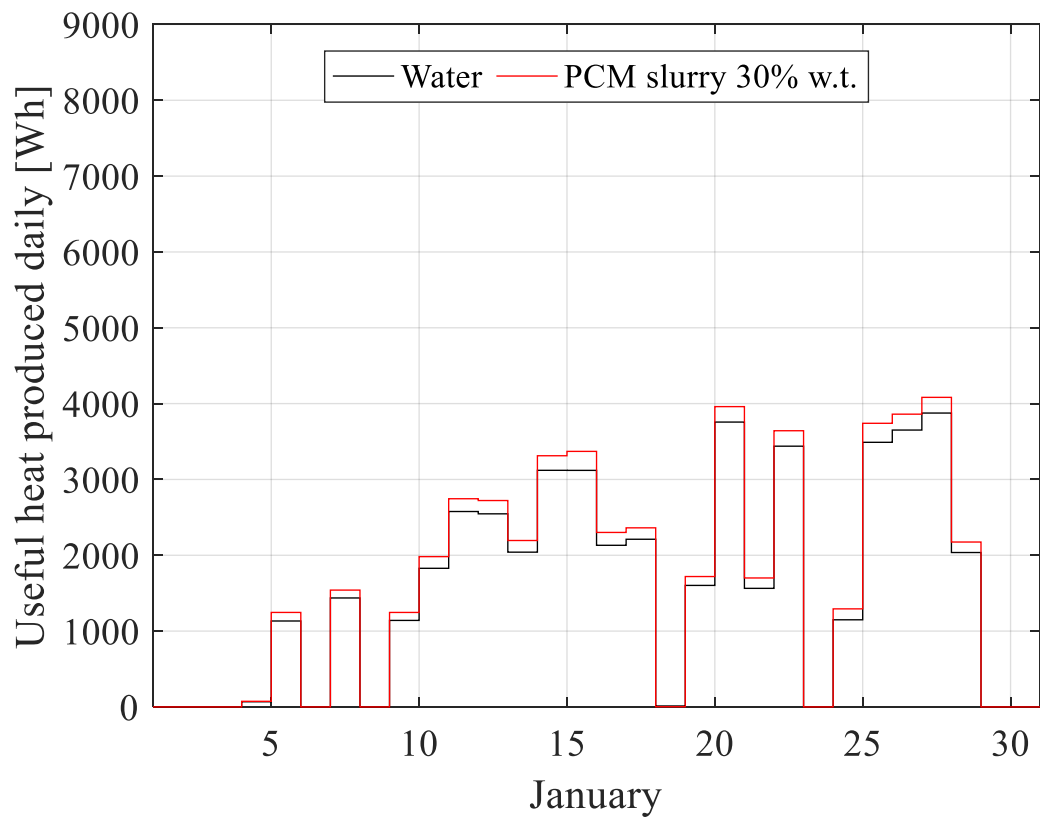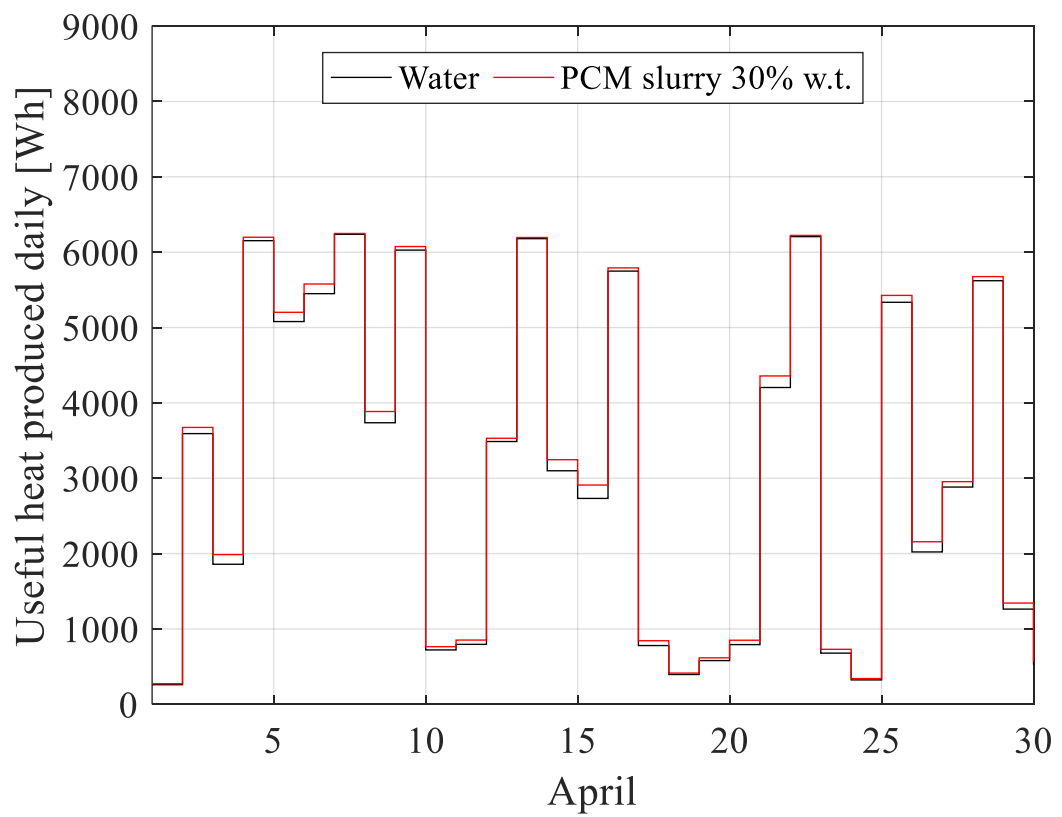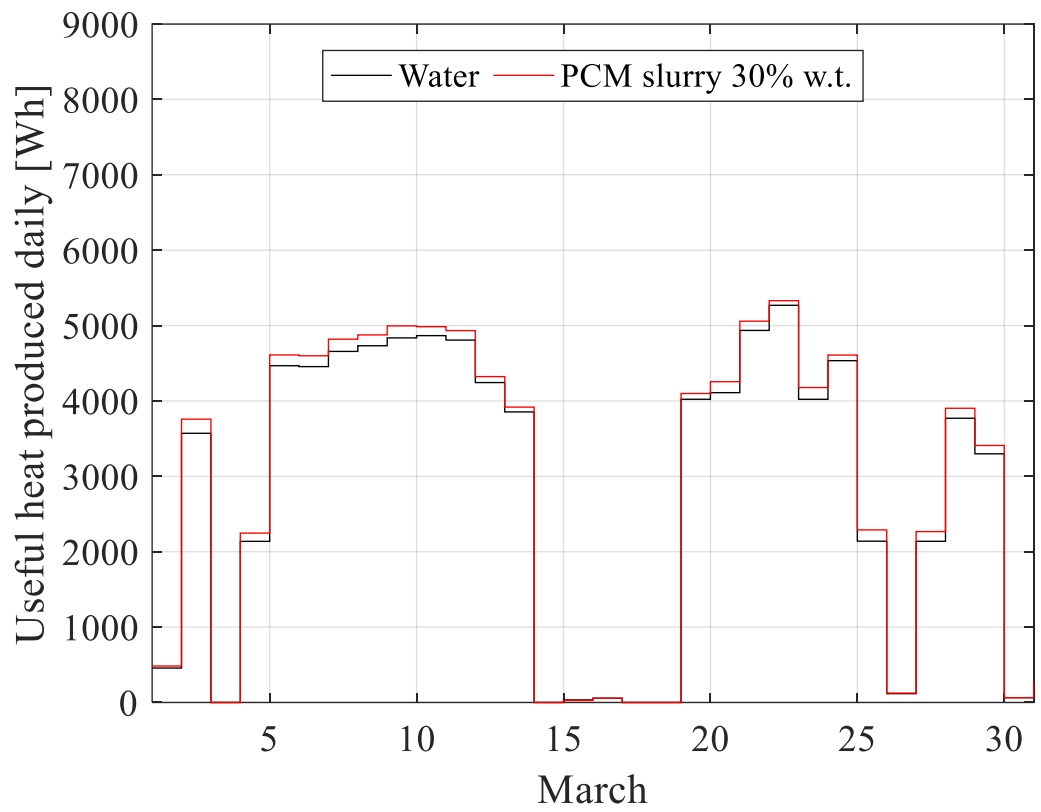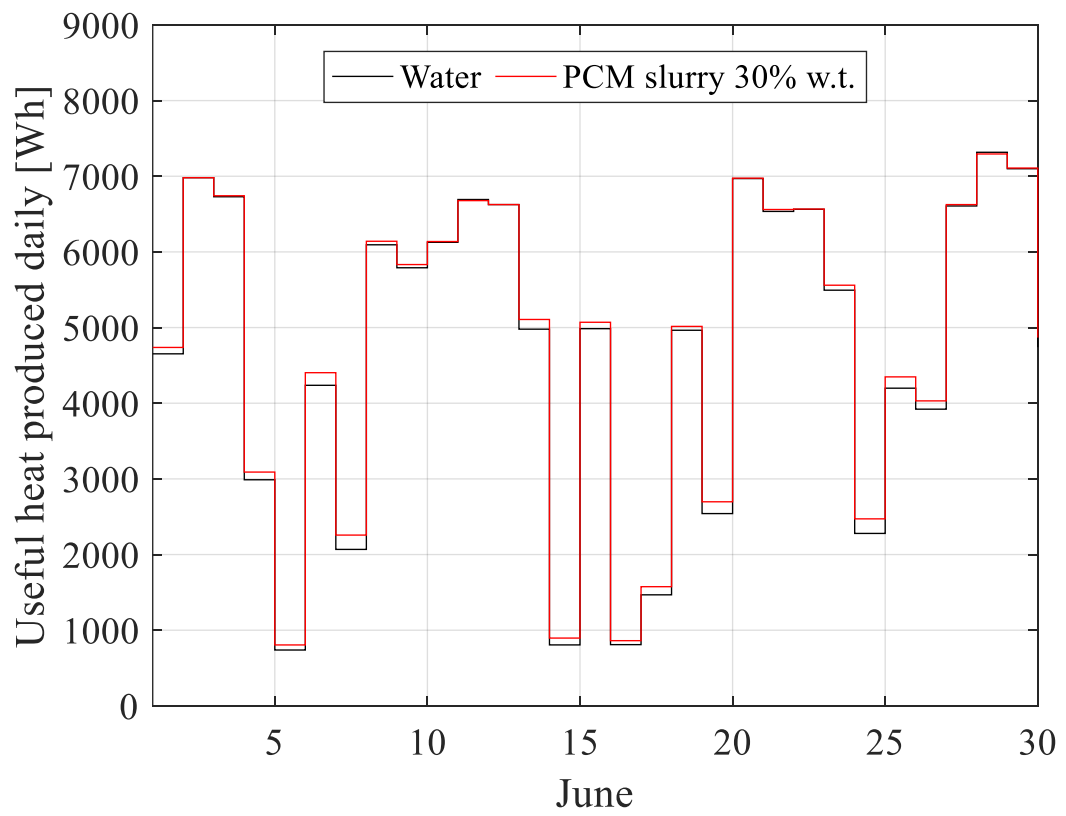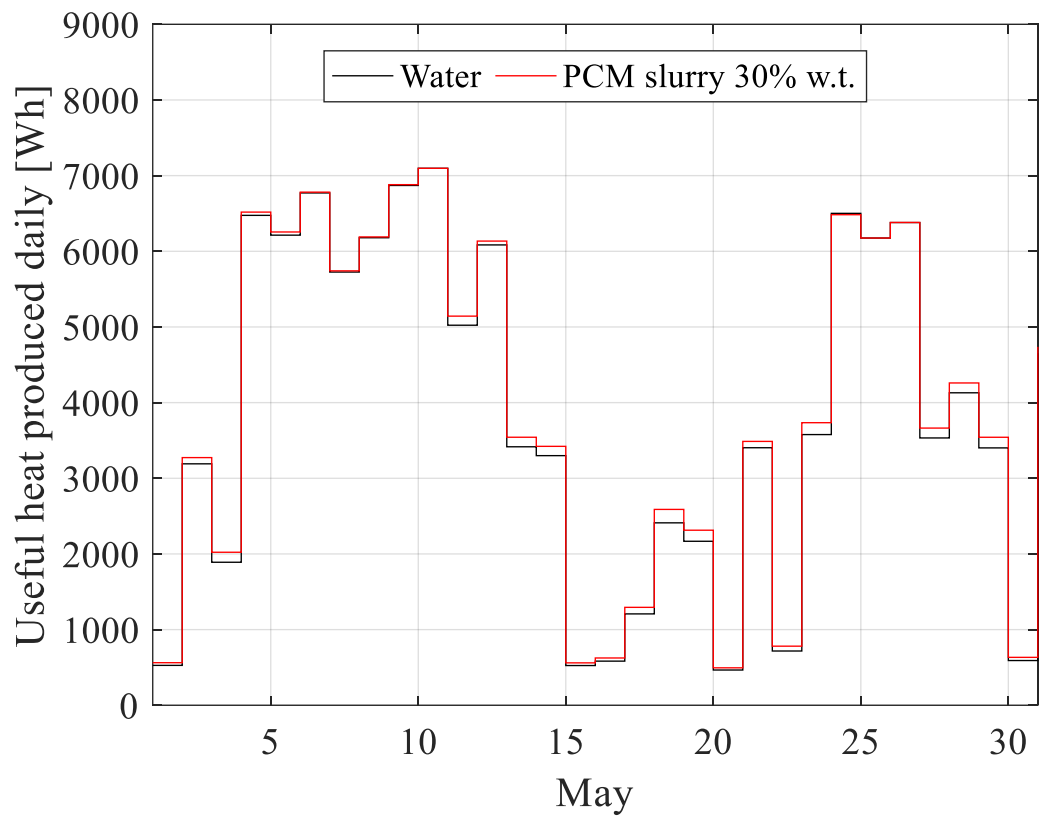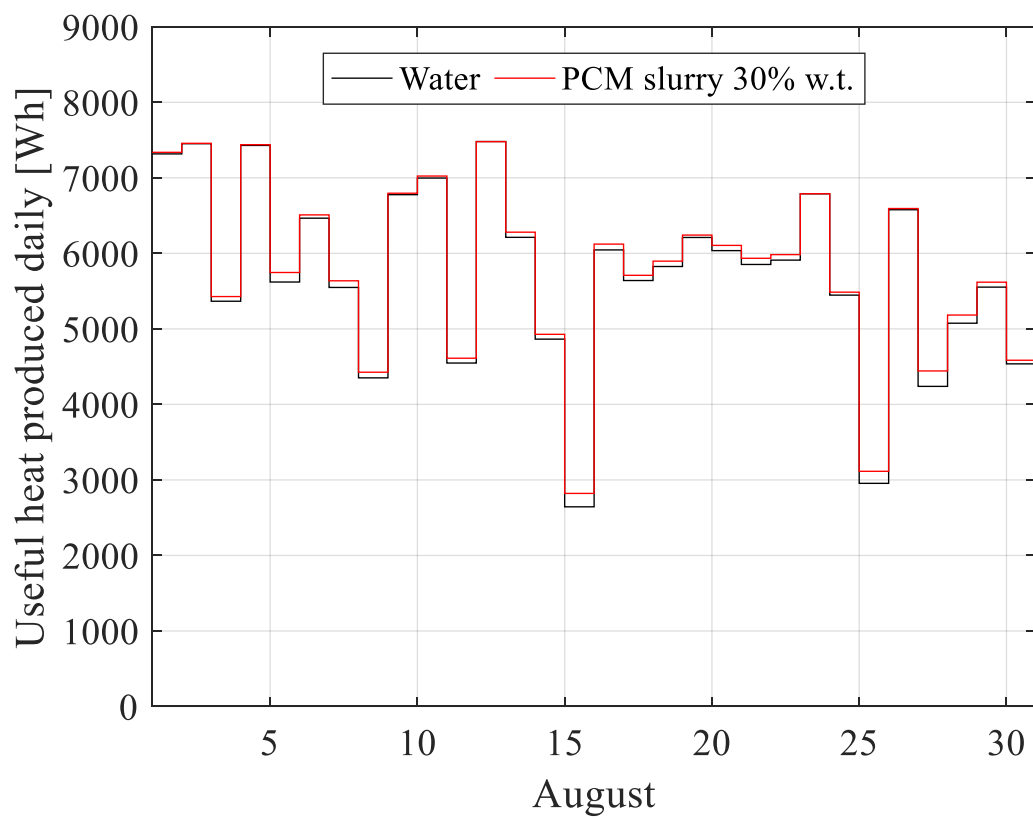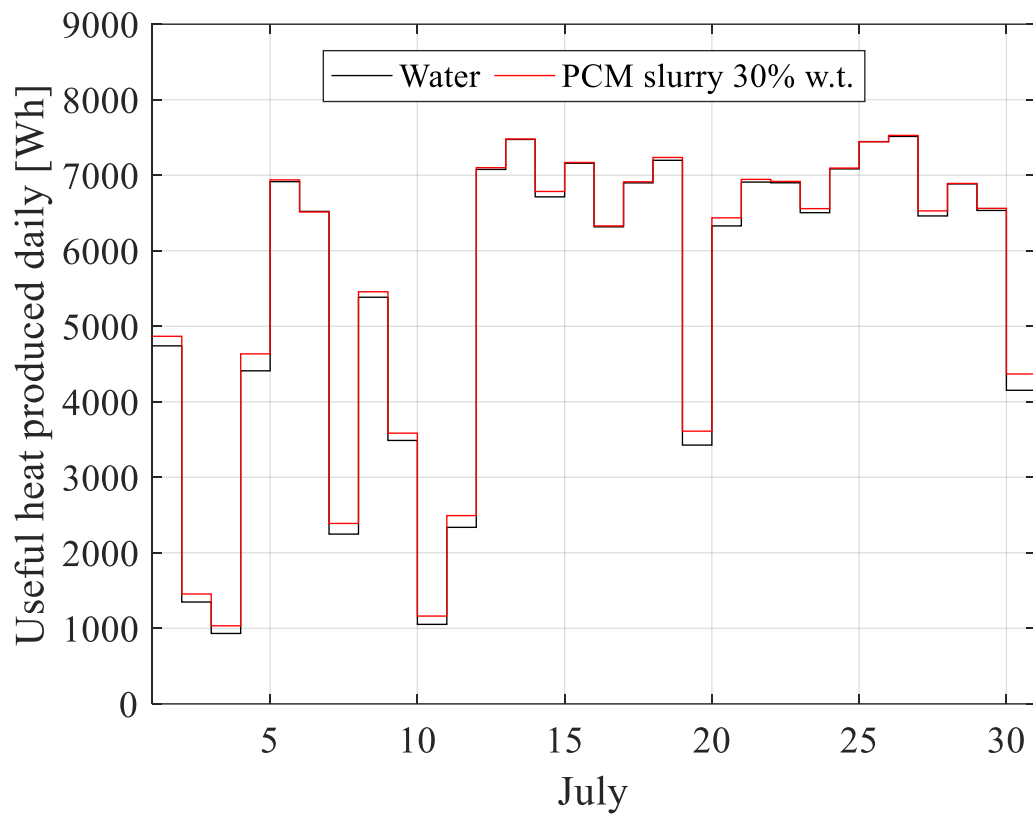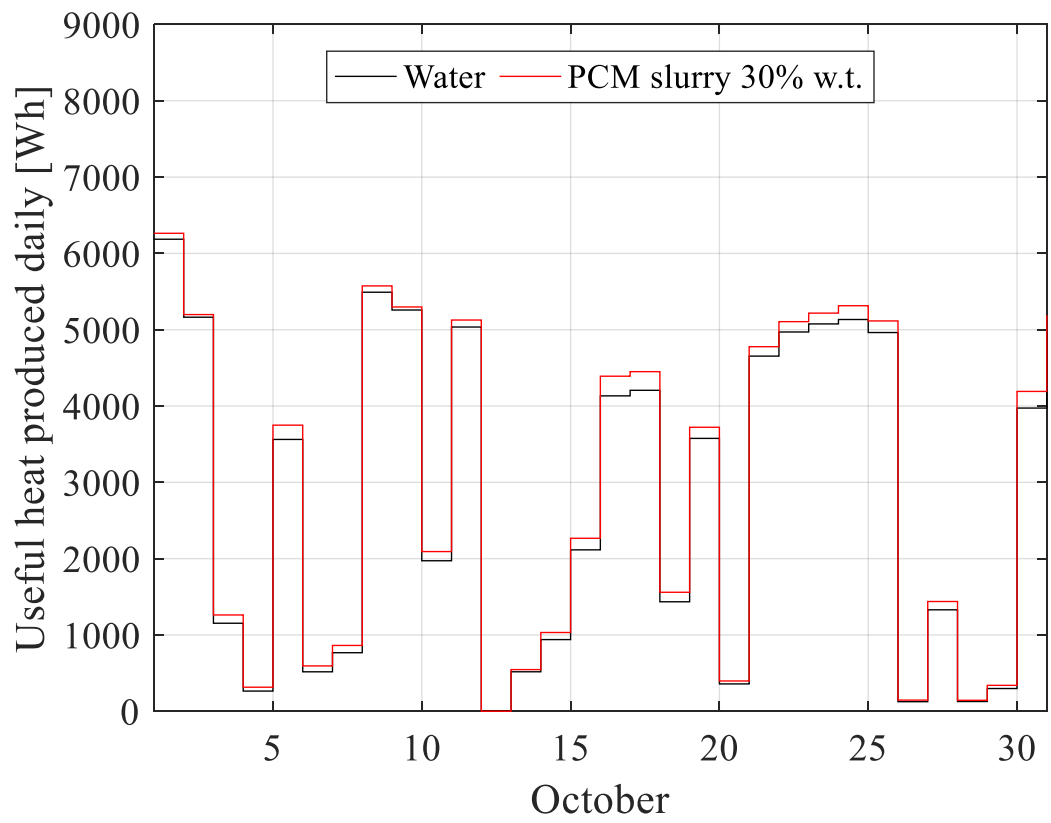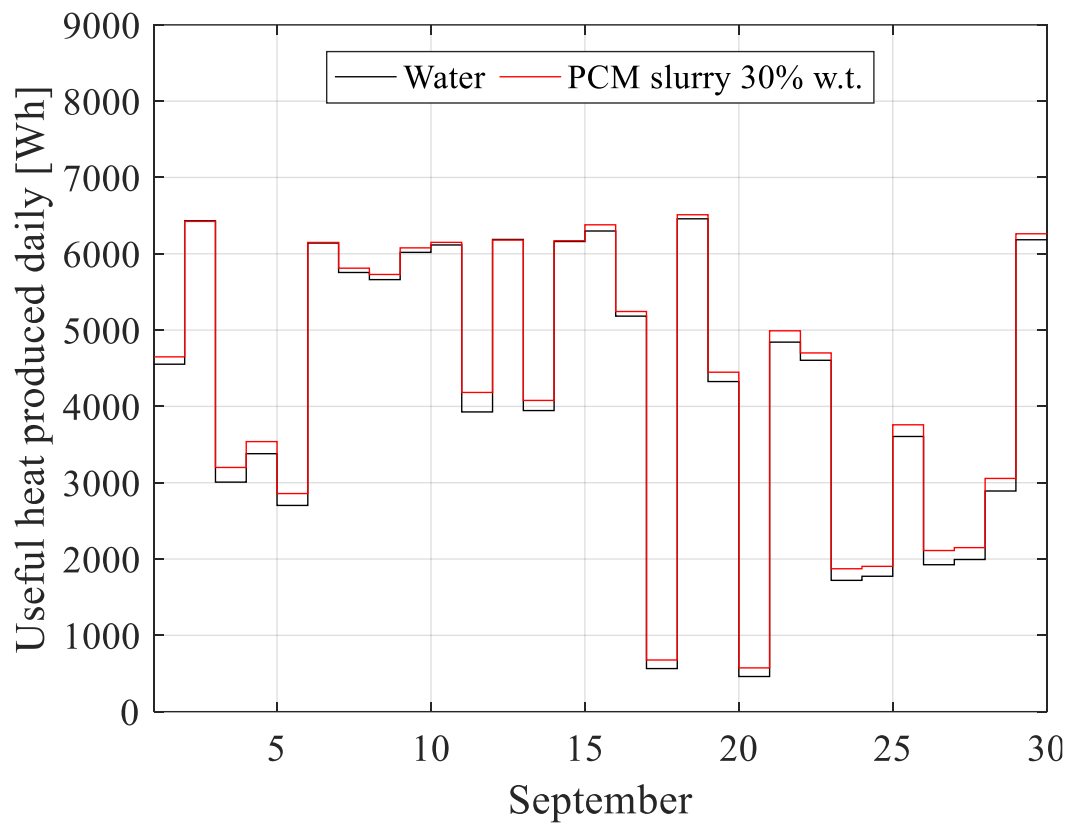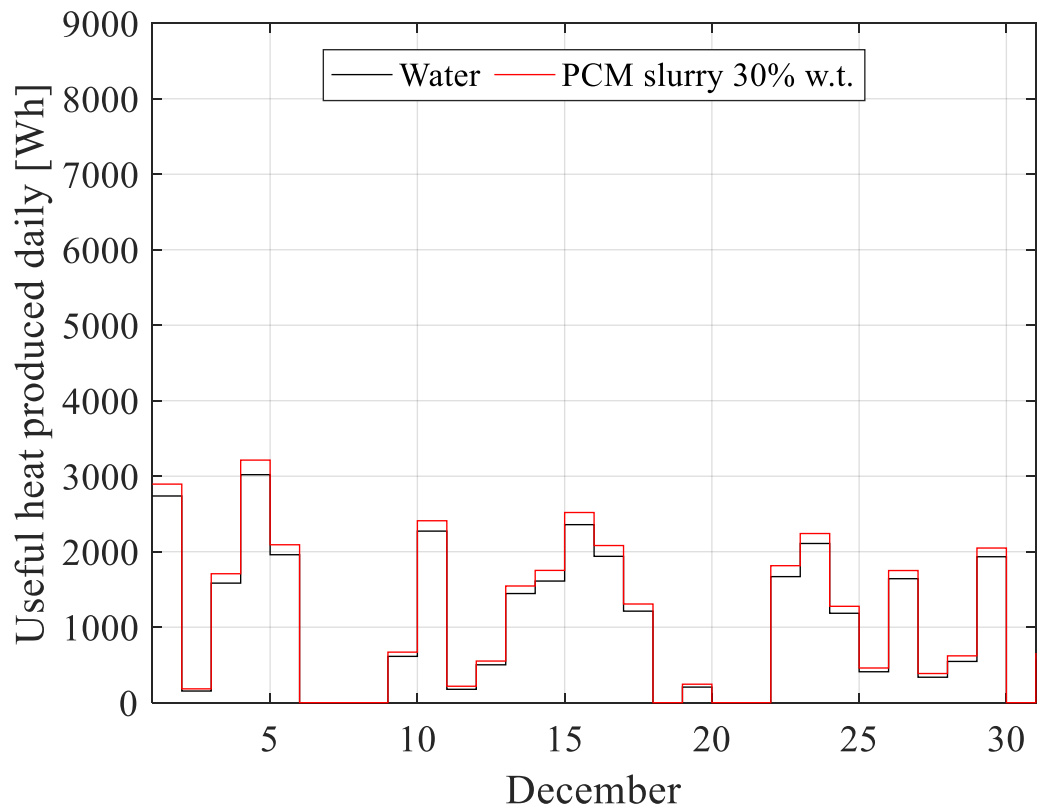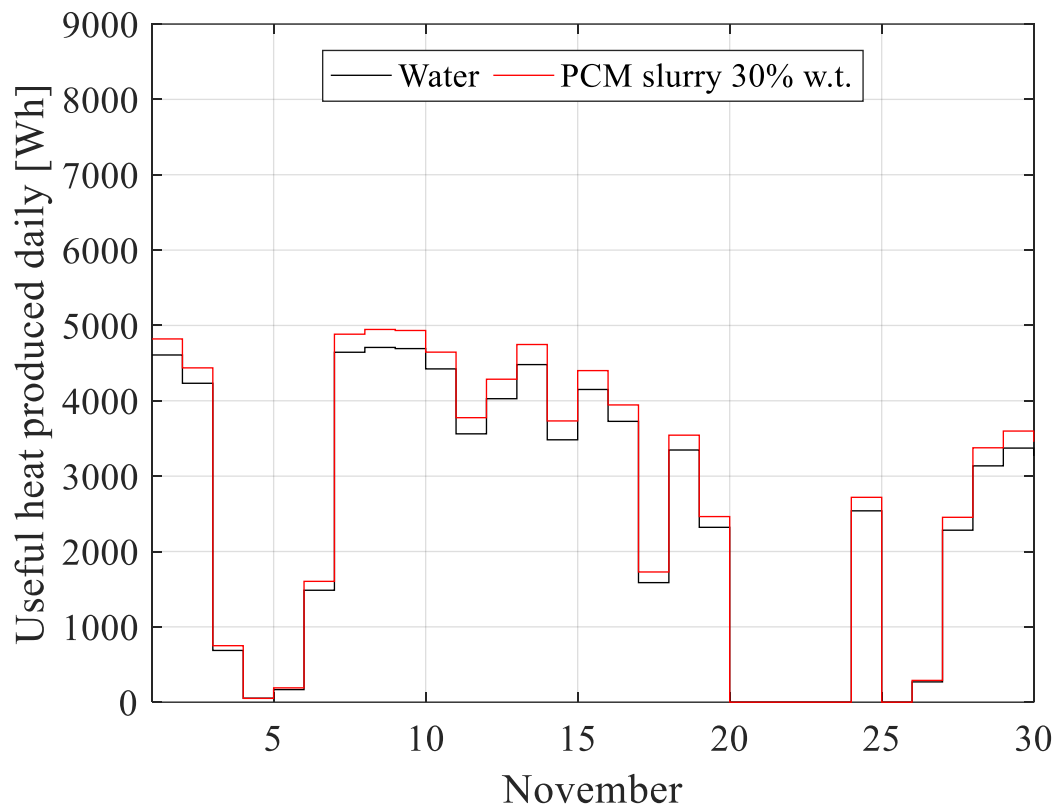
Figure 22. Daily energy production by the collector on monthly basis.

4.2.4 Overall solar thermal system

The literature analysis undertaken in Chapter 2 highlighted how the PCMs had been principally used to exploit their large storage capacity. For this reason, it is clear that several of the SolHe-PCM system benefits are directly related to the thermal storage potentialities offered by this technology. Notwithstanding, if it is relatively easy to carry out performance indicators to assess the efficiency of a solar thermal panel, to define the storage performance is not a trivial process.

On the one hand, the collector efficiency can be evaluated by a First law analysis based on the instantaneous useful thermal power production. On the other hand, for a thermal energy storage unit, it is more interesting to evaluate its dynamical evolution during the time. This process is based on the differential equations presented in Section 3.4.2. Since the solution of this differential equations depends on the property of the storage media itself, the thermo-dynamical evolution of mPCM slurry-based and water-based storage units follow two different paths, due to the unique features of the materials (e.g., specific heat capacity, material density, etc.). These different ways strongly affect the possibility of a normalised evaluation of performance indicators to compare the two technologies.
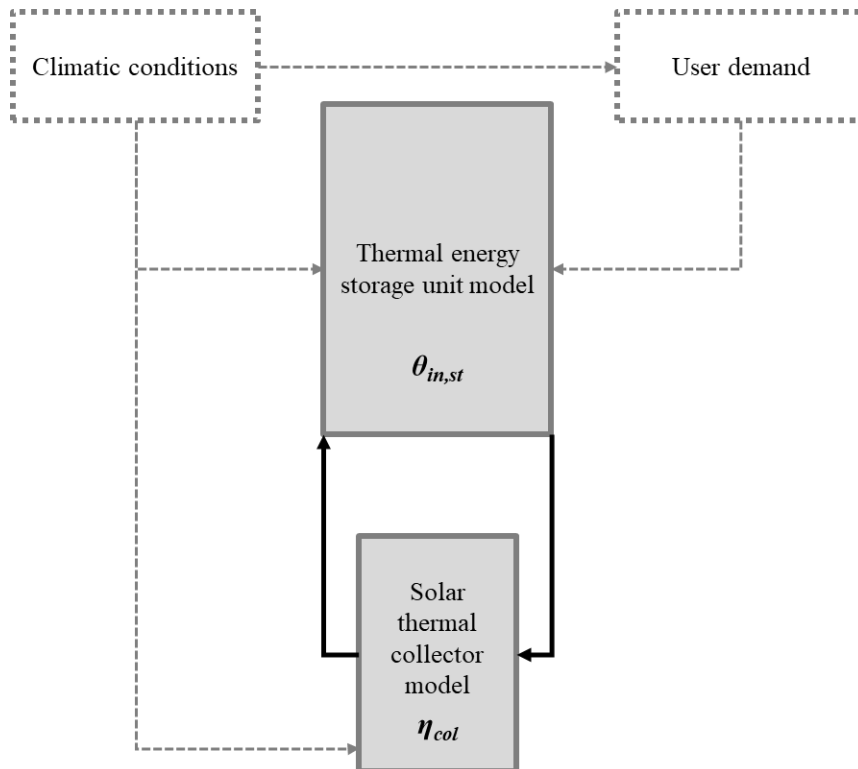
Figure 23. Factors affecting the dynamical evolution of the thermal energy storage unit.

The concepts mentioned above can be better explained with the schematic illustrated in *Figure 23*. The thermo-dynamical behaviour of the thermal energy storage unit is mainly influenced by the uncontrolled external disturbances (e.g., the climatic conditions and the user power demand profiles), the useful thermal power delivered by the solar thermal collector, and the control logic regulating the

overall system. Even if the uncontrolled disturbances and the control logic are the same for the water-based and the mPCM slurry-based circuits, the evolution over time of the system would be influenced by the different performances of the two configurations. Indeed, thermal energy storage unit temperature, θ_{st}, affects inlet temperature of the solar thermal collector; thus it affects its efficiency (see *Figure 18*). Different panel efficiencies cause different amounts of useful thermal power supplied to the thermal energy storage. The thermal energy storage temperature varies as a consequence of the useful thermal power provided. Therefore, this continuous interaction affects the long-term performance of the overall system. For instance, starting with the same initial conditions, assume that a panel A initially produced double useful thermal power than a panel B. After a while, the temperature of the thermal energy storage unit serving the panel A will reach higher values than those of the tank related to the collector B. This temperature rising reduces the panel A relative efficiency. Thus, the evolution of the two systems takes two completely different paths, and the comparison of key performance indicators is not trivial.

Nevertheless, long-term simulations can also be performed in the case of closed-loop configuration. Similarly to the investigations undertaken in Section 4.2.3, the International Weather for Energy Calculation (IWEC) [12] files were used as climatic disturbances. The control logic adopted is the one discussed in Section 3.3.6. The user demand varies according to daily consumption profile and external weather conditions. Engineering methods (or withe-box modelling), statistical, machine learning or artificial intelligence methods (or black-box modelling), or physical-empirical approaches (or grey box modelling) can be adopted for prediction or estimation of the user demand profiles over time (see Section 5.2.5). This represents a vast topic of investigation, which goes beyond out of the goals of the present thesis. In this case, the user demand profiles were calculated as follows:

$$\dot{Q}_{need}(\tau) = A(\tau) \cdot H_{tot} \cdot \left(\theta_i - \theta_a(\tau) \right) \qquad (4.9)$$

Where $\dot{Q}_{need}(\tau)$ is the user demand variation over time τ; H_{tot} is a term that relates the building energy demand with the external temperature, it was assumed equal to 35 W/K according to typical North Italian buildings design loads for space heating; θ_i is the internal building temperature, equal to 20 °C; θ_a is the ambient temperature retrieved by the IWEC file; and $A(\tau)$ is a dimensionless term to consider the hourly variation of the energy demand during a day. In this specific case, this term was calculated by normalising the daily thermal load profile assessed through the method proposed in Ref. [13]. This pattern is representative of the space heating demand of a typical residential building in Turin. *Figure 24* shows the pattern daily profile named *A(τ)*.

Under these hypotheses, the closed-loop simulations were performed for the location of Turin. Since the system was conceived for the satisfaction of the space heating demand the simulation time was limited from the November 15th to the April 15th (conventional heating season of Turin). *Table 11* summarises the most

important indicators to assess the performance obtained with the two configurations of the system, mPCM slurry 30 % w.t. concentration and water-based. The term called "useful heat produced" represent the summation of the instantaneous useful thermal power delivered by the collector over the time span under investigation. The demand was considered unsatisfied when the secondary heat exchanger was not capable of supplying thermal power to the demand side simulator circuit. In general, this fact occurs when the storage temperature drops under 30 °C. Indeed, below this value, a temperature difference significant enough to be compatible with the supply temperature of the demand side simulator is not ensured.
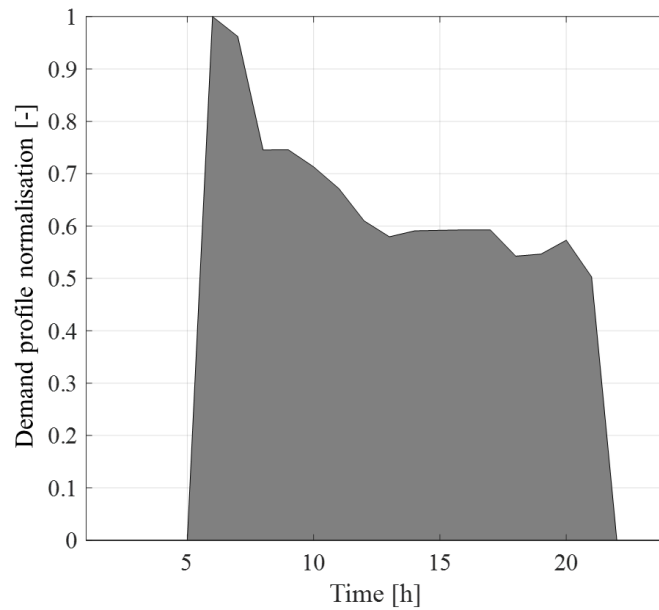
Figure 24. Normalised daily profile of user power demand.

Table 11. Comparison of the performance obtained with a water-based and mPCM slurry-based solar thermal system.

	Water-based	mPCM slurry-based
Useful heat produced [kWh]	401	422
Hours $\theta_s < 30$ °C [h/h]	1393/4416	1131/4416
Demand unsatisfied [kWh/kWh]	153/937	134/937

Figure 25 and *Figure 26* show the frequency distribution of the hours in which the average thermal energy storage temperature is within ranges of 0.5 °C. The comparison between the two figures allows the effect of latent heat storage to be quickly highlighted. In fact, the distribution referring to the mPCM slurry thermal energy storage unit (*Figure 26*) is drastically sharpened in the phase change range. This point allows the temperature involved in the overall process to

be contained. Thus, the dispersions of the thermal energy storage are reduced, and the efficiency of the solar thermal collector is increased.
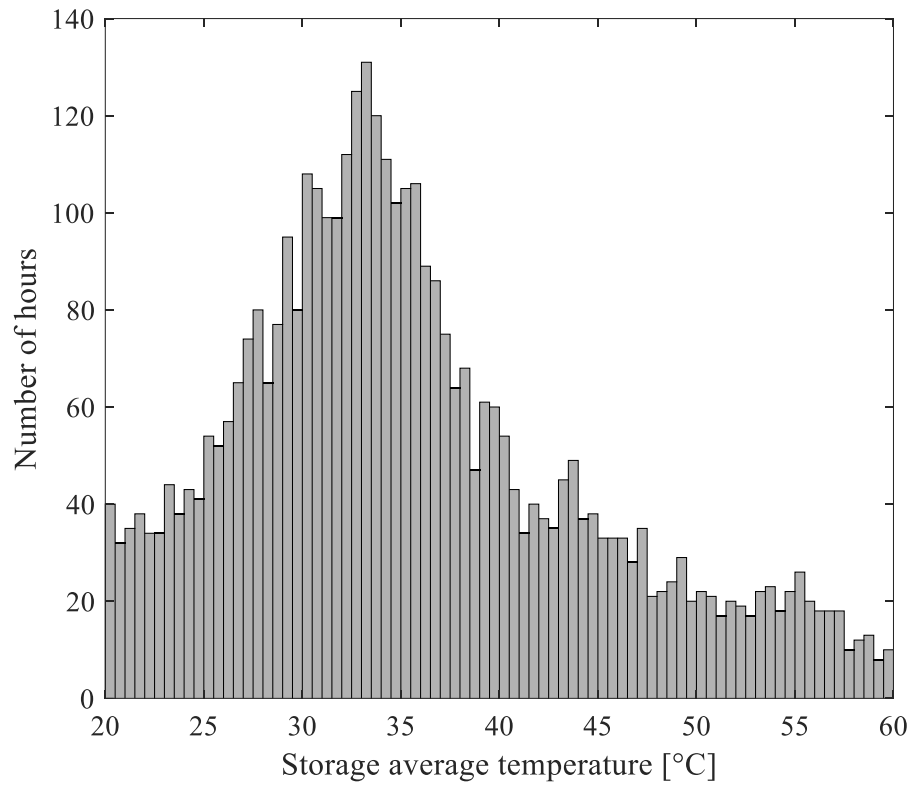
Figure 25. Frequency distribution of the hours in which the thermal energy storage temperature is within bin of 0.5 °C. Water-based solar thermal system.
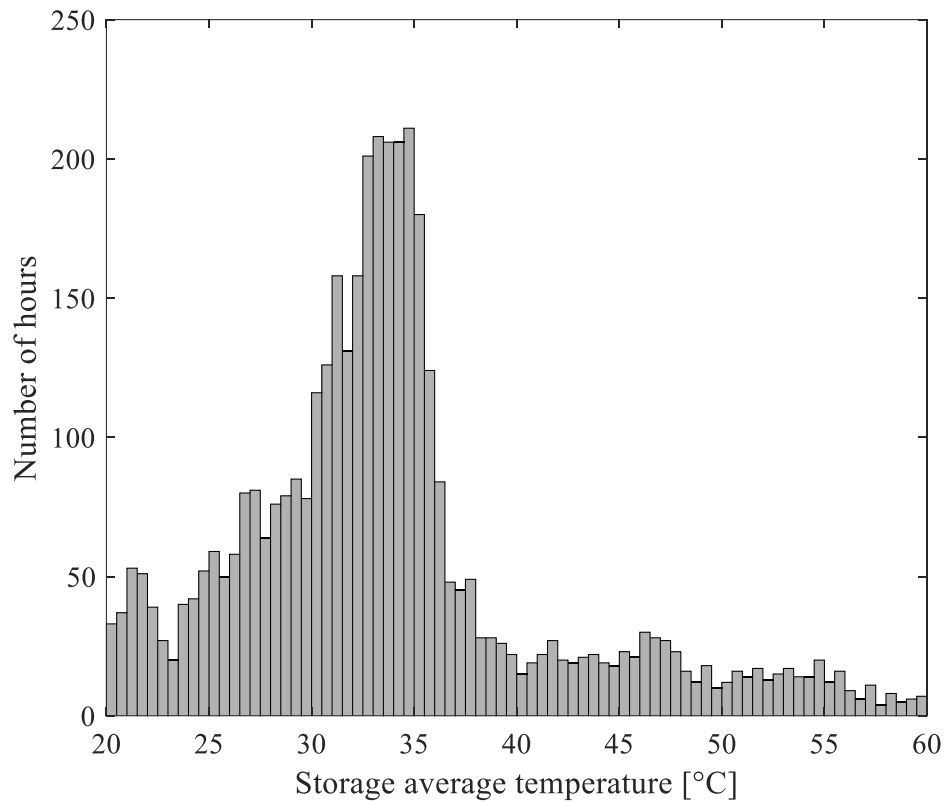
Figure 26. Frequency distribution of the of hours in which the thermal energy storage temperature is within bin of 0.5 °C. mPCM slurry-based solar thermal system.

4.2.5 Overlook on the next investigation steps requiring simulations

Two big questions aroused at this stage. The first one was related to the control paradigms adopted to manage the two systems. To compare the results of the simulations the same regulation logic was assumed for water-based and mPCM slurry-based solar thermal system. However, this assumption can be misleading. Indeed, using controllers that just adapt the logics used for traditional systems can reduce the potential benefit achievable by new technology. For instance, control algorithms based on the monitoring of temperatures can be misrepresentative of a solar thermal system based on the exploitation of the latent heat. This consideration led to the exploration of innovative predictive control paradigms capable of performing recursive optimisation. These aspects are investigated in deep and the entire Chapter 5 has been dedicated to the Model Predictive Control formulation.

The second question was related to the indicators adopted to assess the performance of such an innovative system. From the results mentioned above, it emerged how the First law analysis allowed the potential benefits of the system to be just partially explained. Indeed, the reduction of the temperature levels – both in the collector and in the thermal energy storage unit – opens up to a Second law investigation to better understand the performance benefits achievable by means of the SolHe-PCM technology. Second law analysis is an extensive area of research, and the present thesis does not aim to cover it in detail. The following

Second law analysis should be considered a preliminary investigation that provides a methodological framework and an outlook for future more detailed studies.

4.2.6 Preliminary Second law investigations

The Second law of thermodynamics asserts that losses of useful work unescapably characterise the operations of real systems. By combining the Second law with the First law, it is possible to demonstrate that the destruction of useful work is proportional to the entropy generation rate. Therefore, the entropy generation quantifies the thermodynamic irreversibility, which destroys the useful energy of a system and affects the system performance directly. The Gouy–Stodola theorem is based on this concept:

$$\dot{W}_{max} - \dot{W} = T_0 \cdot \dot{S}_g \qquad (4.10)$$

With $\dot{W}_{max}$ is the maximum work transfer rate (or maximum power transferred), which exists only in the ideal case of reversible operation; $\dot{W}$ is the effective work transfer rate; T_0 is the reference temperature; and $\dot{S}_g$ is the entropy generation rate [14].

Entropy generation and work transfer rate depend on the operating conditions of the system. In detail, the most influencing parameters are the boundary interactions of the system. The performance of a system can be improved by conceiving a new design characterised by a lower entropy generation. This procedure is called Entropy Generation Minimisation (EGM). It aims at minimising the losses of a system subject to a specified set of constraints. In the Entropy Generation Minimisation, the crucial point is the definition of the entropy generation rate as an objective function that has to be minimised. The critical parameters – such as component dimensions or system operating conditions – are chosen as the design variables to minimise the prefixed goals. Contrariwise, an alternative approach can also be undertaken. It is based on the identification and reduction of the thermodynamic irreversibility. This approach is commonly referred as Entropy Generation Analysis (EGA). According to this method, the initial configuration of the system is subsequently improved by introducing possible design modifications [15].

In general, both these approaches are based on the application of principles of computational fluid dynamics and heat-mass transfer for the construction of a realistic model of the system that is under investigation. The model should be sufficiently detailed to capture all the phenomena occurring in the system and how also small modifications affect the performance. In the scientific literature, two different approaches are considered:

•   *The entropy generation studies through a black-box approach*. In this case, the model is drafted as a homogenous sample inside a control volume.

Usually, these models are less detailed, but do not require impressive computational resources;

- *The entropy generation studies through the continuum theory.* In this case, the state variables are considered as continuous functions of the space coordinates and the time. Each infinitesimal volume of a system is considered in thermodynamic equilibrium, although the overall system operates irreversibly. It follows that the intensive thermodynamic properties (e.g., specific entropy, temperature, pressure, etc.) are locally defined even in non-equilibrium situations.

Several papers have indicated that entropy generation is crucial for the performance analysis of the latent heat thermal energy storage units [15]. Both Entropy Generation Minimisation or Entropy Generation Analysis can be considered to increase the system performance. In Ref. [16], a Second law analysis was performed to carefully choose the PCM with the most suitable melting temperature for a specific application. A Second law analysis on the enhancement of the heat transfer rate of a PCM through the addition of high conductive particles was conducted by CFD studies [17]. Ref. [18] used the Second law analysis to study the efficiency of the solidification process in encapsulated ice thermal energy storage unit with different capsule geometries. The study carried out by [19] represents an interesting example on how the results of an Entropy Generation Analysis led to design improvements of finned shell and tube latent heat thermal energy storage.

It was possible to conduct a preliminary Second law analysis starting from the previously reported simulation results. It was based on an entropy generation balance. This formulation should be considered a preliminary results that opens up at future more detailed investigation. In particular, it porvides an overlook about the problem approach.

The entropy globally generated in a system is determined as the summation of the contributions due to the different heat exchanges in the various system components. For this specific case study, these contributions are due to the thermal energy storage unit ΔS_{st}, the solar thermal collector ΔS_{col}, the secondary heat exchanger supplyng the demand side simulator ΔS_{need}, and the external ambient (or system dispersion) ΔS_{dis}. These four elements were assumed as thermostats at a temperature that varies hourly. The storage unit, the collector and the heat exchanger were supposed at the average temperatures resulting from the model, while the external ambient temperature was retrieved from the weather data. The average collector plate temperature was used as a reference for the entire panel. *Table 12* summarises these features.

Table 12. Definition of the variables influencing the system entropy generation.

Component	Entropy generation	Reference temperature
Thermal energy storage unit	ΔS_{st}	θ_{st}
Solar thermal collector	ΔS_{pa}	θ_{col}

Secondary heat exchanger	ΔS_{need}	θ_{need}
External ambient	ΔS_{dis}	θ_a

The entropy balance of the thermal energy storage tank refers to the equilibrium of an open system. The storage unit is the most crucial element in the overall system since it combines the effects due to all the components considered in the balance. The entropy balance of the storage unit can be expressed with the following formulation:

$$\dot{m} \cdot (s_{in} - s_{out}) - \frac{\dot{Q}_{need}}{\theta_{st}} - \frac{A_{st} \cdot U_{st} \cdot (\theta_{st} - \theta_a)}{\theta_{st}} + B_{irr} = \frac{dS_{st}}{d\tau} \qquad (4.11)$$

Where $\dot{m}$ is the mass flow-rate of the heat transfer fluid flowing in the solar collector loop; s_{in} and s_{out} are respectively the flowing *in* and *out* specific entropies due to open storage system exchanges; $\dot{Q}_{need}$ is the power exchanged in the secondary heat exchanger; θ_{st} is the storage unit average temperature; A_{st} is the surface of the thermal energy storage; U_{st} is the storage unit thermal transmittance; θ_a is the ambient temperature; B_{irr} are the entropy losses due to internal irreversibilities; dS_{st} is the storage entropy generation; and $d\tau$ is the time. If the system is considered stationary for each hour, dS_{st} becomes ΔS_{st}, and the transformations can be assumed reversible, thus $B_{irr} = 0$. As a consequence, the previous expression can be rewritten as:

$$\dot{m} \cdot (s_{in} - s_{out}) \cdot \Delta\tau - \frac{\dot{Q}_{need}}{\theta_{st}} \cdot \Delta\tau - \frac{A_{st} \cdot U_{st} \cdot (\theta_{st} - \theta_a)}{\theta_{st}} \cdot \Delta\tau = \Delta S_{st} \qquad (4.12)$$

All the terms of the previous formulation can be retrieved from the results of the previously performed simulations, except for the terms referring to the specific entropies of the open system. Since they are intensive variables, for the water-based heat transfer fluid, some pre-calculated values exist, determined as a function of the other intensive thermodynamic properties (e.g., temperature, pressure). For the mPCM slurry-based system, these values can be determined considering the Gibbs, if the system pressure variations are assumed negligible. This assumption is realistic for the SolHe-PCM case study thanks to the presence of expansion vessels in the system. For the system exploiting the mPCM slurry the previous equation becomes:

$$\dot{m} \cdot \left(\frac{h_{in}}{\theta_{st,in}} - \frac{h_{out}}{\theta_{st,o}}\right) \cdot \Delta\tau - \frac{\dot{Q}_{need}}{\theta_{st}} \cdot \Delta\tau - \frac{A_{st} \cdot U_{st} \cdot (\theta_{st} - \theta_a)}{\theta_{st}} \cdot \Delta\tau = \Delta S_{st} \qquad (4.13)$$

Where h_{in} and h_{out} respectively are the specific enthalpies at the inlet and the outlet of the thermal energy storage unit; while θ_{st} and θ_{st} respectively are the temperature at the inlet and the outlet of the thermal energy storage unit. The

entropy balances referred to the other components of the overall SolHe-PCM system can be formulated similarly wise:

$$-\frac{\dot{Q}_{useful}}{\theta_{col}} \cdot \Delta\tau = \Delta S_{col} \tag{4.14}$$

$$\frac{\dot{Q}_{need}}{\theta_{need}} = \Delta S_{need} \tag{4.15}$$

$$\frac{A_{st} \cdot U_{st} \cdot (\theta_{st} - \theta_a)}{\theta_a} \cdot \Delta\tau = \Delta S_{dis} \tag{4.16}$$

Eventually, the entropy balance of the overall system is formulated as:

$$\Delta S_{tot} = \Delta S_{col} + \Delta S_{dis} + \Delta S_{need} + \Delta S_{st} \tag{4.17}$$

From the simulation results discussed above, the total entropy generated during the cycle of a typical heating season day was 2.78 kJ/K in the case of water, while 2.30 kJ/K in the case of the mPCM slurry. This results highlighted how the SolHe-PCM system can lead to a reduction of the entropy generation up to 17.2 %. Even if it was very preliminary study, this entropy analysis has been useful in the thesis to further underline how - when latent heat exchange processes are considered - it is particularly necessary to adopt approaches that are capable to consider also the temperatures and the thermal levels involved.

One of the outcome of this Section 4.2.4 is exactly to provide to the reader an outlook about how a process involving latent heat exchanges should be approached. Indeed, for certain elements (i.e., the thermal energy storage unit) the First law performance calculation is not sufficient itself to carry out significant long-term results. In this cases, the performance should be evaluated both in terms of energy balances and entropy (or exergy) balances. This work lays the foundations of more detailed investigation. Future works will be focused on the improvement of this Second law analysis. Moreover, exergy/entropy generation evaluations could be adopted to improve the design of each element of the innovative system, particularly the heat exchangers.

4.3 Experimental activities undertaken on the full-scale prototype of a mPCM slurry based solar thermal system

4.3.1 Design and retrofit of the full-scale prototype

The experimental campaign on the full-scale prototype operating with the mPCM slurry as the heat transfer fluid was the most critical path of the present thesis. The full-scale prototype was constructed on the roof of the DENERG Energy Department of Politecnico di Torino. This system construction activity was carried out with the aid of two industrial partners: TechnoEnergy (an Italian solar thermal panel manufacturer) and Teseo (an Italian-French company of industrial automation and control). First of all, the system was *tested with water* as the heat transfer fluid to check the operational behaviour of all the components. Measurement gathered in this phase were also used for a preliminary *calibration the numerical models*. Furthermore, the water-based system was used as benchmark and baseline to compare the performance achievable employing an innovative solar thermal system based on mPCM slurry.

Second of all, a similar long-term experimental campaign was planned to investigate also the effectiveness of the mPCM slurry-based solar thermal system. Nevertheless, some drawbacks occurred at this stage, which delayed the experimental activities from the planned schedule. The experimental campaign started again at the end of October 2015. First of all, a mixture of 200 litres of water and mPCM was prepared. The mixture had 30 % w.t concentration. The mPCM preparation consisted of five steps:

- The weighting of the various mixture components on a scale to divide the exact shares of each material. 200 litres of mPCM at 30 % w.t. concentration corresponds to about 197 kilograms of solution distributed as follow: 59 kilograms of mPCM, 55 kilograms of glycol, and 83 kilograms of water;
- The pouring of the raw materials together in plastic containers. Four tanks of 50 litres each were used for this purpose;
- The steering of the mixture to create a homogenous media;
- The filtration of the mixture to remove any inhomogeneity and mPCM grains;
- The filling up of the thermal energy storage tank with the mPCM slurry.

Since the tests started, it emerged that the mPCM slurry was affected by physical instability problems. The creaming phenomenon in the storage unit was more severe than expected. In fact, the secondary pump P2 – conceived to mix the storage media when steady in the storage tank – was not able to contrast creaming occurrence. After a day of measurements, the mPCM slurry showed a critical creaming separation. Moreover, since the storage tank internal envelop was not realised with stainless steel, the storage inspection visors were matted with a layer of rust. Even if this layer was thin, it did not allow the direct visual inspection of

the creaming phenomenon and was not possible to quantitatively evaluate the problem.

Figure 27. The thin layer of rust deposit affecting the inspection visors.

This shortcoming strongly affects the reliability of the experimental results. Indeed, the exact concentration of the mPCM in the slurry flowing in the primary collector loop remained always unknown. Since the peristaltic pump P3 drew from the lower part of the storage tank, it dealt with the storage media more affected by the creaming phenomenon. Therefore, the lower layer of the storage is where the concentration of mPCM becomes lighter after the creaming occurrence (see Section 3.2.5). In fact, after a couple of days of tests, the material flowing in the pipes of the collector loops seemed to have a mPCM concentration approximately 0 % (almost pure water and glycol with only some particles of mPCM).

After some unsuccessful attempts to solve these drawbacks changing the control settings of the system, the experimental campaign to test the behaviour of the SolHe-PCM prototype was temporarily stopped. A retrofit of the system was necessary to face the challenges due to the creaming manifestation. For this reason, a new thermal energy storage tank solution was designed. It consisted of moving forward to the Version 2 of the storage unit described in Section 3.3.2. The latest version of the storage had two main features that allowed to cope with the drawbacks mentioned above:

• It was made by a transparent plastic envelope that has avoided rust formation (furthermore all the circuit pipes are copper made) and has allowed the visual inspection to be easily carried out;
• It was equipped with a mechanical mixer regulated by a timer and an inverter that has stirred the mPCM slurry every hour to prevent the creaming formation.

The previously described improvements required some months to be designed, provided, and integrated into the existing full-scale prototype. Consequently, the long-term experimental campaign to examine the mPCM slurry as heat transfer fluid in the SolHe-PCM full-scale prototype began at the very end of the Ph.D. programme.

4.3.2 Preliminary results of the tests undertaken exploiting mPCM slurry as heat transfer fluid of the solar thermal system

The abovementioned retrofit of the full-scale prototype was completed by the end of January 2018. The ultimate retrofit activity was the electrical wiring of the inverter that regulates the mechanical mixer of the storage tank. Afterwards, the experimental campaign started again aiming at completing the following steps:

- Water tightness test of the overall hydraulic circuit. It consisted of testing again after the system retrofit all the circuit components (pipes, valves, hydraulic fittings, pumps) using the water as the heat transfer fluid. This stage lasted from January 20th 2018 to January 29th 2018.
- Preliminary mPCM slurry tests. The goal of this stage was twofold. On the one side, testing if drawbacks still occur after continuous operating of the circuit with mPCM slurry used as the heat transfer fluid. On the other side, scheduling the timer that regulates the mechanical mixer stirring operations, necessary to solve the creaming problem. This stage lasted from February 10th 2018 to February 17th 2018;
- Data gathering for numerical model calibration and validation with water as the heat transfer fluid. Since the storage unit was changed a new calibration procedure was required to verify the reliability of the numerical model (in this case it must refer to the single-node version 2 of the storage unit). This stage lasted from February 19th 2018 to February 22th 2018;
- Data gathering for numerical model calibration and validation with mPCM slurry as the heat transfer fluid. This stage was planned for the beginning of March, but the adverse weather conditions (heavy snow) postponed this phase after the ultimate deadline of the present thesis;

The two preliminary stages outlined positive results. The circuit was capable of operating correctly both with water and mPCM slurry used as the heat transfer fluid and storage media. *Figure 28* illustrates a moment of this initial experimental investigation.

Figure 28. The version 2 of the thermal energy storage unit filled with mPCM slurry.

The internal settings of the timer that regulates the mechanical mixer allow 17 cycles only to be planned daily. Two different scenarios were outlined:

- Storage media stirred at constant intervals all day long. In this case, every 1 hour and 23 minutes the mechanical mixer is activated for 2 minutes.
- Storage media stirred more frequently during the daytime. Since the creaming phenomenon does not represent a particular problem during night time, it can be selected to shorten the mechanical mixer activation cycles by considering the daytime only. In this case, from 8 am to 8 pm every 45 minutes the mechanical mixer is activated for 5 minutes. During night time the mechanical mixer remains switched-off. The first activation in the morning lasts a longer time span to cope with the nocturnal creaming occurrence.

The following *Figure 29* illustrates the outdoor weather conditions affecting the solar thermal system performance during the experimental campaign.
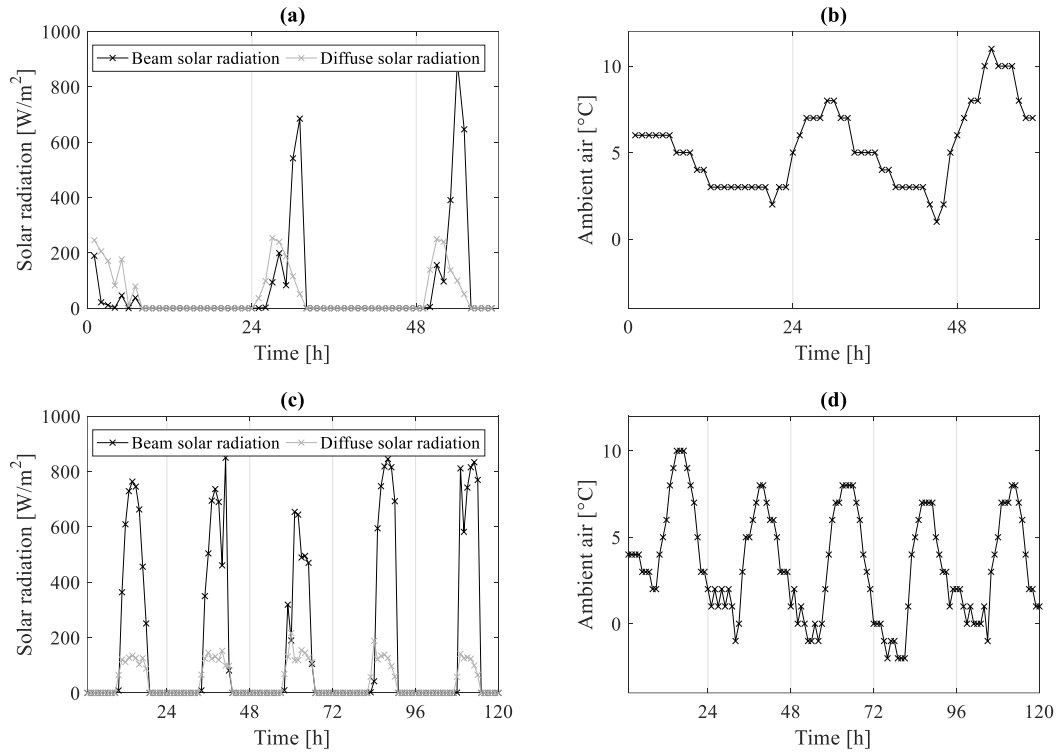
Figure 29. Weather conditions influencing the solar thermal system during the experimental campaign. Beam and diffuse solar radiations (a) during the tests with water and (c) during the tests with mPCM slurry. Ambient temperature (b) during the tests with water and (d) during the tests with mPCM slurry.

In the case of the water-based system the useful thermal power produced by the collector was easily retrieved by the following formulation:

$$\dot{Q}_u = \dot{m} \cdot c_p \cdot (\vartheta_{out} - \vartheta_{in}) \tag{4.16}$$

Where $\dot{m}$ is the mass flow rate controlled by the peristaltic pump P3, c_p is the specific heat capacity of water (set equal to 4186 $Jkg^{-1}K^{-1}$), θ_{out} is the temperature at the outlet of the collector (recorded by the thermocouple TC7), and θ_{in} is the temperature at the outlet of the collector (recorded by the thermocouple TC1). Once the useful thermal power was calculated, it was possible to evaluate the instantaneous efficiency of the system with the following formulation:

$$\eta = \frac{\dot{Q}_u}{A_c \cdot G_T}$$

(4.17)

Results are displayed in *Figure 30*. The experimental campaign with water as heat transfer fluid last only three complete days since adverse weather conditions aroused.
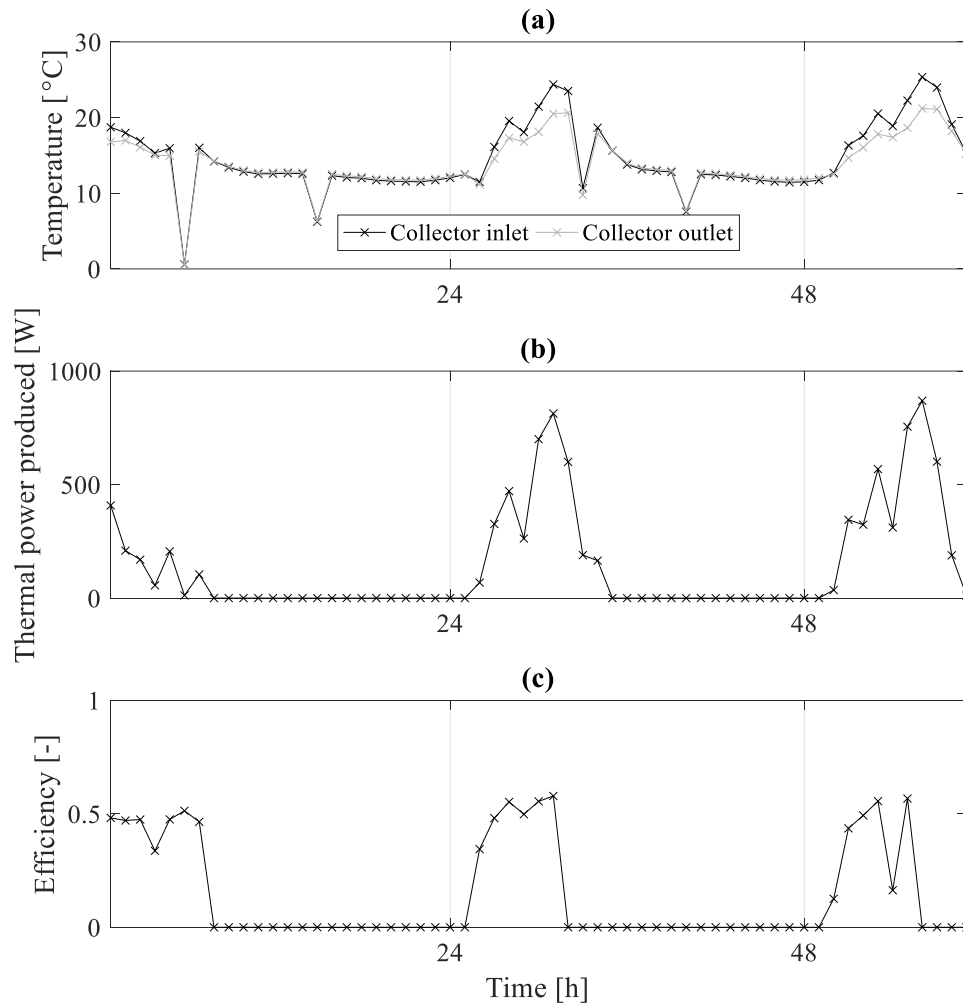
Figure 30. Tests on the water-based circuit with the retrofitted version of the thermal energy storage unit. (a) Comparison between the temperature recorded at the collector inlet and outlet; (b) Useful thermal power produced by the collector; (c) Calculated instantaneous efficiency of the collector.

The preliminary tests adopting the mPCM slurry were conceived to set up the experimental apparatus and verify the non-occurrence of the creaming phenomenon within the new storage unit. In this preliminary tests, the mPCM slurry used in the system before the retrofitting was recycled to avoid the waste of the material. This mPCM slurry presented the drawback of not being a pure mixture since rust was dispersed in the solution, as described in Section 4.3.1.

However, these tests were used to define the steps necessary to correctly evaluate the performance of the panel also in case of adoption of the mPCM slurry as heat transfer fluid. Indeed, in this circumstance the useful thermal power produced by the panel can be retrieved by the following formulation:

$$\dot{Q}_u = \dot{m} \cdot (h(\vartheta)_{out} - h(\vartheta)_{in}) \tag{4.18}$$
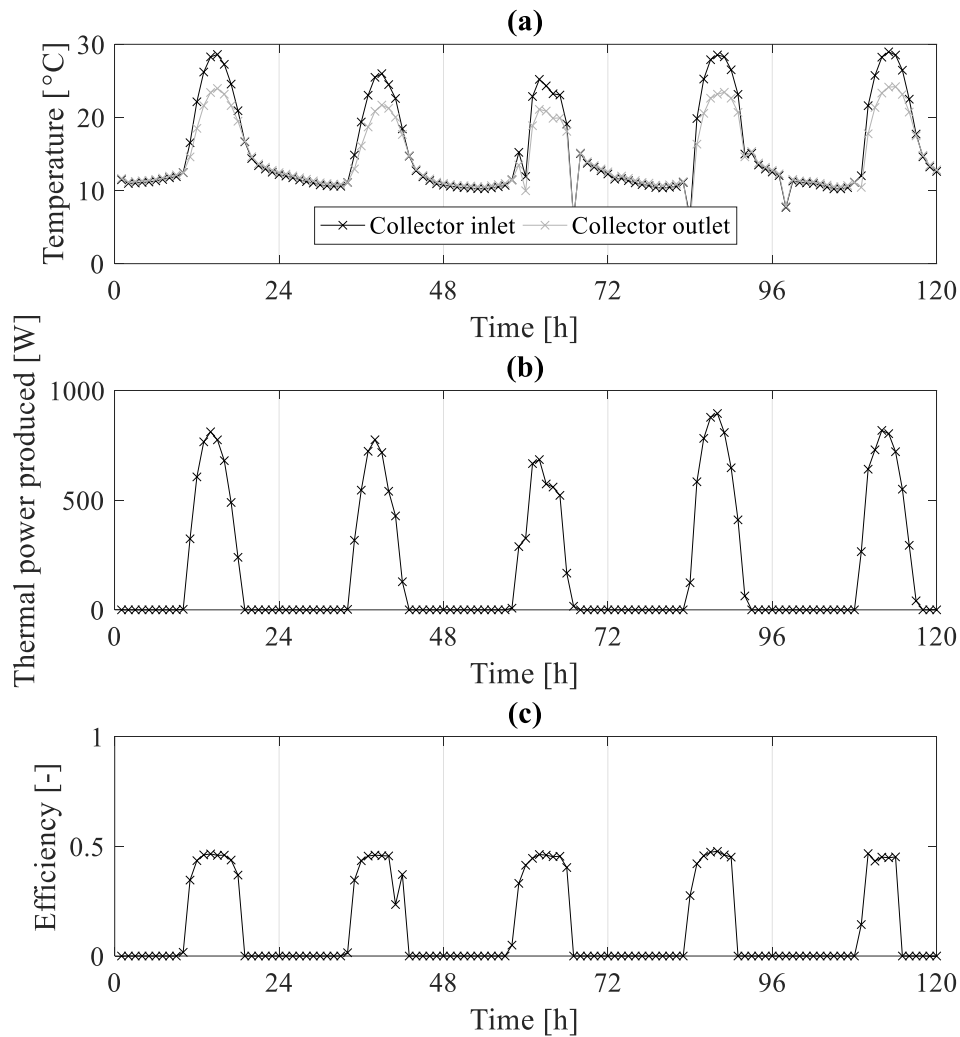
Figure 31. Tests on the mPCM slurry circuit with the retrofitted version of the thermal energy storage unit. (a) Comparison between the temperature recorded at the collector inlet and outlet; (b) Useful thermal power produced by the collector; (c) Calculated instantaneous efficiency of the collector.

Where $h(\theta)_{out}$ and $h(\theta)_{in}$ are the specific mPCM slurry enthalpies at the outlet and the inlet of the collector respectively. They can be derived as a function of the recorded temperature by means of the temperature versus specific enthalpy curves obtained with the T-History experiments (see Section 3.2.2). For this purpose, it is necessary to carefully evaluate the concentration of PCM microcapsules in the mixture. This was possible taking some mPCM slurry samples from the circuit and performing a gravimetric test, which consisted of drying the samples in a ventilated oven until constant weight was reached. Results of the gravimetric tests showed a concentration of about 10 % w.t. of PCM micro-particles dispersed in the mixture. Therefore, the temperature versus specific enthalpy curve referring to that specific concentration was adopted to define the specific enthalpies. Once the useful thermal power is calculated, the system efficiency can be evaluated using Equation 4.17 again. *Figure 31* outlines the results for the mPCM slurry case.

4.4 Key-findings of the present chapter

On the one hand, the present chapter used the numerical model described in Chapter 3 to assess the performance of the SolHe-PCM solar thermal system. On the other hand, experimental tests were undertaken by means of the full-scale prototype whose construction has been outlined in the previous chapter. First of all, the findings of the experimental campaign were used to calibrate and validate the numerical model. Indeed, The Key Performance Indicators used to evaluate the worthiness of the calibration procedure delineated a maximum discrepancy between actual experimental and simulated data lower than 12 %. Since these results were extremely satisfactory, it was possible to consider the outcomes of the model simulations as a reliable tool to assess the SolHe-PCM system performance.

A comparison of the performance of the SolHe-PCM system with a traditional water-based system was performed in the subsequent sections of the current chapter. These analyses were undertaken using both instantaneous parametrical simulations (to evaluate the influence of a single variable on the overall system performance) and year-long simulation (to assess the system performance in different climatic location). In all the simulated scenarios, the SolHe-PCM system demonstrated to overperform the water-based reference system. The simulation results showed that the SolHe-PCM collector could improve the production of useful heat up to 7 % throughout the year and up to 19 % considering the heating season only. A brief dissertation about a Second law analysis of the system has also been undertaken, opening a path for future investigations more detailed.

Eventually, the final section of the chapter describes the attempts of long-term monitoring of the technology. This part has strongly influenced also the full-scale prototype design and construction. Indeed, the system performance was optimised with a trial-and-error procedure (typical of each novel technology), which consisted in re-defining the design of a single system element when shortcomings show that better solution are necessary. This fact was particularly true for the thermal energy storage tank, where the physical instability due to the creaming phenomenon affected the experimental campaign.

References

[1] Yinping Z, Yi J, Yi J. A simple method, the -history method, of determining the heat of fusion, specific heat and thermal conductivity of phase-change materials. Meas Sci Technol 1999;10:201–5. doi:10.1088/0957-0233/10/3/015.

[2] Haberl JS, Bou-Saada TE. Procedures for Calibrating Hourly Simulation Models to Measured Building Energy and Environmental Data. J Sol Energy Eng 1998;120:193. doi:10.1115/1.2888069.

[3] Reddy TA, Maor I, Panjapornpon C. Calibrating detailed building energy simulation programs with measured data - Part I: General methodology (RP-1051). HVAC R Res 2007;13:221–41. doi:Article.

[4] Hyndman RJ, Koehler AB. Another look at measures of forecast accuracy. Int J Forecast 2006;22:679–88. doi:10.1016/j.ijforecast.2006.03.001.

[5] Willmott CJ, Matsuura K. Advantages of the mean absolute error (MAE) over the root mean square error (RMSE) in assessing average model performance. Clim Res 2005;30:79–82. doi:10.3354/cr030079.

[6] Chai T, Draxler RR. Root mean square error (RMSE) or mean absolute error (MAE)? -Arguments against avoiding RMSE in the literature. Geosci Model Dev 2014;7:1247–50. doi:10.5194/gmd-7-1247-2014.

[7] Duffie JA, Beckman WA. Solar Engineering of thermal processes. 4th Editio. New York, New York, USA: Wiley; 2013.

[8] LBLN. WINDOW| Windows and Daylighting 2018. https://windows.lbl.gov/.

[9] Lewis Gladius. Optimum tilt of a solar collector. Sol Wind Technol 1980;4:407–10.

[10] Shariah A, Al-Akhras M-A, Al-Omari IA. Optimizing the tilt angle of solar collectors Optimizing the tilt angle of solar collectors. Renew Energy 2013;26:587–98. doi:10.1016/S0960-1481(01)00106-9.

[11] CTI. UNI EN 12975-1:2011 Impianti solari termici e loro componenti - Collettori solari - Parte 1: Requisiti generali Impianti solari termici e loro componenti - Collettori solari - Parte 2: Metodi di prova 2011.

[12] ASHRAE. International Weather Files for Energy Calculations n.d.:2. https://www.ashrae.org/technical-resources/bookstore/ashrae-international-weather-files-for-energy- calculations-2-0-iwec2.

[13] Kazas G, Fabrizio E, Perino M. Energy demand profile generation with detailed time resolution at an urban district scale: A reference building approach and case study. Appl Energy 2017;193:243–62. doi:10.1016/j.apenergy.2017.01.095.

[14] Lucia U. Gouy-Stodola Theorem as a variational principle for open systems. arXiv Prepr arXiv 2012:1–16.

[15] Sciacovelli a., Verda V, Sciubba E. Entropy generation analysis as a design tool—A review. Renew Sustain Energy Rev 2015;43:1167–81. doi:10.1016/j.rser.2014.11.104.

[16] Kousksou T, Strub F, Castainglasvignottes J, Jamil a, Bedecarrats J. Second law analysis of latent thermal storage for solar system. Sol Energy Mater Sol Cells 2007;91:1275–81. doi:10.1016/j.solmat.2007.04.029.

[17] Jegadheeswarana S, Pohekar SD. Exergy analysis of particle dispersed latent heat thermal storage system for solar water heaters. J Renew Sustain Energy 2010;2:2010.

[18] MacPhee D, Dincer I, Beyene A. Numerical simulation and exergetic performance assessment of charging process in encapsulated ice thermal energy storage system. Energy 2012;41:491–8. doi:10.1016/j.energy.2012.02.042.

[19] Guelpa E, Sciacovelli A, Verda V. Entropy generation analysis for the design improvement of a latent heat storage system. Energy 2013;53:128–38. doi:10.1016/j.energy.2013.02.017.

[20] Serale G, Fabrizio E, Perino M. Design of a low-temperature solar heating system based on a slurry Phase Change Material (PCS). Energy and Buildings 2015;106:44-58. doi: 10.1016/j.enbuild.2015.06.063.

[21] Serale G, Baronetto S, Goia F, Perino M. Characterization and energy performance of a slurry PCM-based solar thermal collector: a numerical analysis. Energy Procedia 2015; 48:223-232. doi: 10.1016/j.egypro.2014.02.027.

[22] Fabrizio E, Monetti V. Methodologies and Advancements in the Calibration of Building Energy Models. Energies 2015; 8(4): 2548-2574. doi:10.3390/en8042548.

[23] Ruiz GR, Bandera GF. Validation of Calibrated Energy Models: Common Errors. Energies 2017; 10(10): 1587. doi:10.3390/en10101587.

[24] American Society of Heating, Ventilating, and Air Conditioning Engineers (ASHRAE). Guideline 14-2014, Measurement of Energy and Demand Savings; Technical Report; American Society of Heating, Ventilating, and Air Conditioning Engineers: Atlanta, GA, USA, 2014.

[25] Efficiency Valuation Organization. International Performance Measurement and Verification Protocol: Concepts and Options for Determining Energy and Water Savings, Volume I; Technical Report; Efficiency Valuation Organization: Washington, DC, USA, 2012.

[26] Webster L, Bradford J, Sartor D, Shonder J, Atkin E, Dunnivant S, Frank D, Franconi E, Jump D, Schiller S, et al. M&V Guidelines: Measurement and Verification for Performance-Based Contracts. Version 4.0. Technical Report. U.S. Department of Energy Federal Energy Management Program: Washington, DC, USA, 2015.

Chapter 5

Model Predictive Control (MPC) for enhancing buildings and HVAC systems energy efficiency. Problem formulation, applications and opportunities for the solar thermal system based on PCM slurry

The increasing spread of renewable energy sources and small-size poly-generation systems in buildings (likewise the SolHe-PCM project), is definitively changing the paradigm of energy distribution and the role of buildings. Energy needs are partially or completely satisfied by on-site energy production employing small renewable energy conversion systems. This process is introducing new challenges to face for compensating the mismatch between renewable sources availability and effective building occupants demand. For instance, the SolHe-PCM prototype can produce useful thermal energy only when solar radiation is available, while space heating demand can also occur during night time.

These challenges are particularly complicated when buildings and the energy delivery system are grid connected (e.g., buildings in a district heating network, small-size building integrated PV systems). Buildings' occupants are becoming "prosumers" (producers and consumers at the same time), and their behaviour during building operation is becoming of vital importance in enhancing energy performance. The implementation of active demand initiatives and peak-shaving strategies is expected to increase in the next future to foster the integration of these distributed resources and generation systems in smart distribution grids [1]. Furthermore, a new concept of active buildings – characterised by construction components (like floors, walls, roofs, foundations, façades, etc.) with adaptive and

responsive features – is increasingly penetrating in the market. In this paradigm, building elements and HVAC systems – coupled and integrated – are becoming capable of changing their behaviour and operating modes, in to face different and contrasting requirements related to different boundary conditions and objective functions. Indeed, responsive and adaptive technologies need to be controlled in an optimised way to exploit their potential completely. This feature is particularly true for innovative building elements such as systems with embedded PCM technologies, which require advanced control approaches to adequately manage their peak shifting potentialities and benefit entirely from their implementation in buildings.

In this context, the implementation of effective energy management strategies through advanced control methods represents an attractive solution to reduce the operational energy consumption of buildings. Moreover, it can be useful to minimise the mismatch between energy demand and on-site generation, maximising the exploitation of renewable energy sources. Many investigations proved that the more advanced control methods could ensure significant energy savings when compared to traditional control strategies [8].

Moreover, the increasing penetration of Information and Communication Technologies (ICT) in buildings has allowed a significant amount of building-related data to be more readily available and accessible. For this reason, if this information is appropriately processed through data-driven procedures, it may provide crucial knowledge on the actual building performance and the influence of occupant behaviour on the building energy consumption [2]. As a consequence, the analysis of this monitored data might represent a very effective opportunity to translate the extracted knowledge into ready-to-implement energy saving techniques and active demand strategies to enhance energy efficiency in buildings and HVAC systems.

Considering that usually indoor thermal comfort and building energy consumption are contrasting needs, optimisation procedures that aim at finding a trade-off between them are one of the primary goals of engineers and researchers worldwide [3]. Furthermore, buildings should be not considered as stand-alone systems, but they should be actively integrated into smart grids. In the last decades, many advances have been made in the building design stage to address these requirements, more recently opportunities to optimise the building behaviour also during its operation have been increasingly explored. This fact is in general achieved by studying and implementing advanced control techniques.

These are enabled thanks to the decreasing cost, accessibility and advances of electronic items and Building Energy Management Systems (BEMS), which allow the collection, storage and analysis of a vast amount of building-related data. Due to this fact, much effort is going to be devoted to the implementation of more sophisticated and prediction-based control strategies aimed at optimising the energy performance of buildings. The application of model- and prediction-based control techniques capable of searching optimal trade-offs between conflicting objectives is therefore highly desirable.

Model Predictive Control (MPC) is a well-established method for constrained control in industrial applications. Recently, it is receiving full attention from researchers in the field of control of buildings and active components. MPC merges principles of feedback control and numerical optimisation. It opens up possibilities of exploiting energy storage capabilities and optimisation of renewable energy sources on-site generation. MPC is able to exploit both the predictions of future disturbances (e.g., internal gains, weather, etc.) and given requirements (e.g., comfort ranges), in order to anticipate the energy needs of the building and optimise its thermal behaviour on the basis of the defined control goals. Constraints are included directly in the optimisation problem that is solved at each sampling step. Until the past decade, the MPC framework found a steep path to the practical implementation, because of its high computational demand in massive optimisation problems. With the development of new processors, graphics processing units, and cloud computing (and therefore with the exponential increase of available computational power), MPC is increasingly applied in various types of buildings and energy systems. Just in 2009, predictive optimal controllers, such as MPC, were considered marginal strategies by a review of advanced building control systems [4]. However, from that date, the application of MPC in buildings received continuously increasing attention, as it can be inferred by *Figure 1*. The papers included in this survey were selected with a search of the keywords "Model Predictive Control", "MPC", "Predictive Control/Controller", "Building" and "HVAC", on Scopus and Web of Science. A total of 211 papers were identified and, after screening and removal of studies that were not in line with the definitions of a Model Predictive Control strategy applied to buildings, 161 papers were included in this survey. An additional 36 documents were used for defining the overall framework and individuating possible alternative control methods of the building thermal behavior.
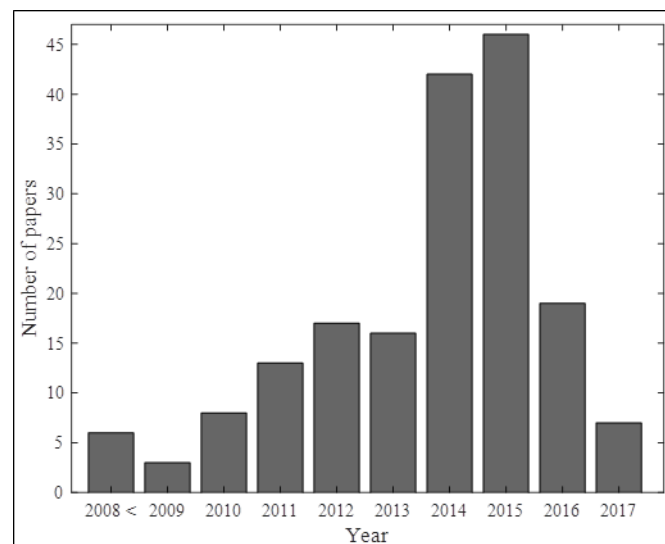
Figure 1. Yearly frequency distribution of scientific papers dealing with MPC formulation for buildings and HVAC systems.

When MPC formulation is undertaken, one of the leading problem arising is the definition of a simplified control oriented model that should be used in the iterative optimisation procedure. However, in the case of SolHe-PCM, a simplified lumped model of the controlled system was already formulated (see Section 3.4). For this reason, MPC algorithms seemed to be the ideal choice to devise a controller capable of maximising the SolHe-PCM system potentialities. Indeed, since a new technology was proposed, new control paradigms had to be formulated to enhance all its benefits.

So that, the present Chapter is divided into two main Sections. The first one aims at reviewing previous works about MPC for building and HVAC system thermal regulation, defining a comprehensive framework to formulate a model-based control problem effectively. In this direction, the entire review part contains many schematics that allow the MPC problem to be conceptually expressed, promoting a clearer comprehension for the readers. The second part of the chapter introduces the steps necessary to implement the MPC regulation in the SolHe-PCM prototype. Close-loop simulations were also carried out aiming at obtaining results to be compared with the ones obtained with a baseline Rule-Base Controller used as a benchmark.

The first part of the present Chapter (Section 5.1) was started during the research period spent at IMT Alti Studi Lucca. Some portions were included in the scientific paper:

- Model Predictive Control (MPC) for enhancing buildings and HVAC systems energy efficiency. Problem formulation, applications and opportunities. Authors: Gianluca Serale, Massimo Fiorentini, Alfonso Capozzoli, Daniele Bernardini, Alberto Bemporad. Journal: Eenergies 11(3) 1-35.

The second part of the present Chapter (Section 5.2) represents an outcome of the research period spent at Sustainable Building Research Centre at University of Wollongong. This work was presented at the international scientific conference 12th SDEWES2017 held in Dubrovnik. Some portions have been included in the scientific paper "Formulation of a Model Predictive Control Algorithm to Enhance the Performance of a Latent Heat Solar Thermal System" (authors: Gianluca Serale, Alfonso Capozzoli, Paul Cooper, Marco Perino) that is currently under review in the Elsevier journal Energy Conversion and Management.

5.1 A framework for Model Predictive Control to improve thermal management of buildings: review of previous works, problem formulation, applications and opportunities

A broader discussion on MPC formulation, applications and opportunities as a whole was necessary before focusing on the definition of the MPC algorithm to regulate the SolHe-PCM prototype. For this purpose, the main scope of the first part of this chapter is to lay the foundation of an imaginary bridge linking automation and control engineers with building and mechanical engineers involved in building and HVAC system design and operation. Indeed, so far, a lack of literature work providing a common dictionary and a taxonomy to enhance the relationship between those two professional categories was observed. Furthermore – even if the MPC control problem for buildings has been well-discussed in many studies found in the literature – a unique, clear and robust framework summarising the necessary steps to formulate the control problem does not exist. The remarkable work of Afram and Janabi-Sharifi [5] gave a significant contribution in this direction, but it only refers to studies done up to 2013 and significant research work in this area has been undertaken since then. Furthermore, compared to that work, more extended discussions and schematics to represent the operation of an MPC controller in a building could be useful to clarify the central concepts of this control framework that are sometimes misinterpreted. As a matter of fact, the lack of clear direction in the literature has generated confusion in some authors, and sometimes the term "Model Predictive Control" has been improperly used (e.g., calling MPC what actually is a day-ahead optimisation procedure or Dynamic Programming).

5.1.1 Short overview on building and HVAC system control methods

Before focusing on Model Predictive Control, a short overview on the most diffused control strategies adopted to manage the building and its HVAC system was necessary. A particular focus was given to the most innovative control techniques exploiting benefits achievable by data gathering. Indeed, over the past decades the implementation of wired and wireless sensors and embedded controllers in building systems has increased rapidly. The increase in computational power, the availability of low cost sensors and the availability of accurate weather predictions allow the control designers to explore some possible advanced control strategies for optimising an efficient building climate control.

The optimisation of the living space climate regulation is a problem that has no unique solution, since many variables can be included in the optimisation process, in particular when on site generation and energy storage units are implemented in

the building. In general, the goals of an intelligent management system for energy and comfort include the following goals:

- achieving a high comfort level, concerning thermal, air quality and visual comfort. This can be done by controlling temperature and lighting set-points or ensuring air quality by managing the level of contaminants such as carbon dioxide;
- achieving high energy efficiency, with the implementation of energy saving strategies while assuring an acceptable indoor environment quality. Similarly, it is possible to minimise the running cost of the building, including dynamic energy pricing of energy sources instead of the simple energy consumption.

A variety of control logic approaches for building cooling and heating systems have been proposed and reported in the literature. The ASHRAE handbook [6] offers a thorough review of the existing control methodologies for building energy systems. Classical control has been widely adopted in building energy systems due to its simplicity in design and low computational complexity when determining the control signals. The HVAC subsystems are controlled using Rule Based Controllers (RBC), based on inferential logics like "if–then–else", which are each managing a specific goal. For example, On/Off or bang-bang controllers are very common in old building systems without digital control, and Proportional-Integral-Derivative (PID) control loops are usually implemented in more modern buildings where heating and cooling systems are equipped with digital control and variable frequency drives (e.g., pulse-width modulation controls) [6]. At the level of the whole building, there is generally no optimisation, even though there are often highly sophisticated local controllers. This means that an upper layer capable of optimising the set-point of each controller in general is lacking. This is due to the high complexity that would be required for each Rule Based Controller and the fact that it is practically impossible to generalise their rules at a building level [30]. Although the combination of well-tuned classical control methods can provide satisfactory results. More advanced controllers can better allow the exploitation of renewable sources or of passive techniques for heating, cooling and lighting to minimise the energy needs and the use of non-renewable primary energy consumption as well as to reduce over-shooting and oscillations that contribute to significant increase of energy waste [7].

In the 1990s research started to focus on the development and application of intelligent methods to building control systems. Smart controllers could be optimally tuned for the control of different subsystems of an intelligent building using evolutionary algorithms [8]. For this purpose, the learning-based approaches from Artificial Intelligence techniques offer a different approach to the energy management problem compared to conventional methods. Control methods based on Artificial Intelligence can deal with noisy or incomplete data, and with nonlinearities in the system. After being trained, they can perform predictions at a relatively high speed [9].

The most common Artificial Intelligence methods is the adoption of Artificial Neural Networks. They have been used extensively for the building predictions and HVAC system control strategies [10,11]. Various Artificial Neural Network architectures have been studied for energy predictions, with resulting coefficient of variation in the range of $2-40\%$. These variations in the accuracy of the predictions were primarily dependent on the Artificial Neural Network architecture used, the regularity of the building operation and the accuracy of data measurement devices [12]. Artificial Neural Network controllers were studied for building thermal management, using a Multi-Input, Single-Output (MISO) architecture. Direct Artificial Neural Network controllers have been used in thermal comfort control [13] and in the temperature control of hydronic heating systems [14]. These controllers are practical and, in contrast to indirect Neural Network controllers, do not require identification of the dynamic model of the plant.

Fuzzy Logic Controllers also offer a potential solution, coupling and integrating the management of all the different criteria and components of an HVAC system. Alcala et al. [15] showed that the use of Fuzzy Logic Controllers can enable the implementation of multi-criteria control strategies incorporating expert knowledge, showing a significant building performance improvement when compared to a classical On/Off controller. Fuzzy Logic Controllers demonstrated good potential also in the energy management of a commercial building, coordinating photovoltaic generation, energy storage system, and building demand under dynamic electricity price conditions [16].

Genetic Algorithms (GAs) are optimization tools that can be used to improve the parameters of other control techniques. The use of Genetic Algorithms has been extensively researched for tuning parameters of classical controllers [16] and Fuzzy Logic Controllers [15]. Genetic Algorithms were also used to identify the key thermal parameters of a zone model based on measurements [17], as well as for the optimisation of Artificial Neural Network models [18] for the control of an HVAC system. Moreover, Genetic Algorithms were exploited for the broader scope of optimising the coordination of energy demand, renewable energy generation and energy storage [19].

5.1.2 Previous surveys on Model Predictive Control for building energy management

In the last years, an increasing number of surveys aimed at analysing the opportunity offered by the implementation of techniques based on classical control principles were published. From these works it has emerged that MPC algorithms are an effective method to improve building energy efficiency. In particular, the reviews on MPC can be grouped in those focused on optimal-intelligent control methods adopted for a single HVAC component (e.g., ventilation systems, ground coupled heat pumps, thermal energy storage units, window control, etc.) or those that consider the control strategies for the energy management of the entire

building. Surveys focused on the thermal management of building and HVAC systems can be further classified into two main groups: those that consider MPC just as one among many possible control methods, and those that are entirely focused on MPC.

5.1.2.1 Reviews that consider Model Predictive Control only as one among many possible control methods.

The papers [4,20] are two preliminary surveys dealing with advanced control systems for energy and comfort management in buildings. In detail, in [20] a useful framework of the early studies about the model-based supervisory control methods up to 2006 is provided. In [21,22] Demand Side Management procedures are reviewed with the aim to clarify the possible energy management strategies based on load forecasts and predictions In [22] MPC is considered as the most diffused and effective instrument in an energy management optimisation framework, which represents the higher level of intelligent control of a building for the authors. In [3] an entire section is focused on MPC and a summary of its main features and advantages for energy management, is provided. Moreover, the authors input the low widespread of this control method to the high modelling expertise and monitoring effort required. Similarly, in [23] an entire section is focused on MPC. This paper is more application-oriented, and it summarises the main features of revised studies without a critical framework to discuss the implementation of MPC in buildings. The recent study [24], provides a detailed overview of the various control strategies that can be applied to a building, focusing in particular on model based controllers, such as MPC. This remarkable paper provides a framework that highlights strengths and weakness of those strategies.

5.1.2.2 Reviews that are entirely focused on Model Predictive Control

The work of Afram and Janabi-Sharifi [5] can be considered the most remarkable review on MPC due to the worthy scheme of MPC implementation that it offers, combined with clear classifications criteria. This review highlights all the steps necessary to properly implement the MPC problem and to formulate the optimisation problem for building energy management. Moreover, the papers analysed in the review are classified between those are based on experimental results; it identifies the most important indicators to compare the MPC with other control approaches and it provides an accurate framework of the future challenges for MPC in building energy management. While a good description of different MPC configurations (e.g., centralised, decentralised, distributed, etc.) was provided, the possible MPC types (e.g., tracking, robust, economic, etc.) are roughly considered in this survey. Despite it considers a large number of articles (around 50), this review dates back to 2013. From that time, as far as the author

know, more than 100 new articles have been published about this MPC algorithm for building thermal management, reflecting the increasing magnitude that this topic is getting. Hilliard et al. [25] published in 2014 an excellent review of trend and opportunities for MPC implementation in commercial buildings. After an introductory description of MPC main features, the article summarises details of 19 scientific works using a series of tables that capture the salient points and allow for comparison. In those tables are listed all the various elements affecting the MPC performance (from the software adopted to the problem details). Consequently, a detailed analysis of strengths and weakness of each paper is carried out, also adopting descriptive statistics to find most common peculiarities. Results of this work were used by the same authors also in [26] to define which are the main requirements of a commercial building to be properly controlled by MPC. Despite the very notable discussion and the effective clearness of the article due to a structure organised by tables, compared to [5] these reviews are affected by a relatively low number of considered case studies and a short description of MPC key elements. Papers [27] and [28] are the most recent reviews on MPC applied to building and HVAC system control. They are both not general surveys, but works focused on particular aspects of building related MPC problems. The first one [27] is focused on Artificial Neural Network based MPC and the initial review section part can be considered an extension of the previous work undertaken by the same research group [5], with additional details on Artificial Neural Network control oriented models. The second one [28] is focused on occupant behaviour based MPC problems for internal temperature regulation. In the first part of the paper, the intention of the authors was to provide a general framework of MPC application for building energy management. Eventually, [29] provided a good overview and vision about the current and future potential applications for MPC building thermal regulation.

5.1.3 Model Predictive Control: framework and structure

The dynamic response of the outputs of a system is affected by controlled inputs (or manipulated variables) and uncontrolled inputs (or disturbances) [30]. A dynamical model of the system can capture such dynamics. Afterward, the controller can exploit them to make predictions of the possible future response of the system as a function of future controlled and uncontrolled inputs. MPC uses these predictions to select the best sequence of future manipulated variables, according to specific performance indices. The latter are defined over a time window that starts from the current time and spans a given prediction horizon in the future. The best sequence is obtained by solving a numerical optimisation problem, that also takes into account the constraints on input and output variables that must be satisfied during the operation of the building. The difference between MPC and open-loop optimal control is that the former only applies the first optimal move of the sequence at the current time instant, optimising a new sequence at the following

time-step again. This way of acting and replanning continuously over time is denoted as the "receding horizon" concept, and is sketched in *Figure 2*.
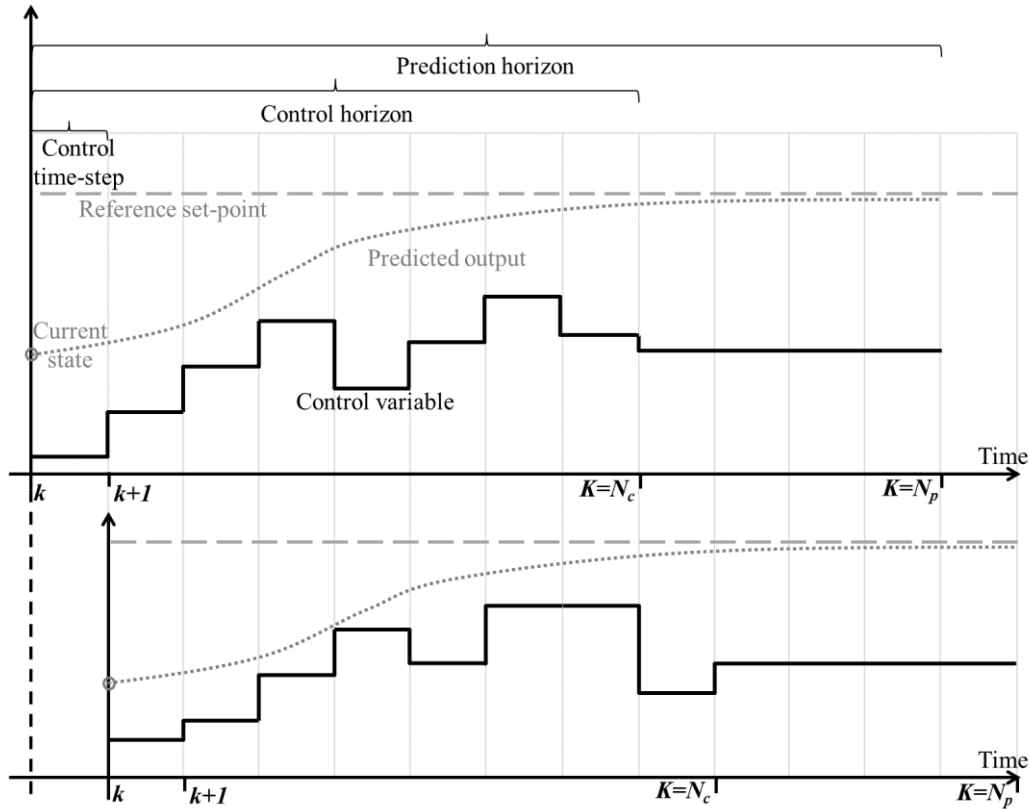
Figure 2. Schematic of the principle of receding horizon. The difference between the top and the bottom figure is one time-step.

The following notation is introduced to describe the receding horizon problem:

- *Current instant* (k): the current sampling step the controller is applied;
- *Control time-step* (T_s): it is the time between control updates and iterative receding horizon optimisations. The discrete variable k is generally used to refer to a specific control time-step;
- *Prediction horizon* (N_p) (also referred to as planning horizon): the number of control time-steps the controller looks ahead in the future to optimise the cost function under constraints;
- *Control horizon* (N_c) (also referred to as execution horizon or manipulated input horizon): the number of possible different values the manipulated variables can take in the future, that relates to the dimension of the optimisation vector.

A general framework of the MPC formulation is shown in *Figure 3*. All the aspects of the MPC framework presented in this figure are discussed in the following sections of this chapter. In *Figure 3*, the boxes filled in dark grey indicate elements that directly influence the optimisation problem; the light grey boxes

denote types of resulting optimisation problems; all the other boxes list the possible forms that the MPC formulation for buildings and HVAC system can take.
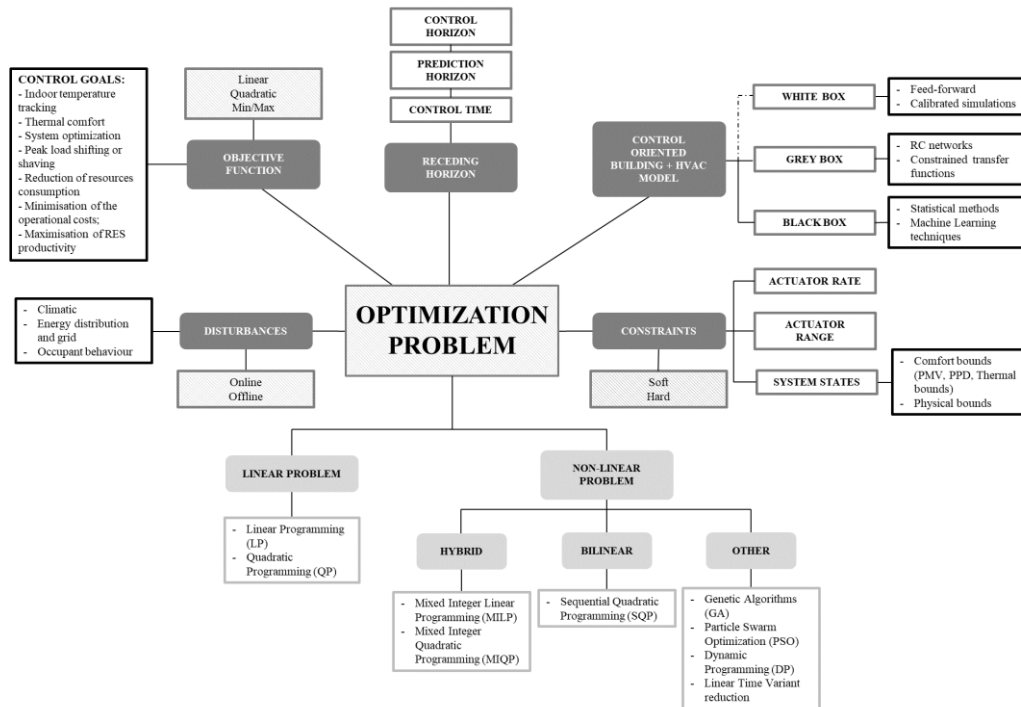
Figure 3. Framework and critical elements of the MPC optimization problem applied to building and HVAC systems. The boxes filled in dark grey indicate factors that directly influence the optimization problem; the light grey boxes denote types of resulting optimization problems; all the other boxes list the possible forms that the MPC formulation for buildings and HVAC system can take.

5.1.4 Typologies of Model Predictive Control

When solving a building control problem, various typologies of MPC can be adopted and they have to be selected according to the nature of the controlled process. In particular, to the type of prediction model that one has developed to describe it. Consequently, also the optimisation algorithms used will differ depending on the nature of the optimisation problem.

The main goal of the so called *standard MPC* (or *tracking MPC*) is to reach and closely track an a-priori defined reference trajectory of a controlled variable. Depending on the nature of the controlled system dynamics, the MPC problem can be either *linear* or *nonlinear*. The extension of MPC from linear to nonlinear problems is not a trivial matter due to additional computational complexity, reliability of nonlinear programming solvers, and lack of general purpose nonlinear systems identification techniques [31].

When the effect of unmeasured disturbances or model mismatch is a concern, sometimes is useful to embed a model of the possible mismatch between the

nominal and real system within the MPC problem formulation. Generally, with an expert knowledge of the controlled process or during the model validation phase from data, it is possible to define the magnitude of the uncertainties affecting the system and their effect on the model response. An MPC is called *robust MPC* when the stability and the performance specifications are maintained for all possible model variations and a class of noise signals (uncertainty magnitude) within a specified range [32]. In this case the uncertainties are bounded and the resulting control strategy always satisfies the defined constraints within the uncertainty range. An alternative solution is offered by the *stochastic MPC*, where a stochastic dynamical model of the process is used to predict its possible future evolution. Disturbances and constraints are included as random variables with a given probability distribution (e.g., Markov Chains). In case of continuous distributions, one allows for unbounded uncertainties and enforces constraints within a finite probability. Contrariwise, in case of discrete distributions, that is if the uncertainty can only take value from a limited set with a given probability, one can optimise stochastic measures (such as a trade-off of expectation and variance, or conditional value at risk) and enforce constraints either for all disturbances (worst-case) or in probability, depending on how critical are the constraints[33]. A stochastic approach in MPC is often used to simulate the occupancy disturbances [34,35]. In [36] an adaptive multi-scenario robust MPC is proposed as an alternative to stochastic MPC. In this case a fuzzy-logic and a hierarchical MPC are used to coordinate the different possible scenarios of building use, ensuring a computational time that is reported lower than that the one required by stochastic MPC to handle the same problem.

The previously described MPC strategies are designed around an objective function that penalizes the deviation of an output of the system from a reference trajectory. Generally, in a hierarchal MPC configuration, the reference trajectories for the set-points are calculated based on economic considerations (e.g., temperature desired values for optimal energy consumption) by the upper supervisory optimisation layer [37]. At a lower level, an MPC can optimise the control sequence of the actuators, minimizing the control effort to track the defined trajectory. *Economic MPC* refers to a strategy where temperature trajectories and system set-points are optimised within the same MPC cost function. The cost function is therefore based on an economic objective rather than the magnitude of the tracking error (e.g., minimising the energy consumption or the operational costs of a building). While this takes into consideration the building operational cost, it also implies that the cost function cannot be used as a traditional Lyapunov function to prove closed-loop stability [38]. Various studies demonstrated that these mathematical issues can be addressed in many practical situations [38]. In particular, in most of the cases, building energy management problems involve processes (i.e., temperature control) with slow dynamics where stability is not an issue, allowing the adoption of an economic MPC strategy [5].

In numerous energy management applications, the system is of a hybrid nature, in the sense that it includes both continuous dynamics (involving real-valued inputs and states) and discrete dynamics (involving finite-state machines and Boolean

input and states), leading to a nonlinear model with discontinuities. In this case, the optimisation most commonly can be cast as a Mixed Integer Programming (MIP) problem, and the MPC formulation is commonly referred as *hybrid MPC* [39]. This MPC approach is commonly used when the operation of the system involves discrete states, functioning modes, open or closed, On or Off or scheduling requirements.

The MPC problem can be formulated in an *implicit* or *explicit* formulation. While in implicit MPC the control law is defined by solving the optimisation problem in real-time, in explicit MPC multi-parametric programming algorithms are run offline to recast the control law as a lookup table of linear gains [40]. Explicit MPC is generally used in those applications of small size where the computing power is limited or a very short computational time is required (e.g., in embedded controllers that are required to perform the online optimisation). Building thermal systems are generally characterised by large time constants and Building Automation Systems normally have sufficient computational power to allow the optimisation of an implicit formulation that can be adopted for the building energy management, and moreover are characterized by large model sizes which would make the explicit MPC approach unpractical, if not impossible.

5.1.5 Models used in Model Predictive Control

The models are mathematical tools capable of describing the physical behaviour of a system with defined input and output variables [41]. Physical processes are *continuous* in nature, however the availability of information on their status is generally *discrete*, due to the sampling nature of the sensors used to monitor and understand the process. A *deterministic* model can completely determine the future and past states of a system knowing its initial conditions. On the other hand, complex random systems with chaotic behaviour require *stochastic* models, which are in general more difficult to implement [42]. It is well-known that the development of an appropriate dynamic model and its identification are often the most difficult and time-consuming tasks of the control design process, in particular when applying an MPC strategy. Indeed, models are the cornerstone of MPC and, following the Camacho and Bordons [31] indications, two different important models can be discerned within the implementation of an MPC controller for buildings and their HVAC systems:

- The *control oriented building and its HVAC system model*, which represents the thermo-dynamical behaviour of the building, used by the MPC for the on-line optimisation. This model should be capable of accurately describe the physics of the controlled process and predicting the future states of the controlled system;
- The *disturbance models* that allow the forecast of the behaviour of the uncontrolled variables affecting the dynamic response of the system.

The control oriented building model is always necessary and its definition is a common issue for those who approach an MPC problem for building control and energy management; while the disturbance models can be in some cases neglected, and data retrieved by external (e.g., Cloud connected) modelling tools or databases can be used instead. While the two aforementioned models are required for the MPC controller implementation, a further model is necessary at the design, simulation and prototype phase:

- The *surrogate simulated building model* that is a virtual, possibly high-accuracy representation of the controlled system necessary to close the control loop in simulation.

5.1.5.1 Modelling the building and the HVAC system

ASHRAE [6] categorises modelling methods into two different approaches: the forward (classical) approach and the data-driven (inverse) approach. On the one side, the *forward approach* (also known as *white box models* or *engineering methods*) presumes detailed knowledge of the various system processes and interactions. The main advantage of this approach is that the system does not require to be physically built in order to evaluate its performance. Thus, in modelling the energy behaviour of a building, the forward approach is usually suitable for preliminary predictions of energy needs and design of system loads. Reduced order models, quasi steady-state methods suggested by standards, modified bin methods and the most common detailed energy simulation tools (e.g., EnergyPlus, TRNSYS, ESP-r and DOE-2) belong to the forward approach methods [43].
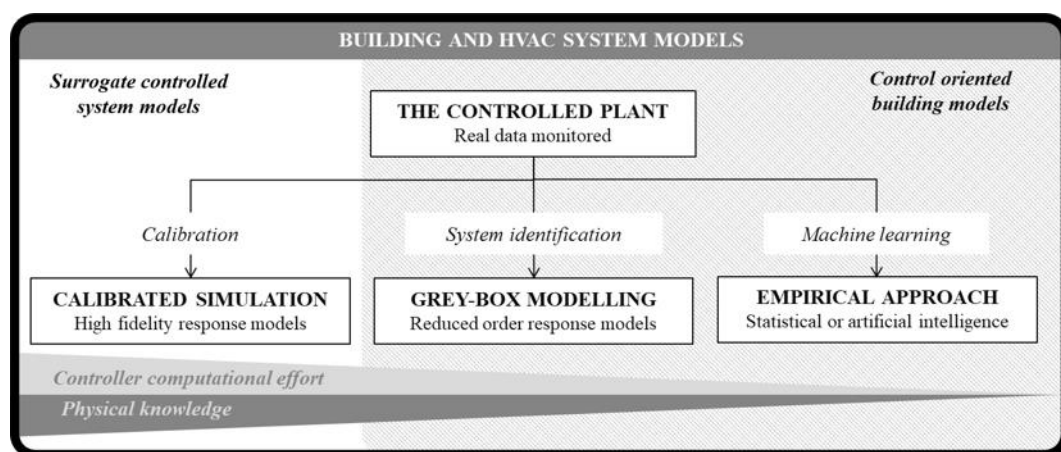
Figure 4. Different modelling approaches according to ASHRAE classification.

On the other side the *data-driven models* were further classified by ASHRAE [6] in three broad groups, highlighted in *Figure 4*, that have also been adopted in the following classifications [2,43–46]:

- *Calibrated simulation models*: are high fidelity response models based on physical principle to calculate thermal dynamics and energy behaviour of whole building level or for sublevel components [46]. The approach is the same as the one mentioned in the forward approach, but in this case the models are calibrated using real data gathered on-field.
- *Black-box models (also known as empirical approach)*: do not require full knowledge of the system or the process. They are developed by fitting parameters of a model to historical behaviour of the system. The parameters subject to identification do not generally have direct physical meaning. For these reasons, black-box models become particularly suitable for predicting the behaviour of processes where a-priori deterministic knowledge of the physical relationship between input and output is not univocally defined (e.g., evolution of climatic disturbances and occupant behaviour related disturbances). In the last few years, much research was focused on this kind of black-box models applied to building data. Various further classifications have been proposed in the literature and interested readers can refer to [43,44,46]. The black-box approach can be either statistical or based on artificial intelligence [2]. For example, linear, multivariate or change-point regression, autoregressive models, conditional demand analysis and Fourier series belong to the category of statistical models. Artificial Intelligence techniques are those are based on machine learning techniques such as Artificial Neural Networks or Support Vector Machines.
- *Grey-box models*: are simplified physical models of system dynamics. While they retain the physical description of the system they represent, their parameters can be estimated using system identification methods. Grey-box models have fitting parameters that include the dynamics of the physical system described. Semi-Deterministic Physical Modelling (DSPM) uses a Resistance-Capacitance (R-C) electrical network analogue to describe the thermodynamics of a system. *Figure 5* represents an example of R-C modelling of a building. Usually the model parameters are estimated by tuning to historical measurements, and this approach has been presented in a wide variety of papers [47–50]. Semi-Probabilistic Physical Modelling (PSPM) - also referred as Bayesan network - approaches the problem using stochastic differential equations for the description of a system to be identified [51]. Various models with increasing complexity have been formulated based on prior physical knowledge, and the parameters of each model are estimated using the maximum likelihood method. Grey-box models, depending on their use, can be either linear or nonlinear, deterministic or stochastic. Non-linear grey-box models require a further effort in the system identification task.

  In *Figure 5* an example of R-C network is shown. Θ_o is the outside temperature, Θ_a is the internal ambient temperature, Θ_a is the internal temperature of a narrow ambient, R_{wo} is the external liminar thermal resistance of the wall, R_{wi} is the internal liminar thermal resistance of the wall, R_w is the thermal resistance of the wall, R_v is a surrogate thermal resistance

associated to ventilation, C_w is the wall thermal capacity, C_a is the internal air thermal capacity, C_f is the floor thermal capacity, ϕ_s is the solar flux incident on the external wall, ϕ_i is the flux due to internal heat gains, ϕ_{HVAC} is the thermal power delivered by radiant panel embedded in the floor.
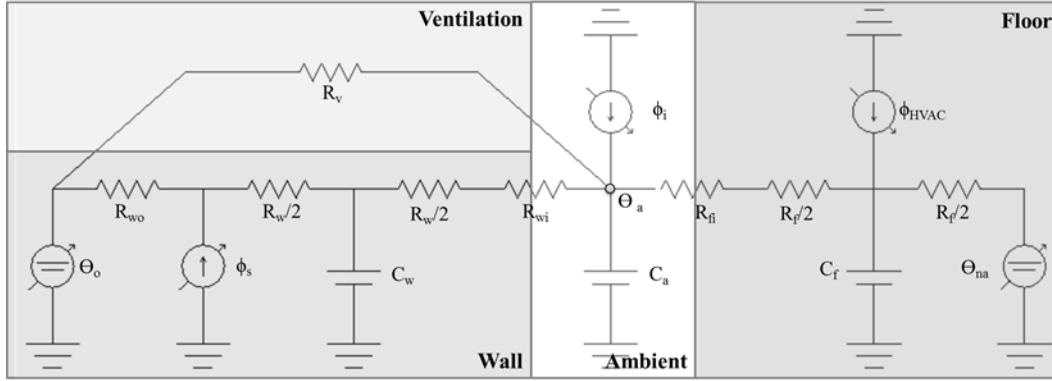
Figure 5. A typical example of an R-C network for MPC applications.

5.1.5.2 The control oriented building and its HVAC system model

It is well known that the development of an appropriate dynamic model and its identification are often the most difficult and time-consuming tasks of the automation process, in particular when applying a MPC strategy. Indeed, for MPC it is necessary to carry out a virtual image of the controlled system, called control oriented building model, capable of describing the physics of such controlled process accurately [52]. This control oriented building model must be accurate enough to ensure satisfactory prediction capabilities and capture the fundamental engineering processes that influence the dynamics of the controlled building, but at the same time has to be simple to ensure a reasonable computational time of the optimisation process [53]. Indeed, the real-time optimisation process could require that the control oriented building model is run numerous times within a defined time interval (represented by the control time-step). The importance of the control oriented building model is highlighted by the fact that many papers have a two-parts structure describing the model: in a first part are focused on the description of the controller and the optimisation process in a second one. In many cases these parts are quite extensive in terms of the amount of research content that the authors decide to split it in two independent articles (e.g., [54] and [55] or [56] and [57]). The control oriented building and HVAC system models, even they are a simplification of the real physical system, are required to represent its response accurately enough for the optimisation to be effective, thus in most cases they are supported by a data-driven approach. In experimental case studies, historical data of states and disturbances, measured by sensors, can be utilized for this purpose. These measurements can also be used in real-time by the controller to perform the optimisation. On the other hand, when the controlled building uses a surrogate

simulated model, the surrogate real-time measurements need to be sent at each control time-step from the simulation platform to the MPC controller.

Inputs to the models for prediction and calibration include the most significant climatic and occupancy related disturbances, as well as controllable inputs such as the thermal energy delivered by the HVAC system. Common inputs to the thermal model include outdoor temperature, solar radiation, internal gains and heating or cooling energy delivered by the HVAC system. The measured response is generally the indoor air temperature; in some cases, mainly simulated, the measured response can also include the average walls or other building components temperature [58]. While the measured indoor air temperatures typically are monitored using sensors integrated into the building automation system, the temperature of the walls, floors, ceilings and other building components are typically estimated, with no feedback from sensors. Furthermore, the temperatures of HVAC system components are also often part of the control oriented model. For example, in [59–61], the thermal energy system operation was optimised, by considering it as a lumped temperature node. The relative difference between the temperature of the thermal energy storage and the building internal temperature represents an additional opportunity for heating and cooling [44,62]. Similarly, to the applications where the control oriented model states relate to temperature nodes, some other authors include in this model also other variables that affect the occupants' comfort. For example, in [63–66] the internal carbon dioxide concentration level is also considered as controlled variable together with the internal temperature. In [65–68] also the light level was taken into account. The light level can be controlled using the blinds position, while the carbon dioxide concentration level was controlled by managed the air change rate. Both these additional variables have an effect on the thermal balance of an indoor environment, affecting the solar gains and the ventilation losses respectively.

From a thermodynamic perspective, a building can be treated as a single zone or as multi zone. The number of zones coincides with the number of internal nodes that are used to model the building dynamics. From the MPC prospective and its use in thermal regulation of indoor spaces, a multi-zone building can be modelled in its entirety in the control oriented building model, in the attempt to find an optimal solution for the operation of the entire building. In other cases, a distributed approach is taken, where various controllers manage a separate zone. A model with reasonable prediction properties is an ultimate condition for excellent performance of the predictive controller, and extensive research has been undertaken to aid the selection of the most appropriate model for the task [58]. Building thermal models used for optimisation generally use less information when compared to high fidelity models, as their complexity and order is reduced and they tend to lump physical characteristics and processes.

It is unlikely that *white-box* or *calibrated simulation models* can be utilised as a control oriented building model, as in general they do not provide an explicit model of the building, the identification and validation of calibrated simulation models are non-trivial processes, and require building blueprints, significant parameter tuning and simulation effort. Moreover, since the complexity, non-linearity and size of the calibrated simulation responsive models, quickly lead

optimisation problems exceed computation time frames required in a practical control application. Nevertheless, many researchers have studied the application of optimal controllers that use those calibrated simulation models, interfaced with different optimisation toolboxes [69–72]. Some of this studies demonstrated how the computational time required by the optimisation of a high fidelity model in TRNSYS exceeds the control sampling time [73]. Moreover, high fidelity simulation models prevent the optimisation solvers from exploring the sparse structure of the resulting optimisation problem [74]. In [29] the further issue of differences between blueprints and actually used materials is introduced. In general, the literature offers numerous works deducing that the calibrated simulation approach is not effective for implementation in controllers [74–76].

In general, *black-box models* these models cannot ensure reliable prediction for operating points outside the range covered by the training data and thus extensive and adequate data training is needed in order to guarantee prediction accuracy. However, state that these models are faster to develop and implement, if sufficient data are available, they are often adopted as control oriented models capable of ensuring an accurate system representation. *Black-box models* are also used to represent the thermal response of a building, and a common representation of a zone heat transfer can be achieved using *transfer functions,* and in the specific case, given that signals are generally discrete, *z-transforms* are used [77]. Arguably, when transfer functions parameters are constrained, they can be considered grey-box models. Other examples of representation of a building response and comfort perception for thermal regulation and HVAC system control using black-box models are Artificial Neural Networks [78], even though they are most commonly used for supervisory optimisation of the energy management [79].

Grey-box modelling is proven to be a comprehensive method to model the thermal response of a building [80]. One of the critical targets in development of a grey-box model for an MPC application is identifying a suitable model is agreement with the physical response of the system and at the same time has a complexity that can embed the information contained in the data, which means that the model should neither be under-fitted nor over-fitted [81]. In buildings, *grey-box models* commonly use the R-C network analogy with an electric circuitry to describe the thermal process dynamics of a building zone. Thermal inertia, modelled as a capacitance in the R-C network, plays a crucial role in the behaviour and optimal operation of Thermally Activated Building Structures. Modular construction of the R-C circuit can be followed to describe the behaviour of a multi-zone building as a combination of single zones. Toolboxes for the automatic generation for control oriented R-C models were also recently developed [82,83]. A forward selection strategy is used to find the best model by an iterative process, using the most meaningful and adequately complex model [81,84]. In [85] the model fit is recalculated every night, taking into account the additional building dynamics data observed each day.

In most of the cases, grey-box models were formulated using a *state-space* representation of Linear Time Invariant (LTI) systems. A discrete state-space model is usually formulated as follows:

$$\begin{cases} x(k+1) = Ax(k) + B_u u(k) + B_v v(k) + Gw(k) \\ \quad y(k) = Cx(k) + D_u u(k) + D_v v(k) + d(k) \end{cases} \qquad (6.1)$$

Where $u(k)$ is the vector of manipulated inputs or controlling variables (e.g., the HVAC system control inputs), $v(k)$ is the vector of measured disturbances affecting the system (e.g., weather), $x(k)$ is the vector of the system states (e.g., the building temperature nodes), $y(k)$ is the vector of the outputs, $d(k)$ is the unmeasured random noise on the outputs, and $w(k)$ is the unmeasured random noise on the measurement of the state. The terms A, B_u, B_v, C, D_u, D_v and G are state matrix, manipulated input matrix, measured disturbances matrix, output matrix, direct transmission matrix for manipulated inputs, direct transmission matrix for measured disturbances, and the matrix of the unmeasured random noise on the states respectively. When the model is grey-box, the parameters in these matrices are estimated using system identification techniques. In building applications, similarly to other industrial processes, the output is not a function of manipulated inputs, resulting in a zero D_u matrix. The outputs $y(k)$ can be either measured (e.g., the indoor air temperature) or unmeasured (e.g., the wall internal temperature). An observer – typically a Kalman filter – is employed to reconstruct the current state vector at time k based on the measured signals. In MPC, an alternative to the *output-feedback* formulation discussed above is referred to as *state-feedback*, and assumes that all the states are measured. In that case the output vector is typically neglected. This formulation is also frequently adopted for building applications.
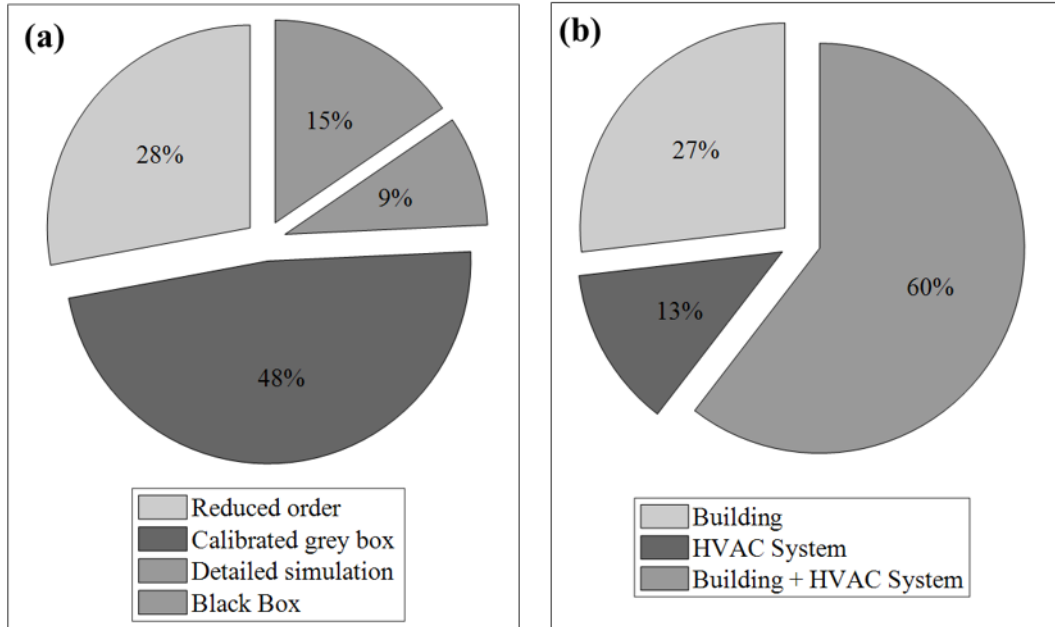
Figure 6. (a) Proportion of reviewed literature papers using either white, grey or black-box models as control oriented building models; (b) proportion of literature papers considering in the control oriented model either the building only, the HVAC only, or both.

On the one hand, some authors prefer not to include the HVAC system model in the MPC formulation. In this case, the MPC solves a higher level optimisation problem, which returns the building set-points to be utilised, while it does not provide information on the HVAC system and its actuators states or behaviour.

On the other hand, other authors consider the mathematical description of the HVAC system and its energy components, together with the building model, crucial for a reliable optimisation of the building operation. In these cases, the HVAC system model can be either integrated with the building model, solving a complete optimisation problem, or the building (or the precinct) demand can be sometimes introduced as an external disturbance with a forecasted profile in the optimisation problem, which is mainly focused on the HVAC system. *Figure 6* reports the fraction of papers found in the literature that use different control oriented building models and approaches to the HVAC system modelling.

In the first case the optimisation can take into account the mutual interaction of the two systems in the thermoregulatory and energy problem, resulting in a more complete formulation, which comes though with a higher cost in terms of problem complexity and computational effort. In the case of Air Handling Units and Variable Air Volume boxes for example [86], the problem acquires a non-linear nature, specifically bi-linear, where one of the states (e.g., the room temperature) multiplies one of the controlled inputs (e.g., the system air flow rate) [87–90]. A similar configuration can also be found in the regulation of Fan Coil Units [91].

Additional complexity can also derive from an intermittent nature of the energy delivery, which leads to the formulation of an optimal controller of a hybrid system, due to the combination of continuous and Boolean variables in the optimisation problem [92]. HVAC systems integrating renewable energy source thermal generation and energy storage can also exhibit a hybrid nature, since they can operate in various defined operating modes [59,61], and MPC is particularly relevant for them since renewable thermal energy resources are highly weather-dependent and energy storage allows an offset of the generation to allow a better match with the demand.

In other cases, the MPC mainly focuses on the control of the HVAC system, considering the thermal demand of the building only as a disturbance to the controlled system. This approach is more common when the complexity or the research focus lies on the HVAC system itself (e.g., in [93] where the optimisation of renewable generation and storage for a solar cooling system is studied), or where the HVAC system has to supply energy to a number of buildings, as in a university campus, and the focus is on the energy management [48,94].

A general framework of the alternative scenario dealing with HVAC system modelling in MPC problems is provided in *Figure 7*.
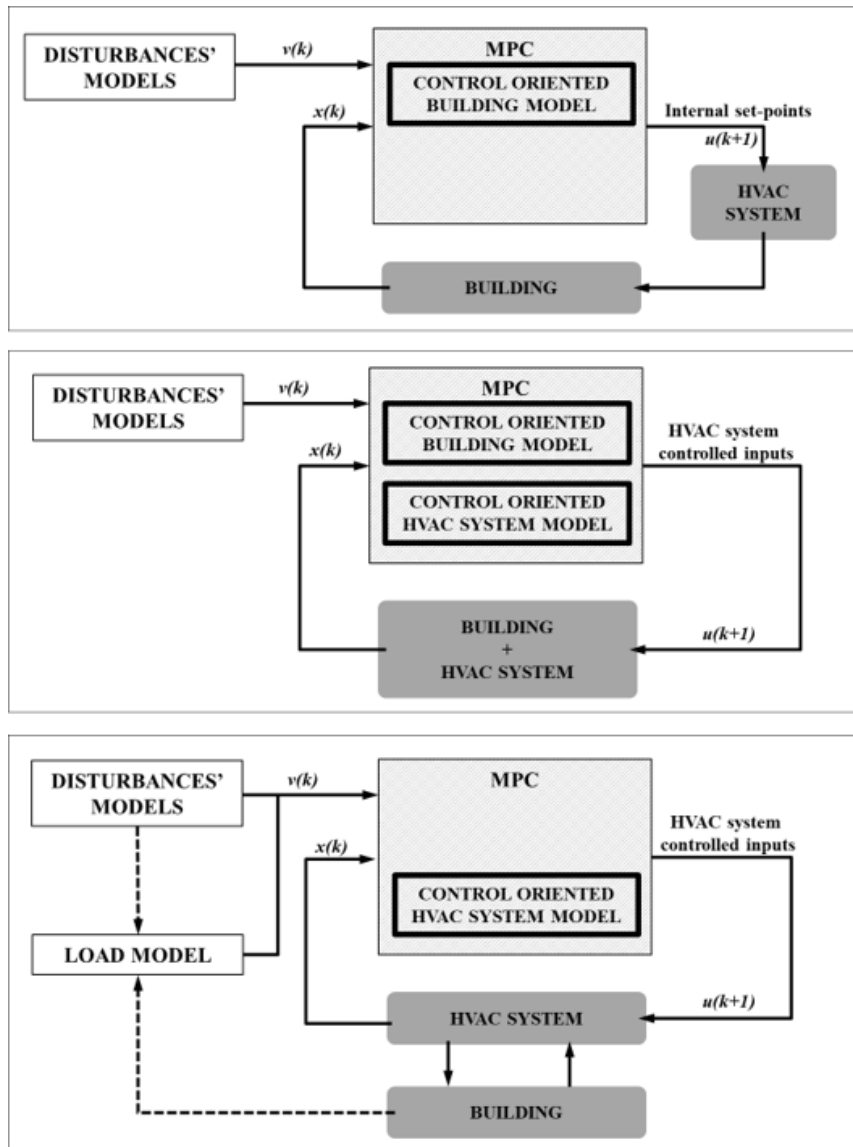
Figure 7. Possible alternative scenario of HVAC system modelling in MPC problems. (a) HVAC system not considered in the MPC formulation; (b) MPC integrating both building and its HVAC system; (c) building not considered in the MPC formulation.

5.1.5.3 The prediction models of disturbances

Disturbances can be either measured or unmeasured. The *measured disturbances* are generally part of the dynamic building model, and their effect on the system response is directly captured by the model. The *unmeasured disturbances* can have a small or large effect on the system response, affecting the uncertainty and the accuracy of the model response. In some cases, even if a sensor is not providing a direct measurement of the disturbance, the disturbance or at least its magnitude can be estimated beforehand [95].

The measured disturbances can be considered as *ideal* measurements or as measurements *affected by uncertainty* (e.g., white noise, stochastic noise, etc.). Signal processing tools generally help in discriminating the signal noise from the

signal itself. Data retrieved from existing data sets can be considered ideal predictions or further elaborated adding a noise to model the uncertainty affecting the disturbances. This action generally is addressed using a Kalman filter that implements white noise to the signal [96].

There are three main categories of measured disturbances affecting a MPC problem for HVAC system and building energy management:

- *Climatic* disturbances (e.g., ambient temperature, humidity ratio, relative humidity, wet-bulb temperature, dew-point temperature, solar radiation, wind velocity, ground temperature;
- *Occupant behaviour related* disturbances (e.g., occupied/unoccupied, variation in the scheduled comfort set-points, internal heat gains/loads, adjacent zones set-points);
- *Grid and energy distributor related* disturbances (e.g., Time of Use or real-time prices, peak load penalties, demand response incentives).

Climatic disturbances affect the energy balance of the building and the performance of system components. The occupant behaviour can also significantly influence the operation objectives, constraints and system response [97]. The disturbances related to the energy distribution becomes crucial where building Demand Side Management strategies are considered in the MPC formulation (e.g., reduction of daily energy cost or peak load shifting or shaping). In other cases, though the building demand can be treated as a single disturbance where the climatic conditions, the occupant behaviour and factors affecting the building energy consumption are lumped together.

The most straightforward method to determine disturbances affecting a building is to utilise commonly available disturbances patterns, such as the Example Weather Year, the Representative Meteorological Year, the Typical Meteorological Year, or the International Weather for Energy Calculation weather files or ASHRAE building demand and occupation patterns [6]. In this case the disturbances can only be used when assessing seasonal macro trends, but would not be accurate enough to be utilised for the short term predictions used by optimisation methods. For this reason, considering the disturbances to be equal to the ones provided in these datasets can be used to assess, at a design stage, the simulated controller performance only, but cannot be used for implementation on a real-time controller.

A more accurate representation of the disturbances affecting the building and its HVAC system can be achieved for example by analysing historical data gathered from the Building Automation System. In this case the disturbances will be modelled around an existing system and they can be used for predicting the performance of an MPC controller when compared to existing classical control logic. The results from such analysis can lead to the development of a real-time controller that can be deployed on the considered building. For the real-time applications, accurate short term predictions are necessary and two primary possible methods of forecast can be adopted:

- *Online predictions* rely on the availability of an internet connection and the possibility to acquire forecasts from a third party source, that has the capability to provide accurate prediction using complex models. For climatic disturbances, these third party sources can include models for weather forecast, which normally use complex numerical climatic models to predict most of the influencing disturbances. The accuracy of these online models has been validated and several papers state that they are highly reliable. Future energy prices are also often predicted using data retrieved from the internet, by means of information supplied by the electricity provider or national/regional energy regulators.

- *Offline predictions* do not need an internet connection and they only rely on the data which has been measured on site; on the other hand, they require a model that can predict the future disturbances behaviour. Moreover, these methods are compulsory for the forecast of occupancy related disturbances that are specific to each case study. The simplest method for offline predictions is the so-called *lazy-man prediction* method. It is based on a rule of thumb that states that "the conditions of the next hours would be only slightly different from those of the previous time period" [35,98,99]. For this reason, data collected on-site referring to previous hours can be used as a prediction for next hours, simply averaged or modified with small corrections (e.g., coefficients assessing higher weights to the measurement closer to the current state). More accurate offline prediction methods are those are based on statistical or machine learning models. Likewise building black-box response models, the literature offers many available methods for modelling the disturbances in these ways[98–100].
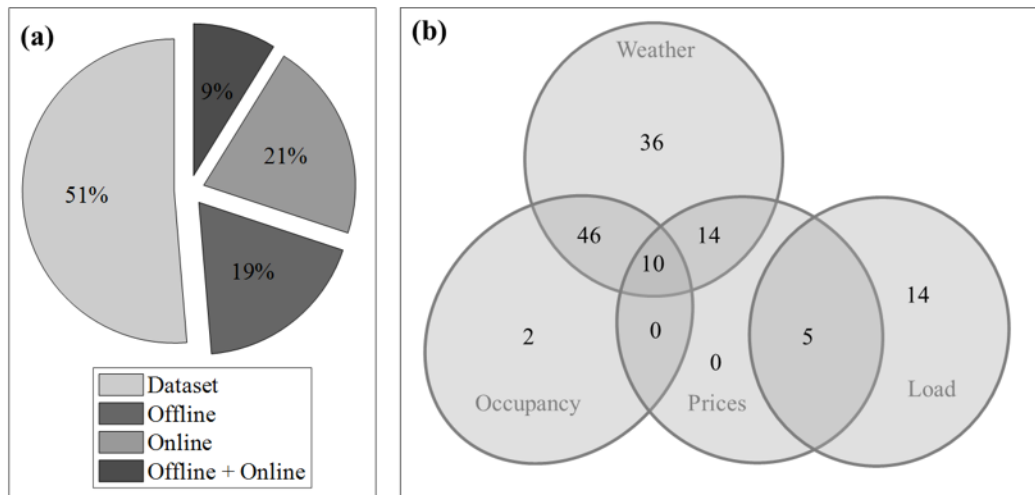
Figure 8. (a) Proportion of literature papers using as disturbances forecast method either online predictions, offline predictions or a combination of the two; (b) number of scientific papers grouped according to combination of forecasted disturbance variables.

A further prediction method often used in the literature combines the predictions of both offline and online methods. Indeed, combining the predictions of external models with data gathered on-site can be useful to calibrate external forecasts - reducing the uncertainty due to discrepancies between the location of weather stations and building site - and to address the risk of sudden internet service interruptions. Furthermore, a more straightforward online forecast can be used to adjust an offline prediction. For example in [101] minimum and maximum daily forecasted temperature were used to correct the trajectory of an offline prediction; or in [102] the Support Vector Machine method was used to forecast day-ahead electricity tariff prices based on past spot market prices and grid load levels.

Figure 8(a) shows the forecasting methods used by previous scientific works and *Figure 8*(b) summarises the scenarios concerning the type of disturbances subject to these predictions.

5.1.6 The controlled systems

The MPC framework is suitable for the management of buildings, regardless of their typology and classification (e.g., residential, educational, commercial, institutional). *Figure 9(a)* shows that theoretical and experimental studies available in the literature cover very heterogeneous building classifications and final uses.
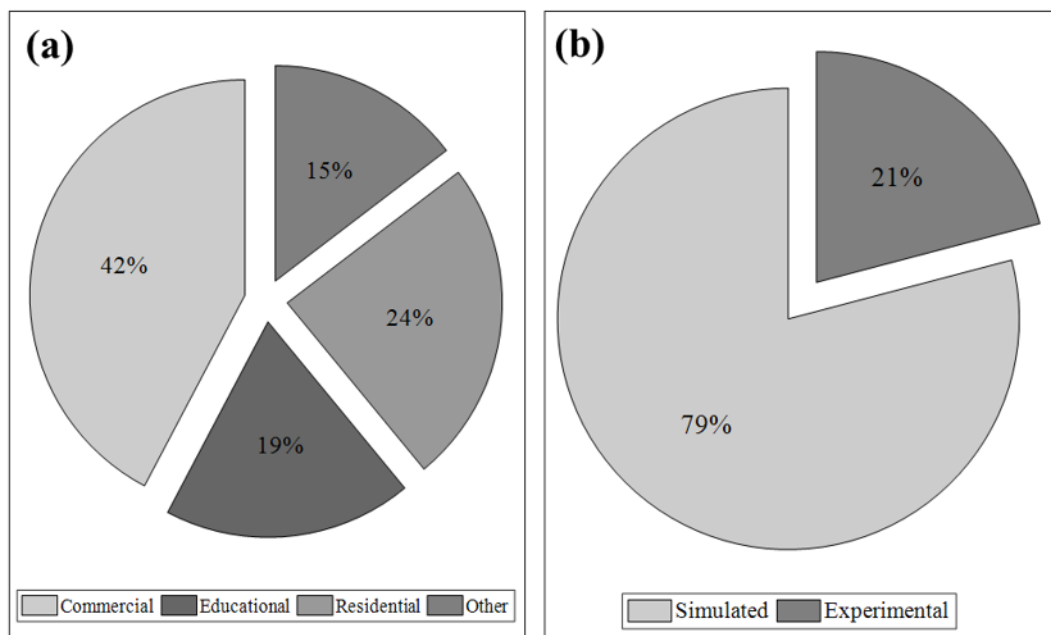
Figure 9. (a) Proportion of building typologies considered for MPC scientific literature studies; (b) proportion of simulated versus experimental cases of MPC for building and HVAC systems in the scientific literature.

The prototyping and testing of an MPC algorithm can be achieved by implementing the controller on an *experimental* case study or a *simulated surrogate*

building model. In any experimental case study, simulations (even if using simplified models) are still necessary during controller design to properly set up the controller parameters and ensure a reliable performance under different boundary conditions. Despite MPC is becoming one of the most promising algorithms for building energy management, o available in the literature there are only few experimental studies compared to the number studies in which the MPC was applied to a simulated surrogate building. The pie chart in *Figure 9(b)* highlights the unbalance between experimental and simulated works.

When the MPC algorithm is applied experimentally, an adequate Building Automation System and integration platform is necessary. Firstly, the correct sensors integrated into the Building Automation System are required to monitor the variables required for the model embedded in the MPC to estimate the response of the system, and that adequate control inputs are associated to the process components. The MPC algorithm, especially in a research study or testing phase, is not embedded in the local controller of the building, but a separate computer performs the online optimisation and exchanges information with the Building Automation System at each control time-step employing a communication protocol. The computation of the solution and therefore the communication can be either local (using a computer and a communication protocol such as Modbus, BacNet, Obix, etc…) or the optimisation can be done off-site, where there is a remote server and the exchange of information is done over the internet. A typical schematic of real experimental implementation of MPC is shown in *Figure 10***Errore. L'origine riferimento non è stata trovata.**.
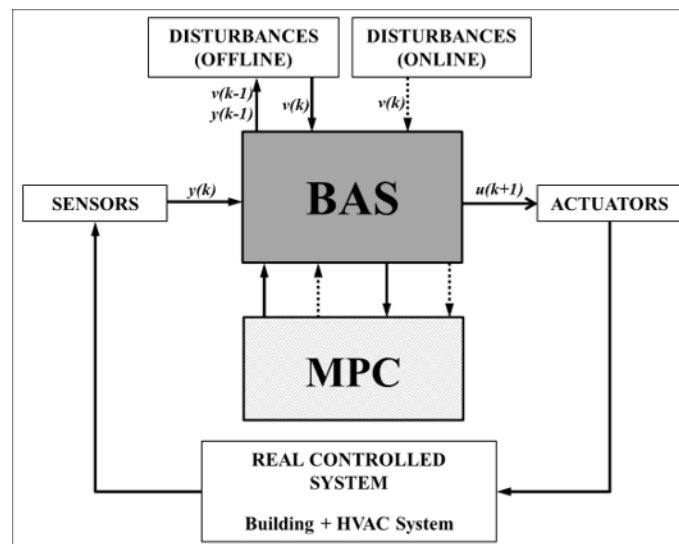
Figure 10. Schematic of MPC implementation in a real controlled system. Dashed lines represent possible connections by the internet.

In most of the cases available in the literature, surrogate simulated building models have been used to test MPC performance. On the one hand, when the building is ideal or monitoring data is not available, the surrogate simulated building model follows a forward approach. This one is the typical case of the theoretical studies on the MPC performances or the evaluation of MPC at building

design stage. In particular, for theoretical studies the building can be represented by an archetype that allows to carry out some performance indicators about MPC management of a category of buildings. On the other hand, when there is an existing case study building, where operative data can be gathered in the field, the surrogate simulated building model can be built using either a forward approach or a data-driven approach. This scenario occurs when it is necessary to investigate the possible benefits achievable through the MPC algorithm compared to an existing logic already implemented in the Building Automation System.

Surrogate simulated building models do not require a control oriented modelling approach and reducing the computational effort is not a primary issue. Indeed, it is only a surrogate of the real experimental application, thus the higher the surrogate simulated model reliability the better.

The most common issue when testing an MPC algorithm on a simulated building is that it is quite challenging to integrate an MPC controller into a building simulation software, leaving the MPC algorithm in most cases on a different external software platform. The two platforms must be interfaced at each control time-step with each other to evaluate the performance of the controller. In this interface, the surrogate building model sends information on the current states and disturbances to the controller, which computes the optimisation and responds with the set of actions that the surrogate building model has to apply at the next time-step. Sometimes, when a detailed simulated surrogate building model is not available, simulation studies can be performed utilising the control oriented building model also as surrogate building model to test the closed-loop performance of the MPC controller and speed up the procedure.

This aspect can be achieved by utilising software that already embed an external interface (e.g., TRNSYS - Type 155) or using packages that have been developed for time-step coupling of two platforms, such as Building Controls Virtual Test Bed (BCVTB) or MLE+ for Matlab/Simulink interfacing with EnergyPlus.

5.1.6.1 Building Automation System and Model Predictive Control architecture

The control inputs calculated by the MPC, which coincides with the outputs that the controller uses to actuate the system, are used to affect the system to reach the control goals. The output of an MPC algorithm is the optimal control sequence for each control input over the controlling horizon, and at each time-step only the first element of this array is applied. The physical actuation of the control inputs is generally achieved using actuators at different levels, which can regulate the heating and cooling delivery, the fans or pumps speeds, or the dampers, valves and windows positions.

The MPC problem can be formulated contemplating different levels of controller outputs. In the configuration presented in *Figure 11(b)*, the MPC controls the actuators directly, while in the configuration presented in *Figure 11(a)*, which is a hierarchical controller, the MPC provides the trajectories that lower level

controllers have to follow. The upper supervisory controller can also be called Real-Time Optimisation layer [38]. The lower layer controllers can be either Tracking MPCs or classical controllers (e.g., RBC, PID, etc...). Generally, in the case where the MPC problem is formulated without considering the HVAC system, see *Figure 6(b)*, the scope of the MPC algorithm is to define the trajectory of the internal set-points, and how to track them is demanded to various lower level controllers. When all the controllers of the lower layer are MPC the configuration is defined as *hierarchical MPC*. Hierarchical MPC is composed at least by an upper MPC layer with a more extended control time-step and horizon that decides the operation of the building processes also addressing complex optimisation goals. The output of this upper layer enters in a number of lower layer MPC controllers, that have a shorter control time-step and prediction horizon, and are designed to track the set-point trajectories defined by the upper control layer. Another similar architecture is represented by the *cascade* MPC, which presents various layers that run optimisations at the same frequency, without a higher level controller that acts as a supervisor. Those distinctions are quite formal and strongly affected by the problem formulation, thus in many cases the difference between cascade and hierarchical is not significant and many papers do not discriminate between the two. In the cases where the MPC also model the HVAC system it controls the set-points of the supply and return temperatures, the system air or water flow rates, amount of fresh air intake, heating and cooling generation systems activation or scheduling, evaporator and condenser loop pressures and refrigerant temperatures, etc. Finally, the MPC optimisation can define higher level decisions. For instance, the building and its HVAC system can be set into a specific operating mode (e.g., thermal storage charging or discharging modes, natural or mechanical ventilation modes [59,61]). These are typical applications of Hybrid MPC [92,101,103–105].
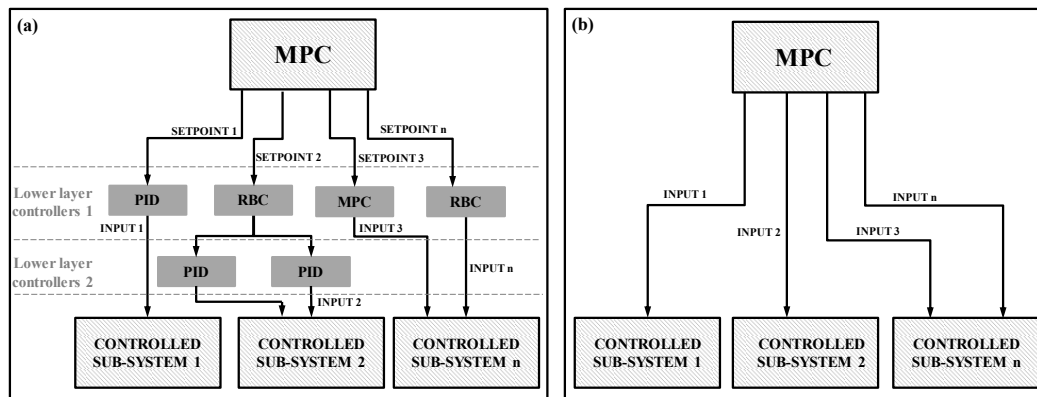
Figure 11. (a) MPC used as supervisory hierarchical controller; (b) MPC used directly for actuation.

A further classification of MPC architectures must be discussed. *Figure 12* shows the three possible configurations of the MPC architecture and their interface to the building. The *centralised MPC* configuration, shown in *Figure 12*(a), is a solution for the management of an entire building and its HVAC system, using a single MPC law. The building and its systems dynamics, their interaction and the

disturbances by which they are affected are considered in a single optimisation problem, which takes into consideration their constraints and mutual influences. While this configuration allows explicit modelling of the system dynamics, the computational effort can grow quite significantly with the system and process complexity. Moreover, a failure of the central MPC controller could cause severe issues with the entire building energy management, making it harder to isolate the problem. In the *decentralised MPC* approach, shown in *Figure 12(b)*, each component is regulated by an independent controller that does not consider events occurring to other elements of the control chain/structure. The mutual interactions among factors are regarded as unknown external perturbations to the model using this approach; the stronger the correlations of performance between these components, the more the reliability of the controller can be affected. Thus, on one hand there is a risk of achieving a significantly suboptimal solution, on the other hand a computational effort is drastically reduced and a higher tolerance to local failures when compared to a centralised solution is obtained. The *distributed MPC* approach, shown in *Figure 12*(c), has been considered an attractive solution for large-scale dynamically coupled building systems by many researchers [91,106–112], because it incorporates positive features of both centralised and decentralised configurations, merged in a single controller. This cooperative behaviour of every individual controller improves the global control performance when compared to decentralised structure. At the same time, the computational effort is significantly reduced when compared to the centralised control method, due to the possibility of sharing the computational workload between controllers. A very good comparison between the performance of centralised, decentralised and distributed in building energy management MPC configurations is presented in [91,107]. In [109] a comparison between centralised and decentralised MPC performances is provided and a compromise solution with a decentralised approach that clusters together some thermal zones to achieve a balanced trade-off between performance and robustness to faults is discussed.
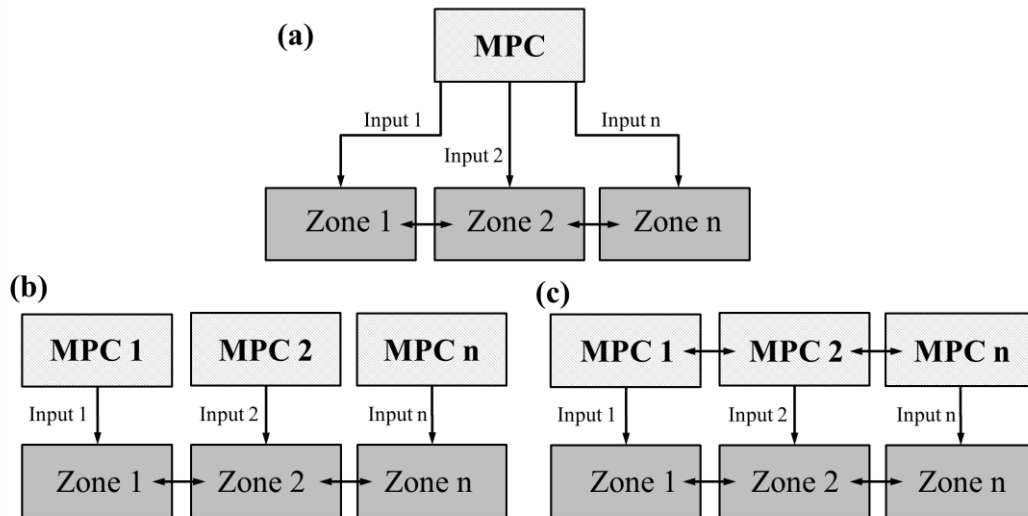
Figure 12. (a) Centralised MPC formulation; (b) decentralised MPC formulation; (c) distributed MPC formulation.

5.1.7 Definition of the receding finite horizon problem for building applications

The control horizon must be smaller or equal to the prediction horizon. Typically, the added value of having many free control moves is limited, as the accuracy of the prediction model decreases with the prediction horizon. In many research works there is no clear distinction between the two horizons, and possibly assume that they were set to equal length.
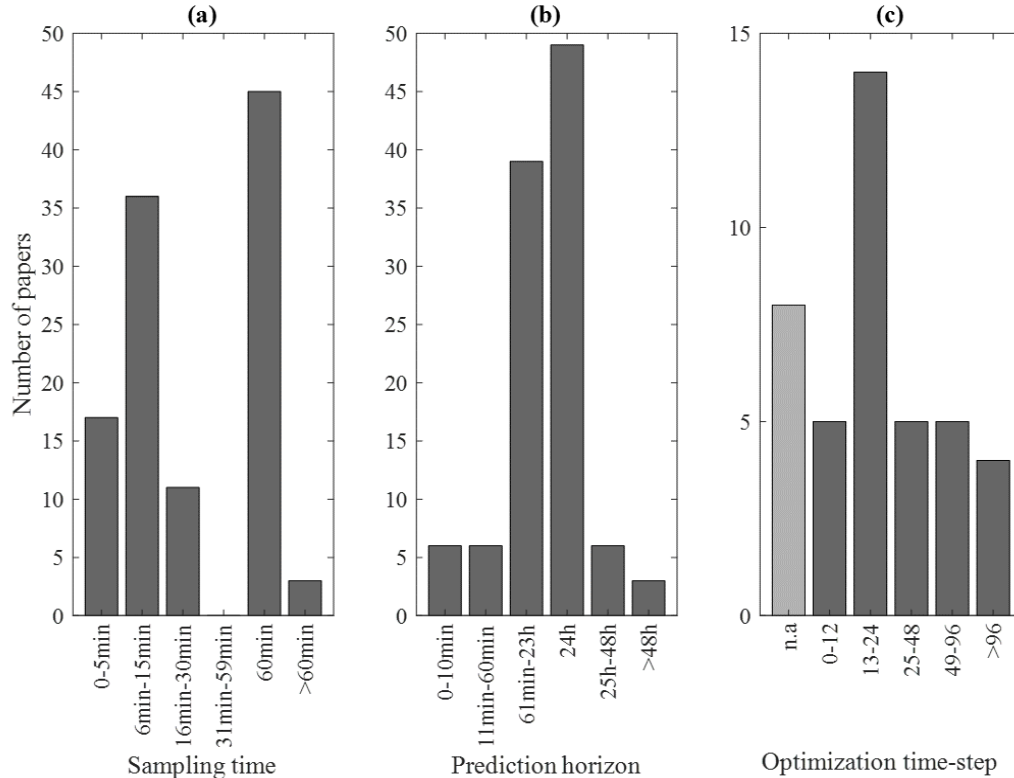
Figure 13. Frequency distributions emerging from the survey of the scientific literature of MPC problems for building and HVAC system regulation: (a) sampling times; (b) prediction horizons;(c) ratio of prediction horizon on sampling time (number of optimisation steps).

The selection of time-step, control horizon and prediction horizon is influenced by the time constants and the dynamical behaviour of the controlled processes. Heat and mass transfer processes in buildings are prolonged, thus the control time-step can be relatively widened when compared to other industrial processes. Typically, because of HVAC systems have faster dynamic responses, they require smaller control time-steps (from a few seconds to a few minutes) compared to when the MPC only manages the building' dynamics (from a minute to an hour). The authors of [113] believe that MPC algorithms should require shorter control time-steps and prediction horizons if they are managing cooling processes when compared to heating ones, due to factors with a faster profile that influence the process response. If on the one hand short horizons reduce the computational effort of the controller,

on the other hand they can affect its reliability by neglecting the effect of a portion of the dynamics of the system. If the horizons are set too long compared to the control time-step, this could lead to much higher computational times, without a significant improvement in the controller performance.

Moreover, because the optimal solution is based on disturbances forecast with inherent uncertainty, an excessive length of the horizons can affect the reliability of the forecasts and therefore the optimality of the solution found. Referring to the applications reviewed in this section, *Figure 13* shows the frequency distribution of: *Figure 13*(a) sampling times, *Figure 13*(b) the prediction horizons and *Figure 13*(c) the ratio of prediction horizon on sampling time (number of optimisation steps). From the distribution of *Figure 13*(c) can be inferred how small time-steps also require short horizons, so that the number of optimisation steps remains of the same order of magnitude and consequently the computational effort to solve the optimisation problem.

5.1.8 Typical constraints used in Model Predictive Control formulations for building energy management

One of the main advantages of utilizing MPC to control building systems is the possibility to include physical constraints into the formulation of the control problem, embedding them in the optimisation algorithm. *Table 1* summarises the possible constraints features.

Constraints can be formulated both as *equalities* or *inequalities*, according to how they relate to their counterpart of the real system. When the problem constraints are rigid and it is mandatory that they are satisfied, they are defined as *hard constraints*, while they are defined as *soft constraints* if they represent a flexible boundary and it is not strictly required that they are satisfied. Generally, soft constraints are formulated using a slack variable that can move the boundary of a certain amount, with an associated penalty in the cost function. The higher is the cost associated to this slack variable, and the closer the solution of the problem will be to the one where the constraints are considered to be hard. From a time perspective, constraints can be either *constant* or *time varying* limits that change according to a schedule, the occurrence of events or variations of the problem boundary conditions.

Table 1. Constraints features in an MPC formulation.

Formulation	Position	Restriction	Time variation	Kind
Equality	System states	Hard	Constant	Rate
Inequality	Actuators	Soft	Time varying	Range

Constraints can be allocated to *system states* and *system inputs*. Constraints on systems states are generally used to handle the occupants' comfort (e.g., maximum or minimum bounds for the indoor temperature [114]), or the allowable temperature range affecting an active building component (e.g., thermal energy storage unit operating range [115]). The constraints allocated to system inputs refer to physical limitations or imposed bounds on the system *actuation components*, or *input variables*. The actuation components' constraints can include maximum and minimum limits both for the *range* (e.g., minimum or maximum power of a heat pump[116] or a terminal unit [107], valve/damper position limits [117]) and for the *rate of change* of their operation (e.g., boiler or heat pump response rate[116], valve/damper/pump/fan change rate [118]). Likewise, the input variables can be constrained on their range and rate of change and they represent imposed or feasible limits (e.g., the maximum or minimum supply/return temperature [118]or the flow rate limits [48,86]). Because of their physical meaning, constraints on actuators are generally formulated as hard constraint, while the constraints on the system states can be softened in some cases [116,119]. For example, softening a constraint on an indoor temperature operation range, represents an undesirable situation that might be considered acceptable and advantageous under specific circumstances. Moreover, state constraints are typically imposed as soft constraints to preserve the feasibility of the optimisation problem, i.e., to make sure that a solution exists.

Additional terms that effect how the controller states behave at the end of the prediction horizon are the *terminal constraint* and the *terminal weight*. The terminal constraint imposes the desired state configuration to be attained at the end of the prediction horizon, while the terminal weight acts as an incentive (but not a necessary condition to satisfy) to the same goal. Both are often used to guarantee closed-loop stability. For example, a terminal constraint can be used to ensure that a thermal energy storage unit continuously stores a minimum level of energy to satisfy the demand of the following day [94].

5.1.9 Control goals and objective functions used in Model Predictive Control problem for building thermal management

The construction of the optimisation function depends on the global objectives that it is desired to achieve in the controlled process. One of the primary goals is ensuring that the controller meets the constraints and operates reliably. The stability of the controller and minimization of the control effort (variation of control inputs in two subsequent time instants) are two typical objectives of the optimisation. Other key objectives could be defined by the preferences the building occupants, the requirement of stakeholders or energy managers. In the first case these requirements are mostly related to *comfort factors* (e.g., target tracking for indoor temperature regulation, maintaining the internal ambient temperature in bounds ensuring the thermal comfort, minimizing occupants' thermal discomfort hours),

whether in the latter the drivers are mostly *economic factors* (e.g., reduction of overall energy demand or greenhouse gas emissions, minimisation of the operational costs, maximisation of renewable energy sources productivity). *Other factors* commonly considered in the objective function are the constrained on-line system operations optimisation or the peak load shifting or shaving. The cost function has to be chosen based on the requirements of the specific application.

The MPC cost function aims at reducing a multi-objective problem into a scalar objective. This is achieved by weighting and adding the various terms of the cost function, where each of these terms represent a specific performance criterion. Properly defining the weights of this objective function is one of the key tasks of the controller designer, because they represent the trade-off between the different control goals. The following expression represents a general formulation of an objective function for an MPC controller [31]:

$$
\min. \sum_{k=1}^{N_p} \left[W_x \| x(k) - x(k)_{ref} \|_{n_x} + W_y \| y(k) - y(k)_{ref} \|_{n_y} \right]
$$

$$
+ \sum_{k=0}^{N_{p-1}} \left[W_u \| u(k) - u(k)_{ref} \|_{n_u} \right. \tag{6.2}
$$

$$
\left. + W_{\Delta u} \| u(k) - u(k-1) \|_{n_{\Delta u}} \right]
$$

Where x is the vector of system states, y is the vector of outputs, and u is the vector of manipulated variables or control inputs. Typically, only x or y is employed in the cost function, the first one when the control oriented building model is formulated as *state-feedback*, while the second one in *output-feedback* formulations. The discrete index k denotes time steps along the prediction horizon. The term *u(k) – u(k-1)* indicates inputs increment over the prediction horizon and is an indication of the control effort. The subscripts *ref* were adopted to indicate the *reference* trajectories or set-points. W_x, W_y, W_u, and $W_{\Delta u}$ are the weight matrices, which can vary along the prediction horizon. N_p is the prediction horizon. If the prediction horizon N_p is larger than the control horizon N_c, then the control inputs following N_c are assumed constant. The terms n indicate the norm dimensions in the cost function. When the 2-norm is used each vector multiplying a weighting matrix is transposed and multiplied a second time (for example, we define $x^T W_x x$ for the costs associated to the states*)*. The solution of the minimisation of the objective function under constraints yields an optimal control sequence u^*. This is a trajectory of the optimal control moves along the prediction horizon that optimises the problem requirements according to the cost function weights and subject to the constraints defined by the user. Only the first control input $u^*(0)$ is applied to the controlled building. Afterwards, the receding horizon moves one control time-step ahead and the optimisation procedure is repeated. Alternative formulations of the objective function are possible according to the problem peculiarities (e.g., the most common alternative in building applications is the hybrid MPC formulation).

One of the most common objectives of the optimisation is ensuring the thermal comfort requirements of building occupants, by scheduling or regulating the set points of the HVAC system or other equipment. When formulating an MPC algorithm, the occupant comfort is generally considered as a pre-determined *set-point* or *set-point trajectory* to track or as *thermal bounds*. This is the simplest way to ensure a positive thermal sensation of the occupants. This formulation avoids adding computational effort to the optimisation problem due to non-linearities. Moreover, it allows a simple implantation of a sensor feedback to the controller in experimental applications. The set-point trajectory can be constant in time (e.g., indoor ambient temperature equal to a pre-defined set point [120]) or time varying (e.g., using a set-point when the building is occupied and a set-back set-point for unoccupied periods [121–123]). The time varying formulation introduces the possibility to vary the target of the building based on occupants' feedback or adaptive thermal comfort theories [124] (e.g., adjusting the set-point according to the external temperature running mean [125]). This set-point can be included in the formulation of a tracking MPC problem, entering in the objective function as a state reference $x_{ref}(k)$ or a system output reference $y_{ref}(k)$. It is also possible to include multiple set-points as thermal bounds, which do not affect the problem linearity and allow the indoor temperature to oscillate in a range of admissible values (e.g., in [61] variable limits of admissible indoor temperature were used as bounds, while [126] introduced two comfort ranges, one can be violated from time-to-time and another one should not be violated at almost any cost). This can be either introduced as a hard constraint of the optimisation problem or as a soft constraint, where the violation of these limits is weighted in the cost function. In this case the slacking variable that allows the softening of the thermal bound constraint is weighted together with the other inputs in the matrix W_u with the reference equal to zero.

In order to better assess the occupants' comfort, detailed thermal sensation indices can be introduced in the MPC formulation. For example, the Predicted Mean Vote (PMV) is an index that represents the average human thermal sensation under certain conditions. Since Fanger introduced this index in the 70's [127], the Predicted Mean Vote is one of the most widely recognised indices to evaluate thermal comfort[128,129]. Even if it provides a more detailed indication of the human thermal sensation than set-points or thermal bounds, the introduction of Predicted Mean Vote in an MPC problem has significant drawbacks [130,131]. Firstly, since Predicted Mean Vote is intrinsically nonlinear, it affects the formulation of the MPC by dramatically increasing the computational effort of the optimisation. In general, it is introduced as a further non-linear function in the MPC objective function. This formulation therefore requires the adoption of non-linear optimisation methods (e.g., Genetic Algorithms or Particle Swarm Optimisation), that cannot guarantee that the optimisation will reach the optimal solution. Secondly, in real applications, Predicted Mean Vote poses issues in the possibility to monitor all the environmental and occupants' variables affecting its calculation. Several studies the possibilities of implementing the comfort indices evaluation into MPC formulations [71,78,132–136]. Some authors use a comparison between Predicted Mean Vote and Actual Mean Vote to merge information from occupants'

feedback and data from sensors [135,137] to improve the decision of their thermal comfort. Predicted Percentage of Dissatisfied (PPD) - an index which calculation is based on the Predicted Mean Vote value and that represents the predicted percentage of occupants would feel thermally uncomfortable – can be adopted as a comfort indicator as well and sometimes it is preferred for its easier user comprehensibility. However, since it is based on the Predicted Mean Vote value, the control of a building based on the Predicted Percentage of Dissatisfied value is affected by the same drawbacks as a Predicted Mean Vote control.

The weighting matrix W_u assigns a cost to the usage of the control inputs in comparison to references defined in the array $u_{ref}(k)$. Generally, the term W_u contains the cost of the actuation of each energy resource and it is utilized to minimize the factors affecting the building operational costs and energy consumption. In the economic MPC formulation it can be directly related to the energy prices of the different energy sources adopted in the process. A typical example is trying to minimise the energy consumption of an HVAC system. Since the model generally considers the thermal delivery to the building, it is necessary to convert this energy to the electrical demand of this equipment. This can be achieved either by including a constant or linear representation of the Coefficient of Performance (CoP) of the studied unit in the control oriented model or in the linear cost function [61,89,103]. In other cases, where the Coefficient of Performance is described by a more detailed non-linear function (e.g., non-linearly dependent on system states and disturbances), it can be included in the optimisation problem with a non-linear cost function, similarly to the case of the Predicted Mean Vote [138,139]. This is a typical example of finding the best trade-off between a more accurate representation of the real system and the computational performance of the MPC problem. The weighting matrix $W_{\Delta u}$ assigns instead a cost to the derivative of the control inputs and therefore their rate of change, ensuring the stability of the system and avoiding excessive fluctuations that can damage the actuators.

The objective function can be expressed in the following forms:

- *Quadratic*, also referred as "norm 2" (*n = 2*). Quadratic cost functions are more common in tracking MPC problems, where the distance from a reference trajectory (e.g., the internal set-point temperature [120,140]) has to be minimised and the fact that the penalty function is quadratic helps with stability and reduced computational effort of the controller (e.g., the on/off switching of the HVAC system and its components [34,103,108,109,126,132,141,142]) ;
- *Linear*, also referred as "norm 1" (*n = 1*). Linear cost functions are the most common in building energy management in problems where the costs allocated to the elements of the weighting matrices must be comparable with each other, for example when trying to minimise building operating cost or maximise RES exploitation in an economic MPC;
- *Min/Max*, also referred as "norm infinite" (*n = ∞*). This configuration is the less frequent for building and its HVAC system control purposes. It is mainly

used when the control goals focus on the peak values [111,143–149], such as reducing or shifting the power peak load or minimizing the maximum daily Predicted Percentage of Dissatisfied value [69].

•
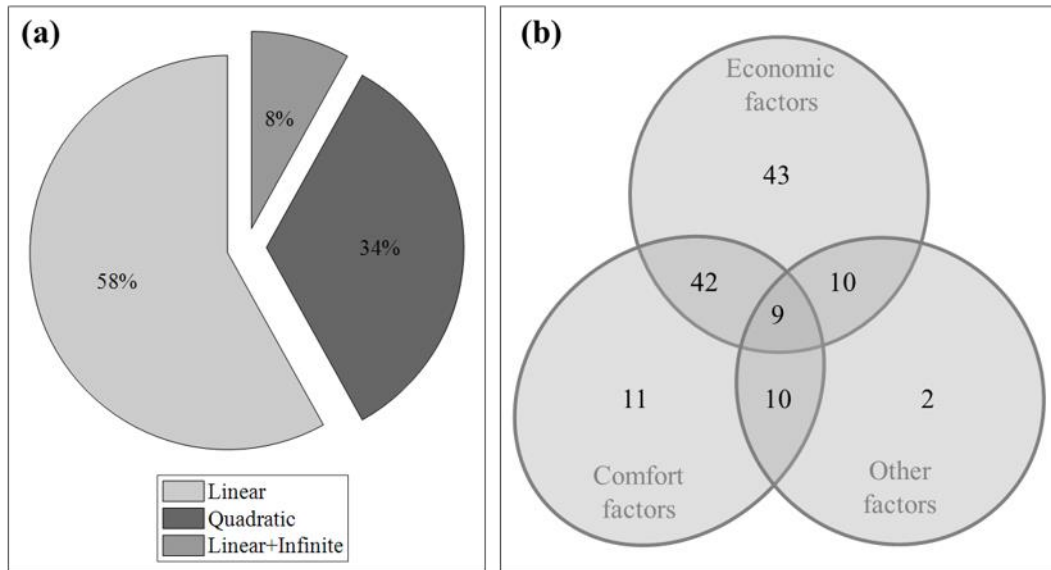
Figure 14. (a) Proportion of different MPC objective function formulation in the scientific literature; (b) number of scientific papers grouped according to different combination of goals considered in the MPC objective function.

5.1.10 Algorithms and programming languages

The optimisation problems that the MPC has to solve highly depend on the nature of the controlled system and the objective cost function defined to assess the control goals. The simplest formulation of an MPC controller is the one applied to a Linear Time-Invariant system. The nature of heat and mass transfer phenomena affecting buildings is intrinsically non-linear [150], however those processes can be treated as a Linear Time-Invariant system, under proper assumptions and simplifications in the control oriented model (e.g., R-C networks with fixed material features and linearised radiative heat transfer coefficient). The constrained problem that includes these Linear Time-Invariant systems to be optimised, generally leads to a Linear Programming (LP) or a Quadratic Programming (QP) optimisation problem, depending on if a linear or quadratic cost function was chosen.

Thermo-dynamical processes in buildings are generally characterised by long response times, and therefore stability is not a primary concern, allowing all the three forms of cost function to be commonly utilised in the optimisation problems [5].

Figure 14(a) shows the fraction of different objective function formulations in MPC applied to building and HVAC system management found in the literature

survey; while *Figure 14*(b) clusters the possible factors considered as optimisation goals.

Systems that contain discrete variables, such as Boolean variables (e.g., heater on/off) or defined operating modes (e.g., natural/mechanical ventilation mode or charging/discharging of a battery [59,61]), or scheduling problems (e.g., heating system operation time[151]), generally have a hybrid nature (formulated as Mixed Logical Dynamical (MLD) or Piecewise Affine (PWA) systems), and they lead to a Mixed Integer Programming (MIP) optimisation problem, as shown in *Figure 15*. Also in this case, depending on the cost function, the problem can take the form of a Mixed Integer Linear Programming (MILP) or Mixed Integer Quadratic Programming (MIQP) problem, which are generally solved using a Linear Programming - or Quadratic Programming -based branch-and-bound algorithm. The problem complexity grows significantly with the number of discrete variables included in the optimisation problem.
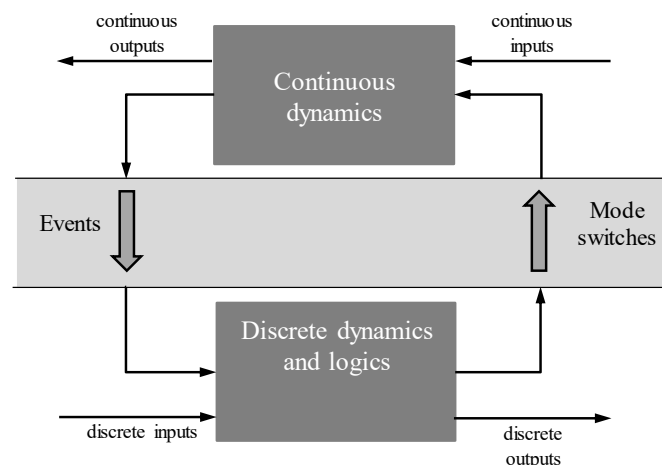
Figure 15. Logic-based discrete dynamics and continuous dynamics interacting through events and mode switches.

Another typology of non-linear system, commonly found when developing models for MPC applied to building HVAC systems, is the bilinear system. This typically occurs when modelling Variable Air Volume boxes. In this case, either non-linear optimisers or Sequential Linear Programmers (SLP) or Sequential Quadratic Programmers (SQP) can be employed to solve the problem. These approaches solve the problem by iteratively linearizing around the state trajectory computed in the previous iteration until convergence is achieved.

When the problem to be solved has a non-linear nature and a mathematical solution is not possible (e.g., the only way to find the response of the system to variable inputs is to entirely simulate the response of the model iteratively), a near optimal solution can be found. This solution can be reached using optimisation algorithms that can at least reduce the number iteration when compared to a "brute force" method, where all the possible combinations of inputs have to be iteratively simulated. This case is typical when black-box or white-box models are employed to model the response of the system. Furthermore, non-linear optimisation methods

are also required when the objective function handles non-linear terms, such as the Predicted Mean Vote calculation or a non-linear Coefficient of Performance formulation. To this purpose, the commonly used optimisation methods are Genetic Algorithms and Particle Swarm Optimisation (PSO), which can reduce the number of iterations necessary to find a near-optimal solution. Due to the iterative nature of these optimisation methods, the computational effort required to simulate the model becomes very significant, making the use of white box models not viable in most cases.

A framework of the frequency distribution of the optimisation methods used in the various MPC problems available in the scientific literature is highlighted in *Figure 16*.
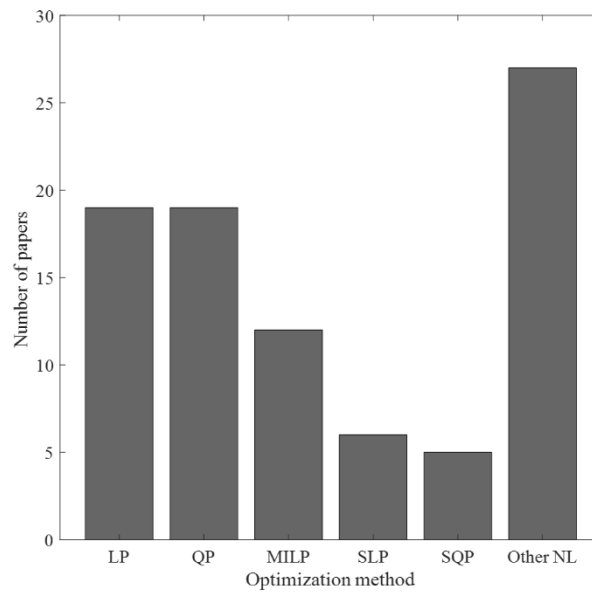
Figure 16. Frequency distribution of the optimisation methods used in the various MPC problems available in the scientific literature.

The most commonly utilised platforms for the implementation of an MPC algorithm are Matlab, for which a number of toolboxes have been developed to make the development of an MPC controller more manageable (e.g., Matlab MPC Toolbox, MPT Toolbox, Hybrid Toolbox, Yalmip), Scilab (open-source software similar to Matlab), Python and C++. To solve the optimisation problem many open-source solvers are available (e.g., GLPK), as well as faster commercial solvers (e.g., CPLEX, Gurobi).

5.1.11 Critical discussion

This survey has so far aimed at providing a clear framework and a complete overview of the applications of MPC algorithms to regulate buildings and their HVAC systems. However, some questions still remain open at this point of the

discussion. *How is it possible to evaluate the performance of a building predictive controller? What are the actual benefits of its application? What are the drawbacks? Is it possible to define general guidelines to drive the penetration of MPC control strategies in buildings? What is the current utilisation of such algorithms?* To answer those not easy questions a holistic approach should be adopted. Some answers can be found exploring and discussing the trends emerging from the survey undertaken. Some of the studies that were not directly cited in the text of the aforementioned survey [152–197], were still considered in the general statistics presented in the figures and in the discussion of this section.

A controller performance is generally evaluated considering its robustness to disturbances, its response time and stability, the suitability of its computational time for the building system dynamics, and the capability to guarantee the achievement of the control goals. In the papers analysed in this survey, the MPC formulation demonstrated a higher performance in each of those aspects when compared to classical building controllers.

The MPC formulation allows the controller to perform an on-line multi objective optimisation, finding an optimal trade-off between contrasting objectives. However, quantitatively evaluation of such benefit is not a simple task. Indeed, a comparable benchmark is necessary for this purpose and this is not always readily available. When the MPC is retrofitted to an existing building, the building baseline performance before the MPC implementation could be used as a reference [198]. Nevertheless, if the study is completely based on theoretical simulations, the baseline controller that defines this reference performance has to be arbitrarily set by the authors of the paper. Furthermore, in experimental implementations, different boundary conditions normally occur in different tests – in terms of weather conditions, occupancy patterns, etc. - and therefore it is not simple to compare consistently the performance of controllers that were acting on the same building at different times.

In building thermal energy management problems, the computational time is not a primary issue contrarily to other industrial processes. Indeed, well formulated MPC problems require from a few seconds (e.g., simple Quadratic Programming problems) to a few minutes (e.g., complex Mixed Integer Linear Programming or non-linear MPC formulations). Those intervals are perfectly compatible with building and HVAC system dynamics, since they generally have a large time constant (from several minutes to hours). To the best of the author's knowledge, the computational time was an issue for a successful MPC implementation only where the control problem was not properly formulated. For instance, when detailed simulation tools were used as control oriented model for the MPC.

As it is possible to infer from *Figure 14*(b) the most common goal included in the objective function of the MPCs surveyed is the reduction of the building energy consumption or operative costs. *Figure 17*(a) shows the average percentage of energy reduction related to an MPC implementation in the surveyed papers. These results are similar to the qualitative analysis of expected potential energy reduction outlined in 2010 by Oldewurtel et al. [65] and reported in *Figure 17*(b). In almost all these studies the MPC algorithm outperforms the baseline controller also in

terms of satisfaction of the comfort requirements [154]. Since in these studies different long term comfort indicators were used [150], a detailed comparison of the results was not achievable. Furthermore, MPC controllers also led to dramatic reductions of peak loads when they were considered part of the control goals (generally around 30 %) either with an explicit formulation in the objective function or with an indirect variable energy prices policies. Peak load reduction is particularly significant when the MPC was managing either an active or passive thermal storage (e.g., managing the charge/discharge of thermal energy storage unit or pre-heating/cooling of thermal activated building structures). This represents a strong opportunity for peak load shifting, demand side management and reduction of the overall energy costs.
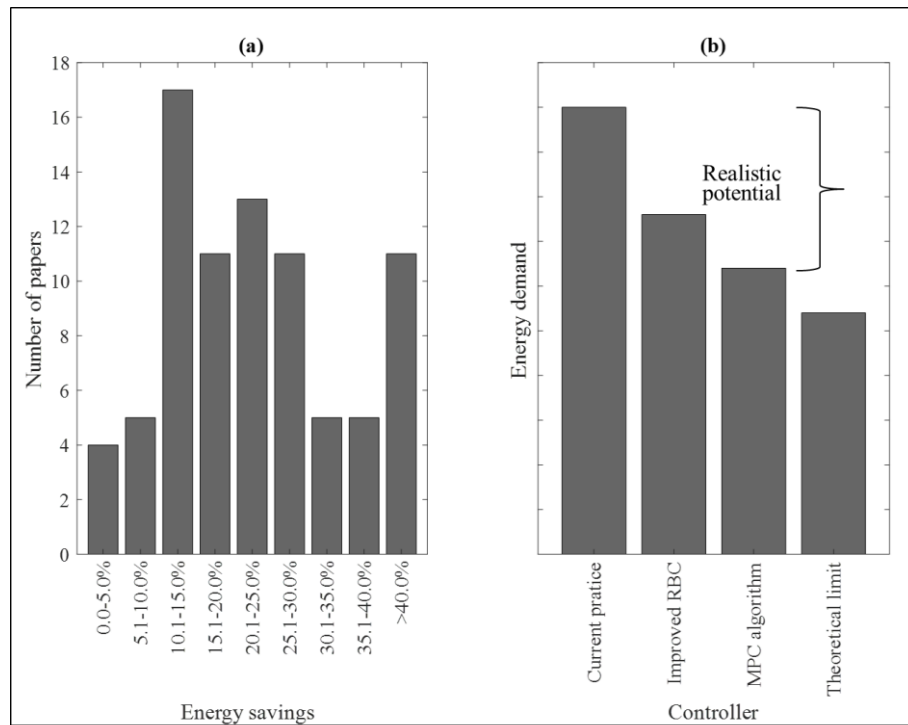
Figure 17. (a) Frequency distribution of the papers about the extent of energy saving consequent to the implementation of MPC algorithms; (b) estimation of energy saving potential exploitable by means of the implementation of MPC algorithms for building energy management

.

A further advantage of MPC is given by its ease of reconfiguration and adaptability to changes in the controlled system. For example, in building and HVAC system applications the objective function may include terms describing the cost of energy. In this case, it is straightforward to update the weights to reflect fluctuations in the energy price, with no other changes to the controller. Also, due to malfunctions or wear and tear, an actuator may operate with a reduced range in some conditions or for some time. This can be very easily taken into account in the MPC problem, by simply updating the corresponding constraints, without having to redesign or recalibrate the controller. This aspect, which is also critical for

scalability of MPC technologies, is barely evaluable in terms of key performance indicators and was usually not considered in the literature papers.

It is possible to individuate three main critical aspects in the implementation of MPC algorithms in buildings, which can significantly affect its operative performance. Firstly, the accuracy of the models (e.g., the control oriented model, or the disturbances prediction model) strongly affects the performance of MPC optimisation and the potential benefits achievable in terms of control goals satisfaction. For this reason, great attention to all these aspects should be paid when formulating the MPC problem. Secondly, utilising an MPC algorithm in the supervisory control layer requires sufficient computational power and proper system calibration to ensure bumpless integration with existing low level controllers. The last and probably most significant issue is related to the existing great variety of building classifications and architectures. Indeed, every building is unique in terms of thermodynamic response – due to the different geometry, construction, end uses, occupancy patterns, weather location, etc. – and MPC algorithms must be customised to fit the specific building features. As an example, the control oriented building models cannot be easily standardised to represent the whole variety of buildings, introducing a significant challenge in the controller development.

Table 2. Categories used in the present survey to undertake statistical trend in MPC formulation for buildings and HVAC systems.

Model type	Model of	Study	Building classification	Forecast method
Reduced order	Building	Simulated	Commercial	Offline
Detailed simulation	Building + HVAC	Experimental	Educational	Online
Calibrated grey-box	HVAC system		Residential	Database
Black-box			Other	Offline + online

Horizons	Disturbances	Formulation	Goal	Optimisation
Control	Weather	Linear	Economic	LQ
Prediction	Occupancy	Quadratic	Comfort	QP
Sampling time	Prices	Infinite	Other	MILP
	Load	Combo	Combo	MIQP
	Combo			SLP
				SQP
				Other NL

Such singularities also cause difficulties in providing a pre-defined general step-by-step guideline for the development of a building MPC control strategy. Nevertheless, the statistics undertaken in the present survey allowed the main trends to be outlined. These trends are based on the classification proposed in *Table 2*. In certain cases, some information was not clearly outlined by the authors of the analysed papers. For this reason, *Table 2* can be viewed as a suggested guideline for the necessary information to be included in a study for a comprehensive description of an MPC algorithm implemented to control buildings and HVAC systems. Furthermore, authors should clearly indicate in the problem description the control sampling time, the prediction horizons and the control horizon.

Despite the growing diffusion of theoretical works, from *Figure 9*(b) it emerges that the number of real buildings actually implementing MPC strategies was relatively small. Up to date, the Illawarra Flame house [59–61] in Wollongong and 10 households in Brugg [114], the 3E Headquarters in Brussels [152] and a commercial Building in Allschwil [75,119], a building of the Czech Technical University in Prague [118,156], the University of California Merced Campus [48] and the Engineers Construction Engineering Research Laboratory in Champaign [155], and the airport of Adelaide [104,153,199] represent the most interesting examples of practical implementation of MPC algorithms in buildings. These applications cover all building classifications - residential, commercial, educational, and other respectively – and are located in various climatic locations.

In this context a last question remains open, related to potential future market penetration rate of MPC for building energy management. *Why do such promising algorithms, which proved to outperform traditional controllers, reach just a small fraction of real building applications?* The answer to this question needs to take into account that only ten years ago MPC was almost not considered as a potential building control method. Afterwards, dozens of theoretical studies and prototype implementations clearly demonstrated the high potential of this control methodology. Killian and Kozek [29] compared this situation for MPC in building control systems to the one in the early 90's of MPC in the process industry. In the early 90's only very few experts in the field knew how to set up and commission an MPC control system successfully in the industrial processes. However, after a massive adoption of these controllers in the last decades, MPC proved to be one of the most widespread, reliable and best performing methods in the processes industry [200].

Nowadays, the primary barrier to a more substantial MPC adoption in the building industry is the intrinsically tricky scalability of the technology, since every building is unique, significantly increasing the controller cost. In order to reach a larger adoption, MPC designers should find a solution to this drawback, otherwise well-tuned traditional controllers with lower performance but easily adjustable to different applications would remain the preferred choice [121,171]. For this purpose, tools that help with the design of the control oriented model should be introduced, in order to reduce the effort and the know-how required in the controller set up. Furthermore, building archetypes coupled with proper setting guidelines should be constructed to standardise the control oriented models partially.

This literature review showed that these algorithms lead to meaningful energy savings, which approximately are around 15-20 %. These values prove that MPC implementation represents an excellent opportunity to reduce buildings carbon footprint and achieve a substantial cost benefits. Furthermore, the established effectiveness whereby MPC algorithms deal with peak shifting and demand side management allow this technology to be considered as one of the most suitable for integration of buildings in smart grids. This fact represents a crucial perspective for the energy market, which continuously requires further flexible loads to mitigate the renewable energy source supply fluctuation.

From the theoretical perspective, it is crucial to investigate better how the occupant behaviour and the occupancy patterns affect the algorithm performance and how to best predict them. At the same time, it is important to study further the robust, stochastic or scenario-based formulations, which allow the uncertainty related to the forecast of disturbances in the optimisation problem to be considered. Important steps in this direction were already made in [34,35,67,90,110,148]. Besides, benchmarking strategies for experimental applications should be defined. Promising solutions for comparing experimental tests on the same building at different times were proposed in [114,152].

In conclusion, to accelerate the market penetration of MPC algorithms it is necessary to explicitly identify which are the most promising building classifications and stakeholders that can take advantage of its implementation. The papers of Hilliard et al. [26,201] provided an excellent overview on the building requirements that allow MPC algorithms to be really effective. The size of the building must be large enough to make an MPC algorithm a cost effective technological solution. In large buildings the capital investment to implement the MPC technology is relatively smaller when compared to the reduction in operating cost. The benefits are more marginal when the MPC is applied to smaller buildings. Moreover, possibilities of active and passive storage strategies, flexibility of the constraints and alternation between occupied and unoccupied periods were individuated as the essential requirements for a worthy building predictive control. The Building Automation System must be at a sufficient technological level to be able to integrate an MPC controller input and output signals. In general, modern commercial, institutional and educational buildings satisfy these requirements and therefore are the most likely candidates for a straightforward practical implementation of an MPC in their supervisory building control system.

It can be misleading to consider that existing manufacturers of building automation system components are the only stakeholders that can benefit from the deployment of an MPC controller. Large organisations can be fairly conservative in the adoption of disruptive control strategies, due to the risks associated with potential failures and the sunk costs related to their existing strategies. For this reason, the author believes that a higher adoption rate of MPC in buildings can be led by control system installers, capable of involving both Building Automation System manufacturers and stakeholders that would directly benefit from the MPC implementation. For example, building owners, energy managers or Energy Saving COmpanies could see in MPC a real possibility to maximise both occupants'

comfort and energy savings, reducing at the same time users' complains and energy bills. Energy providers could also see the potential of MPC as an opportunity to implement demand response strategies directly.

5.2 Model Predictive Control formulation for the regulation of the SolHe-PCM solar thermal system

When a novel technology is introduced, novel control paradigms have to be investigated. Indeed, to adequately control the system and efficiently exploit all its potentialities the existing control logic could be not sufficient. This fact is particularly true when disruptive solutions are proposed. For instance, shifting the thermal energy storage from sensible to latent solutions also influences the system regulation. Indeed, traditional controllers – based and tuned for sensible heat solutions – exploit information deriving from the measurements of process temperatures or incident solar radiation. In latent based solution, the temperature measurement can be misleading because neglecting the additional enthalpy exchanges occurring in the phase change process.

For these reasons, innovative PCM-based solar thermal systems and thermal energy storage units – likewise the SolHe-PCM prototype – need to be controlled in an innovative optimal way to be effective and to fully exploit their potential. In these cases, the classical control methods are not always able to obtain the maximum benefits from these technologies. The investigation of new control paradigms is therefore necessary. Additionally, when poly-generation energy supply systems integrate solar thermal or energy storage systems (e.g., renewable energy sources coupled with auxiliary heaters or boilers, combined heat and power systems, heat pumps, etc.), dynamic optimisation methods may be used to recursively define which is the most advantageous generation source to be selected [202].

The previous review and framework showed how in recent years MPC algorithms have been successfully implemented in various thermal and energy management strategies concerning buildings or building elements. Moreover, MPC has been effectively applied to active energy storages, as well as for the optimal management of on-site renewable energy sources. All these studies showed that the MPC could effectively contribute to the reduction of energy consumed by the HVAC system and the integration of buildings in more flexible energy grids. Nevertheless, the main drawback that has limited the widespread implementation of MPC controllers in building automation systems has been the bottleneck represented by the need of having a reliable mathematical model of the building at disposal [203]. However, in the SolHe-PCM case, a simplified mathematical model capable to accurately describe the physical behaviour of the prototype system was already developed (see Section 3.4). In this case, the main limitation for model-based predictive controllers can be effortlessly addressed. Furthermore, compared to an entire building model, the control oriented model for a solar thermal system and thermal energy storage units can consider almost similar even in very different contexts and applications. This fact led to a control system that can be easily scalable and which can adapt its behaviour in different backgrounds with minimum effort in the controller development phase.

On the other hand, using an MPC algorithm for smart control of a solar thermal system and thermal energy storage unit is not a trivial problem. Indeed, the use of MPC algorithms can arise some issues and proper assumptions are necessary for its effective formulation. In Refs. [61] and [60], air heater collectors were integrated into an MPC algorithm that regulated the building automation system of a single story house. In this case, the storage unit and the solar system had an open loop configuration. This implementation eliminated the mutual interactions between those elements, allowing a straightforward linearisation of the system. Halvgaard et al. [116] investigated the regulation of water-based thermal energy storage designed to couple the space heating system of an apartment and a solar thermal system, neglecting the mutual interaction between the panel and the storage unit. Zambrano et al. [204] stated that controlling a solar system and storage equipped with an absorption chiller to provide space cooling can be used as a benchmark problem for the implementation of hybrid MPC algorithms. Indeed, the hybrid nature of the controlled system that exploits multi-energy sources and has multiple operating modes introduces additional challenges, which required a mixed logical dynamical formulation. Menchinelli and Bemporad in Ref. [93] also faced a similar problem highlighting how for closed-loop solar thermal systems, the heat exchange processes involved are intrinsically non-linear; thus the optimization problem presents a particular challenge. Also in this case, the Mixed Logical Dynamical formulation of a hybrid MPC allowed the problem to be solved.

The MPC problem for solar thermal systems is complicated by the heat exchanges processes involved in the system that are intrinsically non-linear. Thus the optimisation problem presents a particular challenge. Moreover, the adoption of PCM in the controlled process introduces further non-linearities that have to be included in the model. These non-linearities are due to the change of phase and latent heat transfer process at nominal operating temperatures. The next Sections present the formulation of an MPC problem that deals with these challenges for the SolHe-PCM project. A particular focus was undertaken on the controlled system model, the forecasting models for the disturbances affecting the system, the generation system and building demand constraints, and the formulation of the objective function to be optimised. Simulations of the MPC behaviour in a closed loop test rig were performed with the aim of assessing the performance associated with the application of an optimal control strategy when compared to an existing baseline RBC. The baseline RBC was used for analysing key-performance indicators and for benchmarking the system performance in terms of demand satisfaction and electrical energy consumption. Results of the simulations showed that the predictive controller was able to anticipate future disturbances, and therefore optimises the utilisation of the more efficient energy sources.

In the present discussion, the MPC algorithm was not implemented in the real control system embedded in the SolHe-PCM prototype. The existing prototype controller is based on a National Instrument Compact Rio solution, and the MPC algorithm is programmed in Matlab-Simulink. The interconnection of these two programming environments on an embedded controller is a very tricky process that requires efforts beyond the primary goals of the present thesis.

5.2.1 SolHe-PCM configuration selected to test the Model Predictive Control performance

A configuration of the SolHe-PCM prototype must be selected to investigate the MPC features properly. Since the present study is simulation based, what influences the system behaviour is the selection of the numerical model used as a test rig. In detail, on the one side the second version of the collector model, which discretises the panel in ten segments of equal length, was chosen collector (see Section 3.4.1). On the other side, the thermal energy storage tank unit was simulated with a model that uses a thermo-energetic balance of a single lumped node (see Section 3.4.2).

In addition to the prototype configuration presented in Chapter 3.3, an additional auxiliary heat exchanger was added to the system with the scope to operate when renewable energy source generation is insufficient to meet the space heating demand. This assumption was necessary to bring back the prototype to a case study that is capable of simulating real technological solutions, where multi-source energy systems are generally coupled in the thermal energy storage unit. Indeed, non-renewable energy conversion systems are commonly used to integrate the energy delivery when the renewable production is not sufficient. Since the secondary heat exchanger that delivers heat to the building is 2 kW, the auxiliary heater was selected of a similar size. In detail, for these simulations, a 1.5 kW auxiliary electrical heater was chosen. In further simulations, the auxiliary electrical heater can be substituted by different auxiliary heat sources (e.g., a natural gas boiler, electric heat pump, combined heat and power systems, etc.). Therefore, the MPC formulation can be easily adapted to optimise different multi-energy system coupled with a thermal energy storage unit just taking into consideration the different energy conversion efficiencies that characterise the various energy generation systems. The solar thermal system prototype investigated in these simulations is shown in *Figure 18*.
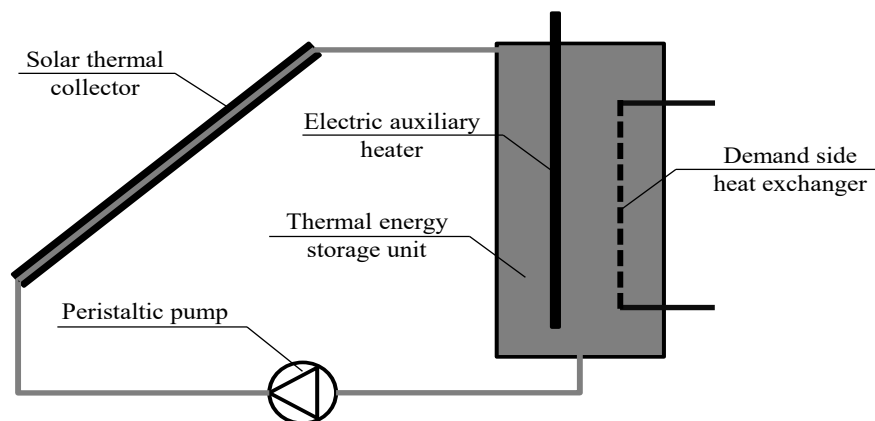
Figure 18. Schematic of solar thermal system prototype.

Eventually, it was already primarily discussed how the whole system performance is influenced by the mPCM concentration chosen for the PCM slurry used as heat transfer fluid and storage media. The system studied in the simulation

herewith presented used a constant concentration of 30 % w.t. of micro-capsules in the PCM slurry mixture. Knowledge of the specific enthalpy versus temperature curve of the PCM slurry at 30 % w.t concentration was necessary to determine the thermo-dynamical behaviour of the material. For this purpose, the results of the T-History experimental procedure outlined in Section 3.2.2 were used to define the specific enthalpy versus temperature curve of the PCM slurry.

5.2.2 Regulation strategies

5.2.2.1 Definition of the baseline Rule-Based Controller

The system controller regulates the pump flow-rate and the power delivered by the auxiliary heater. The existing baseline controller is based on an RBC regulation. In this case, the control of the pump and the electric heater are independent each other. The pump adopted in the full-scale prototype is a peristaltic pump that is capable of operating at four fixed operating flow-rates (0 l/h, 10 l/h, 60 l/h and 90 l/h) to maximise the exploitation of the solar source. The existing baseline controller uses an open-loop control logic, which selects the flow rate from the measurement of the beam solar radiation incident on the solar thermal collector. The pump is activated at the lowest speed (10 l/h) when the beam solar radiation is higher than 50 W/m^2, increased to 60 l/h when the radiation exceeds 225 W/m^2, and further increased to 90 l/h the radiation exceeds 500 W/m^2. These thresholds are listed in Table 1 together with the corresponding electrical energy consumption of the pump at each fixed PCM slurry flow-rate. For safety reasons, the maximum temperature that could be reached in the thermal energy storage unit was 60 °C. If this value was detected, the pump was automatically switched off. The auxiliary electric heater controller's goal was to maintain the thermal energy storage mean temperature as close as possible to a reference set-point temperature. The set-point chosen at the design stage was 35 °C, which is the average of the temperature range within which phase transition occurs.

Table 3. Pump flow-rates, baseline controller thresholds and related electric power consumptions.

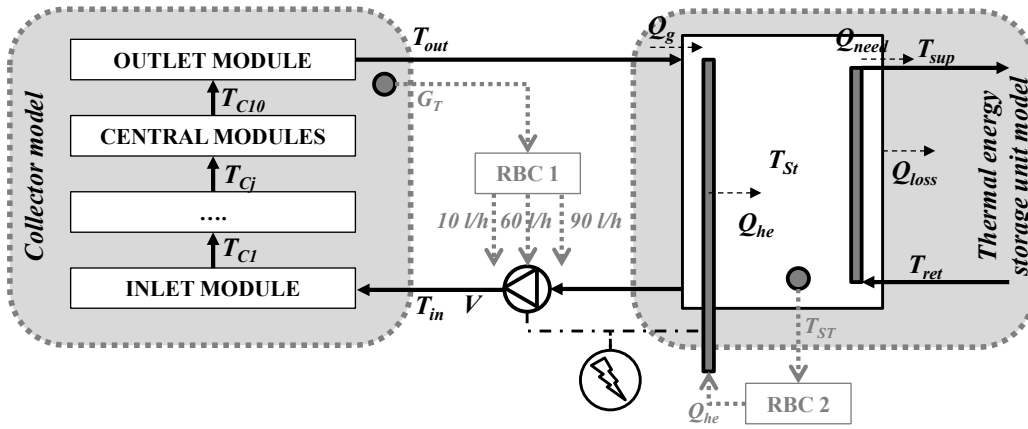| Flow-rate		Power
l/h	*m^3/s*	*W*
10	2.78·10^{-6}	5
60	1.67·10^{-5}	25
90	2.50·10^{-5}	55

Figure 19. Schematic of the solar thermal system with RBC implemented.

5.2.2.2 Model Predictive Control formulation

The dynamic response of the outputs of a system is affected by controlled inputs (or manipulated variables) and uncontrolled inputs (or disturbances). Such dynamics can be captured by a dynamical and simplified control-oriented model of the controlled system and exploited by the controller to make predictions of the possible future response of the system as a function of future controlled and uncontrolled inputs [30]. MPC uses these predictions to select the best sequence of future manipulated variables, according to a specific performance index. The latter is defined over a time window that starts from the current time and spans a given prediction horizon in the future. The best sequence is obtained by solving a numerical optimisation problem, that also takes into account the constraints on input and output variables one must satisfy during the operation of the controlled system. The difference between MPC and open-loop optimal control is that the former only applies the first optimal move of the sequence at the current time instant, optimising a new sequence at the following time-step again. This way of acting and replanning continuously over time is denoted as the "receding horizon" concept [205].

The MPC problem for the current study was formulated using a control time step of 1 hour. It is clear to the author that the control time-step can be reduced to smaller intervals (e.g., a quarter of hour or five minutes) to further improve the quality of the results. However, for the sake of conciseness, the present work has been limited to the hourly basis. In this way, it was possible to use directly the climatic data retrieved from IWEC datasets avoiding any interpolation. Furthermore, even if one-hour time step would be too long for a low-level controller, it can be sufficient for a supervisory controller regulating the set-points exploiting recursive optimisation, such as the MPC algorithms. The control and prediction horizons were assumed to be of the same length and were set equal to 24 hours. According to the classification proposed in *Table 2*, *Table 4* summarises the principal features of the MPC algorithm used to control the system.

It is well-known that prediction models are the cornerstone of MPC and, following the Camacho and Bordons indications [205], two different important

model categories can be discerned within the implementation of an MPC controller: the models required to forecast the external disturbances (external weather conditions and space heating demand, in this case) and the control-oriented model of the controlled system (the thermal management of the thermal energy storage unit, in this case). The models adopted in the close loop simulations are outlined in *Figure 20*.

Table 4. Summary of the peculiarities of the MPC algorithm used to regulate the operation of the SolHe-PCM solar thermal collector and thermal energy storage unit.

Model type	Model of	Study	Building classification	Forecast method
Reduced order	HVAC system	Simulated	Residential	Database

Prediction/ control horizon	Time step	Disturbances	Formulation	Goal	Optimisation
24 h / 24 h	1 h	Weather Load	Linear	Economic Comfort	MILP
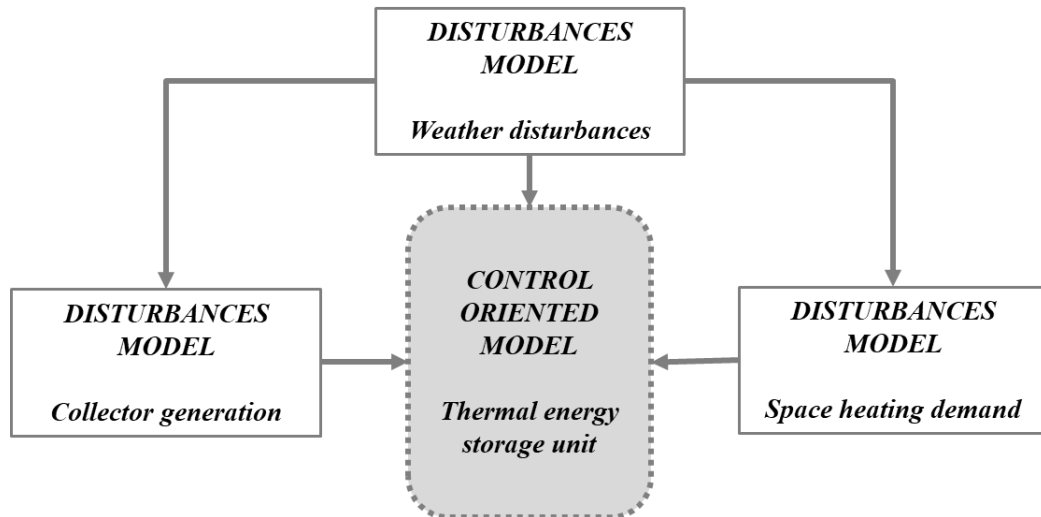
Figure 20. Schematic of the models necessary to formulate the MPC problem for the solar thermal system based on PCM slurry.

5.2.2.3 General assumptions for the problem linearisation

The schematics of the model with the implementation of MPC is presented in *Figure 21*. The MPC algorithm aimed at optimising the operation of the collector by controlling the PCM slurry flow-rate and the utilisation of the auxiliary heater. That is, by dynamically finding the optimal set of control inputs without the need for predefined set-points or schedules.

To ensure the linearity of the model, as required by the MPC optimisation, experimental data related to specific enthalpy versus temperature curve of the PCM slurry were approximated by three-segment piecewise-linear correlations (*Figure 22*). The first and the third segment represent the relation between temperature and specific enthalpy of the PCM slurry with the core material in its solid and liquid state. The central portion is representative of the melting/solidification phase of the material. The phase change occurred not at a specific temperature but within a temperature range (around 2 °C) bounded by a lower and a higher phase change temperature [206]. The results which provided the best match between the experimental data and the piecewise approximation are given in *Figure 22* and Table 5.
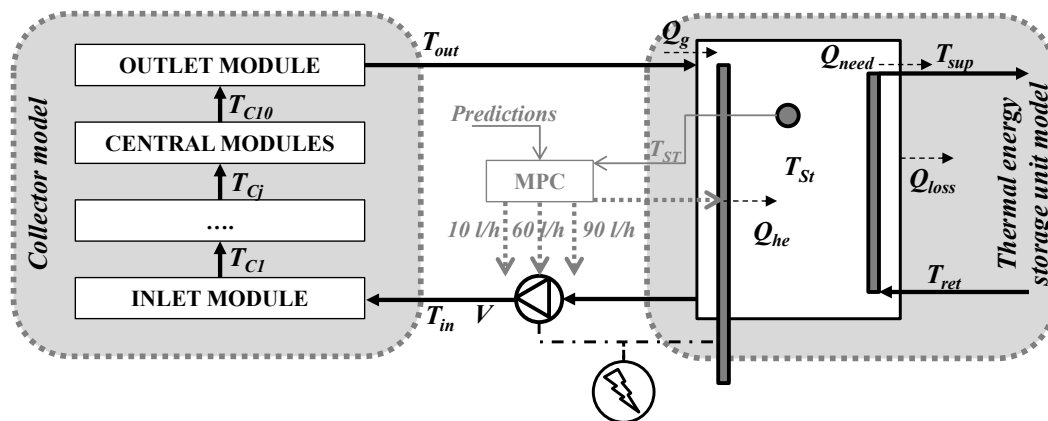
Figure 21. Schematic of the solar thermal system with the Model Predictive Controller implemented.

Table 5. The PCS thermo-dynamical characteristics.

$T_{inf,PCM}$	33.9	$^{\circ}$C	Lower phase change temperature of the PCM slurry
$T_{sup,PCM}$	36.1	$^{\circ}$C	Higher phase change temperature of the PCM slurry
$c_{p,PCM,li}$	5.47	kJkg$^{-1\circ}$C^{-1}	Specific heat capacity of the PCM slurry in solid phase
$c_{p,PCM,tr}$	26.10	kJkg$^{-1\circ}$C^{-1}	Dummy specific heat capacity of the PCM slurry during transition
$dh_{PCM,tr}$	57.42	kJkg^{-1}	Total phase change specific enthalpy of the PCM slurry

$c_{p,PCM,so}$	3.52	kJkg^{-1}°C^{-1}	Specific heat capacity of the PCM slurry in liquid phase

The material specific heat capacity as a function of temperature was derived from this piecewise approximation for numerical simulations. In the phase-change range a constant fictitious specific heat capacity (named: dummy specific heat capacity of the PCM slurry during the transition) was considered. The PCM slurry was a 30 % w.t. mixture of water and a micro-encapsulated PCM material characterised by a nominal specific heat capacity slightly lower than water (n-eicosane solid/liquid specific heat capacity: 1.92/2.46 kJkg^{-1}°C^{-1}). However, from Table 2 it is possible to notice that when the PCM slurry is in the solid phase, its specific heat capacity is slightly higher than that of water. This fact is due to a small amount of phase change transition, caused by rotator–crystal transition occurring in the interval below 30 °C [207].
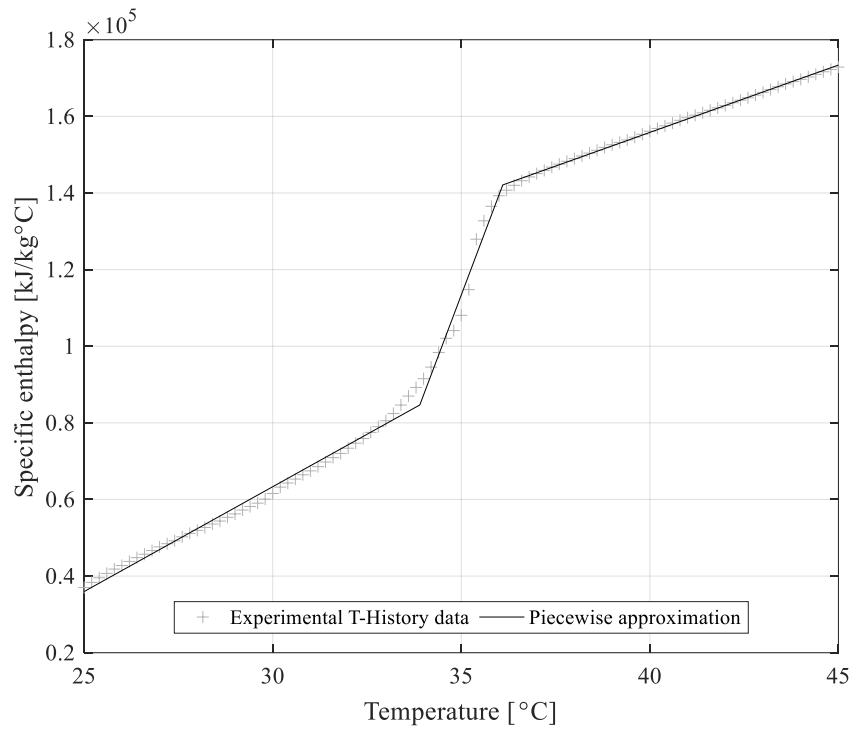
Figure 22. Three-segment piecewise approximation of specific enthalpy versus temperature curve carried out by means of the T-History method.

It is well known that the control-oriented model of the controlled system has to be accurate enough to ensure satisfactory prediction capabilities and capture the fundamental thermal dynamics of the processes influencing the controlled system, whilst at the same time be simple enough to ensure a reasonable computational time for optimisation [53]. In order to ensure the feasibility of the MPC optimisation problem within a prescribed computational time (e.g. lower than the control time-step), the control-oriented model should be formulated to be as close as possible to a Linear Time Invariant model [204]. A subclass of nonlinear systems, that include both continuous and discrete variables (e.g. Boolean variables describing operating

modes), are known as hybrid systems which can be formulated as Mixed Logical Dynamical or Piecewise Affine system [39].

The hybrid system formulation approach adopted for the solar system studied in this paper helped with many challenges that appeared when formulation of an MPC for such a system was attempted. A solar thermal system is intrinsically non-linear in nature, and the formulation of MPC problems requires specific precautions. When a PCM slurry is adopted as a heat transfer fluid the non-linearities further increase due to the phase change processes, as the specific enthalpy stored by the PCM slurry at different temperatures follows a non-linear trend. This problem was addressed by means of the aforementioned piecewise linearisation of the enthalpy versus temperature curves. This allowed the system to be considered as a Piecewise Affine linear system, separating the PCM slurry properties in three linear regions depending on its state of aggregation (solid, liquid or in phase change transition). The heat exchange processes of the solar thermal collector are also strongly influenced by non-linear thermal phenomena (e.g., radiation heat exchange, laminar flow coefficients). Furthermore, the collector performance is influenced by the thermal energy storage unit temperature and vice versa. This non-linearity problem was overcome by excluding the solar collector model from the control-oriented model, and considering the solar generation as an external "switchable" input to the thermal energy storage unit. In this way, the heat flux delivered by the collector was calculated off-line at every time step and treated as a measured external disturbance. This was made possible under the assumption that the collector inlet temperature remains almost constant over the prediction horizon. This hypothesis was particularly true in a solar collector system filled with PCM slurry, where this temperature can be reasonably set in the phase change temperature range of the material. The heat delivered by the collector is influenced by the flow-rate in the collector and by climatic disturbances (i.e., to ambient air temperature, wind speed, solar irradiance, sky temperature).

5.2.2.4 Climatic disturbances forecast

The predicted climatic disturbances affecting the collector and the thermal energy storage were derived following two different approaches: i) by utilising a "perfect prediction", using the same 24-hours weather conditions derived from the Example Weather Year (EWY) of Turin used for the simulation of the controlled system. This simplification can be useful to assess, at a design stage, the simulated controller performance only, but afterward cannot be used for the implementation of a real-time controller; and ii) by providing an estimated weather forecast to the MPC controller. Ref. [99] presented a number of approaches for weather forecast estimation. The Deterministic-Stochastic method was adopted in the current study to predict both external dry-bulb temperature and solar radiation.

The predicted weather was then utilised to calculate the estimated thermal energy generation of the collector and boundary weather conditions over the 24-hour horizon. The comparison between the performance of the controller with ideal

and estimated weather prediction can be used to estimate the effect of a real-time weather forecast on the MPC controller implemented on a real system.

5.2.2.5 Space heating demand forecast

The forecasted space heating demand was considered deterministic and known a-priori. In this study, the space heating demand was calculated in advance by re-scaling the daily thermal load profile assessed using the method proposed in Ref. [208]. This pattern was representative of a typical profile of residential buildings in Piedmont, the same region where the experimental test rig presented in this study is located. The dwellings considered in Ref. [208] were located in Turin (2617 Heating Degree Days and heating design temperature equal to -8 °C) with an annual average space heating energy demand around 90 kWh/m^2.

As the current paper aimed to understand the influence of weather and generation forecast uncertainty, rather than heating demand uncertainty, on the performance of the proposed MPC controller, perfect heating demand forecasts were provided to the MPC with a 24-hours forecast period.

5.2.2.6 Control oriented model

Using the assumptions discussed above, the control-oriented model that represents the thermal energy storage unit dynamics was formulated, based on the system schematic shown in *Figure 23*. The present MPC formulation is defined as a *Hybrid* MPC, since it required a Mixed Logical Dynamical formulation due to the three pump operating modes and the three PCM specific heat capacities. The measured disturbances affecting the thermal energy storage model were the ambient air temperature, the space heating demand and the heat delivered by the collector. The controller was able to regulate the heat delivery of the auxiliary heater and to switch between the three speeds of the solar collector pump and thus to regulate the flow-rate in the collector.

The control-oriented model that represents the evolution of the controlled thermal energy storage unit was explicated by means of the following Equation 6.3:

$$\dot{T}_{st}(t) = \frac{\delta_{10} \cdot \dot{Q}_{10}(t) + \delta_{60} \cdot \dot{Q}_{60}(t) + \delta_{90} \cdot \dot{Q}_{90}(t) - \dot{Q}_{need}(t) - U_{st} \cdot A_{st} \cdot (T_{st}(t) - T_a(t))}{\rho_{PCM} \cdot V_{st} \cdot c_{p,PCM,j}(t)} \quad (6.3)$$

Where the terms $U_{st} = 0.47$ Wm^{-2}°C^{-1}, $A_{st} = 1.75$ m^2, and $V_{st} = 0.2$ m^3 are the average thermal transmittance, the total external surface and the volume of the thermal energy storage tank respectively. The terms $\rho_{PCM} = 950$ kg·m^{-3}, and $c_{p,PCS,j}$ are the PCM slurry density and specific heat capacity respectively. The latter depends on the state of aggregation of the material at the time t. T_{st} is the thermal

energy storage unit average temperature; T_a is the ambient temperature; $\dot{Q}_{g10}$, $\dot{Q}_{g60}$ and $\dot{Q}_{g90}$ are the available heat generations produced by the solar thermal collector at the various pump speeds calculated by means of the external model of the solar thermal collector, $\dot{Q}_{he}$ is the heating delivered by the auxiliary heater; and $\dot{Q}_{need}$ is the heating power delivered to address the space heating demand. The indices δ_{10}, δ_{60} and δ_{90} are the Boolean variables that represent the activation, or not, of the pump at a defined speed. Two pump speed cannot be activated simultaneously.
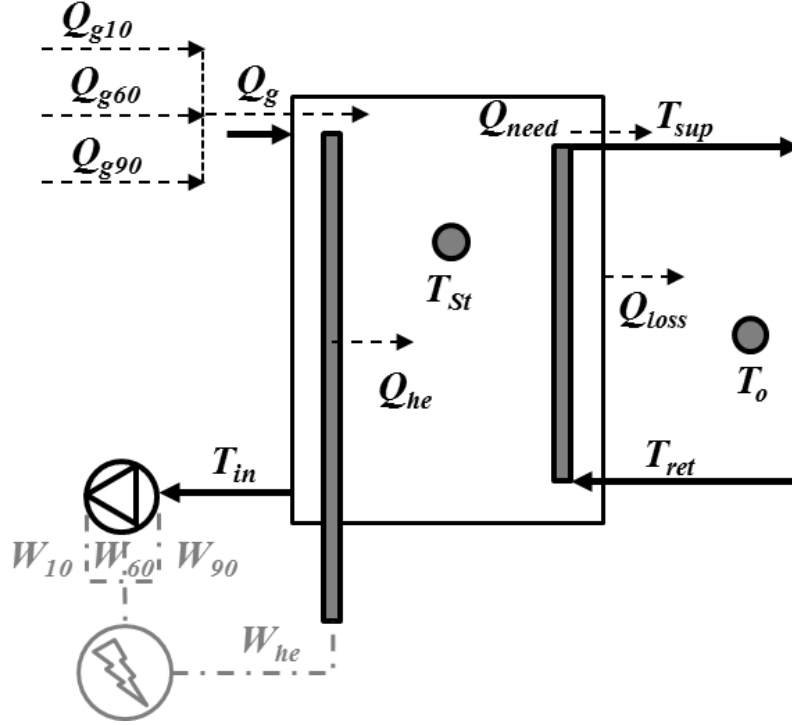
Figure 23. The control-oriented model of the thermal energy storage. Thermal fluxes are marked in black, while electrical energy consumptions are in grey.

To formulate the MPC problem, the system is formulated in the form:

$$\begin{cases} \dot{x}(t) = Ax(t) + B_u u(t) + B_v v(t) \\ y(t) = Cx(t) + D_u u(t) + D_v v(t) \end{cases} \tag{6.4}$$

Where $x = \text{T}_{st}$ is the system state, $u = [\text{e}, \dot{\text{Q}}_{he}, \delta_{10}, \delta_{60}, \delta_{90}]^\text{T}$ is the vector of continuous and Boolean manipulated inputs containing the slacking variable e that allows the minimum temperature constraint to be relaxed, $v = [\dot{\text{Q}}_{need}, \text{T}_a]^\text{T}$ is the vector of measured disturbances affecting the system, and y is the vector of the outputs. A, B_u, B_v, C, D_u and D_v are the state matrix, the manipulated input matrix, the measured disturbances matrix, the output matrix, the direct transmission matrices for manipulated inputs and measured disturbances respectively. These matrices are defined as:

$$A = 1 - \frac{U_{st} \cdot A_{st}}{\rho_{PCM} \cdot V_{st} \cdot c_{p,PCM,j}} \qquad (6.5)$$

$$B_u = \frac{1}{\rho_{PCM} \cdot V_{st} \cdot c_{p,PCM,j}} [1 \quad \dot{Q}_{10}(t) \quad \dot{Q}_{60}(t) \quad \dot{Q}_{90}(t)] \qquad (6.6)$$

$$B_v = \frac{1}{\rho_{PCM} \cdot V_{st} \cdot c_{p,PCM,j}} [-1 \quad U_{st} \cdot A_{st}] \qquad (6.7)$$

$$\boldsymbol{C = 1 \quad D_u = 0 \quad D_v = 0} \qquad (6.8)$$

Where at each time-step the value of the PCM specific heat capacity is:

$$c_{p,PCM,j} = \begin{cases} c_{p,PCM,1} & \text{if} & T_{st}(t) \le T_{inf,PCM} \\ c_{p,PCM,2} & \text{if } T_{inf,PCM} \le T_{st}(t) \le T_{sup,PCM} \\ c_{p,PCM,3} & \text{if} & T_{st}(t) > T_{sup,PCM} \end{cases} \qquad (6.9)$$

5.2.2.7 Constraints

The controlled system had to respect a number of constraints, which reflected the boundaries of the real system. This includes the maximum heating power that the auxiliary electric heater can deliver ($Q_{he,max}$ equal to 1.5 kW), the maximum temperature allowed in the thermal energy storage ($T_{st,max}$ = 60 °C) due to the material performance limits, and the impossibility to operate two pump speeds at the same time. These constraints are summarised in Equation 6.10, Equation 6.11 and Equation 6.12 respectively.

$$0 \le \dot{Q}_{he} \le \dot{Q}_{he,max} \qquad (6.10)$$

$$T_{st} \le T_{st,max} \qquad (6.11)$$

$$\sim(\delta_{10} \,\&\, \delta_{60}) \,\&\, \sim(\delta_{10} \,\&\, \delta_{90}) \,\&\, \sim(\delta_{60} \,\&\, \delta_{90}) \qquad (6.12)$$

An additional soft constraint reported in Equation 6.13 was introduced to ensure that the temperature of thermal energy storage unit remains high enough to be able to deliver the required heating demand building at each time step, considering the physical design of the secondary loop that extracts heat from the tank to supply the thermal energy, while allowing the possibility to relax it to ensure the feasibility of the problem and the stability of the controller:

$$T_{st,min} + e \le T_{st} \qquad (6.13)$$

Where $T_{st,min}$ is the minimum temperature of the thermal energy storage unit. $T_{st,min}$ was determined as a function of $\dot{Q}_{need}$ assuming that the system works with a fixed flow-rate and with a constant return water temperature equal to 25 °C. For this reason the profile of $T_{st,min}$ is directly related to the heating energy demand profile.

5.2.2.8 Objective Function

The MPC problem was formulated in an *Economic* way, since the objective function was calculated in first-norm with minimization of energy needs as the primary control goal (Equation 6.14).

In particular, the objective function was minimised over the control horizon time-span (N_c = 24-hours) targeting the minimal overall electrical energy consumption components and the violation of the slacking constraint e.

$$\min_{\{u\}_0^{N-1}} \quad J = \sum_{k=1}^{N-1} \|Q(x(k) - x_r)\|_p + \|R(u(k) - u)\|_p \qquad (6.14)$$

Where Q and R are the weighting matrices on the states and the manipulated input respectively. The problem was formulated as an *economic MPC*, assuming a linear objective function corresponding to norm-1 ($p=1$). In this cost function, only the manipulated inputs contribute to the overall cost, through: i) the energy consumption associated to the electric heater; ii) each possible operating mode of the circuit pump, and; iii) the violation of the slacking variable e used as a soft constraint. The cost associated with each input variable is summarised in *Table 6*. The MPC algorithm was formulated using the Multi Parametric Toolbox (MPT3) for Matlab [209] and the control-oriented model was defined in HYSDEL [210]. The optimisation was achieved using the CPLEX as a solver for the Mixed Integer Linear Programming (MILP) problem. The average solving time at each control time step was around 0.5 s on a laptop computer with an Intel core I7 processor and 32 GB of RAM.

Table 6. The weighting matrix parameters.

Input variable	Cost	Units
e	$0.90 - 0.95 - 1$	kWh$_{el}$/°C
Q_{he}	1	kWh$_{el}$/ kWh$_{th}$
δ_{10}	0.005	kWh$_{el}$
δ_{60}	0.025	kWh$_{el}$
δ_{90}	0.050	kWh$_{el}$

5.2.3 Results of the application of the MPC algorithm

The results presented below refer to one week of closed loop simulation. Specifically, the 7th week of the Example Weather Year was selected for the analysis, as it was considered representative of winter conditions in Turin because of its average temperature and solar conditions (average ambient air temperature equal to 4.2 °C and average daytime direct beam radiation equal to 320 Wm^{-2}), as well as the alternation between sunny and cloudy days. *Figure 24* shows the disturbances affecting the solar thermal system. In *Figure 24*(a) the main weather disturbances, including ambient air temperature, direct beam solar radiation, and horizontal diffuse solar radiation are shown. *Figure 24*(b) presents the potential solar thermal collector heat generation profile at the various pump speeds, calculated using the numerical model presented in Chapter 3. The procedure was repeated at each control time step for the 24-hours ahead using the future weather disturbances, forecasting the three potential generation profiles. *Figure 24*(c) presents the instantaneous space heating demand profile.

Both the RBC and MPC with perfect disturbances forecast strategies were implemented in close loop with the simulated system and the results were compared. In *Figure 25*(a) and *Figure 26*(a) the closed loop control sequences for the RBC and MPC controllers respectively are shown. The flow-rate corresponding to the different fixed pump speeds is shown on the primary y-axis, while the heat provided by the electric heater is shown on the secondary y-axis. The controlled variable and only system state was the thermal energy storage temperature, which was influenced by the external disturbances and control inputs. The storage temperature profiles of the two simulations are shown in *Figure 25*(b) and *Figure 26*(b). In these charts, the actual thermal energy storage temperature is compared with the minimum thermal energy storage unit temperature required to ensure the complete fulfilling of space heating demand. The temperature bounds of the phase change transition are shown using dashed lines on the chart. The initial temperature of the thermal energy storage unit was set at 35 °C in both cases, assuming that some level of charge was accumulated in the previous days.
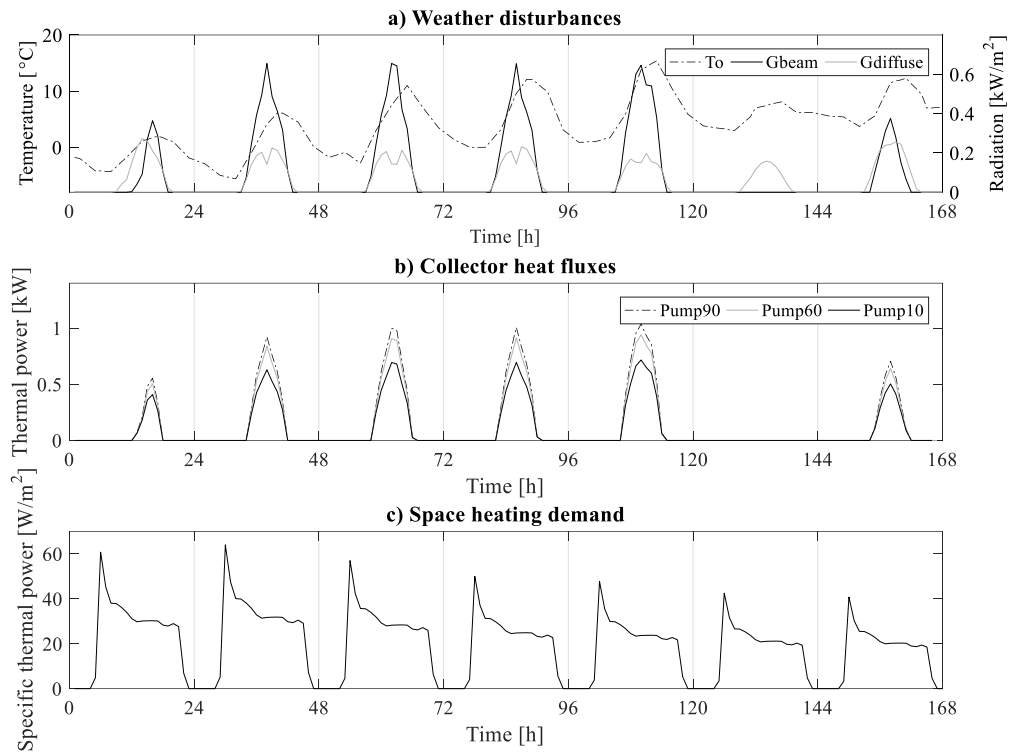
Figure 24. Disturbances affecting the controlled system. (a) Weather disturbances. (b) Forecasted solar thermal collector heat generation profiles at the various fixed pump speeds. (c) Space heating demand profile.
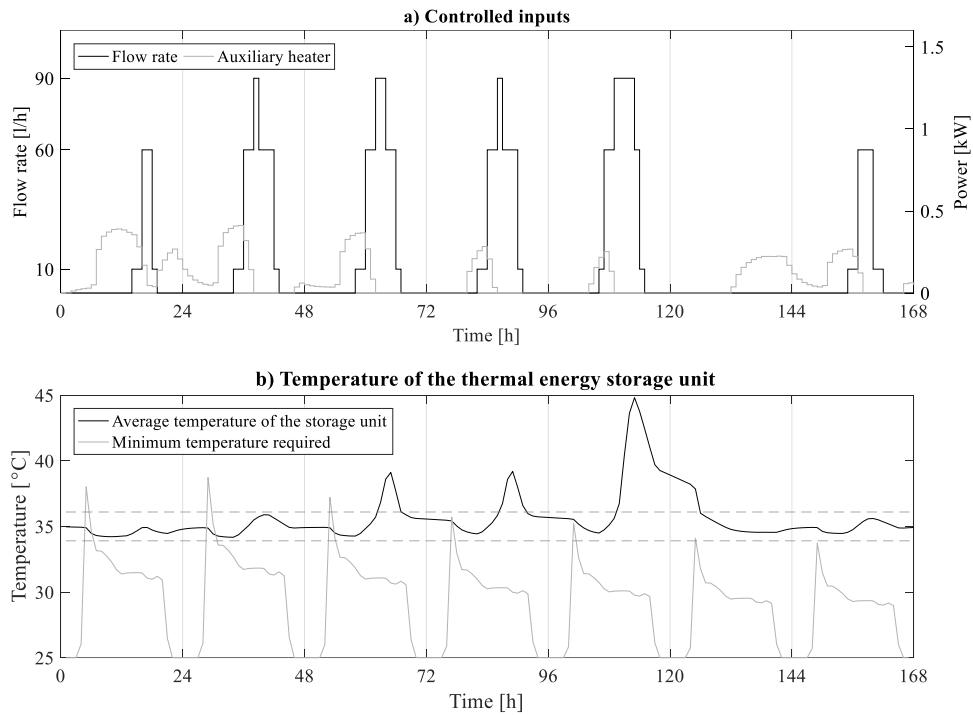
Figure 25. RBC regulation (a) System controlled inputs (pump flow-rate and electric heater power). (b) Temperature evolution of the thermal energy storage unit compared with the minimum temperature required for the thermal energy storage unit.

Figure 26. MPC regulation with perfect disturbances prediction (slacking variable e equal to 1.0 kWh$_{el}$/°C) (a) System controlled inputs (pump flow-rate and electric heater power). (b) Temperature evolution of the thermal energy storage unit compared with the minimum temperature required for the thermal energy storage unit.
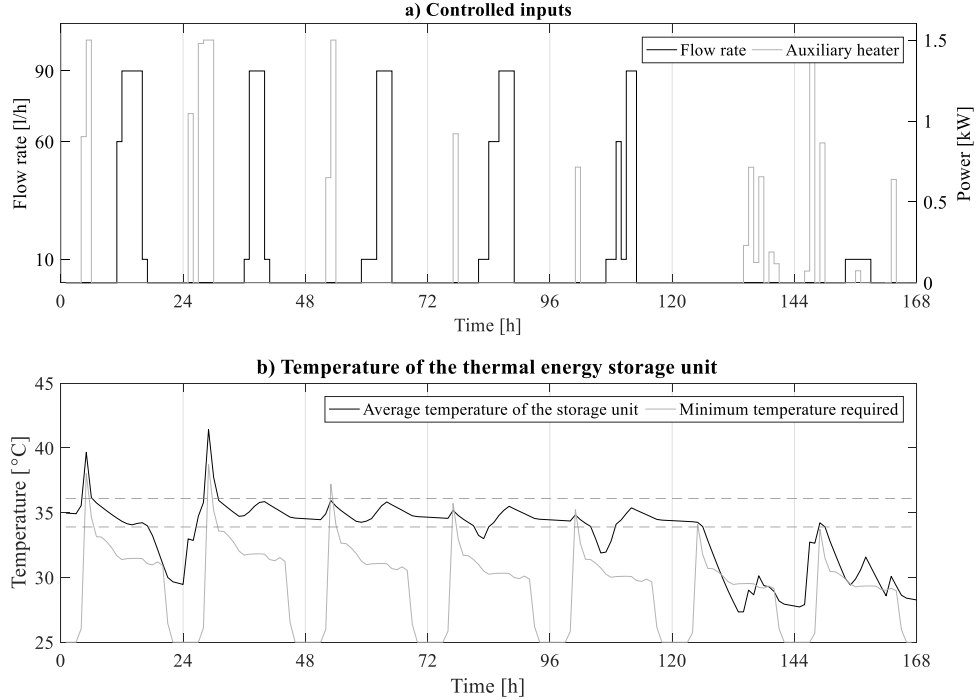
Figure 27. MPC regulation with estimated disturbances prediction (slacking variable e equal to 0.95 kWh$_{el}$/°C). (a) System controlled inputs (pump flow-rate and electric heater power). (b) Temperature evolution of the thermal energy storage unit compared with the minimum temperature required for the thermal energy storage unit.

244

The MPC controller was also simulated using the imperfect weather prediction in the MPC controller, replicating what a real-time controller would experience if an online weather prediction method was implemented together with the MPC logic on an embedded controller. The closed loop control sequences and storage temperature profiles of this simulation are shown in *Figure 27*(a) and *Figure 27*(b).

To quantitatively evaluate the potential benefits achievable by means of a control strategy is not a simple task. Comparable benchmark indicators are necessary for this purpose and must be selected appropriately. *Table 7* summarises the main results and key performance indicators of the controllers in the performed week of close loop simulations, where for example MPC (1.00) represent the results 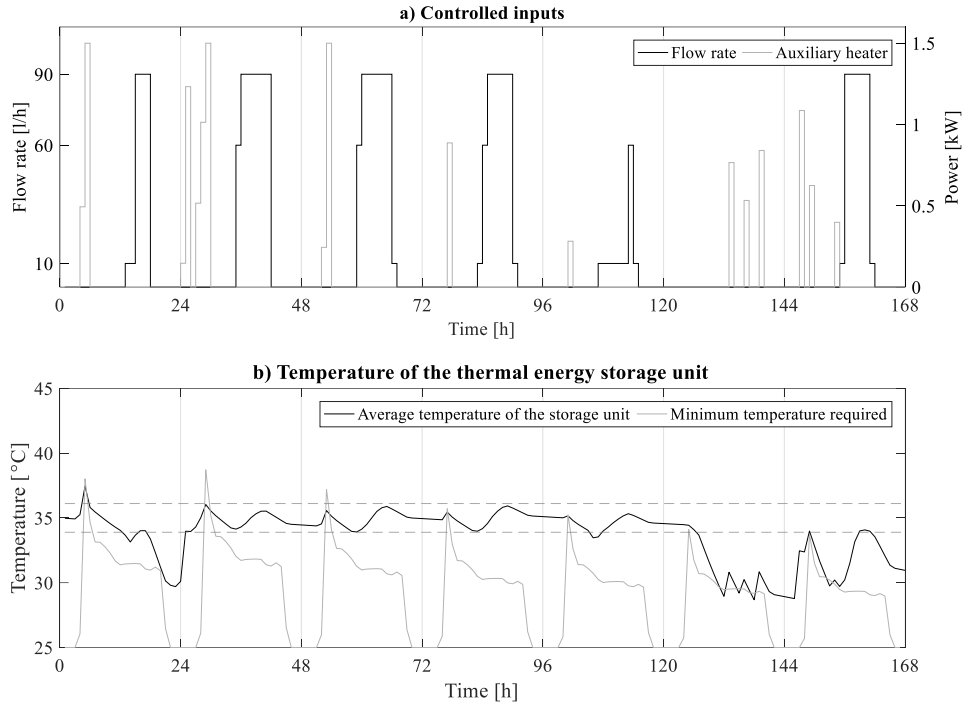of the MPC controller with perfect disturbances forecast and slacking variable equal to 1 kWh$_{el}$/$^\circ$C, RBC the Rule-Based Controller baseline benchmark, and MPC (dist) the MPC controller with estimated disturbances forecast (slacking variable was only considered to be equal to 0.95 kWh$_{el}$/$^\circ$C in this case). These key performance indicators include the overall energy system consumption (W_{tot}) and the split between pump and electric heater consumption (W_{pump} and W_{heater} respectively), the unsatisfied heating demand ($Q_{unsatisfied}$, which only depends on the temperature difference between the minimum required and the actual storage temperature, since the secondary flow to the building is considered to be constant), and the details on the panel energy generation (Q_{pan}, SF and COP_{pan}, which represent total energy extracted, solar fraction and system COP). Furthermore, G and Q_{need} represent the total available solar energy and the total demand. Finally, Q_{st} represents the energy difference in the storage between the beginning and end of the simulation.

Table 7. Energy consumption and performance indicators resulting from the close loop simulation for the system operating with RBC or MPC regulation.

	G	Q_{pan}	SF	W_{pump}	COP_{pan}	W_{heater}	W_{tot}	Q_{need}	Q_{st}	$Q_{unsatisfied}$	
	[kWh]	[kWh$_{th}$]	[%]	[kWh$_{el}$]	[kWh$_{th}$/kWh$_{el}$]	[kWh$_{el}$]	[kWh$_{el}$]	[kWh$_{th}$]	[kWh$_{th}$]	[kWh$_{tl}$]	[%]
RBC		22.0	38.1%	1.6	13.93	17.6	19.2		0.1	2.6	7.7%
MPC (1.00)		21.3	36.8%	1.0	20.64	14.4	15.5		6.1	0.3	1.0%
MPC (0.95)	57.8	22.1	38.3%	1.0	22.21	13.6	14.6	33.3	5.8	1.8	5.3%
MPC (0.80)		23.1	40.1%	0.8	30.65	12.4	13.1		6.1	4.6	13.9%
MPC (dist)		22.1	38.3%	1.2	18.26	16.8	18.0		6.7	2.8	8.2%

5.2.4 Discussion of the results

A comparison of the key-performance indicators was necessary to evaluate the performance of the MPC and the RBC regulation. To initially perform this comparison, the results related to MPC with perfect weather forecast and slacking variable e equal to 1 kWh$_{e}$/$^\circ$C were used to this purpose.

The total weekly energy demand for space heating was 33.3 kWh. To define the overall energy required by the system the energy losses towards the ambient

should be added to this value. Since these losses depend on the thermal energy storage unit temperature, the RBC and MPC algorithm resulted in different losses amounts, which were equal to 8.9 kWh in the RBC simulation and 8.8 kWh in the MPC simulation case. Thus, the resulting total weekly energy demand was equal to 42.2 kWh in the case of system controlled with RBC and equal to 42.1 kWh for the MPC regulation.

In the case of the RBC regulation, the collector delivered 57.6 % of the total thermal energy generated by the system (22.0 kWh), while the remaining 42.4 % was provided by the electric heater (17.6 kWh). In this case, the thermal energy storage level at the end of the simulation was the same as the one at the beginning (same temperature of the heat transfer fluid stored in the tank – see *Figure 25*(b)), with Q_{st} equal to 0.1 kWh.

The MPC regulation used the collector to generate 59.7 % of the total thermal energy generation (21.3 kWh), and used the electric heater for the remaining 40.3 % (14.4 kWh). However, to fulfil the demand an additional 6.1 kWh were discharged from the storage when comparing the initial and final energy stored in the tank, Q_{st}, (as the final heat transfer fluid temperature was lower than the one at the beginning of the simulation – see *Figure 26*(b)).

From the demand satisfaction perspective, the RBC simulation showed that 7.7 % of the space heating demand was not satisfied (2.6 kWh), while in case of MPC regulation this amount was only 1.0 % (0.3 kWh). The failure to satisfy the energy demand occurred when thermal energy storage unit temperature was lower than the minimum temperature required by the space heating system. While the RBC controller cannot increase the thermal energy storage unit temperature when energy demand peaks occur, as it does not have this knowledge available, the MPC algorithm can act in advance and prepare for peak demand, as can be seen in the first two days of the simulation in *Figure 25*(b) and *Figure 26*(b).

While managing the ability to satisfy more or less demand in favour of energy efficiency is non-trivial with a RBC controller, with an MPC this trade-off (or violation of the temperature boundary constraint in favour of energy) can be managed by varying the slacking variable value and therefore by relaxing or hardening the temperature boundary constraint.

The MPC in the initial setup (with a slacking variable value equal to 1.0 $kWh_{el}/°C$) outperforms the RBC controller in terms of both meeting the heating demand and in total energy consumption (total energy consumption was reduced by 19.2 % when compared to the RBC case).

The effect of varying the slacking variable value can be seen in the results from the simulations presented in *Table 7*. Relaxing the boundary allows the controller to meet less demand (5.3 % and 13.9 % of unmet demand in the cases of *e* equal to 0.95 $kWh_{el}/°C$ and 0.8 $kWh_{el}/°C$ respectively), but at the same time this creates an opportunity to utilise more the solar resource (solar fraction increases to 38.3 % and 40.1 % respectively, from the initial 36.8 %) and more efficiently (the COP of the solar system increases to 22.21 kWh_{th}/kWh_{el} and 30.65 kWh_{th}/kWh_{el} respectively, from the initial 20.64 kWh_{th}/kWh_{el}). This leads to a further reduction of the energy consumption when compared to the RBC case, by 24.0 % and 31.8 % respectively.

Specifically, in the case of e equal to 0.95 kWh$_{el}$/$^{\circ}$C, this further energy reduction is achieved whilst maintaining a smaller amount of unmet heating demand relative to the RBC case.

Considering the case where the MPC was operating using estimated weather and generation predictions, the MPC performed less efficiently compared to the benchmark MPC with perfect predictions, using 18 kWh$_{el}$ in total. The MPC with estimated weather and generation still outperformed the RBC in terms of total energy consumption, but with a slight decrease in performance when considering the unmet demand (8.2 %).

It is particularly noticeable that the use of an estimated prediction causes a decrease in the COP of the solar system (18.26 kWh$_{th}$/ kWh$_{el}$) and result in a higher compensation of the missing solar generation with the electric heater (16.8 kWh$_{el}$).

The methods by which the MPC algorithm regulates the solar thermal system to achieve superior performance can be seen in *Figure 26*(a). Given that the electric heater has a considerably lower efficiency compared to the solar system driven by a pump with a low electrical consumption, the MPC controller attempted to exploit the renewable energy source as much as possible to fulfil the demand, charging the storage whenever possible. During the days in which the solar energy generation is low and not sufficient to fulfil the energy demand, the electric heater was mostly utilised to maintain the storage temperature above the lower temperature boundary constraint. The lower the pump speed, the lower the electrical energy consumption (*Table 3*), but also the lower the amount of energy delivered by the collector (*Figure 24* (b)). The MPC ensured an optimal regulation and trade-off between these two contrasting objectives, using high pump speeds with high energy generation levels and only when necessary. It can be seen in *Figure 26*(b) that the MPC algorithm tends to maintain the thermal energy storage unit temperature within the PCM slurry phase transition range when solar energy is available, and maintains a lower temperature when there is no generation available (likely in order to minimise the thermal losses). Furthermore, *Figure 26*(b) highlights how the receding horizon formulation allowed the space heating demand requirement to be anticipated by the control system, overheating the thermal energy storage unit before a demand peak, and when the more efficient renewable energy source was available. Comparing *Figure 27*(a) and (b) with *Figure 26*(a) and (b) it is possible to observe the difference between the MPC controller with perfect predictions and with an estimated forecast. There is a sudden change in weather and available generation in the last two days of the simulated period. This was not well predicted by the weather estimation algorithms, as they only use past data to predict the future disturbances. This unpredicted weather caused a more extensive and less efficient (in terms of meeting the demand) use of the electric heater. In reality better disturbances prediction models can be implemented which do not only rely on past data, but also access on-line forecast via internet.

Using estimated disturbances reduced the performance of the Model Predictive Control algorithm from both the energy consumption and demand satisfaction when compared to using perfect predictions, highlighting the importance of reliable model and disturbances prediction to ensure effective operation of a Model

Predictive Controller. Better disturbances prediction models than the one implemented in this study, which do not only rely on past data, but also access on-line forecast via internet, could improve the controller performance towards the perfect prediction benchmark performance. The findings of the work have proved the effectiveness of MPC in properly exploiting the benefits of the latent heat of fusion/solidification at the base of the investigated solar system, which is expected to penetrate the market in the near future.

5.3 Key-findings of the present chapter

The aim of this chapter has been twofold. On the one side, a detailed survey on the recent advances of Model Predictive Control (MPC) for regulating the building thermal processes was carried out. On the other side, a MPC algorithm was developed to optimally regulate the SolHe-PCM full-scale prototype.

The first part of the chapter was more theoretical. A total of 211 papers were identified on Science Direct and Google Scholar database and, after screening and removal of studies that were not in line with the definitions of a MPC strategy applied to buildings, 161 papers were included in an extended survey. The scope of this study was not only to review the recent findings of the scientific literature, but also and chiefly to define a clear and exhaustive framework capable of pointing out the steps required for a correct implementation of MPC algorithms to building thermal regulation. The various subsection of this parts examined each single aspect that should be carefully considered when devising an MPC formulation. Particular effort was given to the section dedicated the building control oriented model. In fact, defining a correct model of the controlled system represents a great challenge in the development of a model-based controller. Great emphasis was given to critically examine the pros and cons encountered during the devising of an MPC algorithm for regulating building energy processes. The entire final section of this chapter part was dedicated to this purpose.

Since the previous survey has demonstrated that the benefits attributable to an MPC algorithm overtake the shortcomings a practical application to a case study was studied in the second part of the chapter. In detail, it was clear to the author that the controller of SolHe-PCM had to be improved. Indeed, innovative PCM-based solar thermal systems and thermal energy storage units – likewise the SolHe-PCM prototype – need to be controlled in an innovative optimal way to be effective and to fully exploit their potential. In these cases, the classical control methods are not always able to obtain the maximum benefits from these technologies. The investigation of new control paradigms was therefore necessary. Additionally, when poly-generation energy supply systems integrate solar thermal or energy storage systems (e.g., renewable energy sources coupled with auxiliary heaters or boilers, combined heat and power systems, heat pumps, etc.), dynamic optimisation methods may be used to recursively define which is the most advantageous generation source to be selected. MPC proved to be reliable and efficient for satisfying these purposes. A MPC algorithm was devised to regulate the operation of the SolHe-PCM solar thermal collector and thermal energy storage unit. The MPC formulation with different soft constraint parameters and disturbances forecasted with ideal and deterministic-stochastic methods was compared with the baseline RBC. Compared to the traditional RBC formulation the MPC regulation produced energy savings of up to 19.2 % with lower unmet energy demand. Moreover, when the slacking variable, which was used to constrain the requirement to meet space heating demand, was relaxed energy savings increase to 31.8 %, but with a slightly higher unmet energy demand.

References

[1]   Lawrence TM, Boudreau M, Helsen L, Henze G, Mohammadpour J, Noonan D, et al. Ten questions concerning integrating smart buildings into the smart grid. Build Environ 2016;108:273–83. doi:10.1016/j.buildenv.2016.08.022.

[2]   Capozzoli A, Cerquitelli T, Piscitelli M. Enhancing energy efficiency in buildings through innovative data analytics technologies. In: Ciprian Dobre, Fatos Xhafa, editors. Next Gener. Platforms Intell. Data Collect., Elsevier; 2016, p. 353–89.

[3]   Shaikh PH, Nor NBM, Nallagownden P, Elamvazuthi I, Ibrahim T. A review on optimized control systems for building energy and comfort management of smart sustainable buildings. Renew Sustain Energy Rev 2014;34:409–29. doi:10.1016/j.rser.2014.03.027.

[4]   Dounis AI, Caraiscos C. Advanced control systems engineering for energy and comfort management in a building environment-A review. Renew Sustain Energy Rev 2009;13:1246–61. doi:10.1016/j.rser.2008.09.015.

[5]   Afram A, Janabi-Sharifi F. Theory and applications of HVAC control systems - A review of model predictive control (MPC). Build Environ 2014;72:343–55. doi:10.1016/j.buildenv.2013.11.016.

[6]   ASHRAE. 2013 ASHRAE Handbook - Fundamentals (SI Edition). American Society of Heating, Refrigerating and Air-Conditioning Engineers, Inc.; 2013.

[7]   Kolokotsa D. Comparison of the performance of fuzzy controllers for the management of the indoor environment. Build Environ 2003;38:1439–50. doi:10.1016/S0360-1323(03)00130-6.

[8]   López A, Sánchez L, Doctor F, Hagras H, Callaghan V. An evolutionary algorithm for the off-line data driven generation of fuzzy controllers for intelligent buildings. Conf Proc - IEEE Int Conf Syst Man Cybern 2004;1:42–7. doi:10.1109/ICSMC.2004.1398270.

[9]   Hagras H, Packharn I, Vanderstockt Y, McNulty N, Vadher A, Doctor F. An intelligent agent based approach for energy management in commercial buildings. 2008 IEEE Int Conf Fuzzy Syst (IEEE World Congr Comput Intell 2008:156–62. doi:10.1109/FUZZY.2008.4630359.

[10]   Beghi A, Cecchinato L, Rampazzo M, Simmini F. Load forecasting for the efficient energy management of HVAC systems. 2010 IEEE Int Conf Sustain Energy Technol 2010:1–6. doi:10.1109/ICSET.2010.5684414.

[11]   Curtiss PS, D P. Examples of Neural Networks Used for Building System Control and Energy Management. ASHRAE Trans 1997;103:909–13.

[12]   Kumar R, Aggarwal RK, Sharma JD. Energy analysis of a building using artificial neural network: A review. Energy Build 2013;65:352–8. doi:10.1016/j.enbuild.2013.06.007.

[13]   Liang J, Du R. Thermal comfort control based on neural network for HVAC application. Proc 2005 IEEE Conf Control Appl 2005 CCA 2005 2005:819–24. doi:10.1109/CCA.2005.1507230.

[14]   Kanarachos a., Geramanis K. Multivariable control of single zone hydronic heating systems with neural networks. Energy Convers Manag 1998;39:1317–36. doi:10.1016/S0196-8904(98)00015-6.

[15]   Alcala R, Benitez JM, Casillas J, Cordon O, Perez R. Fuzzy control of

HVAC systems optimized by genetic algorithms. Appl Intell 2003;18:155–77. doi:10.1023/A:1021986309149.

[16] Zhang H, Davigny A, Colas F, Poste Y, Robyns B. Fuzzy logic based energy management strategy for commercial buildings integrating photovoltaic and storage systems. Energy Build 2012;54:196–206. doi:10.1016/j.enbuild.2012.07.022.

[17] Platt G, Li J, Li R, Poulton G, James G, Wall J. Adaptive HVAC zone modeling for sustainable buildings. Energy Build 2010;42:412–21. doi:10.1016/j.enbuild.2009.10.009.

[18] Nassif N. Modeling and optimization of HVAC systems using artificial neural network and genetic algorithm. Build Simul 2013;7:237–45. doi:10.1007/s12273-013-0138-3.

[19] Arabali A, Ghofrani M, Etezadi-Amoli M, Fadali MS, Baghzouz Y. Genetic-algorithm-based optimization approach for energy management. IEEE Trans Power Deliv 2013;28:162–70. doi:10.1109/TPWRD.2012.2219598.

[20] Wang S, Ma Z. Supervisory and Optimal Control of Building HVAC Systems: A Review. HVAC&R Res 2008;14:3–32. doi:10.1080/10789669.2008.10390991.

[21] Esther BP, Kumar KS. A survey on residential Demand Side Management architecture, approaches, optimization models and methods. Renew Sustain Energy Rev 2016;59:342–51. doi:10.1016/j.rser.2015.12.282.

[22] Lazos D, Sproul AB, Kay M. Optimisation of energy management in commercial buildings with weather forecasting inputs: A review. Renew Sustain Energy Rev 2014;39:587–603. doi:10.1016/j.rser.2014.07.053.

[23] Naidu DS, Rieger C. Advanced control strategies for heating, ventilation, air-conditioning, and refrigeration systems—An overview: Part I: Hard control. HVAC&R Res 2011;17:2–21. doi:10.1080/10789669.2011.540942.

[24] Aste N, Manfren M, Marenzi G. Building Automation and Control Systems and performance optimization: A framework for analysis. Renew Sustain Energy Rev 2017;75:313–30. doi:10.1016/j.rser.2016.10.072.

[25] Hilliard T, Kavgic M, Swan L. Model predictive control for commercial buildings: trends and opportunities. Adv Build Energy Res 2015;2549:1–19. doi:10.1080/17512549.2015.1079240.

[26] Kavgic M, Hilliard T, Swan L. Opportunities for implementation of MPC in commercial buildings. Energy Procedia 2015;78:2148–53. doi:10.1016/j.egypro.2015.11.300.

[27] Afram A, Janabi-sharifi F, Fung AS, Raahemifar K. Artificial neural network (ANN) based model predictive control (MPC) and optimization of HVAC systems : A state of the art review and case study of a residential HVAC system. Energy Build 2017;141:96–113. doi:10.1016/j.enbuild.2017.02.012.

[28] Mirakhorli A, Dong B. Occupancy behavior based model predictive control for building indoor climate - A critical review. Energy Build 2016;129:499–513. doi:10.1016/j.enbuild.2016.07.036.

[29] Killian M, Kozek M. Ten questions concerning model predictive control for energy efficient buildings. Build Environ 2016;105:403–12. doi:10.1016/j.buildenv.2016.05.034.

[30] Rawlings JB, Mayne DQ. Model Predictive Control : Theory and Design. 5th ed. Madison, Wisconsin: Nob Hill Pub; 2012.

[31] Camacho EF, Bordons CA. Model Predictive Control. 2nd ed. London: Springer-Verlag; 2007. doi:10.1007/978-0-85729-398-5.

[32] Bemporad A, Morari M. Robust model predictive control: a survey. Lect

Notes Control Inf Sci 2007;245:207–26. doi:10.1007/BFb0109870.

[33] Bernardini D, Bemporad A. Stabilizing model predictive control of stochastic constrained linear systems. IEEE Trans Automat Contr 2012;57:1468–80. doi:10.1109/TAC.2011.2176429.

[34] Mady AE, Provan GM, Ryan C, Brown KN. Stochastic Model Predictive Controller for the Integration of Building Usage and Temperature Regulation. Proc. Twenty-Fifth AAAI Conf. Artif. Intell., 2011, p. 1371–6.

[35] Oldewurtel F, Parisio A, Jones CN, Morari M, Gyalistras D, Gwerder M, et al. Energy efficient building climate control using Stochastic Model Predictive Control and weather predictions. Am Control Conf (ACC), 2010 2010:5100–5. doi:10.1109/ACC.2010.5530680.

[36] Kim SH. Building demand-side control using thermal energy storage under uncertainty: An adaptive Multiple Model-based Predictive Control (MMPC) approach. Build Environ 2013;67:111–28. doi:10.1016/j.buildenv.2013.05.005.

[37] Ma J, Qin SJ, Salsbury T. Application of economic MPC to the energy and demand minimization of a commercial building. J Process Control 2014;24:1282–91. doi:10.1016/j.jprocont.2014.06.011.

[38] Tran T, Ling K-V, Maciejowski JM. Economic Model Predictive Control - A Review. Proc. 31st Int. Symp. Autom. Robot. Constr. Min. (ISARC 2014), 2014, p. 1–8.

[39] Bemporad A, Morari M. Control of systems integrating logic, dynamics, and constraints. Automatica 1999;35:407–27. doi:10.1016/S0005-1098(98)00178-2.

[40] Bemporad A. A multiparametric quadratic programming algorithm with polyhedral computations based on nonnegative least squares. IEEE Trans Automat Contr 2015;60:2892–903. doi:10.1109/TAC.2015.2417851.

[41] Beck J V., Arnold KJ. Parameter estimation in engineering and science. 1st ed. John Wiley & Sons Inc; 1977.

[42] de Cursi ES, Sampaio R. Uncertainty Quantification and Stochastic Modeling with Matlab. 1st ed. London: ISTE Press - Elsevier; 2015.

[43] Li Z, Han Y, Xu P. Methods for benchmarking building energy consumption against its past or intended performance: An overview. Appl Energy 2014;124:325–34. doi:10.1016/j.apenergy.2014.03.020.

[44] Zhao H, Magoulès F. A review on the prediction of building energy consumption. Renew Sustain Energy Rev 2012;16:3586–92. doi:10.1016/j.rser.2012.02.049.

[45] Wang S, Yan C, Xiao F. Quantitative energy performance assessment methods for existing buildings. Energy Build 2012;55:873–88. doi:10.1016/j.enbuild.2012.08.037.

[46] Magoulès F, Zhao H. Data Mining and Machine Learning in Building Energy Analysis: Towards High Performance Computing. 1st ed. John Wiley & Sons Inc; 2016.

[47] Privara S, Vana Z, Zacekova E, Cigler J. Building modeling: Selection of the most appropriate model for predictive control. Energy Build 2012;55:341–50. doi:10.1016/j.enbuild.2012.08.040.

[48] Ma Y, Borrelli F, Hencey B, Coffey B, Bengea S, Haves P. Model Predictive Control for the Operation of Building Cooling Systems. IEEE Trans Control Syst Technol 2012;20:796–803. doi:10.1109/TCST.2011.2124461.

[49] Gyalistras D, Gwerder M. Use of weather and occupancy forecasts for optimal building climate control (OptiControl): Two years progress report.

2009.

[50]   Verhelst C, Logist F, Van Impe J, Helsen L. Study of the optimal control problem formulation for modulating air-to-water heat pumps connected to a residential floor heating system. Energy Build 2012;45:43–53. doi:10.1016/j.enbuild.2011.10.015.

[51]   Cigler J (Čvut/Fel). Issues in nonlinear stochastic grey box identification. Int J Adapt Control Signal Process 2010;9:465–90. doi:10.1002/acs.4480090603.

[52]   Li X, Wen J. Review of building energy modeling for control and operation. Renew Sustain Energy Rev 2014;37:517–37. doi:10.1016/j.rser.2014.05.056.

[53]   Prívara S, Cigler J, Váňa Z, Oldewurtel F, Sagerschnig C, Žáčeková E. Building modeling as a crucial part for building predictive control. Energy Build 2013;56:8–22. doi:10.1016/j.enbuild.2012.10.024.

[54]   Hazyuk I, Ghiaus C, Penhouet D. Optimal temperature control of intermittently heated buildings using Model Predictive Control: Part I - Building modeling. Build Environ 2012;51:379–87. doi:10.1016/j.buildenv.2011.11.009.

[55]   Hazyuk I, Ghiaus C, Penhouet D. Optimal temperature control of intermittently heated buildings using Model Predictive Control: Part II - Control algorithm. Build Environ 2012;51:388–94. doi:10.1016/j.buildenv.2011.11.008.

[56]   Salakij S, Yu N, Paolucci S, Antsaklis P. Model-Based Predictive Control for building energy management. I : Energy modeling and optimal control 2016;133:345–58. doi:10.1016/j.enbuild.2016.09.044.

[57]   Yu N, Salakij S, Chavez R, Paolucci S, Sen M, Antsaklis P. Model-based predictive control for building energy management : Part II – Experimental validations 2017;146:19–26. doi:10.1016/j.enbuild.2017.04.027.

[58]   Prívara S, Váňa Z, Žáčeková E, Cigler J. Building modeling: Selection of the most appropriate model for predictive control. Energy Build 2012;55:341–50. doi:10.1016/j.enbuild.2012.08.040.

[59]   Fiorentini M, Cooper P, Ma Z. Development and optimization of an innovative HVAC system with integrated PVT and PCM thermal storage for a net-zero energy retrofitted house. Energy Build 2015;94:21–32. doi:10.1016/j.enbuild.2015.02.018.

[60]   Fiorentini M, Cooper P, Ma Z, Robinson DA. Hybrid model predictive control of a residential HVAC system with PVT energy generation and PCM thermal storage. Energy Procedia 2015;83:21–30. doi:10.1016/j.egypro.2015.12.192.

[61]   Fiorentini M, Wall J, Ma Z, Braslavsky JH, Cooper P. Hybrid model predictive control of a residential HVAC system with on-site thermal energy generation and storage. Appl Energy 2017;187:465–79. doi:10.1016/j.apenergy.2016.11.041.

[62]   Henze GP, Felsmann C, Knabe G. Evaluation of optimal control for active and passive building thermal storage. Int J Therm Sci 2004;43:173–83. doi:10.1016/j.ijthermalsci.2003.06.001.

[63]   Parisio A, Fabietti L, Molinari M, Varagnolo D, Johansson KH. Control of HVAC systems via scenario-based explicit MPC. Proc IEEE Conf Decis Control 2014;2015–Febru:5201–7. doi:10.1109/CDC.2014.7040202.

[64]   Maasoumy M, Sangiovanni-Vincentelli A. Total and Peak Energy Consumption Minimization of Building HVAC Systems Using Model

Predictive Control. IEEE Des Test Comput 2012;29:26–35. doi:10.1109/MDT.2012.2200871.

[65] Oldewurtel F, Gyalistras D, Gwerder M, Jones CN, Stauch V, Lehmann B, et al. Increasing Energy Efficiency in Building Climate Control using Weather Forecasts and Model Predictive Control. REHVA World Congr Clima 2010:8pp.

[66] Lehmann B, Gyalistras D, Gwerder M, Wirth K, Carl S. Intermediate complexity model for Model Predictive Control of Integrated Room Automation. Energy Build 2013;58:250–62. doi:10.1016/j.enbuild.2012.12.007.

[67] Gondhalekar R, Oldewurtel F, Jones CN. Least-restrictive robust periodic model predictive control applied to room temperature regulation. Automatica 2013;49:2760–6. doi:10.1016/j.automatica.2013.05.009.

[68] Favoino F, Fiorito F, Cannavale A, Ranzi G, Overend M. Optimal control and performance of photovoltachromic switchable glazing for building integration in temperate climates. Appl Energy 2016;178:943–61. doi:10.1016/j.apenergy.2016.06.107.

[69] Ascione F, Bianco N, De Stasio C, Mauro GM, Vanoli GP. Simulation-based model predictive control by the multi-objective optimization of building energy performance and thermal comfort. Energy Build 2016;111:131–44. doi:10.1016/j.enbuild.2015.11.033.

[70] Ascione F, Bianco N, De Stasio C, Mauro GM, Vanoli GP. A new comprehensive approach for cost-optimal building design integrated with the multi-objective model predictive control of HVAC systems. Sustain Cities Soc 2017;31:136–50. doi:10.1016/j.scs.2017.02.010.

[71] Zhao J, Lam KP, Ydstie BE, Loftness V. Occupant-oriented mixed-mode EnergyPlus predictive control simulation. Energy Build 2016;117:362–71. doi:10.1016/j.enbuild.2015.09.027.

[72] Corbin CD, Henze GP, May-Ostendorp P. A model predictive control optimization environment for real-time commercial building application. J Build Perform Simul 2013;6:159–74. doi:10.1080/19401493.2011.648343.

[73] Zakula T, Armstrong PR, Norford L. Modeling environment for model predictive control of buildings. Energy Build 2014;85:549–59. doi:10.1016/j.enbuild.2014.09.039.

[74] Ma Y. Model Predictive Control for Energy Efficient Buildings. University of California, Berkeley, 2012.

[75] Sturzenegger D, Gyalistras D, Gwerder M, Sagerschnig C, Morari M, Smith RS. Model Predictive Control of a Swiss office building. 11th Clima-RHEVA world Congr., 2013, p. 10.

[76] Hensen J, Lamberts R. Building performance simulation for design and operation. 1st ed. Routledge; 2012.

[77] Armstrong P, Leeb S, Norford L. Control with building mass-Part I: Thermal response model. ASHRAE Trans 2006;112:449–62.

[78] Ferreira PM, Ruano AE, Silva S, Conceição EZE. Neural networks based predictive control for thermal comfort and energy savings in public buildings. Energy Build 2012;55:238–51. doi:10.1016/j.enbuild.2012.08.002.

[79] Foggia G, Thi Thu Hà P, Wurtz F, Warkosek, G. Wurtzijaem F. Optimizing energy management in buildings with Neural Networks. Int J Appl Electromagn Mech 2009;30:237–344.

[80] Bloem J. System Identification Applied to Building Performance Data. Joint

Research Centre European Commission; 1994.

[81] Bacher P, Madsen H. Identifying suitable models for the heat dynamics of buildings. Energy Build 2011;43:1511–22. doi:10.1016/j.enbuild.2011.02.005.

[82] Sturzenegger D, Gyalistras D, Morari M, Smith RS. Semi-automated modular modeling of buildings for model predictive control. Proc Fourth ACM Work Embed Sens Syst Energy-Efficiency Build - BuildSys '12 2012:99–106. doi:10.1145/2422531.2422550.

[83] David Sturzenegger. Model Predictive Building Climate Control - Steps Towards Practice. 2012.

[84] Andersen KK (Dtu), Madsen H (Dtu), Hansen LH (Risø). Modelling the heat dynamics of a building using stochastic differential equations. Energy Build 2000;31:13–24. doi:10.1016/S0378-7788(98)00069-3.

[85] West SR, Ward JK, Wall J. Trial results from a model predictive control and optimisation system for commercial building HVAC. Energy Build 2014;72:271–9. doi:10.1016/j.enbuild.2013.12.037.

[86] Kelman A, Ma Y, Borrelli F. Analysis of local optima in predictive control for energy efficient buildings. J Build Perform Simul 2017;6:236–55. doi:10.1080/19401493.2012.671959.

[87] Kelman A, Borrelli F. Bilinear Model Predictive Control of a HVAC System Using Sequential Quadratic Programming. Int Fed Autom Control World Congr 2011:9869–74. doi:10.3182/20110828-6-IT-1002.03811.

[88] Sturzenegger D. Bilinear Modeling of an Air Handling Unit for Model Predicitive Control Technical Report Models of the Components Nonlinear AHU model. 2015.

[89] Henze GP, Kalz DE, Liu S, Felsmann C. Experimental analysis of model-based predictive optimal control for active and passive building thermal storage inventory. HVAC&R Res 2005;11:189–213. doi:10.1080/10789669.2005.10391134.

[90] Borrelli F. Fast stochastic predictive control for building temperature regulation. 2012 Am Control Conf 2012:3075–80. doi:10.1109/ACC.2012.6315347.

[91] Lauro F, Longobardi L, Panzieri S. An adaptive distributed predictive control strategy for temperature regulation in a multizone office building. 2014 IEEE Int. Work., IEEE; 2014, p. 32–7.

[92] Siroky J, Cigler J, Ferkl L. Hybrid MPC approach to reconfiguration of building heating system. Eur Control Conf 2013:2675–80.

[93] Menchinelli P, Bemporad A. Hybrid Model Predictive Control of a Solar Air Conditioning Plant. Eur J Control 2008;14:501–15. doi:10.3166/ejc.14.501-515.

[94] Yudong M, Borrelli F, Hencey B, Packard A, Bortoff S. Model Predictive Control of thermal energy storage in building cooling systems. Decis. Control. 2009 held jointly with 2009 28th Chinese Control Conf. CDC/CCC 2009. Proc. 48th IEEE Conf., 2009, p. 392–7. doi:10.1109/cdc.2009.5400677.

[95] Pannocchia G, Rawlings JB. Disturbance models for offset-free model-predictive control. AIChE J 2003;49:426–37. doi:10.1002/aic.690490213.

[96] Ricker NL. Model predictive control with state estimation. Ind Eng Chem Res 1990;29:374–82. doi:10.1021/ie00099a013.

[97] Jia M, Srinivasan RS, Raheem AA. From occupancy to occupant behavior: An analytical survey of data acquisition technologies, modeling

methodologies and simulation coupling mechanisms for building energy efficiency. Renew Sustain Energy Rev 2017;68:525–40. doi:10.1016/j.rser.2016.10.011.

[98] Foucquier A, Robert S, Suard F, Stéphan L, Jay A. State of the art in building modelling and energy performances prediction: A review. Renew Sustain Energy Rev 2013;23:272–88. doi:10.1016/j.rser.2013.03.004.

[99] Ren MJ, Wright JA. Adaptive Diurnal Prediction of Ambient Dry-Bulb Temperature and Solar Radiation. HVAC&R Res 2002;8:383–401. doi:10.1080/10789669.2002.10391297.

[100] Florita A, Henze G. Comparison of Short-Term Weather Forecasting Models for Model Predictive Control. HVAC&R Res 2009;15:835–53. doi:10.1080/10789669.2009.10390868.

[101] Khakimova A, Kusatayeva A, Shamshimova A, Sharipova D, Bemporad A, Familiant Y, et al. Optimal energy management of a small-size building via hybrid model predictive control. Energy Build 2017;140:1–8. doi:10.1016/j.enbuild.2017.01.045.

[102] Kim SH, Augenbroe G. Using the National Digital Forecast Database for model-based building controls. Autom Constr 2012;27:170–82. doi:10.1016/j.autcon.2012.05.012.

[103] Mayer B, Killian M, Kozek M. Management of hybrid energy supply systems in buildings using mixed-integer model predictive control. Energy Convers Manag 2015;98:470–83. doi:10.1016/j.enconman.2015.02.076.

[104] Huang H, Chen L, Hu E. A hybrid model predictive control scheme for energy and cost savings in commercial buildings: Simulation and experiment. 2015 Am Control Conf 2015:256–61. doi:10.1109/ACC.2015.7170745.

[105] Vaghefi SA, Jafari MA, Zhu J, Brouwer J, Lu Y. A Hybrid Physics-Based and Data Driven Approach to Optimal Control of Building Cooling / Heating Systems. IEEE Trans Autom Sci Eng 2014:1–11. doi:10.1109/TASE.2014.2356337.

[106] Moros P, Bourdais R, Dumur D, Buisson J. Distributed model predictive control for building temperature regulation 2010:3174–9.

[107] Moroşan P-D, Bourdais R, Dumur D, Buisson J. Building temperature regulation using a distributed model predictive control. Energy Build 2010;42:1445–52. doi:10.1016/j.enbuild.2010.03.014.

[108] Ma Y, Anderson G, Borrelli F. A Distributed Predictive Control Approach to Building Temperature Regulation. Am Control Conf 2011:2089–94. doi:10.1109/ACC.2011.5991549.

[109] Scherer HF, Pasamontes M, Guzmán JL, Álvarez JD, Camponogara E, Normey-Rico JE. Efficient building energy management using distributed model predictive control. J Process Control 2014;24:740–9. doi:10.1016/j.jprocont.2013.09.024.

[110] Long Y, Liu S, Xie L, Johansson KH. A scenario-based distributed stochastic MPC for building temperature regulation. IEEE Int Conf Autom Sci Eng 2014;2014–Janua:1091–6. doi:10.1109/CoASE.2014.6899461.

[111] Barata FA, Neves-silva R. Distributed MPC for Thermal Comfort in Buildings with Dynamically Coupled Zones and Limited Energy. Dr. Conf. Comput. Electr. Ind. Syst., 2014, p. 305–12.

[112] Béguery P, Industries S, Merlin- PL. Model predictive control for energy management in buildings Part 2 : Distributed Model Predictive Control. 4th IFAC Nonlinear Model Predict. Control Conf., 2001, p. 226–31.

[113] Dong B, Lam KP. A real-time model predictive control for building heating and cooling systems based on the occupancy behavior pattern detection and local weather forecasting. Build Simul 2014;7:89–106. doi:10.1007/s12273-013-0142-7.

[114] Lindelof D, Afshari H, Alisafaee M, Biswas J, Caban M, Mocellin X, et al. Field tests of an adaptive, model-predictive heating controller for residential buildings. Energy Build 2015;99:292–302. doi:10.1016/j.enbuild.2015.04.029.

[115] Halvgaard R, Bacher P, Perers B, Andersen E, Furbo S, Jørgensen JB, et al. Model predictive control for a smart solar tank based on weather and consumption forecasts. Energy Procedia 2012;30:270–8. doi:10.1016/j.egypro.2012.11.032.

[116] Halvgaard R, Poulsen NK, Madsen H, Jørgensen JB. Economic Model Predictive Control for building climate control in a Smart Grid. 2012 IEEE PES Innov Smart Grid Technol 2012:1–6. doi:10.1109/ISGT.2012.6175631.

[117] Huang G. Model predictive control of VAV zone thermal systems concerning bi-linearity and gain nonlinearity. Control Eng Pract 2011;19:700–10. doi:10.1016/j.conengprac.2011.03.005.

[118] Siroky J, Oldewurtel F, Cigler J, Privara S. Experimental analysis of model predictive control for an energy efficient building heating system. Appl Energy 2011;88:3079–87. doi:10.1016/j.apenergy.2011.03.009.

[119] Sturzenegger D, Gyalistras D, Morari M, Smith RS. Model Predictive Climate Control of a Swiss Office Building: Implementation, Results, and Cost-Benefit Analysis. IEEE Trans. Control Syst. Technol., vol. 24, 2016, p. 1–12. doi:10.1109/TCST.2015.2415411.

[120] Wallace M, McBride R, Aumi S, Mhaskar P, House J, Salsbury T. Energy efficient model predictive building temperature control. Chem Eng Sci 2012;69:45–58. doi:10.1016/j.ces.2011.07.023.

[121] Goyal S, Barooah P, Middelkoop T. Experimental study of occupancy-based control of HVAC zones. Appl Energy 2015;140:75–84. doi:10.1016/j.apenergy.2014.11.064.

[122] Huchuk B, Gunay HB, O'Brien W, Cruickshank CA. Model-based predictive control of office window shades. Build Res Inf 2016;44:445–55. doi:10.1080/09613218.2016.1101949.

[123] Hilliard T, Swan L, Kavgic M, Qin Z, Lingras P. Development of a whole building model predictive control strategy for a LEED silver community college. Energy Build 2016;111:224–32. doi:10.1016/j.enbuild.2015.11.051.

[124] de Dear, Richard; Brager GS. Developing an Adaptive Model of Thermal Comfort and Preference. ASHRAE Trans 1998;104.

[125] Nicol JF, Humphreys MA. Adaptive thermal comfort and sustainable thermal standards for buildings. Energy Build 2002;34:563–72. doi:10.1016/S0378-7788(02)00006-3.

[126] Váňa Z, Cigler J, Široký J, Žáčeková E, Ferkl L. Model-based energy efficient control applied to an office building. J Process Control 2014;24:790–7. doi:10.1016/j.jprocont.2014.01.016.

[127] Fanger P. Thermal comfort. Analysis and applications in environmental engineering. New York: McGraw-Hill; 1972.

[128] ISO/TC159/SC5. ISO 7730:2005 - Ergonomics of the thermal environment -- Analytical determination and interpretation of thermal comfort using calculation of the PMV and PPD indices and local thermal comfort criteria

2005.

[129] ASHRAE. Standard 55 - Thermal environmental conditions for human occupancy 2016.

[130] Cigler J, Prívara S, Vána Z, Záceková E, Ferkl L. Optimization of Predicted Mean Vote index within Model Predictive Control framework: Computationally tractable solution. Energy Build 2012;52:39–49. doi:10.1016/j.enbuild.2012.05.022.

[131] Jiri C, Samuel P, Zdenek V, Eva Z, Lukas F. On Predicted Mean Vote Optimization in Building Climate Control. 2012 20th Mediterr. Conf. Control Autom., Barcelona, Spain: 2012, p. 1518–23.

[132] Álvarez JD, Redondo JL, Camponogara E, Normey-Rico J, Berenguel M, Ortigosa PM. Optimizing building comfort temperature regulation via model predictive control. Energy Build 2013;57:361–72. doi:10.1016/j.enbuild.2012.10.044.

[133] Castilla M, Álvarez JD, Normey-Rico JE, Rodríguez F. Thermal comfort control using a non-linear MPC strategy: A real case of study in a bioclimatic building. J Process Control 2014;24:703–13. doi:10.1016/j.jprocont.2013.08.009.

[134] Garnier A, Eynard J, Caussanel M, Grieu S. Predictive control of multizone heating, ventilation and air-conditioning systems in non-residential buildings. Appl Soft Comput J 2015;37:847–62. doi:10.1016/j.asoc.2015.09.022.

[135] Chen X, Wang Q, Srebric J. Model predictive control for indoor thermal comfort and energy optimization using occupant feedback. Energy Build 2015;102:357–69. doi:10.1016/j.enbuild.2015.06.002.

[136] Klauco M, Kvasnica M. Explicit MPC approach to PMV-based thermal comfort control. Proc. IEEE Conf. Decis. Control, 2014, p. 4856–61. doi:10.1109/CDC.2014.7040147.

[137] Daum D, Haldi F, Morel N. A personalized measure of thermal comfort for building controls. Build Environ 2011;46:3–11. doi:10.1016/j.buildenv.2010.06.011.

[138] De Ridder F, Diehl M, Mulder G, Desmedt J, Van Bael J. An optimal control algorithm for borehole thermal energy storage systems. Energy Build 2011;43:2918–25. doi:10.1016/j.enbuild.2011.07.015.

[139] Li S, Joe J, Hu J, Karava P. System identification and model-predictive control of office buildings with integrated photovoltaic-thermal collectors, radiant floor heating and active thermal storage. Sol Energy 2015;113:139–57. doi:10.1016/j.solener.2014.11.024.

[140] Preglej A, Rehrl J, Schwingshackl D, Steiner I, Horn M, Skrjanc I. Energy-efficient fuzzy model-based multivariable predictive control of a HVAC system. Energy Build 2014;82:520–33. doi:10.1016/j.enbuild.2014.07.042.

[141] May-Ostendorp P, Henze GP, Corbin CD, Rajagopalan B, Felsmann C. Model-predictive control of mixed-mode buildings with rule extraction. Build Environ 2011;46:428–37. doi:10.1016/j.buildenv.2010.08.004.

[142] Liang W, Quinte R, Jia X, Sun JQ. MPC control for improving energy efficiency of a building air handler for multi-zone VAVs. Build Environ 2015;92:256–68. doi:10.1016/j.buildenv.2015.04.033.

[143] Jingran M, Qin SJ, Bo L, Salsbury T, Ma J, Li B. Economic model predictive control for building energy systems. 2011 IEEE PES Innov. Smart Grid Technol. ISGT 2011, 2011, p. 1–6. doi:10.1109/ISGT.2011.5759140.

[144] Salsbury T, Mhaskar P, Qin SJ. Predictive control methods to improve

energy efficiency and reduce demand in buildings. Comput Chem Eng 2013;51:77–85. doi:10.1016/j.compchemeng.2012.08.003.

[145] Ma J, Qin J, Salsbury T, Xu P. Demand reduction in building energy systems based on economic model predictive control. Chem Eng Sci 2012;67:92–100. doi:10.1016/j.ces.2011.07.052.

[146] Maasoumy M, Razmara M, Shahbakhti M, Vincentelli AS. Handling model uncertainty in model predictive control for energy efficient buildings. Energy Build 2014;77:377–92. doi:10.1016/j.enbuild.2014.03.057.

[147] Wei T, Zhu Q, Maasoumy M. Co-scheduling of HVAC control, EV charging and battery usage for building energy efficiency. IEEE/ACM Int. Conf. Comput. Des. Dig. Tech. Pap. ICCAD, 2015, p. 191–6. doi:10.1109/ICCAD.2014.7001351.

[148] Maasoumy M, Razmara M, Shahbakhti M, Sangiovanni Vincentelli A. Selecting building predictive control based on model uncertainty. Proc. 2014 Am. Control Conf., 2014, p. 404–11. doi:10.1109/ACC.2014.6858875.

[149] Kircher KJ, Zhang KM. Model Predictive Control of Thermal Storage for Demand Response. 2015 Am. Control Conf., 2015, p. 956–61. doi:10.1109/ACC.2015.7170857.

[150] Cengel YA, Ghajar AJ. Heat and Mass Transfer: Fundamentals and Applications. 5th ed. New York: McGraw-Hill; 2014.

[151] Lu Y, Wang S, Sun Y, Yan C. Optimal scheduling of buildings with energy generation and thermal energy storage under dynamic electricity pricing using mixed-integer nonlinear programming. Appl Energy 2015;147:49–58. doi:10.1016/j.apenergy.2015.02.060.

[152] De Coninck R, Helsen L. Practical implementation and evaluation of model predictive control for an office building in Brussels. Energy Build 2016;111:290–8. doi:10.1016/j.enbuild.2015.11.014.

[153] Huang H, Chen L, Hu E. A new model predictive control scheme for energy and cost savings in commercial buildings: An airport terminal building case study. Build Environ 2015;89:203–16. doi:10.1016/j.buildenv.2015.01.037.

[154] Hazyuk I, Ghiaus C, Penhouet D. Model Predictive Control of thermal comfort as a benchmark for controller performance. Autom Constr 2014;43:98–109. doi:10.1016/j.autcon.2014.03.016.

[155] Bengea SC, Kelman AD, Borrelli F, Taylor R, Bengea SC, Kelman AD, et al. Implementation of model predictive control for an HVAC system in a mid-size commercial building. HVAC&R Res 2014;20:121–35. doi:10.1080/10789669.2013.834781.

[156] Privara S, Siroky J, Ferkl L, Cigler J. Model predictive control of a building heating system: The first experience. Energy Build 2011;43:564–72. doi:10.1016/j.enbuild.2010.10.022.

[157] Oldewurtel F, Ulbig A, Parisio A, Morari M. Reducing Peak Electricity Demand in Building Climate Control using Real-Time Pricing and Model Predictive Control. 49th IEEE Conf. Decis. Control, Atlanta (GA): 2010, p. 1927–32.

[158] Paris B, Eynard J, Grieu S, Talbert T, Polit M. Heating control schemes for energy management in buildings. Energy Build 2010;42:1908–17. doi:10.1016/j.enbuild.2010.05.027.

[159] Coffey B, Haghighat F, Morofsky E, Kutrowski E. A software framework for model predictive control with GenOpt. Energy Build 2010;42:1084–92. doi:10.1016/j.enbuild.2010.01.022.

[160] Ghiaus C, Hazyuk I. Calculation of optimal thermal load of intermittently

heated buildings. Energy Build 2010;42:1248–58. doi:10.1016/j.enbuild.2010.02.017.

[161] Karlsson H, Hagentoft C-E. Application of model based predictive control for water-based floor heating in low energy residential buildings. Build Environ 2011;46:556–69. doi:10.1016/j.buildenv.2010.08.014.

[162] Avci M, Erkoc M, Rahmani A, Asfour S. Model predictive HVAC load control in buildings using real-time electricity pricing. Energy Build 2013;60:199–209. doi:10.1016/j.enbuild.2013.01.008.

[163] Berkenkamp F, Gwerder M. Hybrid model predictive control of stratified thermal storages in buildings. Energy Build 2014;84:233–40. doi:10.1016/j.enbuild.2014.07.052.

[164] Hu J, Karava P. A state-space modeling approach and multi-level optimization algorithm for predictive control of multi-zone buildings with mixed-mode cooling. Build Environ 2014;80:259–73. doi:10.1016/j.buildenv.2014.05.003.

[165] Hu J, Karava P. Model predictive control strategies for buildings with mixed-mode cooling. Build Environ 2014;71:233–44. doi:10.1016/j.buildenv.2013.09.005.

[166] Chandan V, Alleyne AG. Decentralized predictive thermal control for buildings. J Process Control 2014;24:820–35. doi:10.1016/j.jprocont.2014.02.015.

[167] Touretzky CR, Baldea M. Nonlinear model reduction and model predictive control of residential buildings with energy recovery. J Process Control 2014;24:723–39. doi:10.1016/j.jprocont.2013.09.022.

[168] Herrera E, Bourdais R, Guéguen H. Predictive and interactive controllers for solar absorption cooling systems in buildings. J Process Control 2014;24:836–45. doi:10.1016/j.jprocont.2014.03.008.

[169] Touretzky CR, Baldea M. Integrating scheduling and control for economic MPC of buildings with energy storage. J Process Control 2014;24:1292–300. doi:10.1016/j.jprocont.2014.04.015.

[170] Dobbs JR, Hencey BM. Model predictive HVAC control with online occupancy model. Energy Build 2014;82:675–84. doi:10.1016/j.enbuild.2014.07.051.

[171] Goyal S, Ingley HA, Barooah P. Occupancy-based zone-climate control for energy-efficient buildings: Complexity vs. performance. Appl Energy 2013;106:209–21. doi:10.1016/j.apenergy.2013.01.039.

[172] Herrera E, Bourdais R, Guéguen H. A hybrid predictive control approach for the management of an energy production-consumption system applied to a TRNSYS solar absorption cooling system for thermal comfort in buildings. Energy Build 2015;104:47–56. doi:10.1016/j.enbuild.2015.06.076.

[173] Zakula T, Armstrong PR, Norford L. Advanced cooling technology with thermally activated building surfaces and model predictive control. Energy Build 2015;86:640–50. doi:10.1016/j.enbuild.2014.10.054.

[174] Boo C-J, Kim J-H, Kim H-C, Lee KY. Building Indoor Temperature Control Using Model Predictive Control in Cooling Systems. IFAC-PapersOnLine 2015;48:316–20. doi:10.1016/j.ifacol.2015.12.397.

[175] Zhao Y, Lu Y, Yan C, Wang S. MPC-based optimal scheduling of grid-connected low energy buildings with thermal energy storages. Energy Build 2015;86:415–26. doi:10.1016/j.enbuild.2014.10.019.

[176] Feng J, Chuang F, Borrelli F, Bauman F. Model predictive control of radiant slab systems with evaporative cooling sources. Energy Build 2015;87:199–

210. doi:10.1016/j.enbuild.2014.11.037.

[177] Marušić A, Lončar D. Model predictive control in small family house: Extravagance or future of energy consumption in households. IFAC-PapersOnLine 2015;28:701–2. doi:10.1016/j.ifacol.2015.05.200.

[178] Brooks J, Kumar S, Goyal S, Subramany R, Barooah P. Energy-efficient control of under-actuated HVAC zones in commercial buildings. Energy Build 2015;93:160–8. doi:10.1016/j.enbuild.2015.01.050.

[179] Killian M, Mayer B, Kozek M. Cooperative fuzzy model predictive control for heating and cooling of buildings. Energy Build 2016;112:130–40. doi:10.1016/j.enbuild.2015.12.017.

[180] Chen X, Wang Q, Srebric J. Occupant feedback based model predictive control for thermal comfort and energy optimization: A chamber experimental evaluation. Appl Energy 2016;164:341–51. doi:10.1016/j.apenergy.2015.11.065.

[181] Yao J, Costanzo GT, Zhu G, Wen B. Power Admission Control with Predictive Thermal Management in Smart Buildings. IEEE Trans Ind Electron 2015;62:2642–50. doi:10.1109/TIE.2014.2387091.

[182] Razmara M, Maasoumy M, Shahbakhti M, Robinett RD. Optimal exergy control of building HVAC system. Appl Energy 2015;156:555–65. doi:10.1016/j.apenergy.2015.07.051.

[183] Razmara M, Maasoumy M, Shahbakhti M, Rush DR. Exergy-Based Model Predictive Control for Building HVAC Systems. 2015 Am. Control Conf., 2015, p. 1677–82.

[184] Zhao J, Lam KP, Ydstie BE, Karaguzel OT. EnergyPlus model-based predictive control within design–build–operate energy information modelling infrastructure. J Build Perform Simul 2015;8:121–34. doi:10.1080/19401493.2014.891656.

[185] Baoti M, Novoselnik B, Cesi J, Petrovi I. Nonlinear Model Predictive Control for Energy Efficient Housing with Modern Construction Materials. IEEE Sensors Appl. Symp., IEEE; 2015, p. 1–6.

[186] Majumdar A, Setter JL, Dobbs JR, Hencey BM, Albonesi DH. Energy-comfort optimization using discomfort history and probabilistic occupancy prediction. 2014 Int. Green Comput. Conf. IGCC 2014, IEEE; 2015, p. 1–10. doi:10.1109/IGCC.2014.7039173.

[187] Rhee K-N, Kim KW, Zakula T, Armstrong PR, Norford L, Mayer B, et al. Cooperative and hierarchical fuzzy MPC for building heating control. Energy Build 2013;58:640–50. doi:10.1016/j.enbuild.2014.10.054.

[188] Mantovani G, Ferrarini L. Temperature Control of a Commercial Building With Model Predictive Control Techniques. IEEE Trans Ind Electron 2015;62:2651–60. doi:10.1109/TIE.2014.2387095.

[189] Carrascal E, Garrido I, Garrido AJ, Sala JM. Model Predictive Control for the heating system of a public building. World Autom. Congr. Proc., IEEE; 2014, p. 433–8. doi:10.1109/WAC.2014.6935986.

[190] Taneja J, Ieee SM, Culler D, Ieee F, Tomlin C, Ieee F. Reducing Transient and Steady State Electricity Consumption in HVAC Using Learning-Based Model-Predictive Control. Proc. IEEE, vol. 100, IEEE; 2012, p. 240–53.

[191] Aswani A, Master N, Taneja J, Krioukov A, Culler D, Tomlin C. Energy-Efficient Building HVAC Control Using Hybrid System LBMPC. IFAC Proc Vol 2012;45:496–501.

[192] Li X, Malkawi A. Multi-objective optimization for thermal mass model predictive control in small and medium size commercial buildings under

summer weather conditions. Energy 2016;112:1194–206. doi:10.1016/j.energy.2016.07.021.

[193] Vega Lara BG, Castellanos Molina LM, Monteagudo Yanes JP, Rodríguez Borroto MA. Offset-free model predictive control for an energy efficient tropical island hotel. Energy Build 2016;119:283–92. doi:10.1016/j.enbuild.2016.03.040.

[194] Acosta A, González AI, Zamarreño JM, Álvarez V. Energy savings and guaranteed thermal comfort in hotel rooms through nonlinear model predictive controllers. Energy Build 2016;129:59–68. doi:10.1016/j.enbuild.2016.07.061.

[195] O'Dwyer E, De Tommasi L, Kouramas K, Cychowski M, Lightbody G. Modelling and disturbance estimation for model predictive control in building heating systems. Energy Build 2016;130:532–45. doi:10.1016/j.enbuild.2016.08.077.

[196] Zong Y, Böning GM, Santos RM, You S, Hu J, Han X. Challenges of implementing economic model predictive control strategy for buildings interacting with smart energy systems. Appl Therm Eng 2017;114:1476–86. doi:10.1016/j.applthermaleng.2016.11.141.

[197] Dwyer EO, Tommasi L De, Kouramas K, Cychowski M, Lightbody G. Control Engineering Practice Prioritised objectives for model predictive control of building heating systems. Control Eng Pract 2017;63:57–68. doi:10.1016/j.conengprac.2017.03.018.

[198] Cigler J, Tomáško P, Široký J. BuildingLAB: A tool to analyze performance of model predictive controllers for buildings. Energy Build 2013;57:34–41. doi:10.1016/j.enbuild.2012.10.042.

[199] Huang H, Chen L, Mohammadzaheri M, Hu E. A new zone temperature predictive modeling for energy saving in buildings. Procedia Eng 2012;49:142–51. doi:10.1016/j.proeng.2012.10.122.

[200] Samad T. A survey on industry impact and challenges thereof. IEEE Control Syst 2017;37:17–8. doi:10.1109/MCS.2016.2621438.

[201] Hilliard T, Kavgic M, Swan L. Model predictive control for commercial buildings: trends and opportunities. Adv Build Energy Res 2016;10:172–90. doi:10.1080/17512549.2015.1079240.

[202] Marinakis V, Doukas H, Karakosta C, Psarras J. An integrated system for buildings' energy-efficient automation: Application in the tertiary sector. Appl Energy 2013;101:6–14. doi:10.1016/j.apenergy.2012.05.032.

[203] Zacekova E, Vana Z, Cigler J. Towards the real-life implementation of MPC for an office building: Identification issues. Appl Energy 2014;135:53–62. doi:10.1016/j.apenergy.2014.08.004.

[204] Zambrano D, Bordons C, García-Gabín W, Camacho EF. A Solar Cooling Plant: a Benchmark for Hybrid Systems Control. IFAC Proc Vol 2006;39:199–204. doi:10.3182/20060607-3-IT-3902.00037.

[205] Camacho EF, Bordons C. Model Predictive Control 1999:51–61.

[206] Mehling H, Cabeza LF. Heat and cold storage with PCM. Handbook. Springler; 2008.

[207] Genovese A, Amarasinghe G, Glewis M, Mainwaring D, Shanks RA. Crystallisation, melting, recrystallisation and polymorphism of n-eicosane for application as a phase change material. Thermochim Acta 2006;443:235–44. doi:10.1016/j.tca.2006.02.008.

[208] Kazas G, Fabrizio E, Perino M. Energy demand profile generation with detailed time resolution at an urban district scale: A reference building

approach and case study. Appl Energy 2017;193:243–62. doi:10.1016/j.apenergy.2017.01.095.

[209] Herceg M, Kvasnica M, Jones CN, Morari M. Multi-parametric toolbox 3.0. Control Conf (ECC), 2013 Eur 2013:502–10.

[210] Torrisi FD, Bemporad A. HYSDEL- A Tool for Generating Computational Hybrid Models for Analysis and Synthesis Problems. IEEE Trans Contr Syst Technol 2004;12:235–49. doi:10.1109/TCST.2004.824309.

Chapter 6

Conclusion and outlook

The pursuit to obtain higher levels of comfort has led to a dramatic increase in the energy demand in buildings. For this reason, in the last decades, one of the primary goals of engineers and researchers has been to optimise the trade-off between the conflicting objectives of increasing the occupants' thermal comfort and reducing the building energy demand. The outcomes of these studies led to improve the performance of energy efficient building technologies significantly and to increase the market penetration of nearly Zero Energy Buildings or passive buildings. However, the adoption of Renewable Energy Sources - directly integrated into buildings or connected to energy grids - has introduced new challenges to face. Indeed, the Renewable Energy Sources variation during the time and the mismatch between Renewable Energy Sources availability and the actual occupants' demand require buildings capable to interact with variable grid and occupants' needs. Exploiting active and passive energy storage technologies is a first possible solution for addressing this requirement. Additional benefits can derive from the implementation of information and communication technologies in buildings. Indeed, electronic components are becoming extremely affordable. Thus their deployment in buildings sharply increased in the last decade, allowing a significant amount of building-related data to be more readily available and accessible. Simultaneously, the increase in computational power and the availability of accurate weather predictions permitted the building designers to explore many possible advanced control strategies for optimising the energy management of buildings.

The research activity outlined in the present thesis has been undertaken in this framework. The primary goal of the work has been to investigate the innovative energy technologies and control algorithms for enhancing demand-side management in buildings. In detail, the thesis has been focused on a solar thermal system for satisfying space heating demand of buildings. The main shortcoming of solar energy (and broadly of renewable energy sources) is the possible mismatch between energy production and exploitation. Indeed, the building energy demand

profiles do not match exactly with the shape of the power pattern supplied by renewable energy production system. For this reason, technologies able to store the energy production and active demand-side management or demand-response strategies must be implemented in buildings. The scope is to enable the reduction in the mismatch between energy availability and demand in buildings. This shortcoming can be faced employing hardware or software solutions. The hardware solutions for thermal demand response of buildings are those technologies that allow the energy loads to be permanently shifted or mitigated. The software solutions for demand response are those that integrate an intelligent supervisory layer in the building automation (or management) system. The present thesis approached the problem from both the hardware technologies side and the software solutions side. This methodology represents itself a novelty in the literature. In fact, innovative hardware technologies and intelligent control layers are generally investigated separately. Contrariwise, in the present thesis, an approach that evaluated the problem holistically was undertaken. This path has allowed the benefits available employing hardware or software solutions to be considered at the same time. This detail enabled the mutual relationships and interactions between the strategies to be appropriately measured.

Most of the findings and outcomes of the current research work has been already discussed in detail in the previous chapters. The goal of this final chapter is providing to the reader not only a simple summary of the results but also a clear perspective about their implication in a global framework and future works.

The technology used as the case study was a low-temperature solar thermal system for satisfying space heating demand, named SolHe-PCM. Current advances in the energy science have marked how the improvement of performance of a conditioning system requires a reduction in the thermal levels involved in the process. This objective can be reached moving the paradigms at the basis of the heat transfer processes involved in the heat conversion, storage, and delivery. For instance, in this thesis, it was possible by switching from a traditional technology that involves sensible heat storage to an innovative solution characterised by latent heat exploitation. A novel heat transfer fluid and storage media based on mPCM slurry was adopted for this purpose. In the first part of the thesis, the features of that material were investigated experimentally and theoretically. In particular, it was demonstrated that the mPCM slurry – up to 45 % w.t. concentrations – can be straightforwardly used in solar thermal systems without particular rheological, pipe clogging, and pumping problems. An increase in pressure drops was monitored, but it assumes significant values only for very high mPCM concentrations (over 35 % w.t.). Tests on thermal properties underlined how the material significantly overperform the water within the phase change range. The higher the PCM concentration in the mixture, the better the overall thermal performance. Future works should find the optimal trade-off between the pressure drops worsening and the thermal properties improving for each system configurations.

Form the material science perspective, the main shortcoming of the mPCM was the physical instability due to the density difference between the dispersed mPCM and the carrier fluid, causing the creaming phenomenon. Firstly, creaming was

studied experimentally. Secondly, technical measures to mitigate its occurrence were adopted on the SolHe-PCM full-scale prototype. Despite these precautions, the first version of the prototype was affected by material instability shortcomings. The creaming caused material segregation in the storage tank and pipe clogging. This fact required the substitution of the storage tank with a new version equipped with a mechanical mixer. This recursive design procedure (trial-and-error) is almost typical of every innovative technology. The experimental campaign was slowed down by the operation of system retrofit required for preventing creaming shortcomings. For this reason, in the time-span of the present thesis, it was not possible to carry out and discuss detailed experimental results. Anyhow, the recursive design led to an operating version of the full-scale prototype, which opens up to future tests on the long-term system performance.

Nevertheless, the experimental campaign was used to calibrate and validate a numerical model of the solar thermal system. This model was developed to define the thermo-energetic behaviour of the technology. It consisted of two mathematical sub-models able to describe the power/energy balances of the flat-plate solar thermal collector and the thermal energy storage unit respectively. In closed-loop configuration, all the Key Performance Indicators used to assess the reliability of the model indicated an excellent comparison between the system monitored outputs and simulation results. For this reason, the model was considered validated and able to explain the real system behaviour adequately. A traditional water-based solar thermal system was used as the reference baseline. Parametrical simulations about the collector performance showed how the heat transfer fluid based on PCM slurry overperforms the baseline according to various boundary conditions. The same results were obtained during year-long simulations referred to three locations, characterised by very different climatic conditions. Compared to a traditional water-based system, the simulation results showed that the SolHe-PCM collector could improve the production of useful heat up to 7 % throughout the year and 19 % during the heating season. The last part of this section explained that the thermal energy storage performance must also be considered Second law analysis to be adequately evaluated. Even if a simplified version of Second law balance was herewith presented, detailed Second law analyses will be demanded for future works. Moreover, exergy/entropy generation evaluations could be adopted to improve the design of each element of the innovative system, particularly the heat exchangers.

Once the hardware technology was defined, the implementation of an innovative control method was necessary to enhance the operational efficiency of the system. In this framework, the increasing penetration of Information and Communication Technologies (ICT) in buildings has allowed a significant amount of building-related data to be more readily available and accessible. For this reason, if this information is appropriately processed through data-driven procedures, it may provide crucial knowledge on the actual building performance and the influence of occupant behaviour on the building energy demand. A specific solution was considered particularly promising for this purpose: the adoption of Model Predictive Control (MPC) formulations for improving the building thermal and

energy management. When MPC formulation is undertaken, one of the leading problem arising is the definition of a simplified control oriented model that should be used in the iterative optimisation procedure. However, in the case of SolHe-PCM, a simplified lumped model of the controlled system was already formulated. For this reason, MPC algorithms seemed to be the ideal choice to devise a controller capable of maximising the SolHe-PCM system potentialities. Indeed, since a new technology was proposed, new control paradigms had to be formulated to enhance all its benefits.

Firstly, this thesis provided a robust and complete framework of the steps required to define an MPC problem for building processes regulation correctly. This scope was reached employing an extended review of the scientific literature and practical application concerning MPC application for building management. The main outcome of this section was to lay the foundation of an imaginary bridge linking automation and control engineers with building and mechanical engineers involved in building and HVAC system design and operation. Secondly, an MPC algorithm was formulated to regulate the SolHe-PCM prototype. Deterministic and estimated external disturbance were considered. A testbed virtual environment was developed to perform closed-loop simulations. The existing rule-based control logic was employed as the reference baseline. Compared to the baseline, the MPC algorithm produced energy savings up to 19.2 % with lower unmet energy demand. Moreover, when the slacking variable used to constraint the fulfilling of the space heating demand was relaxed energy savings ramped up to 31.8 %. Nevertheless, in this case, a slightly higher unmet energy demand was detected. The findings of the work have proved the effectiveness of MPC in adequately exploiting the benefits of the latent heat of fusion/solidification at the base of the investigated solar system. Future works will be focused on the implementation of the control algorithm on the regulation system embedded in the full-scale prototype. Furthermore, a better estimation of the disturbances related to the occupant behaviour will be considered thanks to the advancement in data analytics.

In conclusion, the research activity undertaken in this PhD thesis underlined how topics covered by energy sciences are nowadays heterogeneous and complex. Conducting research investigations able to cover all these aspects seemed to be a hard challenge. However, the thesis outlined how the current advanced technologies offer development potentialities and computational power that are stronger than ever. Engineers and researchers must improve their "soft skills" in problem formulation to correctly select the questions necessary to answer with the aid of these technologies. This path should be carried on with a holistic approach, capable of considering all the possible aspects of the problem and all the possible solutions to face it. At the same time, engineering "hard skills" are necessary to integrate and deploy these technologies appropriately. Two main research paths should be further investigated in this direction: hardware technologies and software solution. Concerning hardware aspects, more than ever, it is necessary to increase the building storage potentialities and better integrate renewable energy sources. On the other hand, software solutions enable to enhance the performance of these innovative hardware technologies. Particularly promising are those solutions

related to energy data analytics for automatic extraction of knowledge and predictive control strategies with recursive optimisation tools.

The geometrical figure used in the introduction of the thesis (*the most unfortunate dodecahedron*) can also be adapted to conclude the work. In fact, even if the present study was focused on a specific case study, it contained aspects belonging to several scientific disciplines. Besides, future works must necessarily deal with further topics. This fact underlines how the current challenges offered by the building physics require more and more a multi-disciplinary approach. This heterogeneous and complex framework can be pinpointed by the dodecahedron represented in *Figure 1*. For similarity with the previous one, this geometric figure was called "*the challenging dodecahedron*".
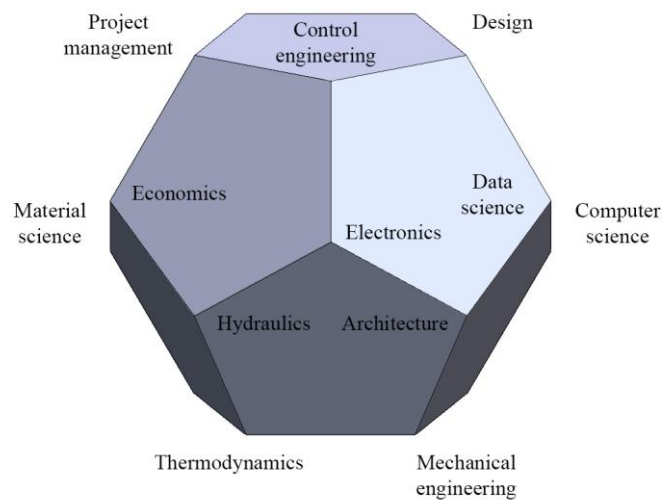
Figure 1. The challenging building physics dodecahedron.

The building physics is represented by *the challenging dodecahedron* itself. The dodecahedron faces represent the several disciplines affecting the development of a novel aspect of the building physics. Most of them have also been approached in the present thesis, while others open up at future studies. The sciences primarily involved in the building physics have been the *mechanical engineering, thermodynamics* and *architecture* which institute the basis of the geometrical figure. The *design* competences intervene in the conceiving of novel technologies and the definition of the initial blueprints, while the *project management* is required to correctly deploy and make full-scale prototypes. *Rheology (hydraulics)* and *material science* (*chemistry*) demonstrated to play a fundamental role in novel HVAC system performance assessment. Mainly the latter will be crucial for the specific case study, in order to individuate a definitive solution to the creaming phenomenon. Up to date, *electronics* is broadly used in building and HVAC systems both for extensive monitoring and practical actuation. *Computer science* leads to connect the components in an Internet of Things framework, which takes advantage of the tremendous computational power offered by Cloud solutions and

data gathered from several resources. The embedded controller used in the present case study only partially covered these topics. Nevertheless, they will be essential for future developments that will estimate system disturbances (e.g., space heating demand or climatic conditions) in a more tailored mode. On the one side, the collected data can be processed to exploit advances in *control engineering*, which allows intelligent energy management strategies to be performed. On the other side, *data scienc*e competencies are becoming more and more central in understanding stochastic processes (e.g., occupancy driven problems). Eventually, the *economic feasibility* of a technology must be investigated considering all the investment and operational costs required for penetrating the market effectively. In detail, cost-optimal analyses represent a valid solution to explore the trade-off between the energy-saving benefits and the additional budgets needed by a novel technology. Future works regarding SolHe-PCM has to approach the problem also from this perspective.